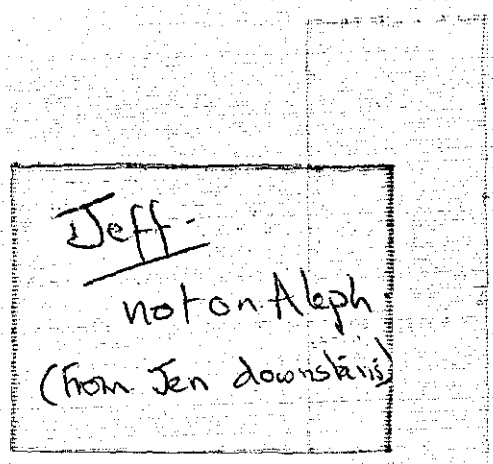
Jeff -
not on Aleph
(from Jen Downskiis)

TOWARD COMMERCIAL REALISATION OF WHOLE FIELD INTERFEROMETRIC ANALYSIS

BY

JOHN R. TYRER

A Doctoral Thesis submitted in
partial fulfilment of the
requirements for the award of
Doctor of Philosophy
of the
Loughborough University of Technology

December 1989

Department of Mechanical Engineering

There are certain Phaenomena of this scatter'd Light,
which when I first observed them,
seem'd very strange and surprizing to me.

Sir Issac Newton
Second Book of Optics
Pt IV, 1704

This work is dedicated to Elizabeth Raymond
for her love and help

and to my parents, Ray and Nita
for their love and support

TOWARD COMMERCIAL REALISATION OF WHOLE FIELD INTERFEROMETRIC ANALYSIS

ABSTRACT

The objective of this work was to produce an instrument which could undertake wholefield inspection and displacement measurement utilising a non-contacting technology. The instrument has been designed to permit operation by engineers not necessarily familiar with the underlying technology and produce results in a meaningful form. Of the possible techniques considered Holographic Interferometry was originally identified as meeting these objectives. Experimental work undertaken provides data which confirms the potential of the technique for solving problems but also highlights some difficulties.

In order to perform a complete three dimensional displacement analysis a number of holographic views must be recorded. Considerable effort is required to extract quantitative data from the holograms. Error analysis of the experimental arrangement has highlighted a number of practical restrictions which lead to data uncertainties. Qualitative analysis of engineering components using Holographic Interferometry has been successfully undertaken and results in useful analytical data which is used in three different engineering design programmes. Unfortunately, attempts to quantify the data to provide strain values relies upon double differentiation of the fringe field, a process that is highly sensitive to fringe position errors. In spite of this, these experiments provided the confidence that optical interferometry is able to produce data of suitable displacement sensitivity, with results acceptable to other engineers.

In order to extend the work into an industrial environment double pulsed lasers are used in Holographic and Electronic Speckle Pattern Interferometry. This work is necessary to determine the possible limits of

the double pulse technique. The experiments did provide confidence that with suitable design effort interferometric arrangements could be constructed to work in the most arduous of industrial environments. Triggering of the laser from a secondary transducer resulted in various electronic configurations which successfully provided temporal and spatial investigations of vibrating component surfaces. However, the problems of data extraction common to holographic techniques again led to questions about data quality and interpretation.

Recognition of the experimental difficulties in using Holographic Interferometry in practical engineering studies suggested Electronic Speckle Pattern Interferometry (ESPI) to be a more suitable technique. The different imaging mechanism of ESPI is able to provide three dimensional results without further data reduction and was investigated further to determine if the technique was able to fulfil the remaining objectives. New designs of interferometer result in equipment able to provide in-plane and out-of-plane data. Experiments undertaken refined time averaged ESPI such that high contrast fringe patterns could be obtained from systems operated using F1.4 lenses.

The design of the existing analogue ESPI processing electronics produced fringes of good visual quality, but this was achieved by simple contrast stretching. Thus the actual $\cos^2$ fringe function was replaced by one of a near square wave type. New digital processing electronics were designed which did not corrupt the fringe pattern intensity distribution. The restoration of the correct fringe function provided suitable input data for computer based fringe pattern analysis. Since the fringe patterns alone do not provide real data it was necessary to determine methods for computer based fringe pattern analysis. After a review of available fringe processing techniques, two step phase stepping was chosen.

Experimentation shows that the phase stepping approach can be successful in tackling the ESPI fringe pattern reduction. Although the demands imposed by the image processors lead to further designs of the

hardware, micro computer and multipage framestores result in the equipment being able to undertake image acquisition and fringe pattern processing in less than 15 seconds. Furthermore these new designs are compact, simple in construction and easy to maintain.

The construction of hybrid in-plane and out-of-plane sensitive interferometers provides the necessary test bed for the image processing equipment. The generation of processed three dimensional displacement data in cartesian coordinate form is considered highly significant to real world engineering design studies. The final effort of the research is the combination of ESPI with novel pulsed lasers to produce the prototype for the required instrument technology. Attempts to incorporate a pulsed ruby laser in a speckle interferometer, whilst experimentally successful, were significant in identifying problems which were endemic of pulsed ruby laser operation. An alternative laser type is identified which can provide suitable pulsed energy and, using a frequency doubled Nd.YAG pulsed laser for ESPI results in real time, high repetition (50Hz) pulsed results. Problems with traditional double pulse operation lead to the novel concept of combining two separate pulsed lasers to form a twin laser system with greater flexibility. The new twin pulse laser concept proves to be very successful, by achieving a trebling of the optical energy output for half the electrical energy requirement of the previous system. Line narrowing with diode laser seeding provides the necessary improvement to laser beam quality. This totally new approach leads to a considerable improvement in flexibility with variable pulse separation from 10 nsec up to 20 msec (20 msec being the camera operating cycle time) being achievable, with a maximum energy of 100 mJ/pulse of consistent output.

ACKNOWLEDGEMENTS

During the course of this work the following people have contributed;

Professor Gordon Wray, Professor Jim Hewit and Brian Bergquist for academic assistance, and remembrance is paid to the late Professor John Butters who acted as supervisor in the early phases of the work.

Dr. Jeremy Davies of Rover Group for providing the original opportunity to undertake this work.

Members of the Optical Engineering Group; Dr. Paul Montgomery, Paul Henry, David Kerr, Dr. Fernando Mendoza, Mike Shellabear, Andy Moore, and Paul King for help and stimulating discussions. Vic Roulstone, Steve Penney and the late Mick Bramley for mechanical instrumentation. Terry West, David Hackett and Mick Smeeton for the electronic instrumentation. Rosemarie Lander and Wendie Pilkington for typing the thesis.

Ken Topley and Margaret Martin for photographic work.

Peter Smith, Guy Richards, Fiona Clouder Richards and Bill Hillier of the SERC for funding.

Dr. Paul Sarkies of Spectron Lasers for loan of the original Nd.YAG laser.

Finally to Dr. Elizabeth Raymond, who got there first and gave me all the needed encouragement and help.

Thank you.

CONTENTS PAGE

CHAPTER 1
OVERVIEW

1.0 Introduction

Prior to this century it was usual in science for the experiment to predate the theory. Holography is in the new category where theory predates experiment. The use of interferometry and interference goes much further back into history but it was the 1960's that saw the emergence of Holographic Interferometry.

Today, with the ready availability of large computer based modelling techniques, it is verification of the computer predictions which is needed to match performance with hypothesis - in some circumstances it is the model alone which enables designs to be completed. It was with this background in mind that endeavours were made to produce instrumentation that could provide wholefield inspection for the engineering community. In particular, it is in the field of engineering design, where the detection of undesirable and potentially catastrophic effects not successfully predicted would be of tremendous value. Theoretical models are continually improving but a need still exists for the model to be experimentally verified. For example, coupled vibration modes are difficult to predict, relying on the response of a structure to the combination of two or more resonant frequencies. The cross coupling of these, together with inhomogeneties of the material used and complexity of boundary conditions, make for difficult prediction of real world conditions. Optical inspection can provide surveys of both the resonant and coupled modes and help designers with the mode shape and frequencies.

Thus a need exists for a measuring instrument able to provide data in a form suitable for engineers to refine a process or device. This work arose from studying the performance of motor cars and their power units in both the laboratory and various test facilities. This required a technique

which could provide experimental data about the wholefield performance of a power train system or an individual device. Many techniques were considered, usually they relied on the overcoating of the surface with suitable material from which a comparative analysis could be performed. The results in all cases were relative and needed calibration. Optical Interferometry is an alternative method which provides absolute data without intruding within the component's environment and does not require any surface modification. Hence the results obtained could be considered representative of the actual response of the surface.

1.1 Holography and Holographic Interferometry

A non-invasive wholefield technique based around the laser was identified as a candidate technology for study. To determine the value of such technology, the suitability of the data had to be considered within the broader requirements of manufacturing industry. Whilst fringe patterns appeared to be of value, the technology had been available for over twenty five years and yet there was no major commercial effort in this area. The apparent value of the data was constrained by three further aspects:

(i) It was a difficult technique to use and consequently automate.
(ii) It was tedious to extract meaningful data.
(iii) Real world studies outside the laboratory had received little attention.

Figure 1.1 outlines the programme of study undertaken, it identifies Holographic Interferometry as a possible technique from the attributes outlined above. Further work was required to confirm this decision:-

(i) The undertaking of suitable engineering problem solving in order to provide confidence in the technique and identify the type of information required.

(ii) Experimental studies to appreciate the subtlety of the technique and thereby attempt to consider automation of the process to widen the appeal.

In retrospect this approach appears somewhat naive. During the heady days of the 1960's when the laser and holography appeared to provide many potential solutions, a great deal of funding and effort attempted similar tasks. The principal conclusions from this initial study highlighted problems in acquiring quantitative data and the real need to tackle problems on components not only in a laboratory situation but in-service performing a real world task.

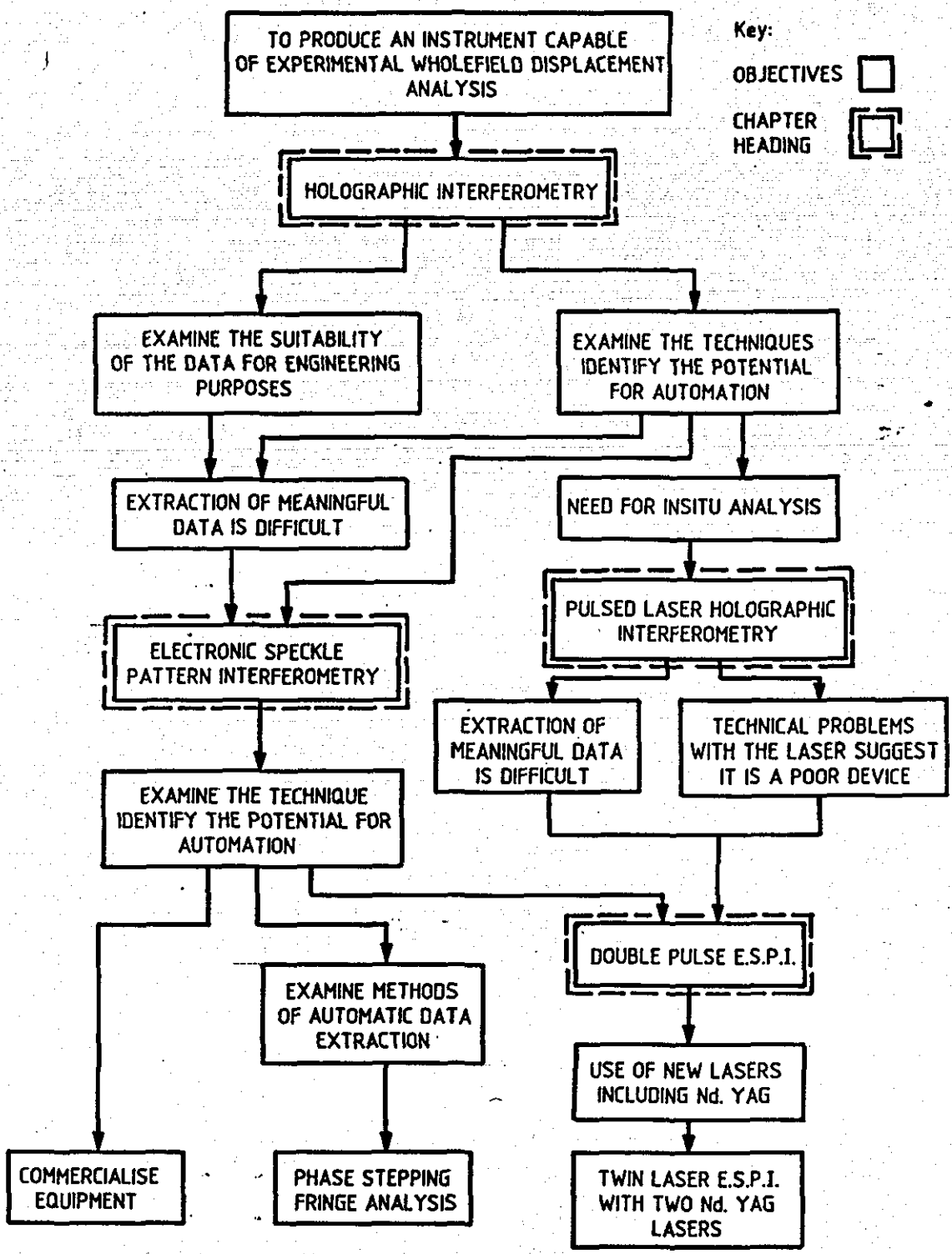

Figure 1

Block Diagram Showing the Work Methodology Undertaken

1.2 Electronic Speckle Pattern Interferometry (ESPI)

Previous post graduate research had acquainted the author with Electronic Speckle Pattern Interferometry (ESPI) and provided some experience in the advantages of this 'noisy' form of interferometry. The advantage of real time viewing and potential utility of the technique were considered to provide the necessary technical solutions. The imaging mechanism of ESPI is different to that of Holographic Interferometry. ESPI relies on electronic correlation of the image picture points whereas holographic interferometry utilises the interference of optical wavefronts in high resolution photographic recording media. Thus ESPI can overcome the photographic processing requirements by the use of television cameras. However, the most significant advantage is the use of correlation techniques against optical wavefronts interference. The arrangement of the optical system provides the flexibility to construct interferometers sensitive to displacement in the three principal orthogonal vectors. Thus separately and independently three views of the displacement of a component can be acquired with no cross correlation between views. Typical arrangements use cartesian vectors (x, y and z) to provide data, whereas with holographic interferometry three views are required from the hologram and only after suitable data extraction can a vector be uniquely described. This becomes a handicap when attempting to extract only the x and y displacement vectors although other optical arrangements are possible which provide just the z displacement vector. A technique existed therefore, which could potentially provide the necessary data but little work had been undertaken into providing arrangements which could be practically exploited. The design of interferometers, which combined optical performance with the simplicity of manufacture and operation, formed a major goal of this work. The design of new electronic pre-processing with advances in digital electronics overcame many of the cost and performance barriers. These designs had to be commercially orientated to attract a wider community of users to provide the basis for the refinement of the technique.

The interferometric designs used throughout this programme have generated fringe patterns which detect relative changes between the optical path lengths of the two interferometer arms. Shearing interferometers produce fringe patterns which relate to the change of slope of the displacement. Conceptually, displacement fringe patterns are somewhat easier to comprehend and consequently highlight any problems. The fringe patterns, whilst able to provide displacement contours in the orthogonal vectors, do not themselves provide data. Manual interpretation of the fringe patterns was a long-winded and inaccurate process. Thus it was necessary to undertake a feasibility study into the possible methods of computerised fringe pattern analysis. Equipment was borrowed to assess likely methods which would be insensitive to the inherent noise problem of speckle interferograms. Two step phase stepping was deemed suitable, though additional effort was necessary to undertake the task of software generation, interferometer evaluation and electronic pre-processor manufacture.

1.3 Double Pulsed Holographic Interferometry

In combination with the evolution of the ESPI instrumentation, one other conclusion of the initial study was the need for real world problem solving. Previous work had demonstrated the ability of double pulsed ruby lasers to undertake interferometric study of such environments. However, the cost, size and complexity had mitigated against significant utility in any industrial facility. The size of the user market had not encouraged the laser manufacturers to invest in the development of pulsed ruby lasers and so produced a chicken and egg problem. A further aspect reflecting their limited usage was the skill level necessary to operate the equipment. Much published literature existed demonstrating the ability of pulsed lasers to acquire interferometric data though little evidence existed of successful applications to problem solving. The industrial facilities utilising such equipment are not primarily concerned

with establishing a wider acceptance of this technology by other potential users. One alternative to pulsed laser technology is the use of common path interferometry which effectively phase locks the object to the recording system. Laboratory trials of this technique demonstrated limited applicability.

1.4 Double Pulsed Electronic Speckle Pattern Interferometry

Experimental investigations using pulsed lasers and holographic interferometry demonstrated the advantages of such equipment, but still retained the problems of data acquisition. The conclusions from the initial experimental work was to attempt to build upon the limited previous work undertaken in double pulsed ruby laser ESPI. The intention being to build upon the instrumentation advantages of ESPI and the potential of the pulsed laser. Trials with alternative stroboscopic and cavity dumped continuous wave lasers proved unsatisfactory.

With suitable re-design of the pulsed laser optical chassis, experiments attempted to harness the ruby laser in an experimental ESPI configuration. This highlighted problems with pulse to pulse energy stability not previously considered a problem with holography. The additional demands of ESPI requiring the synchronisation of the timing and pulse to pulse intensity stability, necessitated further redesign to the electronics and optical arrangement. Consideration of the laser principles and fundamental operating constraints suggested this type of solid state laser to be unsuitable for continuous high repetition double pulsing. An ideal alternative laser source would have a higher optical efficiency to reduce the problems of thermal instabilities and be able to operate at television rates (25Hz for European framing rates or 50Hz for field rates). Furthermore, the laser should operate in the visible part of the optical spectrum. Experience in attempting to align an infra-red pulsed laser interferometer highlighted visible operation as an important feature. With industrial considerations in mind, visible operation presents fewer

concerns from a laser safety aspect. Underwater operation is desirable, which requires the blue/green part of the visible spectrum for maximum transmission in water with minimum absorption. Copper vapour lasers were considered but rejected due to their particular beam profile and limited energy per pulse. A compromise solution was found with Neodymium Yttrium Aluminium Garnet (Nd.YAG) lasers whose fundamental wavelength of 1.06 μm failed to meet the desire for visible operation but could, after suitable discussions and modifications by the laser manufacturers, provide all other aspects of the specification. To reduce the problem of non visible operation, television cameras were identified which could operate successfully with reasonable photometric sensitivity in this part of the spectrum. Fortunately suitable high efficiency (50%) frequency doubling crystals became available which provided operation at 0.53μm thus producing a visible output and so completing the initial specification. Operation of frequency doubled, double pulsed Nd.YAG was successfully demonstrated. One problem with this type of operation is the demands placed upon the pockel cells and intra-cavity etalons, optical components within the laser cavity, which have not previously been operated under such demanding interferometric conditions. Thermal problems associated with the high energy inputs to absorptive devices led to beam jitter, causing laser beam stability problems. One novel approach of this work was the optical injection of diode seeded laser energy into two Nd.YAG lasers to enable high quality, fully variable double pulse operation of an interferometer. Such equipment has been specifically designed and produced for this research. This approach provided all the attributes laid down in the equipment specification. The combination of all three aspects - commercial instrumentation, computerised fringe pattern analysis and twin pulsed Nd.YAG laser based ESPI - provides equipment able to satisfy the needs of the end users and is now acquiring industrial interest.

The layout and arrangement of the work undertaken is given in Figure 1.1 which also highlights work breakdown into chapter headings. The contents of these chapters are:

Chapter 2 - Principles of Holography

The mathematical background is presented with comments on materials and different recording techniques.

Chapter 3 - Holographic Interferometry

This chapter presents the practical studies of how holographic interferometry aided the design of automobile engine components and provided a mechanism to introduce a new type of engine condition monitoring.

Chapter 4 - Double Pulsed Holographic Interferometry

This chapter considers the experimental and theoretical requirements and the problems encountered with the synchronisation electronics. An experimental study is presented which required the equipment to be used for in-situ vibration analysis of a large industrial turbo-compressor.

Chapter 5 - Electronic Speckle Pattern Interferometry

The principles of ESPI operation are outlined and experimental techniques discussed. The initial system configuration is considered followed with the design changes and innovation necessary for commercialisation of an instrument. The basics of computer based fringe pattern analysis are considered.

Chapter 6 - Double Pulsed Electronic Speckle Pattern Interferometry

The principle of operation and the problems encountered with ruby and Nd.YAG lasers are discussed. The background to the twin laser concept is presented with experimental verification of the technique.

Chapter 7 - Conclusions

This chapter details the methodology which brought about the development of new approaches to initiate commercial uptake of the concepts. The experimental studies undertaken have to some extent conditioned the routes taken, problems encountered within industry

have helped formulate the technology programme. All of these factors led to a final experimental unit which was different from the original concept.

Chapter 8 - Future Work

This chapter considers the potential industrial areas of interest and examines areas for future research and development.

Appendix 1 - Pulsed Ruby Lasers and Their Operation

Details the description of solid state lasers and the design changes made to the ruby lasers used. The background necessary to undertake the changes from ruby to Nd.YAG lasers is presented. A full understanding of pulsed laser principles is required to attempt the design of the novel twin laser equipment.

Appendix 2 - Speckle Pattern Image Formation and Correlation Interferometry

Provides the fundamentals of the imaging mechanisms and how speckle pattern correlation interferometry differs from Holographic Interferometry. These differences are turned into operational advantages and provide analytical solutions which can be engineered into instruments.

Appendix 3 - Experimental Vibration Study Using Time-Averaged ESPI on a Clamped Square Metal Plate

Provides a comparison between a theoretical prediction of the first six modes and results obtained using time-averaged ESPI.

CHAPTER 2
PRINCIPLES OF HOLOGRAPHY

2.0 Background

Optics is second only to astronomy as the oldest of the physical sciences to be studied by man. Its real scientific roots are based in classical Greek studies and optics has spawned many fields of interest in modern times. It is interesting to note that as our knowledge base expands and the subjects of studies proliferate, optics is being moved more and more to the sidelines. The development of the laser during the 1960's saw a resurgence of activity and money, which unfortunately diminished during the late 1970's. The lack of industrial acceptance may be due in part to the reliance upon the human eye as the final imaging transducer in a system. Television cameras and other imaging sensors are of comparatively low resolution and have not easily been linked to wholefield data reduction facilities. Today the relatively low cost of digital computing equipment and availability of suitable video to digital interfaces is providing the final vital link. Despite the numerous papers concerned with holography and holographic interferometry dating from the late 1960's that refer to the computerised data reduction as an easy but tedious task - it has been anything but! Unfortunately the imaging sensors which are available still rely upon a detecting system which measures either light amplitude or irradiance (the square of amplitude). No detectors available are sensitive to phase and therefore any recording system still relies on phase discrimination using an intensity method. This approach was identical to, that chosen by Gabor [1,2,3] in his attempts to improve the imaging ability of electron microscopes. His intention was twofold:

1. To correct the spherical aberrations of the lenses used within the microscope.
2. To record the scattered object electrons within the microscope in a fashion which allowed reconstruction of the image using visible light.

A consequence of this later approach was that magnification (M) would be linearly related to the ratio of the wavelength of the electron (λ_E) and the visible wavelength (λ_L) as shown:

$$M = \frac{\lambda_L}{\lambda_E}$$

The information about the size and shape of an object is carried in both the phase and intensity structure of the wavefront and both must be encoded to record the complete object wavefront. Gabor's approach, for which he received the Nobel prize in 1971, was to adopt a technique used in radio, namely to combine a carrier wavelength with that from the signal and use interference between the two to record both intensity and phase. Upon playback, demodulation of the complex wavefront takes place with a second identical carrier wave being diffracted to generate the original complex wavefront. This interference pattern could readily be recorded using a high resolution photographic plate.

Unfortunately whilst this magnification is linear the aberrations increase with the third and fourth power of the ratio. To demonstrate the feasibility of his ideas he first used a high pressure mercury arc lamp (of very limited coherence length) to record a visible hologram. The same arrangement was used to reconstruct the image from his 'on-line hologram,' see Figure 2.1.

This method of 'wavefront reconstruction' as it was described is shown in Figure 2.1. In Gabor's experiment the object was a transparency of a few opaque lines upon a clear background. The major limitation of this approach was the need for the observer to view the reconstructed image along the axis of the illumination. Whilst this demonstrated the recording and playback ability, the second part of the experiment, the image magnification still awaits the availability of a commercially produced coherent electron source.

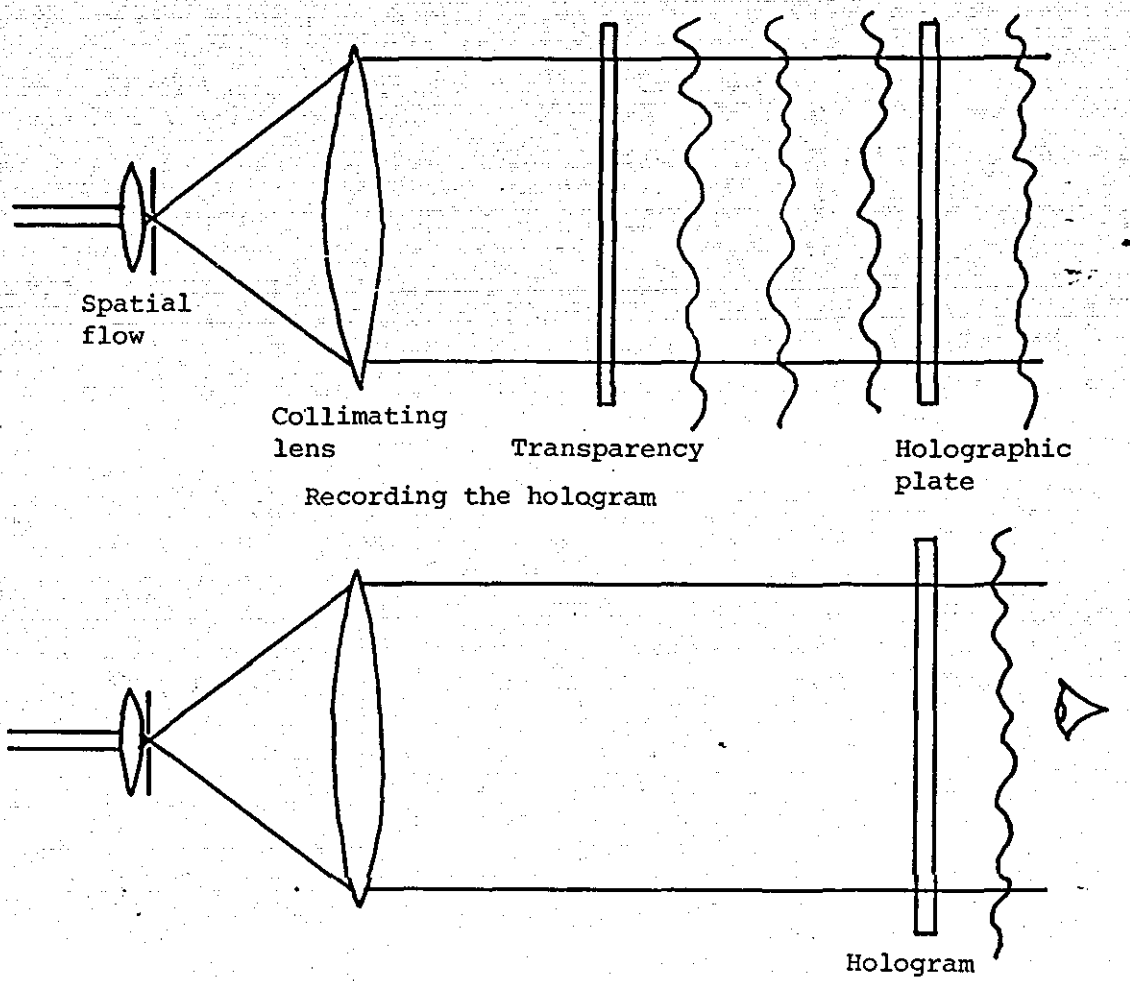

Figure 2.1
Gabor On-line Recording Arrangement

2.1 Off-Axis Holography

The on-axis recording and viewing arrangement was a limitation which remained until longer coherence light sources became available. The advent of the laser enabled an alternative and practical 'off-axis' holographic recording technique capable of imaging diffuse, three dimensional objects. This is accredited to Leith and Upatnieks [4], whilst working in optical processing of synthetic aperture radar data. Whilst they had been able to produce off-axis holograms using mercury arc sources, the laser source resulted in shorter exposures (seconds instead of minutes) and the greatly increased coherence of the laser reduced the physical constraints on the alignment of the optical equipment.

Denisyuk [5] in the Soviet Union reported around the same time, the ability to replay in-line holograms using white light. 1965 saw the most significant application of this branch of optics with reports by several different workers of Holographic Interferometry (HI). This combined the off-axis advantages of holography with the ability to accurately describe object displacement using interferometry. The basic arrangement for recording and replaying an off-axis hologram is shown in Figures 2.2 and 2.3.

When polarized wavefronts combine, the intensity (I) at a point in the field is given by:

$$I = I_1 + I_2 + 2\sqrt{I_1 I_2}\cos\phi \qquad (1)$$

with I_1 and I_2 the intensity vectors and ϕ the phase difference.

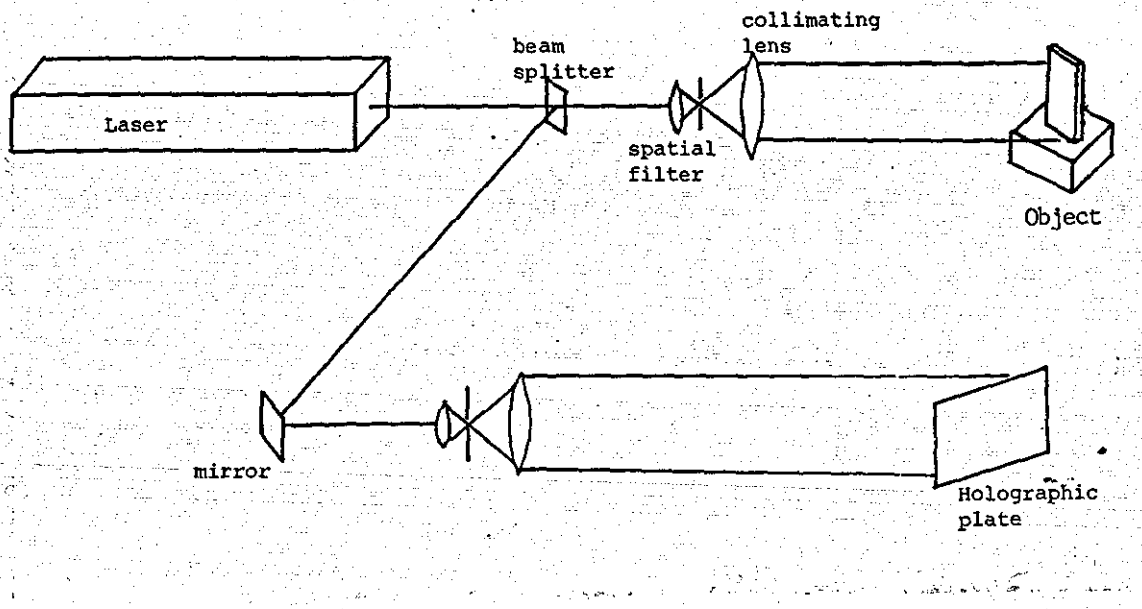

Figure 2.2
Recording the Off Axis Hologram

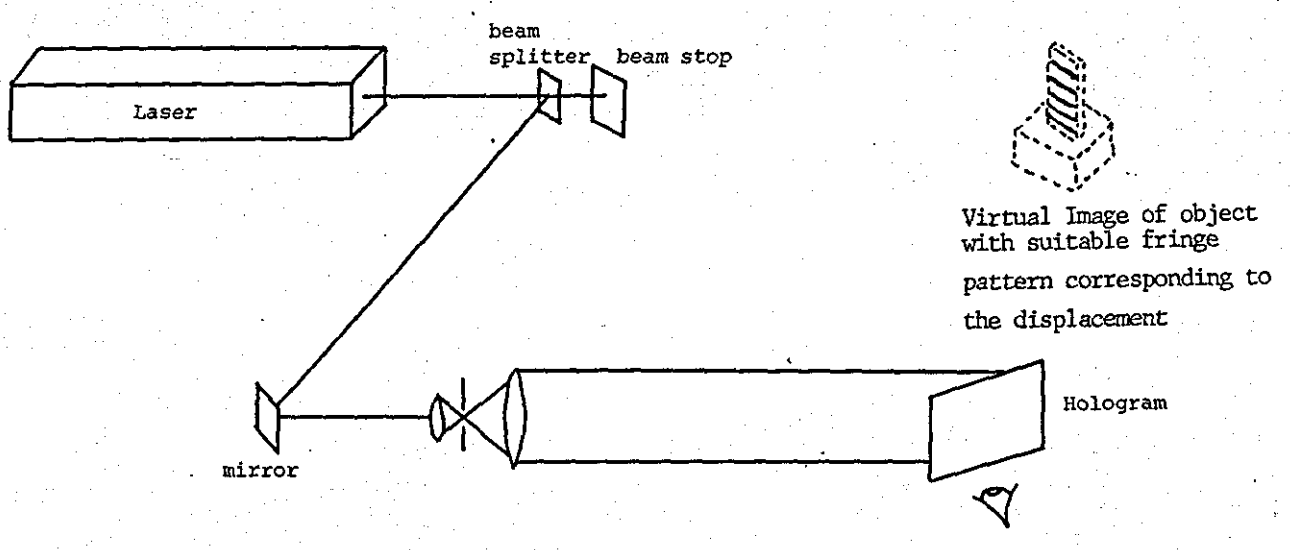

Figure 2.3
Replaying the Off Axis Hologram

Therefore I_{max} occurs when $\cos \phi = 1$

i.e. when $\phi = \phi_1 = 0 \pm 2\pi, \pm 4\pi$ .... etc.

hence

$$I_{max} = I_1 + I_2 + \sqrt{2}\, I_1 I_2 \qquad (2)$$

and I_{min} occurs when $\cos \phi = -1$

i.e. when $\phi = \pm \pi, \pm 3\pi$ .... etc.

$$I_{min} = I_1 + I_2 - \sqrt{2}\, I_1 I_2 \qquad (3)$$

It is usual to refer to the case where $I > (I_1+I_2)$ as constructive interference and $I_1+I_2 > I$ as destructive interference. When $I_1 = I_2$ then

$$I = 2I (1 + \cos \phi)$$
$$= 4I \cos^2 \frac{\phi}{2} \qquad (4)$$

showing the pattern varying with the square of the cosine.

2.2 Recording Principles

The irradiance distribution which is recorded by the photographic emulsion will generally be described by equation (1) and the contrast or fringe visibility (V) is defined as:

$$V = (I_{max} - I_{min}) / (I_{max} + I_{min}) \qquad (5)$$

Since the photographic emulsion responds only to the intensity of the exposing light it is obviously necessary to optimise the response. Hurter and Driffield in 1890 characterised photographic plates by using a plot of optical density (D) of the developed plate against the log of the exposure (E).

The exposure (E) is described by:

$$E = It \qquad (6)$$

where t is the exposure time and I the intensity of the light. The general form of the curve, showing a toe, straight line portion and shoulder is given in Figure 2.4.

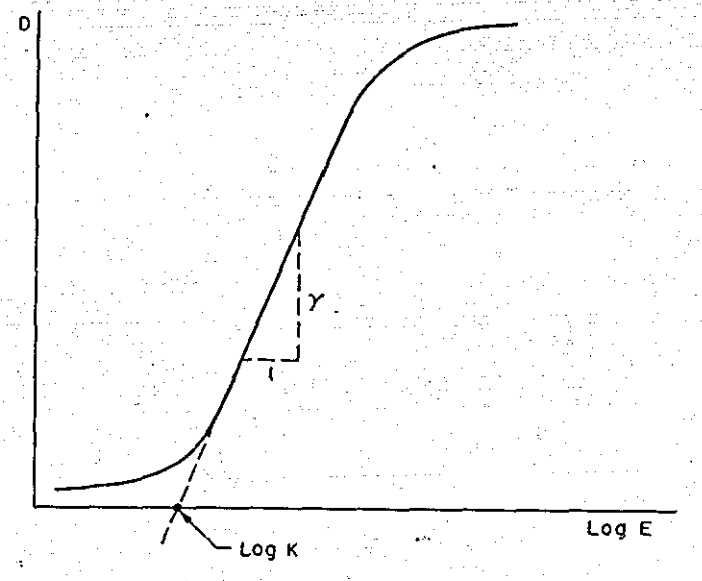

Figure 2.4
The Hurter and Driffield Curve

The straight line portion of the curve is represented by:

$$D = \gamma (\log E - \log K) \qquad (7)$$

where γ is the slope and log K the intercept with respect to the Log E axis. γ is more usually thought of as an indicator of the contrast of the photosensitive material.

On a practical note, it is usual to pass the toe of the Hurter Driffield curve and work within the straight line portion of the curve to ensure a linear response of the photosensitive material. One way of surpassing the toe is to use a stronger reference beam. Theoretically for maximum contrast an object to reference beam ratio of 1:1 is ideal, practically 1:10 is usual to overcome this material constraint.

The purpose of the hologram is to reconstruct the original object wavefront. This requires the regeneration of its complex amplitude (U_1) by replaying the hologram with an identical reference beam (having the save wavelength, wavefront curvature and spatial location - relative to the holographic plate). When re-illuminated in this fashion, the hologram will diffract light away from its plane to recreate the original object wavefront. To do this requires that both the amplitude and phase wavefronts are faithfully reproduced. As stated earlier the recording medium only responds to square of the amplitude (irradiance). The object wavefront irradiance (I_1) is:-

$$I_1 = U_1 U_1^* \qquad \text{where } U_1 \text{ is the complex amplitude}$$
$$U_1^* \text{ is the complex conjugate}$$

This is a real quantity and can be recorded when combined with a reference beam on the photographic emulsion. As shown earlier the phase and intensity distribution of the object wavefront can be reconstructed using the reference wave to demodulate and 'playback' the hologram.

For an off axis hologram the complex amplitudes at the holographic plate are shown in Figure 2.5.

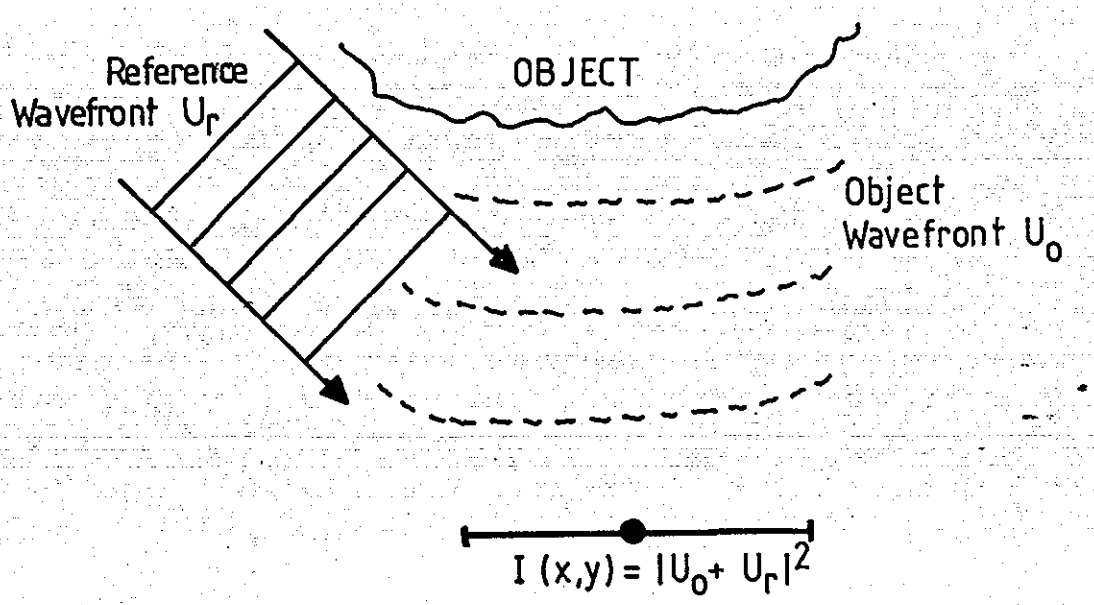

Figure 2.5
A General Description of the Wavefront
Amplitudes Seen at the Holographic Plate

For the generalised point on the emulsion surface the two combining wavefronts are given by:

Object $U_o = a_o e^{-j\phi_o}$ (8)

Reference $U_R = a_R e^{-j\phi_R}$ (9)

$$I(x,y) = |U_o + U_R|^2 = |a_o e^{-j\phi_o} + a_R e^{-j\phi_R}|^2 \quad (10)$$

$$= |a_o\cos\phi_o + ja_o\sin\phi_o + a_R\cos\phi_R + ja_R\sin\phi_R|^2$$

$$= |a_o\cos\phi_o + a_R\cos\phi_R + j(a_o\sin\phi_o + a_R\sin\phi_R)|^2$$

$$= (a_o\cos\phi_o + a_R\cos\phi_R)^2 + (a_o\sin\phi_o + a_R\sin\phi_R)^2 \quad (11)$$

$$= a_o^2\cos^2\phi_o + a_R^2\cos^2\phi_R + 2a_oa_R\cos\phi_o\cos\phi_R$$
$$+ a_o^2\sin^2\phi_o + a_R^2\sin^2\phi_R + 2a_oa_R\sin\phi_o\sin\phi_R$$

$$= a_o^2 + a_R^2 + 2a_oa_R\cos(\phi_o - \phi_R) \quad (12)$$

Then let $\phi_R = \frac{2\pi \sin\theta_R}{\lambda}$

where; the third term in equation 12 is usually referred to as the interference term and consists of carrier fringes of spatial frequency (f), $f = \sin\theta_R/\lambda$ which are modulated in amplitude by $a_o(x,y)$ and phase by ϕ_o.

Assuming the hologram to be correctly exposed and processed, it has a complex amplitude transmittance (T_a) that can be expressed as a function of exposure as shown in Figure 2.6.

$$T_a(x, y) = \beta E(x, y) \qquad (13)$$

where ß is the slope of the amplitude transmittance plotted against the exposure of the recording material in use;

$$T_a(x,y) = \beta\{I_O(x,y) + I_R(x,y) + 2a_O a_R \cos(\phi_O - 2\pi f)\} \qquad (14)$$

The terms $\beta I_O(x,y)$ and $\beta I_R(x,y)$ will usually be uniform over the holographic plate and simply represent a bias level T_o. Thus by the correct balancing of the object and reference beam intensity ratios the best contrast and signal to noise levels can be achieved, within the exposure capability of the holographic emulsion.

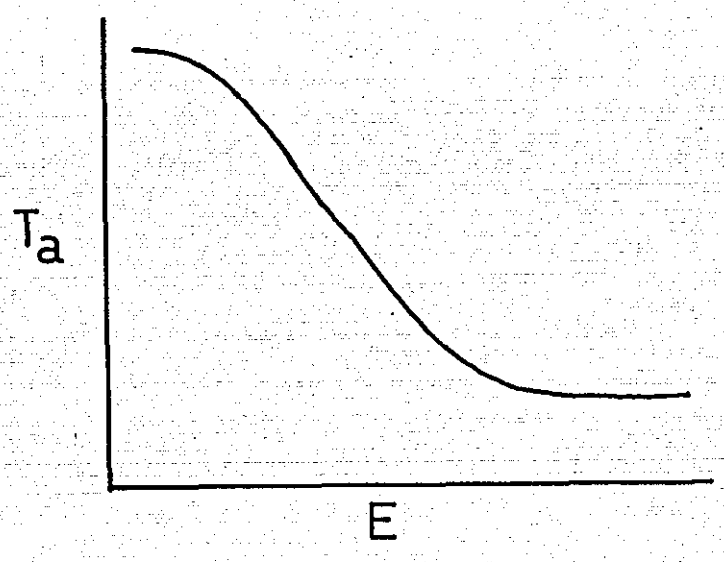

Figure 2.6
Plot of Transmittance-Exposure Sensitometric
Curve for Photographic Emulsion

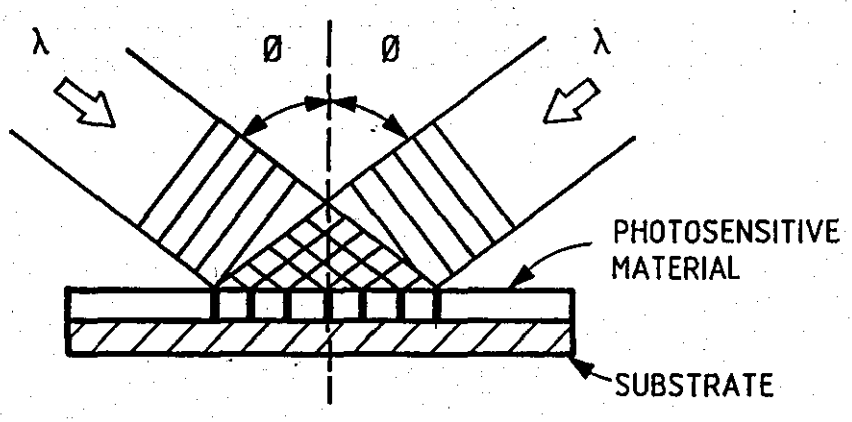

Figure 2.7
A Holographic Diffraction Grating Formed by
Interfering Two Plane Wavefronts $U_R + U_O$

To determine the suitability of the recording material it is necessary to calculate the information density generated by the final term $2a_O a_R \cos(\phi_O - \phi_R)$. The first two terms can be thought of as non-contributory intensity levels. To simplify the analysis, consider two plane wavefronts interfering at the emulsion surface, as with a diffraction grating shown in Figure 2.7.

If U_R and U_O are equal and incident, each at the same angle to the plate normal, the resulting frequency (f) of the fringe pattern will be given by :-

$$f = \frac{2\sin\theta}{\lambda} \qquad \text{let } \theta = 45° \text{ and } \lambda = 633 \text{ nm}$$

then f = 2234 lines mm^{-1} or a fringe spacing of 0.45 μm. The recording material must therefore be able to record up to 2500 lines mm^{-1}, requiring specialist photographic emulsion. Typical photographic emulsions will usually record up to 500 lines mm^{-1}. The price paid for resolution is sensitivity, holographic emulsions require 1×10^{-6} Jcm^{-2}, compared with 1×10^{-8} Jcm^{-2} for a 100 ASA photographic emulsion. The thickness of holographic emulsion is typically 10μm and so care must be taken to ensure sufficient development time to process through the depth of the silver halide emulsion. Realisation that the fringes align themselves with the angular bisector between the two beams requires that all holograms be made with the plate normal aligned with this bisector. In this way any emulsion expansion or contraction does not affect the stored interference pattern, as shown in Figure 2.8.

One minor constraint concerning the angular position of the reference beam is when photographing the resultant hologram. The angle between the reference beam and the plate normal should be greater than 25° to avoid camera flare from the reference beam during photographic recording.

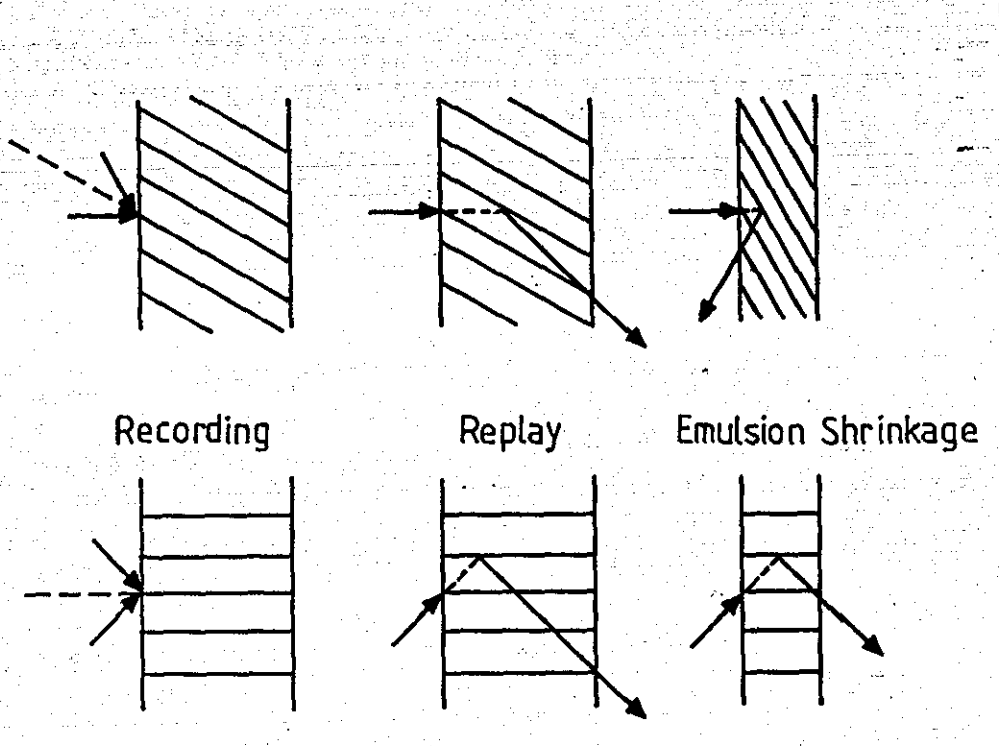

Figure 2.8
Effects of Emulsion Shrinkage on
the Reconstruction Angle

2.3 Silver Halide Emulsions

2.3.1 Introduction

Holographic emulsion consists of a physical support of glass or plastic sheet which is coated with photosensitive emulsion. The emulsion consists of gelatin which is the colloid into which the submicroscopic crystals of silver halide (usually silver bromide) are precipitated and sensitisers which give the silver halide enhanced recording sensitivity to a specific wave band of light. Emulsifiers may be added to control the gelatin hardness and swelling properties.

Holographic emulsions must provide high resolution, or in optical terms a high modulation transfer function (MTF) at high spatial frequencies. This means that the emulsion grain size must be smaller than the interference pattern to be recorded. In order to be able to record optical interference patterns (wavelength range 0.45 - 70μm) the holographic emulsion requires to have a grain size of at least 0.045 - 0.07μm. Commercially available emulsions typically have a grain size of 0.03 - 0.08μm, though the mean grain size, standard deviation etc. are the variables each specific manufacturer controls. In conventional photographic emulsions the grain size is 1 μm and is therefore larger than the wavelength used. The size of the grain directly controls the sensitivity or speed of the emulsion, by presenting a larger volume for the photon to encounter within the gelatin matrix.

It is also necessary that the grain size is smaller than the illuminating wavelength so that Mie scattering and diffusion will not be significant. Whilst these two factors do not directly contribute to the sensitivity of an emulsion the overall effect of size reduction of grains does not produce a linear reduction in speed. Further factors such as the packing density of the grains, the consistency of distribution within the emulsion and the mark space ratio within the entire volume all affect sensitivity. These are significant because the interference pattern is recorded within the full three dimensional volume of the emulsion unlike photography where only

the intensity distribution across an area is significant. Thus the probability of a number of photons being absorbed is proportional to the volume of the crystal or the cube of the mean crystal diameter.

The simplified recording mechanism relies upon the photon supplying energy to the halide ion in order to release an electron. The electron then attracts a silver ion to produce a silver atom. This metastable condition can exist for about one second during which time if two silver atoms congregate then a stable particle will form. In order to produce a stable latent image that can be developed, typically four silver atoms are required.

This process can be summarised as;

$$Br^- + h\nu \rightarrow Br + e^-$$
$$e^- + Ag^+ \rightarrow Ag$$

where hν represents the photon energy, Br the halide, e^- the electron and Ag the silver atom.

The latent image requires an optimum rate of photon adsorption during an exposure, consequently, very long $>10^4$ sec (astronomical photography) or very short $<10^{-6}$ sec (pulsed holography with 10-20 x 10^{-9} sec) exposures do not follow the relationship of E = It. This is known as reciprocity law failure. Thus for pulsed holography a doubling of the suggested energy is required for optimum exposure of the emulsion (given in the manufacturer's data sheets).

Chemical development of the emulsion renders the latent image visible. The thickness of the emulsion and the readiness to allow the chemicals to soak through the gelatin are factors which effect the development time and the quality of processing. The developer reduces the exposed silver halide (the latent image) to metallic silver. Subsequent processing in fixer dissolves the remaining unexposed silver halide leaving the metallic

silver in the gelatin matrix. This results in an amplitude hologram and upon reconstruction, the intensity distribution of the metallic silver diffracts the reference beam to recreate the object wavefront. Bleaching of the silver converts the silver to transparent silver salts which have a different refractive index to the gelatin. This is called a phase hologram hologram because the different refractive indices diffract the reference beam. The advantage is a reduced absorbtion of the beam, i.e. the diffracted beam will be more intense producing a brighter image of the recorded object.

2.3.2 Holographic Emulsions Used

Holographic emulsions manufactured by Ilford and Agfa Gaevert were the two types used, Kodak did not consider the UK market large enough to warrant importing material from the U.S.A. A comparison between them, including spectral sensitivity is given below.

Ilford

Emulsions manufactured by the Ilford company are only recently commercially available. In general, they appeared to have the most consistent performance especially in terms of sensitivity, grain size and emulsion hardness. The quality of control of the emulsion appeared to be the best presently available as did the consistency of the emulsion. Though the emulsion sensitivity is half that of other makes, e.g., Agfa, for red sensitive material but is compatible with Agfa in the green. Figure 2.9 presents the manufacturer's sensitivity data.

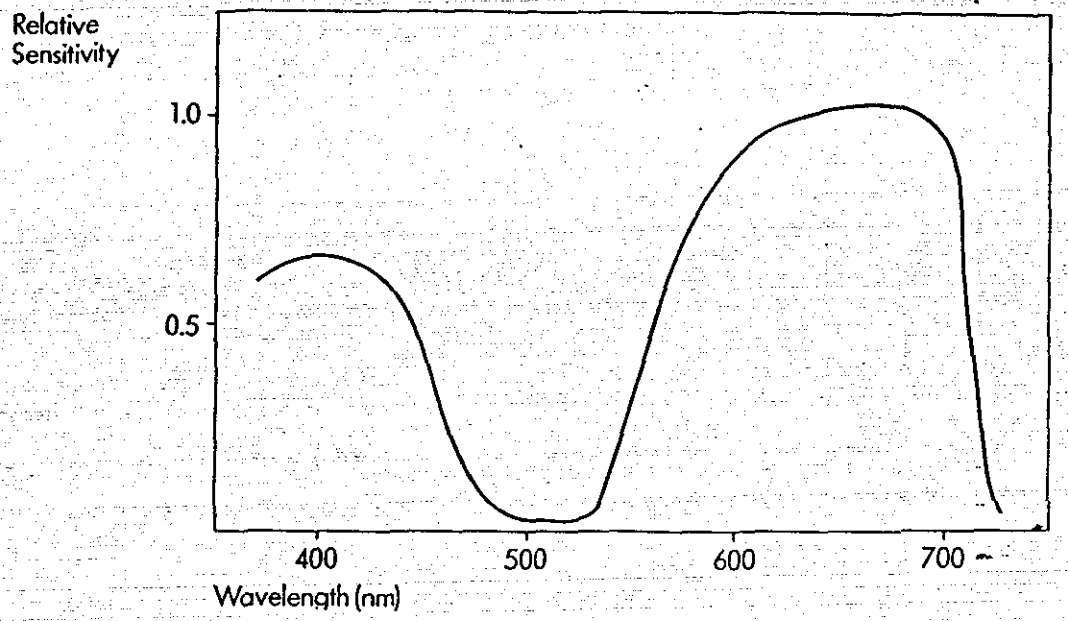

The above curve shows the relative spectral sensitivity of SP673 holographic film to white light flash exposure (10^{-4}s).

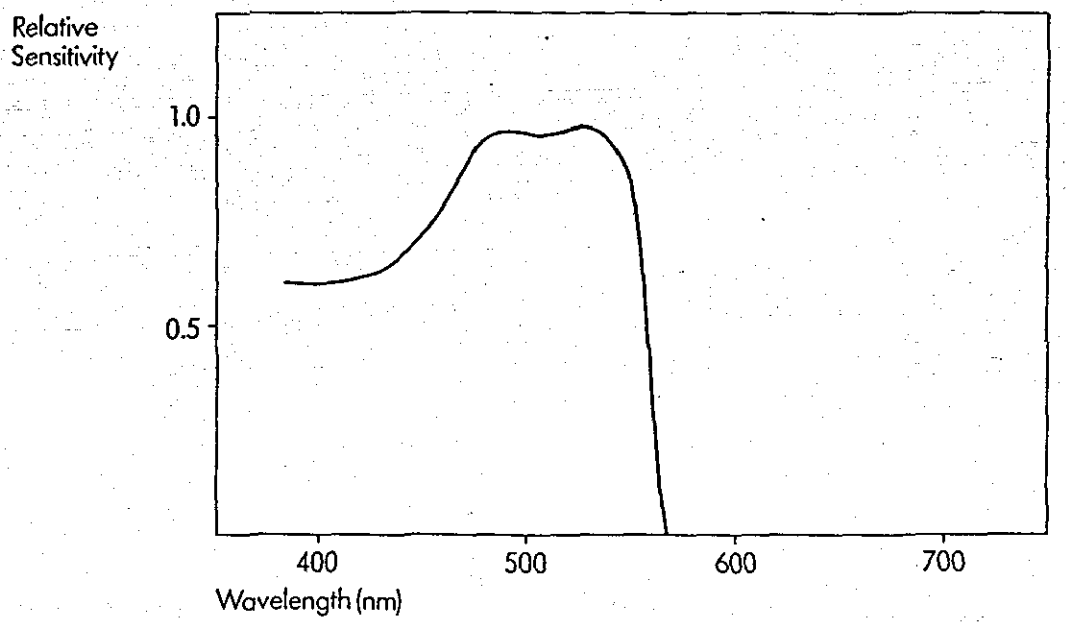

The above curve shows the spectral sensitivity of SP672 holographic film to white light (flash exposure 10^{-4}s).

Figure 2.9

Relative Spectral Sensitivity of Ilford SP673 and SP672 Holographic Emulsion

Agfa 10E75 (red sensitive) and 10E56 (green sensitive) Agfa emulsions have been the standard emulsions for holography in Europe. Figure 2.10 presents manufacturer's sensitivity data. A number of problems were encountered including: supply of fogged plates (approximately 1 in 10 boxes would be damaged in this way), scatter and optical noise - functions of the spread of sizes of the silver halide grains, varying sensitivity from batch to batch requiring a test plate to be exposed for each batch.

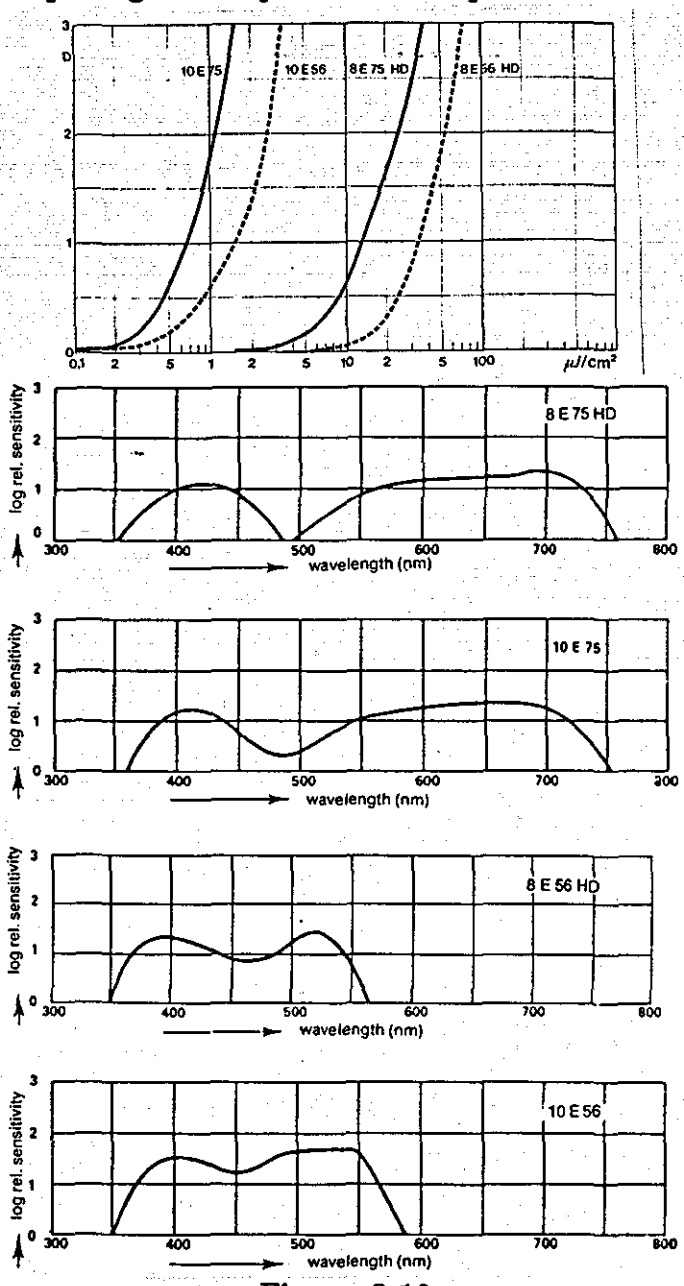

Figure 2.10

Relative Spectral Sensitivity of Agfa 8E75, 10E75, 8E56 and 10E56 Holographic Emulsions

2.4 Assessment of Alternative Holographic Media

Attempts to use the various alternatives to silver halide were made. The recording properties of each material is tabulated below:

Recording Material	Resolution mm^{-1}	Nominal Sensitivity $\mu J/cm^2$	Wavelength nm
Agfa 10E75	2800	2	633
8E75	4000	10	633
10E56	2800	2	514
8E56	4000	25	514
Kodak 120-02	>2500	30	63
Ilford SP672	>7000	50	514
SP673	>7000	50	633
Newport Thermoplastic (Honeywell)	1000	100	633
Rottenkolbe	1000	100	633
Thompson CSF BSO	1000	1000	514
Shipley AZ1450	>4000	10,000	458
Dichromate Gelatin	>5000	400	488

Table A. Comparison of Holographic Materials

2.4.1 Thermoplastic Materials

As an alternative to silver halide recording materials, two commercially available devices using thermoplastic materials were evaluated, they were produced by Rottenkolber (Germany) and Newport Corporation (U.S.A.). Attempts to use the Rottenkolber device were hampered by poor availability and lack of support in this country. Specific tests had to be abandoned and no trials were performed.

The Newport Corporation device was loaned by Metax Ltd., the then U.K. agents for Newport. Holograms were made using Helium-Neon and Argon-Ion continuous wave lasers. Unsuccessful tests were tried using a pulsed ruby laser. The following conclusions were drawn.

The recording device was the Newport HC1000 thermoplastic plate system. This produced reliable and consistent results with no residual fringes. However, the capital cost (£13K) and consumable costs of £1 per hologram made the equipment expensive. No archive results could be produced. The photometric sensitivity of the Newport plates necessitated an increase in laser power of a factor of 10 over silver halide emulsions. The spatial resolution of photo-thermoplastic material is centred at 800 l mm^{-1} (diffractive efficiency of 0.34) with a spread of between 600 l mm^{-1} and 1200 l mm^{-1}. This limits the angle of view to a cone of solid angle 20°. Thus large objects have to be viewed further away than for silver halide materials further reducing the returned object beam intensity and increasing the exposure time. One advantage of this method of recording is that a phase hologram is directly recorded. This eliminates the phase shift associated with the silver halide hologram and provides a bright zero order fringe.

Advantages of Thermoplastic Materials
Compared with Silver Halide Emulsions

... Ideal for in situ recording, processing and reconstruction.
... The emulsion (of dimension 36mm x 24mm) was mounted on a glass plate and was capable of being reprocessed up to 500 times, replacement cost of emulsion £500, (i.e., unit cost ≈£1 per hologram).
... Best suited to real time holographic interferometry.
... High diffraction efficiency (up to 15%).
... Processing takes approximately 10 seconds (1 minute pre-processing prior to exposure for erasure).
... Erasable.

Disadvantages

... Initial capital outlay is high, approximately £10K.
... Quality control of plate manufacture is poor, leading to large variability in plate to plate performance.
... Ghost images can be retained after erasure.
... High voltage device leading to sensitivity to moisture, dust and temperature.
... Complex interdependence between diffraction efficiency and spatial frequency giving rise to process and device specific arrangements.
... Complexity of operation layout and repeatability (numerous holograms failed for no apparent optical reasons).

Conclusions

This was an expensive option best suited to a production line environment. The spatial frequency limit was too restrictive for studying large objects unless positioned a greater distance from holographic plane resulting in reduced object beam intensity.

2.4.2 Electro Optical Crystals

An experiment was conducted in conjunction with Thompson CSF at Mulhouse, Strasbourg, France. A small 8 inch (200 mm) diameter metal disc was illuminated with 500 mWatts of Argon Ion radiation at 514 nm. The results were viewed via a Thompson vidicon television camera in real time. Whilst able to show various real time vibration modes the penalty was light sensitivity. The active optical component was a cube of volume 1 cm^3 of Bismuth Silicon Oxide (BSO) which was activated with a 1 KV standing voltage.

Advantages of BSO Compared with Silver Halide Emulsions

.. In situ recording and processing.
... Suited to real time holographic interferometry.
... Processing takes 5 seconds.
... Erasable.

Disadvantages

... Only available as experimental units.
... Requires high voltage bias voltage for operation.
... Non permanent record.
... Very insensitive to argon laser light.
... Low resolution with consequent object size restrictions.

Conclusions

Not a device best suited for Holographic Interferometry, highly uneconomic in light usage, not fully supported or commercially developed.

2.4.3 Photoresist

The cost of commercially prepared photoresist plates (using Shipley AZ1450 resist) are prohibitively expensive - £14 for a 4"x 4" plate. Therefore a manufacturing facility was established within the department. The surface quality of the coated plate is highly dependant upon plate cleanliness and a dust free coating environment. Enclosing the coating plant within a plastic hood with fan extraction for the fumes improved the plate quality. Development relies on the removal of exposed resist, the developer used was sodium hydroxide with a dilution of 1:4 for 1-3 minutes.

Advantages of Photoresist Compared with Silver Halide Emulsion

... High resolution.
... Surface replication of hologram can be made for copies.

Disadvantages

... Specialist coating techniques needed.
... Very insensitive compared to photographic material.
... High cost per plate
... Peak sensitivity is at 350 nm (i.e. within the UV spectrum). The output power of Argon lasers at this wavelength is less than 50 mW.

Conclusions

Not suitable for Holographic Interferometry.

2.4.4 Dichromate Gelatin

Similar coating requirements to photoresist are needed, although the glass from silver halide plates can be used after the photosensitive material has been removed using fixer. The gelatin needs to be sensitised usually with a solution of ammonium dichromate and exposed within 48 hours of sensitisation.

Advantages of Dichromate Gelatin Compared with Silver Halide

... High resolution.

Disadvantages

... Specialist coating techniques needed.
... Very insensitive.

Conclusions

Not suitable for Holographic Interferometry.

2.5 Conclusions

This chapter has introduced the principles of holography as a wavefront reconstruction process. It has considered the experimental processing requirements and highlighted some optical arrangements necessary to minimise replay errors.

- An appreciation has been gained of the range of media available for producing holograms.
- Based on experimental work, an assessment of the most suitable material - silver halide - allowed the determination of the optimum conditions for processing.
- Requirements of chemical processing were investigated for both continuous wave and pulsed holography.
- Techniques to minimise the effects of emulsion distortion by the experimental arrangements have been considered and solutions determined.
- Little difference in performance between the Agfa and Ilford holographic emulsions was detected. A trade-off of resolution against speed is acknowledged and in this respect Agfa emulsion was used for subsequent experimentation although Ilford emulsions were more consistent in emulsion quality.

CHAPTER 3
HOLOGRAPHIC INTERFEROMETRY

3.0 Background

Shortly after the demonstration of off-axis holography by Leith and Upatnieks [4] the realisation of á new form of interferometry dawned on many workers during the next few years. The reporting of this capability then spawned enormous efforts all over the world. A fundamental attraction was the ability to visualise whole field displacement of a surface undergoing displacement, this should be possible with ease and in a quantitative fashion. Books about Holographic Interferometry used extensively here are those by Vest [6], Erf [7] and Caulfield [8].

In order to design interferometers which generate data in a form that can be usefully analysed it is necessary to describe what the fringes mean, how they are derived and how they can be altered to extract the data required. The location of the object and object illumination relative to the recording material determine the overall sensitivity of the fringe pattern. Sub-fringe interpolation and automatic fringe pattern analysis are left to a later chapter concerned with these matters. Different arrangements and methods are used for the range of experimental measurements needed. This work concentrates on vibration and static displacement studies of diffusely reflecting objects.

3.1 Holographic Interferometry Fringe Formation

3.1.1 Real Time - Live Fringe Analysis

When a correctly processed hologram is kinematically relocated in its original position and re-illuminated with the original reference beam, the reconstructed object beam produced will be identical with the original object recording beam. Thus when the recorded object beam is combined with the original object beam the two constructively interfere and the images re-inforce one another. Any relative movement between the recorded position and the live image shows up as a series of contour fringe patterns outlining the areas of displacement. However, the reconstructed wavefront will have undergone a uniform phase shift of π radians due to the recording process producing a photographic negative. Usually for holography this is not considered because the sign of the irradiance is irrelevant. Therefore the complex amplitude of the reconstructed wavefront will be described by -a(x,y), whilst the current live image will be a(x,y), exp [j$\Delta\phi$(x,y,t)], where $\Delta\phi$ is the consequential phase change under the loading of the object at time t.

The resultant irradiance seen will be the sum of the squares of the two wavefront amplitudes.

$$I(x,y,t) = \{-a(x,y) + a(x,y) \exp [j\Delta\phi (x,y,t)]\} \{-a^*(x,y) + a^*(x,y) \exp \{j\Delta\phi (x,y,t)]\} \quad (15)$$

$$= 2a^2(x,y) [1 - \cos \Delta\phi (x,y,t)] \quad (16)$$

Thus with no phase change a dark fringe will be observed with a phase change of $\pi/2$ a bright fringe will be seen. Points which have undergone identical levels of phase change will be linked and will appear as fringes. If the surface is continuous and no discontinuities are present then fringes will describe contours of constant value. In the context of the nature of this work these fringes represent displacement. The intensity of these fringes vary cyclically with displacement amplitude and be modulated by a cosine function. A comparison between this type of

holographic fringe function and the frozen fringe type is presented in Plates 1 and 2. These show a clamped metal plate centrally loaded with 10μm of displacement. Full experimental details are presented in Section 3.4.

The advantage of this type of interferogram is that the surface can be loaded or excited and provided that no indiscriminate displacement has taken place, fringes will be seen in real time. The disadvantage is the complexity involved in arranging the silver halide emulsion to replay in its original location. Emulsion shrinkage after processing combined with the plate relocation kinematics render this a difficult technique practically, usually leaving several residual fringes over the component.

One technique tried using holographic plates was to immerse the plate in water in a liquid gate (a glass sided developing tank) prior to exposure. Once the plate was exposed the processing chemistry was pumped around the liquid gate with the processed hologram being viewed once again in water. A method best described as cumbersome. The plate would replay well but did not render itself to industrial application. A commercialised version made by Laser Technology Inc. via Ealing Electro Optics PLC was tried but leaked badly during trials and failed to produce holograms in the central third of the 35mm format film used.

3.1.2 Frozen Fringe - Double Exposure Analysis

Initially, real time interferometry was performed on components to determine test conditions worthy of further investigation. Subsequently the various conditions could be permanently recorded by double exposing the holographic plate once at the rest position (U_1) and re-exposing to a second loaded position (U_2). Providing that no other spurious movement took place between the exposures, the processed holographic plate provided fringe pattern data detailing the surface motion as:

$$I(x,y) = |U_1 + U_2|^2 \quad (17)$$

where $U_1(x,y) = a(x,y)\exp[-j\phi(x,y)]$ (18)

$$U_2(x,y) = a(x,y)\exp\{-j[\phi(x,y) + \Delta\phi(x,y)]\} \quad (19)$$

Thus the reconstructed wave front becomes;

$$I(x,y) = \left|a(x,y)\exp(-j\phi(x,y)] + a(x,y)\exp\{-j[\phi(x,y) + \Delta\phi(x,y)]\}\right|^2 \quad (20)$$

$$= 2a^2(x,y)[1 + \cos\Delta\phi(x,y)] \quad (21)$$

A point with no phase change between exposures will be bright, areas which have undergone a phase change of $\pi/2$ will be covered in dark fringes, a plot of the fringe modulation against phase change is given in Figure 3.1. A comparison of this fringe type with live fringe results is given in Plates 1 and 2. Experimental details are given in Section 3.4.

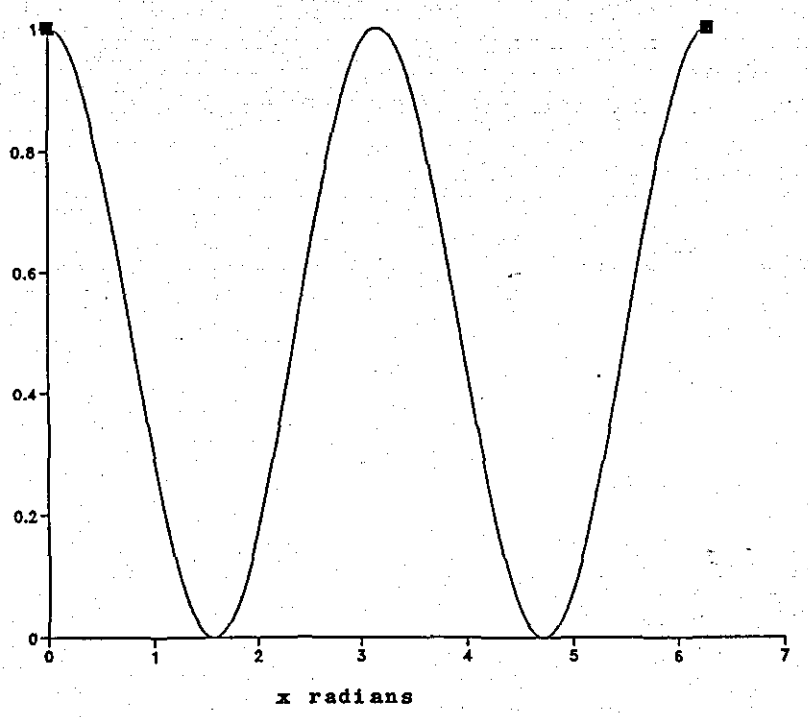

Figure 3.1

Plot of Fringe Pattern Intensity Against Phase Change (Surface Displacement) for a Double Exposed Holographic Study

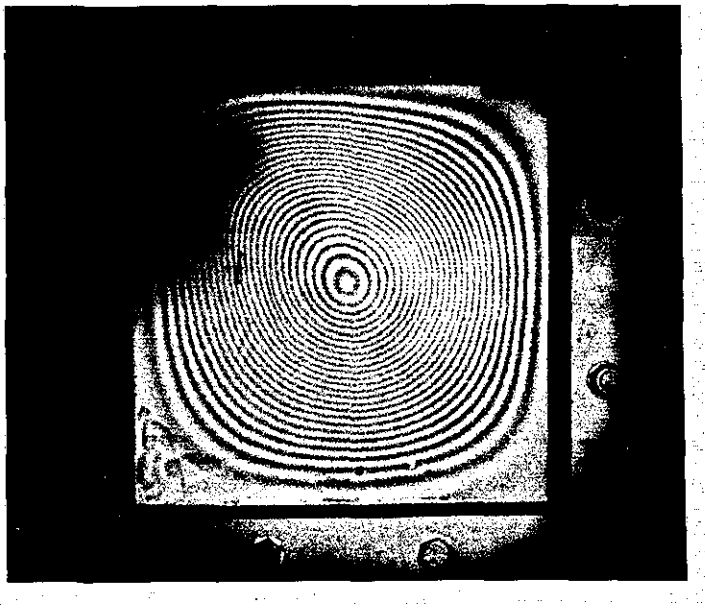

Plate 1.

A Live Fringe Recording of a Clamped Metal Plate Centrally Loaded 9μm of Displacement. (Dark zero order fringe)

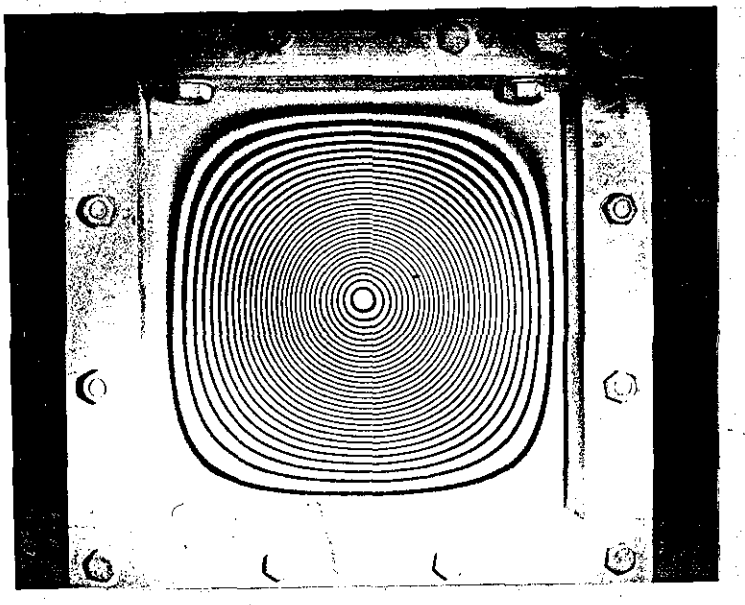

Plate 2.

A Frozen Fringe Recording of a Clamped Metal Plate Centrally Loaded 10μm of Displacement. (Bright zero order fringe)

3.1.2 Time Averaged Holographic Interferometry

In 1965 Powell and Stetson [9] published the results of a holographic recording made whilst the object was sinusoidally vibrating. The resultant displacement analysis can be traced back to Osterberg [10] and is summarised as follows. Using a clamped metal plate as the example, if the plate vibrates sinusoidally, see Figure 3.2. the displacement of any surface point will be described by:

$$D(x,y,t) = z(x,y) \sin \omega t \qquad (22)$$

where D is the Amplitude at position (x,y) and ω the vibration frequency.

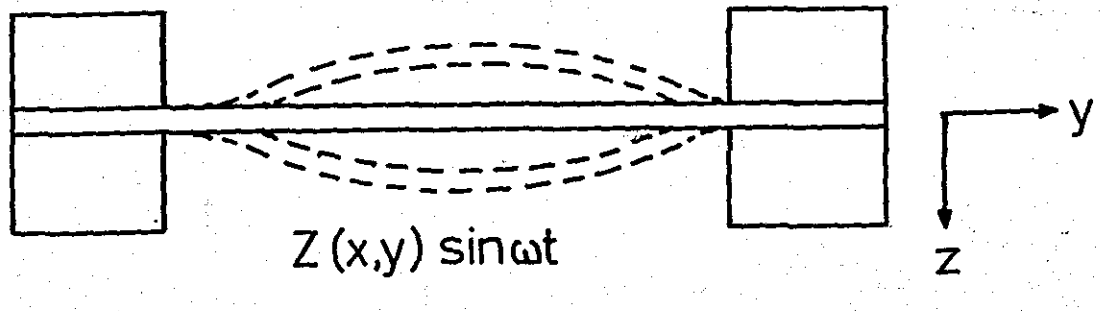

Figure 3.2
Top View of Vibrating Plate, Showing Displacement in z Axis

As discussed earlier equation (8) (with the sign ignored)

$$U_o(x,y) = a_o(x,y) \exp[j\phi_o(x,y)] \qquad (8)$$

If the system is configured to measure pure out of plane displacement and the static path length of the object beam is l_o the surface displacement will vary by $\pm \frac{z(x,y) \sin \omega t}{2}$.

The surface amplitude will cause a path length increase on both the illuminating path and the reflected path i.e. the path length will vary by $\pm z(x,y) \sin \omega t$ hence the peak to peak displacement change to the pathlength will be $2z(x,y) \sin \omega t$. Thus the corresponding phase change will be;

$$\Delta\phi(x,y,t) = \left(\frac{2\pi}{\lambda}\right) 2z(x,y) \sin \omega t \qquad (23)$$

Combining this with equation (8) yields,

$$U_o(x,y) = a_o(x,y) \exp\left[j\phi(x,y) + j\frac{4\pi z}{\lambda}(x,y) \sin \omega t\right] \qquad (24)$$

If the exposure period (T) is much greater than the period of the oscillation ($1/\omega$) then the consequential time averaged hologram will be described by:

$$\frac{1}{T}\int_o^T a(x,y) \exp\left[j\phi(x,y) + j\frac{4\pi z}{\lambda}(x,y) \sin \omega t\right] dt \qquad (25)$$

or

$$U_o(x,y)\frac{1}{T}\int_o^T \exp j\frac{4\pi z}{\lambda}(x,y) \sin \omega t.dt$$

or more usually as

$$J_o\frac{4\pi z}{\lambda}(x,y)$$ where J_o is the Bessel Function of the zero order

The total irradiance seen by the plate will be proportional to

$$I(x,y) = |U|^2$$

$$= a^2(x,y)\, J_o^2 \left[\frac{4\pi z}{\lambda}(x,y)\right] \qquad (26)$$

The difference between the minima and maxima of $J_o^2(x)$ against $\cos^2(x)$ can be seen in Figure 3.3.

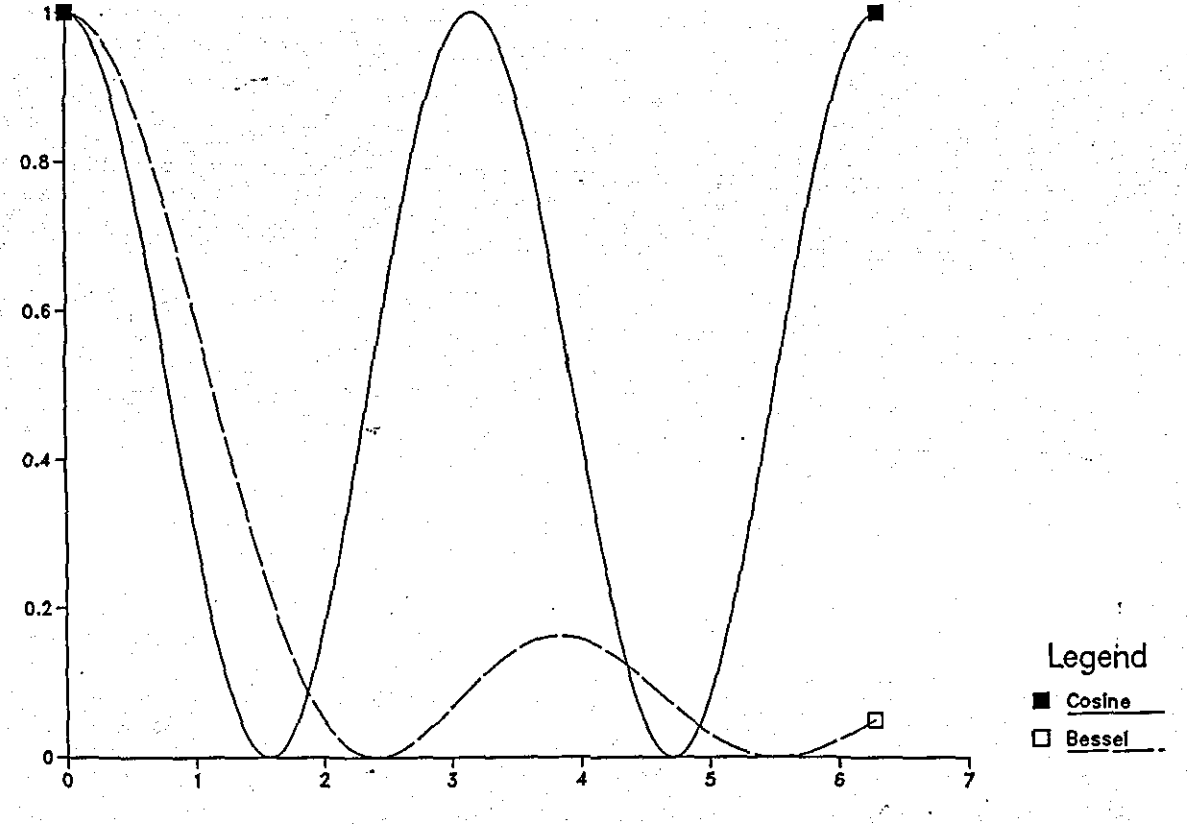

Figure 3.3

Plot of $J_0^2(x)$ and $\cos^2(x)$ Showing Fringe Sensitivity and Intensity

Thus areas of zero movement will be the brightest (the zero order fringe) with subsequent fringe intensity varying in both displacement amplitude sensitivity and brightness. This can be seen in the results of the metal plate where time averaged holographic interferometry was used in the first six modes as shown in Plate 3. A useful representation of fringe pattern function can be gained by comparing Plates 1 and 2 with Plate 3. Details of experimental procedure are given in Section 3.4.

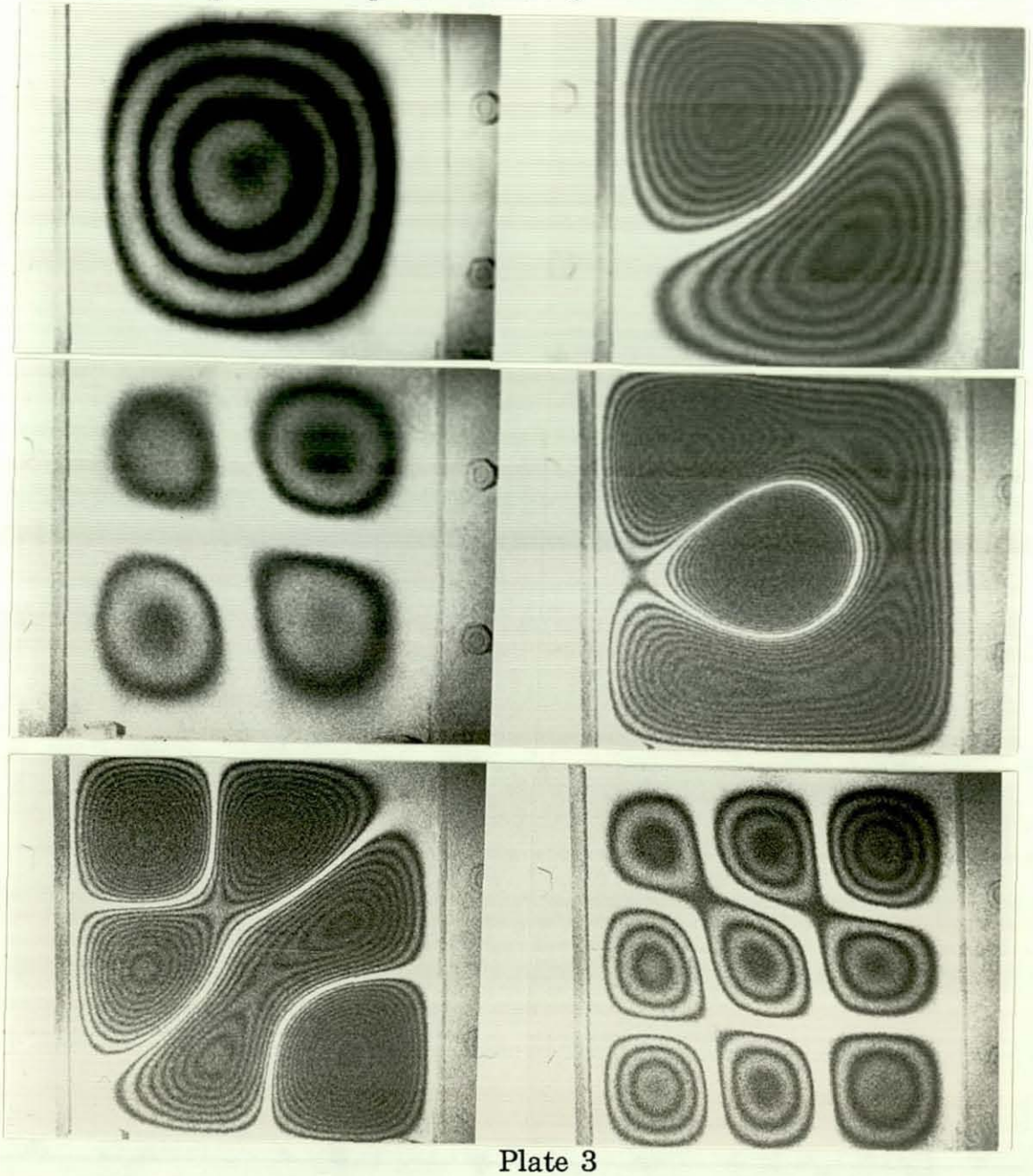

Plate 3

Time Averaged Holographic Analysis of Initial Modes of a Clamped Metal Plate

3.2 Sinusoidal Vibration Studies Using Stroboscopic Holographic Interferometry

Using the same conditions as with the time averaged study (24);

$$U_o(x,y) = a_o(x,y) \exp [\, j\phi\,(x,y) + j\,\frac{4\pi z}{\lambda}\,(x,y) \sin \omega t]$$

this can be rationalised to;

$$U_o(x,y) = a_o(x,y) \exp \{j\,[\phi + \frac{4\pi z}{\lambda} \sin \omega t]\,\} \qquad (27)$$

Ostrovsky et al [11] have undertaken an analysis of this. The intensity of the reconstructed image is proportional to the square of the magnitude of the mean value during exposure time T, therefore;

$$I = \left| \frac{ae^{-j\phi}}{T} \int_o^T \exp\,(j\frac{4\pi z}{\lambda} \sin \omega t)dt \right|^2 \qquad (28)$$

again using the Bessel function series

$$I = \left| \frac{a}{T} \sum_{n=-\infty}^{n=\infty} J_n\,(\frac{4\pi z}{\lambda}) \int_o^T e^{jnwt}\, dt \right|^2 \qquad (29)$$

From Figure 3.4, the exposure is shuttered and synchronized with one of the peaks of displacement. The pulse length (k) is a proportion of the oscillating period τ,

Thus with $T = \frac{2\pi}{k} = \frac{\tau}{k}$

$$I = a^2 \left| \frac{k}{T} \sum_{n=-\infty}^{\infty} Jn(\frac{4\pi z}{\lambda}) \int_{\frac{\tau}{4} - \frac{\tau}{2k}}^{\frac{\tau}{4} + \frac{\tau}{2k}} e^{jn2\pi t/\tau}\, dt \right|^2 \qquad (30)$$

Theintegrandbecomes;

$$\frac{\tau}{k} \frac{\sin(n\pi/k)}{n\pi/k} \exp\left(j\frac{n\pi}{2}\right) dt$$

Giving (30) as;

$$I = a^2 \left| \sum_{n=-\infty}^{\infty} J_n\left(\frac{4\pi z}{\lambda}\right) \frac{\sin(n\pi/k)}{n\pi/k} e^{jn\pi/2} \right|^2 \qquad (31)$$

but $J_{-n} = (-1)^n J_n$ and $\exp\left(J\frac{n\pi}{2}\right) = j^n$ and

$$J_n \exp\left(j\frac{n\pi}{2}\right) = J_{-n} \exp\left(-J\frac{n\pi}{2}\right)$$

Therefore

$$I = a^2 \left| J_o\left(\frac{4\pi z}{\lambda}\right) + 2 \sum_{n=1}^{\infty} J_n \frac{4\pi z}{\lambda} \frac{\sin(n\pi/k)}{n\pi/k} j^n \right|^2 \qquad (32)$$

If the exposure is synchronized with the other extreme of displacement then;

$$I = a^2 \left| \frac{k}{2} \sum_{n=-\infty}^{\infty} J_n\left(\frac{4\pi z}{\lambda}\right) \int_{\frac{3\tau}{4} - \frac{\tau}{2k}}^{\frac{3\tau}{4} + \frac{\tau}{2k}} e^{jn2\pi t/\tau} dt \right|^2 \qquad (33)$$

Giving;

$$= a^2 \left| J_o\left(\frac{4\pi z}{\lambda}\right) + 2 \sum_{n=1}^{\infty} J_n\left(\frac{4\pi z}{\lambda}\right) \frac{\sin(n\pi/k}{n\pi/k} (-j)^n \right|^2 \qquad (34)$$

The hologram will usually be exposed to <u>both</u> extremes of displacement and is described by the superposition of equations (32) and (34).
This can be summarised as;

$$I = a^2 \left| J_o\left(\frac{4\pi z}{\lambda}\right) + 2 \sum_{n=1}^{\infty} J_n\left(\frac{4\pi z}{\lambda}\right) \frac{\sin(n\pi/k)}{n\pi/k} \left[j^n + (-j)^n\right] \right|^2 \qquad (35)$$

when n is odd, the summation is zero and for even integers the square brackets yield $2j^n$, thus:

$$I = a^2 \left| J_o\left(\frac{4\pi z}{\lambda}\right) + 2 \sum_{n=1}^{\infty} J_{2n}\left(\frac{4\pi z}{\lambda}\right) \frac{\sin(2n\pi/k)(-1)^n}{2n\pi k} \right|^2 \qquad (36)$$

If k is put equal to 2 then continuous time averaged analysis takes place and $\sin n\pi = 0$ thus reverting to (26),

$$I = a^2 (x,y)\, J_o^2 \left[\frac{4\pi z}{\lambda} (x,y)\right]$$

with k put equal to ∞ and assuming $\frac{\sin(2n\pi/k)}{2n\pi/k} = 1$

then

$$I = a^2 \left| J_o\left(\frac{4\pi z}{\lambda}\right) + 2 \sum_{n=1}^{\infty} J_{2n}\left(\frac{4\pi z}{\lambda}\right) \cos\frac{2n\pi}{2} \right|^2 \qquad (37)$$

Bessel functions with even subscripts become in this case,

$$\cos^2\left(\frac{4\pi z}{\lambda}\right)$$

thus $$I = a^2 (x,y) \cos^2 \left[\frac{4\pi z}{\lambda} (x,y)\right] \qquad (38)$$

i.e. reverting to simple double exposure or frozen fringe patterns. Hence the shutter period will have direct bearing on the fringe quality and sensitivity of the fringe pattern. A short period will enable higher fringe numbers to be recorded and escape the limitations of the J_o^2 fringe function shown in Figure 3.3. Double pulse fringe patterns with an exposure period of 20 nsec are considered $\cos^2$ fringe patterns.

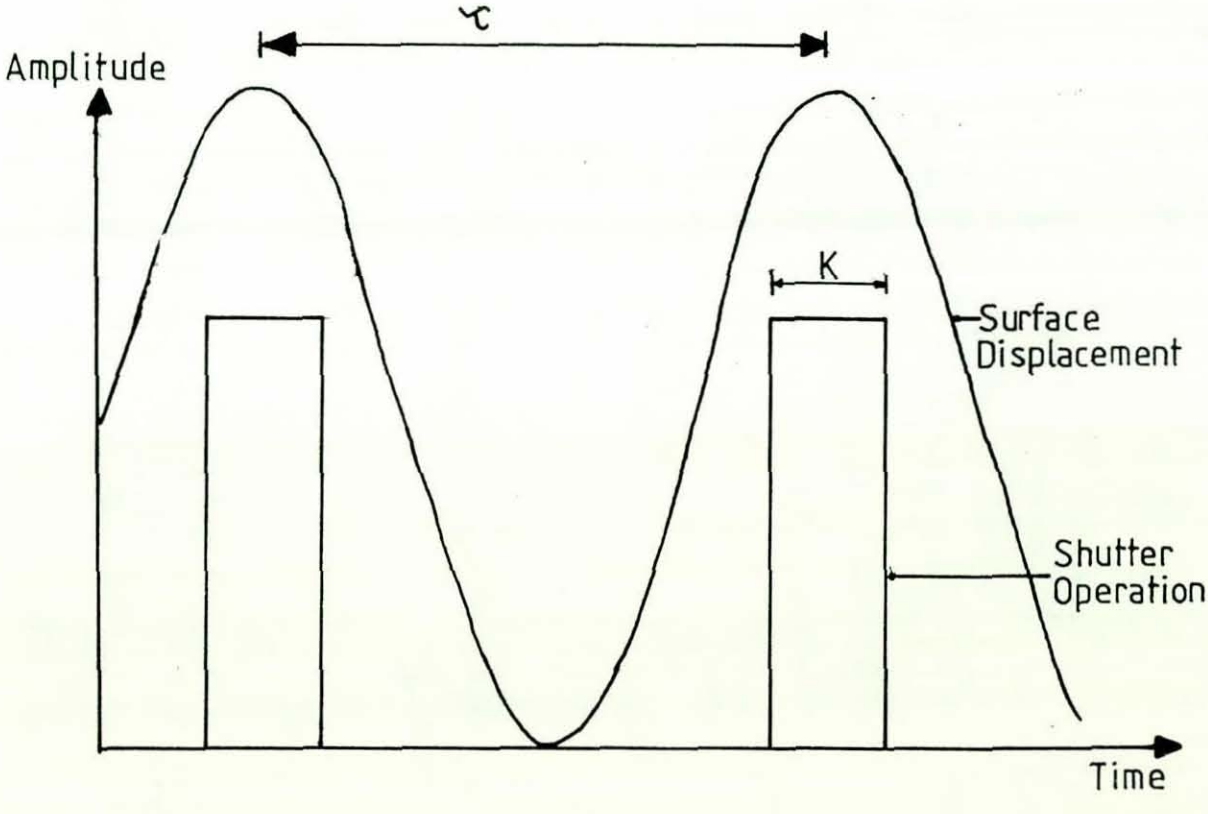

Figure 3.4
Synchronized Shutter Operation for Holographic Vibration Analysis

3.3 Fringe Pattern Definition

Examining the surface displacement in greater detail as shown in Figure 3.5, reveals the overall sensitivity of the holographic process. The actual surface displacement generates :-

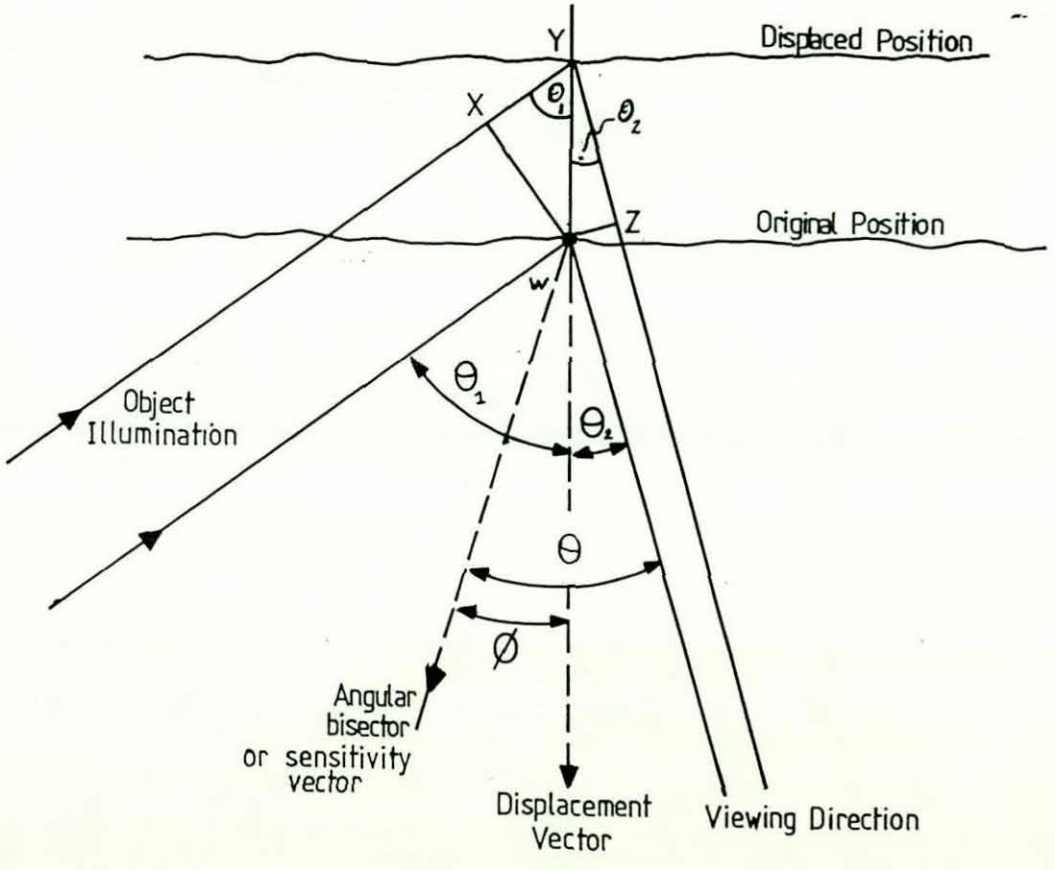

Figure 3.5
Optical Path Difference Produced by a Displaced
Surface Revealing the Sensitivity Vector

The path difference $= XY + YZ$

$= d \cos \theta_1 + d \cos \theta_2$

$= d(\cos \theta_1 + \cos \theta_2)$

$= d(2 \cos \frac{\theta_1 + \theta_2}{2} \cos \frac{\theta_1 - \theta_2}{2})$

let $\frac{\theta_1 + \theta_2}{2} = \theta$ and $\phi = \frac{\theta_1 - \theta_2}{2}$

then path difference $= 2d \cos \theta \cos \phi$ (39)

The path difference will be the number of fringes counted multiplied by the wavelength of the laser therefore;

$$N\lambda = 2d \cos \theta . \cos \phi$$

$$d = \frac{N}{2 \cos \theta . \cos \phi} \quad (40)$$

and is defined along the angular bisector more usually known as the sensitivity vector. Thus if illumination and viewing are along the same axis, $\theta = \phi = 0$

then $d = \frac{N\lambda}{2}$ the condition for maximum sensitivity

Figure 3.6 shows the hologram observed from two horizontally displaced points.

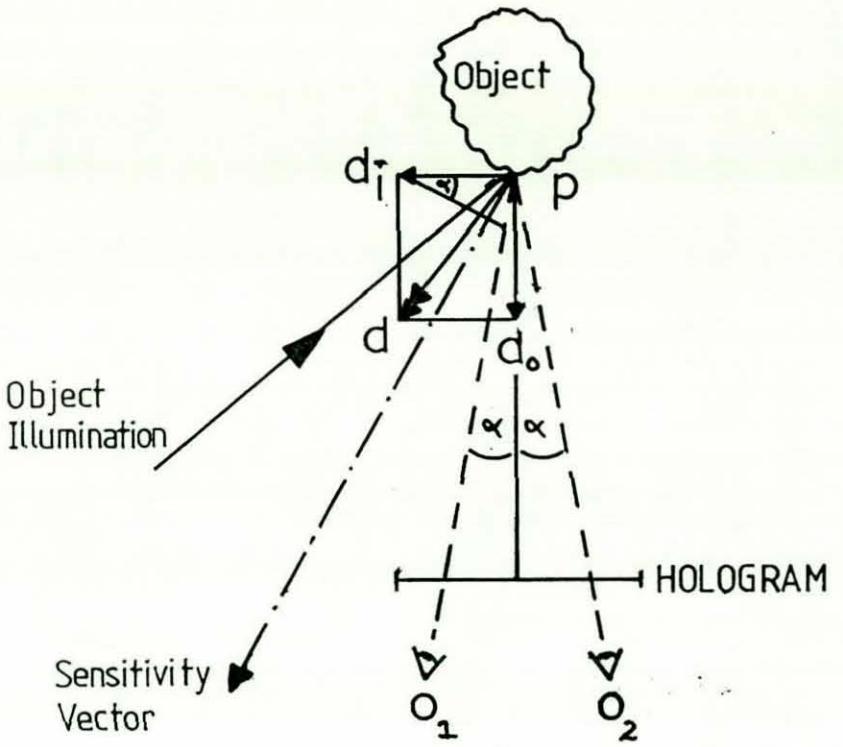

Figure 3.6
Two Point Observation of Holographic Fringe Patterns

Here d_0 represents the surface displacement normal to the holographic plate axis - out-of-plane displacement and d_i represents the horizontal surface displacement parallel to the holographic plate axis - in-plane displacement. The total displacement, assuming no vertical movement, will be d. The angle between the two observation points 0_1 and 0_2 is 2α. The path length difference for d_0 to these observation points will be equal (by symmetry). Let n represent the number of fringes observed, therefore, n_1 and n_2 correspond to fringe numbers at points 0_1 and 0_2, then;

$$d_i = \frac{(n_1 - n_2)\,\lambda}{2\,\sin\alpha} \qquad (41)$$

To extract the in-plane displacement d_i some amount of fringe counting and computation is required. For the generalised case involving three dimensional displacement, three views are necessary. Unfortunately most real world objects tend to be much larger than the 5 x 4" holographic plates used, therefore to minimise the errors associated with small changes in observation angles the arrangement in Figure 3.7 can be used.

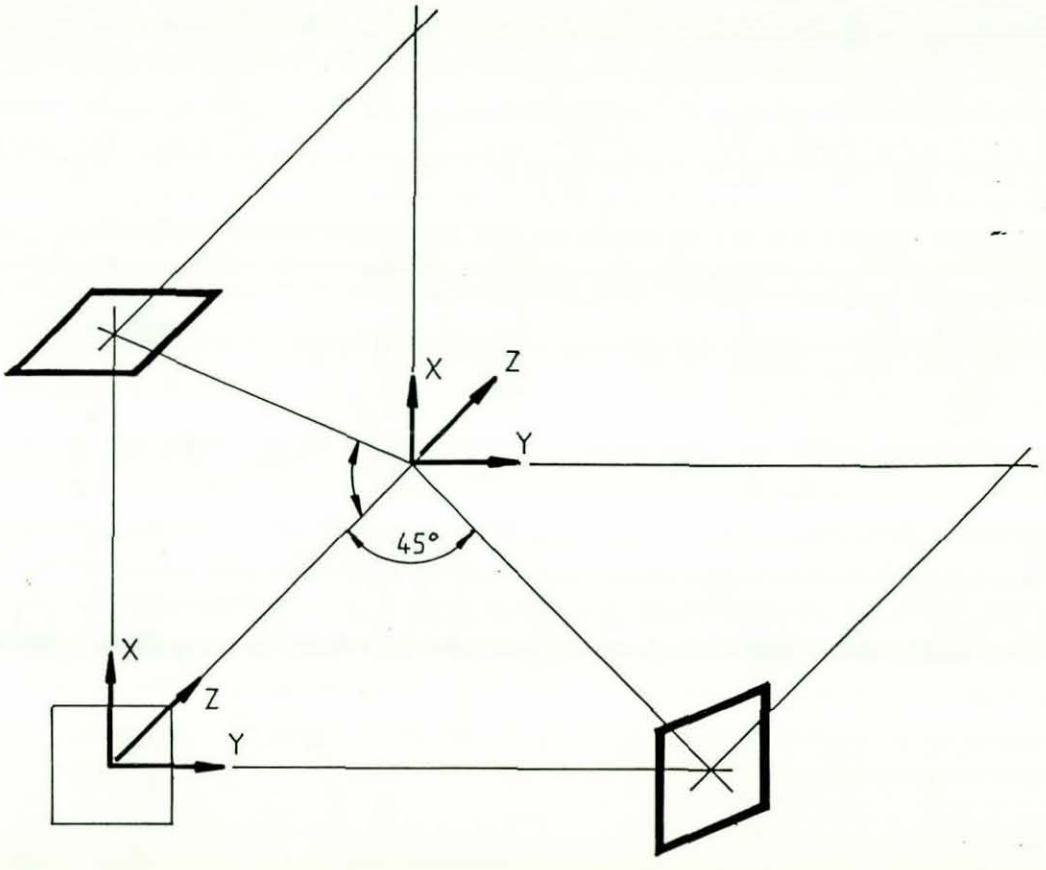

Figure 3.7
Generalised Holographic Analysis

It can be shown that the system can be set up to extract pure out-of-plane displacement but for each of the in-plane vectors computation will be required. Consequently two or more views of any surface position are needed to establish the in-plane movement. For most investigations this is considered cumbersome and error prone since there will be optical aberrations introduced by the viewing system. This is a limitation of holographic interferometry.

3.4 Experimental Verification

For the purposes of confirming the theoretical models presented, a study was undertaken using the clamped metal membrane shown in Figure 3.8. The experimental layout is given in Figure 3.9. Agfa 10E75 5 x 4" glass plates were used for the holographic recording. Object to reference beam intensity ratios of 1:8 were used throughout, with a total of 4 μWatts/cm^2 of Helium Neon (λ = 633nm) linearly polarized radiation from a 15 mWatt NEC laser. The plate processing was as detailed below;

Development:	Ilford SP678C, 2 minutes, 18 C.
Wash:	2 minutes.
Fix:	Ilford Hypam Non-hardening fixer, 2 minutes.
Wash:	2 minutes.
Bleach:	Ferric Nitrate Bleach until clear.
Wash:	2 minutes.
Dry:	Methanol soak, air assist dry.

An exposure time of 1 second was used for all exposures. Vertical polarization of both beams was used prior to the variable polarising beamsplitter, the final polarization being determined by the reference beam. Matching this reference polarisation vector to the object beam was achieved by a rotary half wave plate within the beamsplitter chassis. Photographs were taken using Kodak technical Tech Pan 2495 film rated at 125 ASA developed in D19 for maximum contrast.

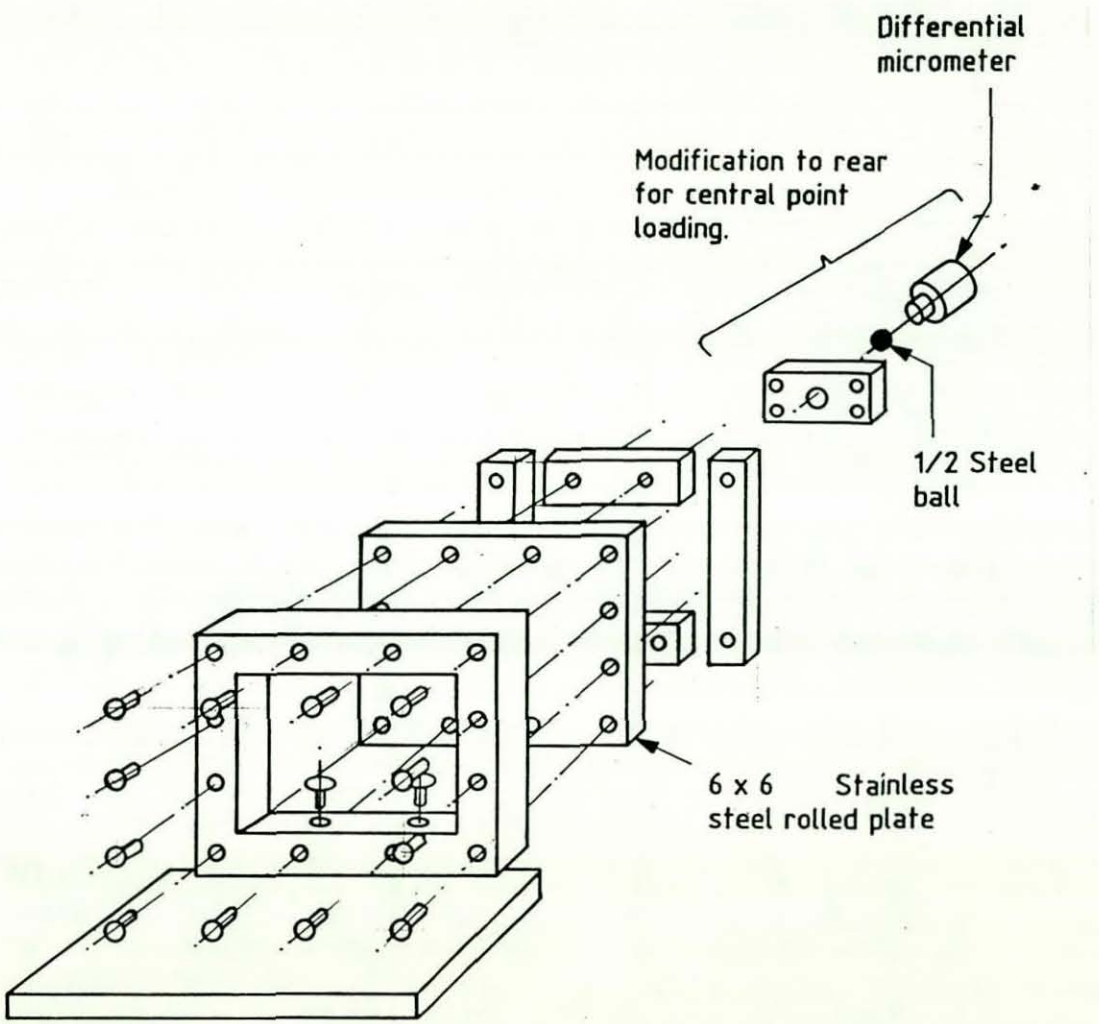

Figure 3.8
Exploded Diagram of the Experimental Test Object
Used for Verification of Theoretical Model

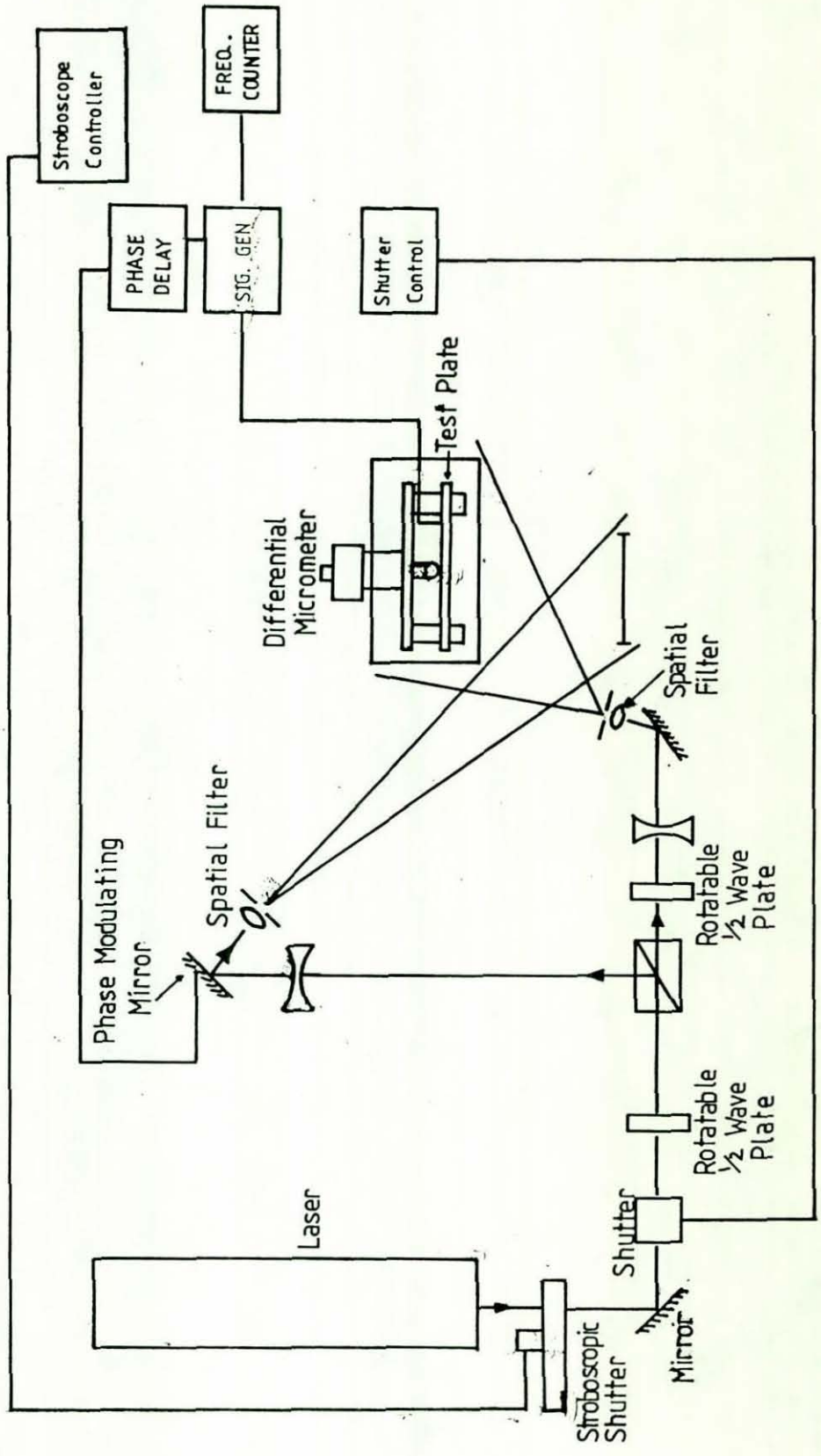

Figure 3.9
Experimental Layout of Opto-Mechanical Equipment
Used for Theoretical Verification

3.4.1 Holographic Study of Mass Modification to a Simply Supported Metal Disc

In attempting to promote the attributes of holographic interferometry within the automobile industry, a common comparison was made with the accelerometer based modal analysis. An experiment was devised to demonstrate the advantages of a holographic study compared with more traditional techniques. Whilst holography does not presently have the ability to undertake software analysis of the data, nor perform mathematical predictions such as mass modification, it offers high data density. Furthermore, being non-evasive, it does not affect the response of the structure. This is demonstrated in Plate 4, where a mass of 78 grams is added to the disc before the second hologram is recorded.

A 30.5cm (12") brass disc of uniform thickness, 1.5875 mm (1/16"), was vibrated with a piezo electric crystal attached to the central point mounting of the disc. Mode 2 was chosen for comparison and the disc excited at 280 Hz. Exposure and processing details were as follows;

Exposure:	10 seconds, Agfa 10E75 emulsion.
Development:	Neofin Blue, 2 minutes, 20 C.
Wash:	2 minutes.
Fix:	Amfix, 2 minutes.
Wash:	2 minutes.
Bleach:	Ferric Nitrate, clearing time + 1 minute.
Wash/Dry:	Methanol soak, air assist dry.

A second hologram was made after the mass had been adhered with IS12, a cyanoacrylate adhesive used for strain gauges and accelerometers. The location of the mass was chosen after consideration of the disc mode shape. The resonant peak was shifted down to 266 Hz with consequential mode shape disturbance. This pair of results was taken from a study of the initial five modes of vibration demonstrating the mass damping and frequency disturbance associated with alternative techniques.

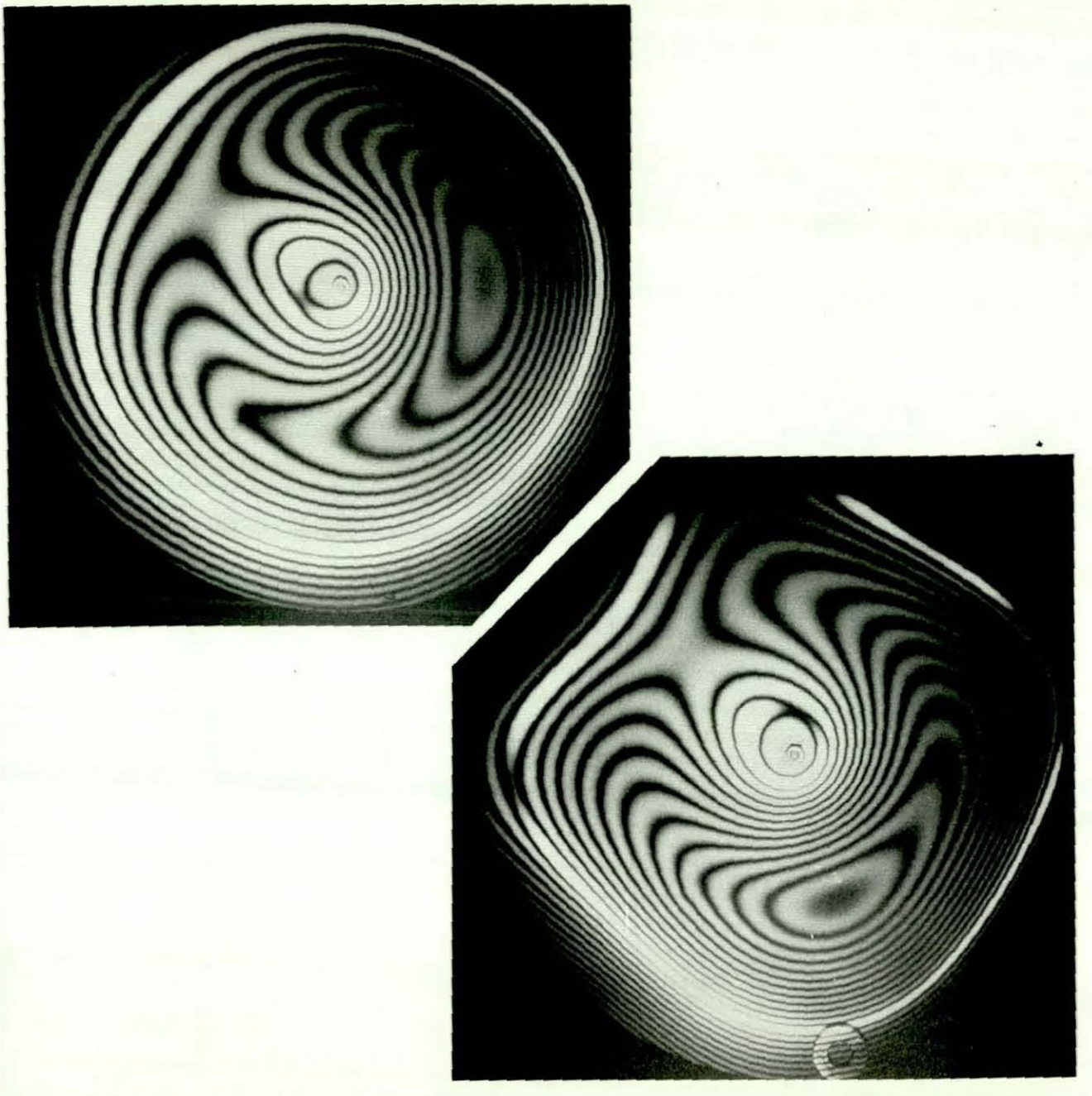

Metal Disc Vibrating
at 280 Hz.

Metal Disc with 78g mass
Vibrating at 266Hz.

Plate 4.
Demonstration of Mass Damping of Vibrating Discs

3.4.2 Holographic Analysis of Triumph Acclaim Baffle Plate

Three months prior to the launch of a new model, the Triumph Acclaim, a request was made for holographic analysis of the engine sump baffle plate, see Figure 3.10. The request suggested that the baffle plate was required for performance reasons, to try to minimise oil migration from the oil pump feed pipe during cornering and reduce oil churning by the crankshaft. A problem existed whereby the engine, either on the test bed, or within a vehicle could fatigue the baffle plate on its three spot welded mounting points which led to a catastrophic collision between it and the rotating crankshaft. The original, known as Type 1 could fail within the first 6000 miles of operation. Two further modified sumps, Types 2 and 3 had been delivered by Honda, the joint model manufacturers, and assessment was required of their suitability. The Noise, Vibration and Harshness (N.V.H.) department had identified 150Hz and 180Hz as potential problem frequencies, which suggested an input derived from engine crankshaft secondary out of balance components at around 4600 rpm. A second source of 120 Hz was also thought to be a possible resonance which suggested engine secondaries of around 3600 rpm. An initial holographic study of the Type 1 sump showed the baffle plate to be driven at 120 and 220 Hz.

The Type 1 baffle plate was a simple flat plate with three attachment areas for spot welding onto the sump wall. Type 2 was modified to include a stiffening lip along the free edge and Type 3 further included a ridge along the plate parallel with the crankshaft. Results from initial studies are summarised in Table B.

The stiffness of the baffle plate increased with each type and a vibration reduction between Types 1 and 2 was expected, however, no significant reduction between Type 2 and 3 was noticed. This was somewhat worrying as the second ridge should have restrained the mode more than actually occurred. Consequently, a further sump was modified by removing the baffle and a comparison made between the response of the

restrained and unrestrained sidewalls of the sump fitted to an engine block. Plate 5 shows the sump with the baffle plate removed and Plate 6 shows a Type 3 baffle plate. It was presumed that the sump had a failure mode associated with side wall fatigue of the drain plug, the baffle plate being a means to reduce the side wall panting. These results enabled a modification to be produced by the engineering works at Longbridge. The modified design called for a second bridging U strap to be mounted at the top of the sump and across the peak displacement of the baffle plate, this was known as a Type 4. Engineers sent from Honda acknowledged our prognosis of the problem and concurred with our findings. The results from Type 3 had been correctly interpreted as providing no real solution. It was satisfying to note that our conclusions were correct and came prior to their engine test bed results, which confirmed our predicted failure location and duty cycle (less than 7000 miles). The ideas put forward for Type 4 bracing were then incorporated into a Type 5 baffle plate which had a series of a, b and c, these being variations of mounting at different points on the sump wall. The final and successful solution, Type 6, was a totally re-designed baffle plate which incorporated the stiffening rib concept mounted toward the bottom of the sump. A comparison of designs driven with the same forcing energy is given in Plates 7.1-.5. Following this holographic survey and analysis, pre-production Type 6 baffle plates were tested in service on vehicles using German Autobahns and engines running on test beds.

Following successful trials, Type 6 baffle plates went into full production and all pre-launch Triumph Acclaims, (three months stockpile) were retro-fitted with Type 6 prior to sale. This provided the automobile industry with a test case showing the design relevance of Holographic Interferometry in producing data not generated by the strain gauged vehicles tested by the production company. The overall assessment and re-design from Type 1 to Type 6, took five weeks prior to highspeed testing of the Type 6 on the Autobahns. On receipt of a new design, four hours were needed to undertake a complete resonance study. This acquisition time was considerably shorter than the traditional N.V.H. test methods. It

did however, reveal the difficulty in providing quantifiable data. Fortunately in this study, the qualitative nature of the problem allowed successful re-designs of the component to be produced.

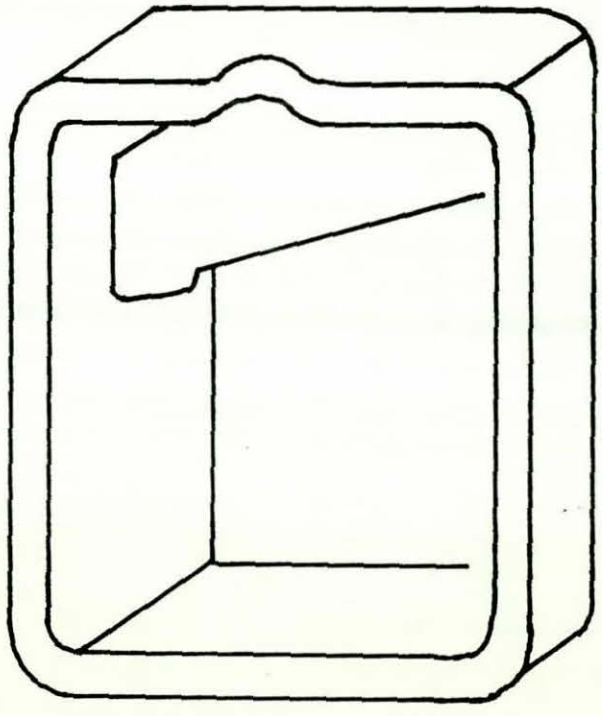

Figure 3.10
General View of Engine Sump and Internal Baffle Plate

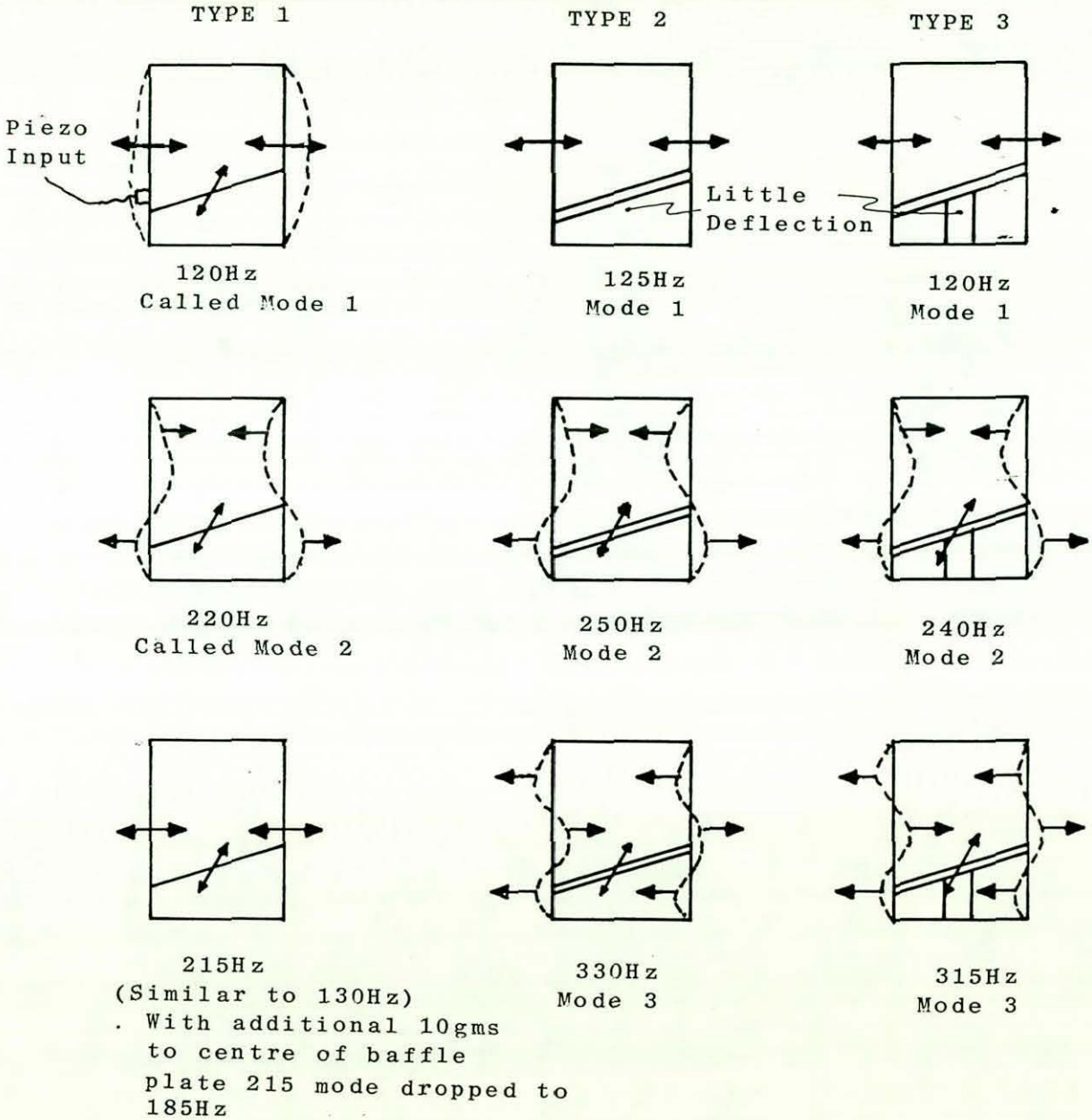

Table B

Summary of Initial Mode Shape of Engine Sump and Baffle Plate

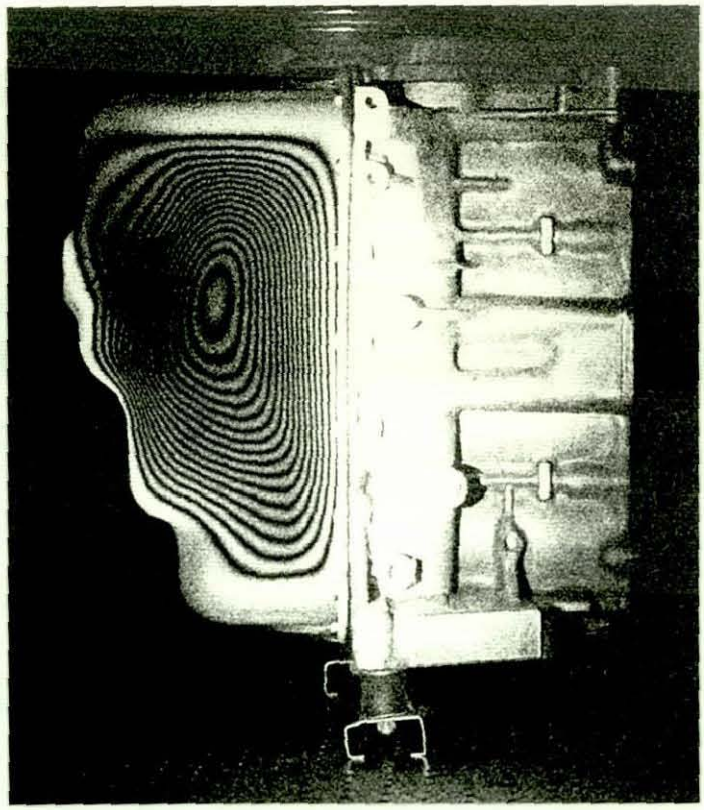

Plate 5

Engine Block and Sump (without baffle) at 240Hz

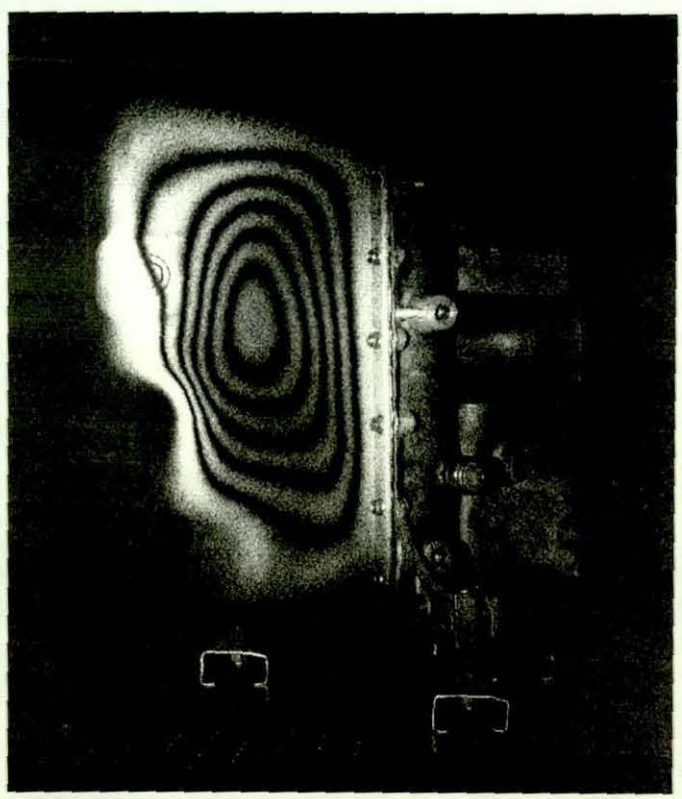

Plate 6

Engine Block and Sump with Type 3 Baffle at 250Hz

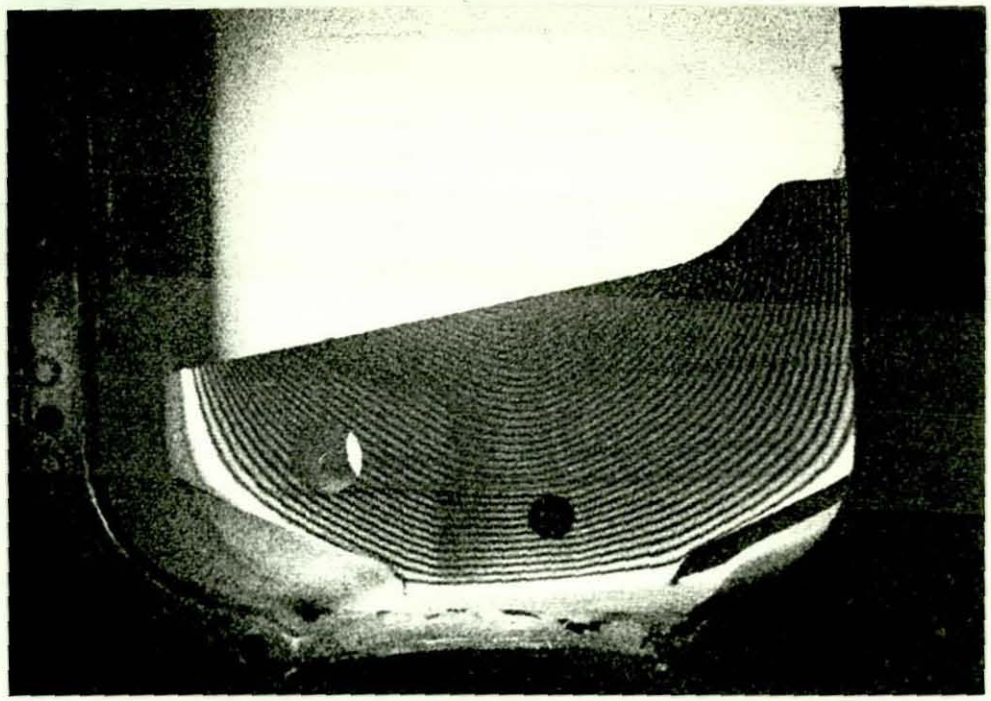

Plate 7.1
Type 1 Sump Baffle Plate at 220Hz

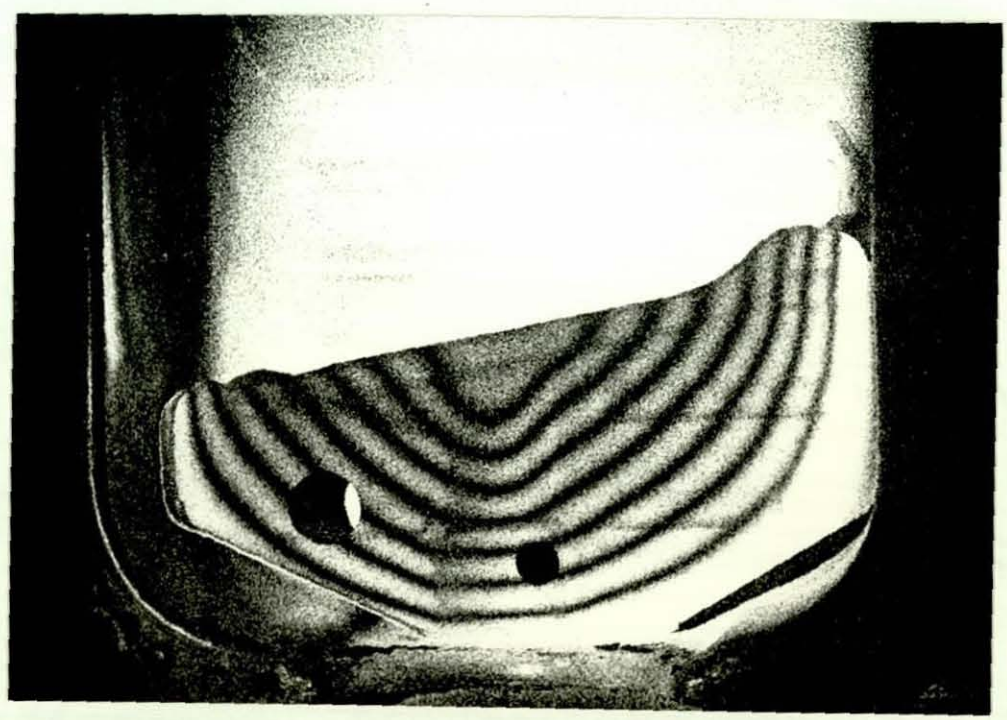

Plate 7.2
Type 2 Sump Baffle Plate at 250Hz

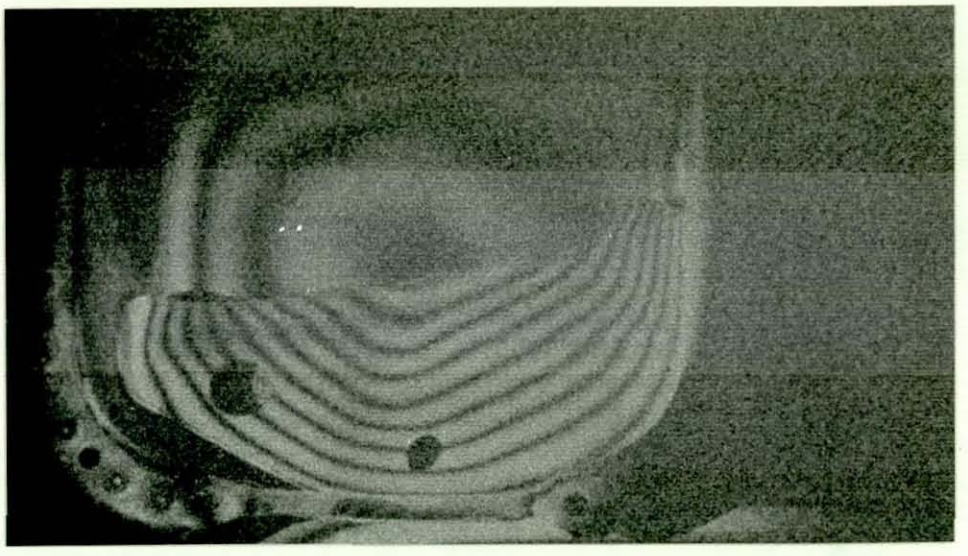

Plate 7.3
Sump Baffle Plate 240Hz

Plate 7.4

Type 5a Sump Baffle Plate at 255Hz

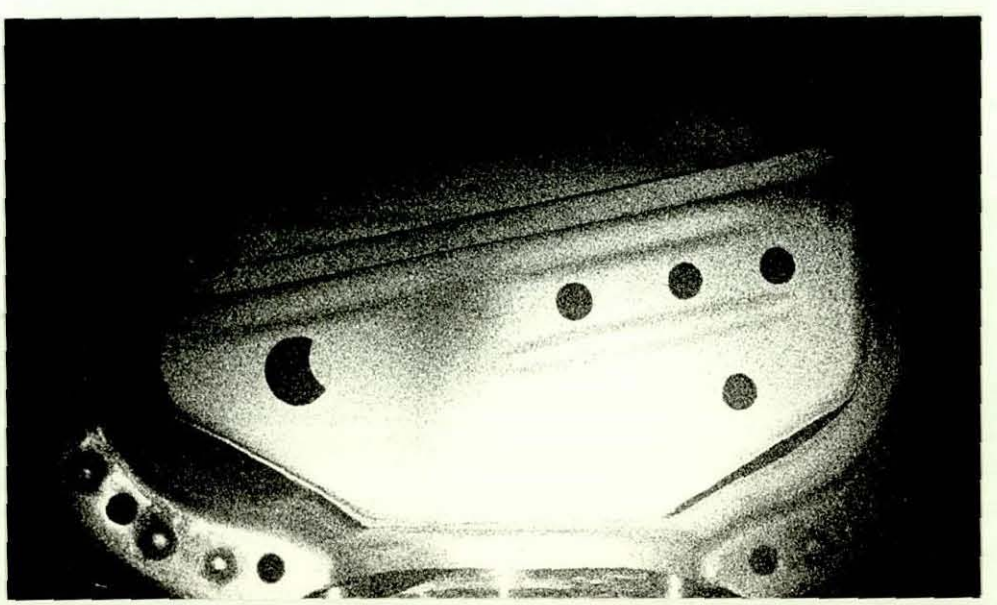

Plate 7.5

Type 6 Sump Baffle Plate at 255Hz

3.4.3 Engine Mode Shape Determination Using Holographic Interferometry

An initial investigation attempted to determine whether;

1. It was possible to excite a four cylinder engine block for study using Holographic Interferometry.
2. It was possible to do the same for an engine if route 1 was successful.
3. Similar resonances could be seen with the engine running in a dynamometer test cell.

Studies undertaken had revealed double pulsed Holographic Interferometry to be used for in-situ analysis of engine/bodyshell interaction. Little published data existed on the time-averaged holographic analysis of large structures. Problems encountered arose from the mounting of such a large structure, with large resonant displacements, upon an interferometric optics table. Initially, four point suspension, using elastic ropes was attempted to provide a free-free response. Unfortunately, elastomeric creep and considerable settling times rendered this approach unworkable.

A subsequent approach relied on utilising the engine mounting points with suitably softened elastomeric isolating suspensions units - typically modified engine mounting rubbers used on the motor vehicle. Excitation of the block was via a Ling Dynamics 10lb force electromagnetic vibrator and a 100 watt variable frequency power amplifier. The mode shape survey was used to compare production aluminium V8 3-5 litre engine blocks to determine if any variation in the initial resonant modes took place. Other than responses which varied by ± 3Hz in the range DC-350Hz no identifiable production variability existed. A consequence of this work was a further survey investigating the response of the block to a reduction in wall thickness. This work, in conjunction with other studies led to a lighter weight block going into full production.

3.4.3.1 Knock Sensor Location

Austin Rover engineers in conjunction with Lucas had attempted to control an E-series, four cylinder, motor car engine with a programmed ignition system which relied upon a knock sensor to detect the onset of engine pre-detonation. Two competitors, Saab and Renault, had successfully implemented engine management systems requiring knock detection. Two cars were provided for study, a Saab 900 Turbo and a Renault 18 Turbo, for assessment of their knock detection systems. The initial study revealed the Saab to have the accelerometer located in the centre of the engine block, whilst the Renault accelerometer was located upon a boss extended from the cylinder head. Both cars relied upon digital electronics to pre-filter the general response of the accelerometer and provide information in the 6-8 kHz region. Engineers at Lucas and the Engine Design Department at Longbridge had requested studies to be made of the cylinder head, intake and exhaust manifolds. A similar route was proposed for the filtration electronics and memory configuration. After suitable discussions with the Advanced Components Group, two new options were considered for pre-filtering of accelerometer input;

a) Resonant tuned accelerometer.
b) Resonant mounting pin for accelerometer.

Option a) was dismissed on cost grounds after discussions with Mullard and Hitachi, the accelerometer manufacturers. Option b) was dismissed as falling beyond the manufacturing capacity of Longbridge engine plant.

A further novel approach suggested was a holographic inspection of the engine block for resonant sites at the knock frequency. Mounting of a broad band, cheap accelerometer at this location would provide a response mechanically tuned to the knock operating frequency and could be tested for suitability on an interfaced engine test bed. The suggested use of the engine block was to ensure maximum sensitivity being close to the excitation and minimise transmission losses through a cast iron

component compared with gasket interfaces and the higher damped aluminium cylinder head. Mounting space was also considered to be more readily available on the block side compared to the highly convoluted side of the cylinder head. The recent holographic noise survey of cylinder blocks had provided confidence and the necessary experimental mounting arrangements.

One proposed advantage of the mechanical resonant filter approach was a reduction in electronics and ability for low cost broad band piezo electric accelerometers to be used. Simplified thresholding circuits could provide suitable information which, combined with an engine flywheel positional encoder, could predetermine the ignition, fuel and turbocharger requirements of each engine cylinder for every ignition cycle.

Initial trials were undertaken to provide a single candidate sensor location to which an accelerometer could be adhered. Lucas had determined engine knock frequencies to be at a maximum at 6.4kHz at 2000 rpm, with an effective range of 6.15-6.60kHz. Holograms were successfully produced within that range, although holograms attempted between 12-13kHz to identify any harmonics produced no meaningful results. Excitation of the block was via a modified cylinder head bolt onto which the electrodynamic transducer was attached. To determine the resonant frequencies, an accelerometer was attached to a centrally located boss and the output monitored to provide initial frequencies. Discussions with Bruel and Kjaer staff suggested a design for a touch probe mounting for an accelerometer to enable a portable contact probe to be constructed. To identify common location sites, it was necessary to sequentially excite the engine from each of the cylinder head bolts. Other parameters studied included: effects of water cooling jacket - 100Hz reduction with two fringe damping, engine wear and production variability of cylinder blocks, both of which produced little change. Example holograms are shown in Plates 8 and 9, where different input locations excite the engine at 6345Hz with 10lb force input energy.

The accelerometer can be seen in Plate 8, the sump cover can also be seen vibrating on Plate 9 although the block modes are reduced.

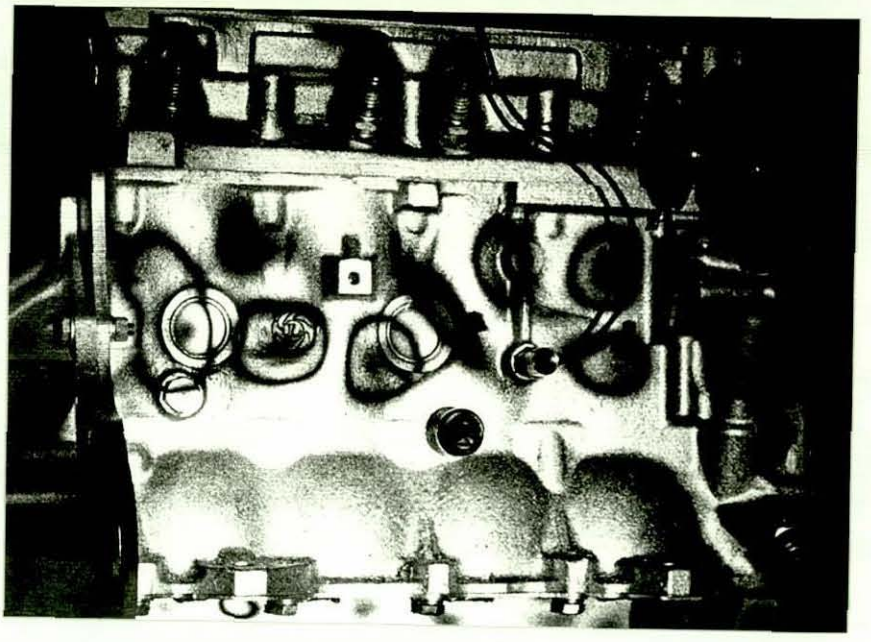

Plate 8. E-Series Engine vibrating at 6345Hz with the input in-line with the accelerometer

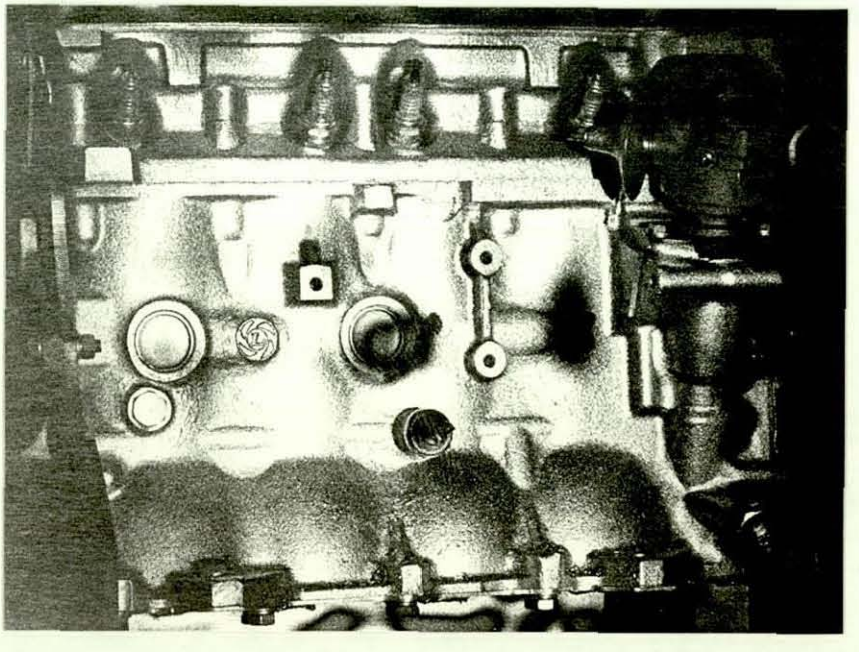

Plate 9. E-Series engine vibrating at 6345Hz with the input in the far left hand side of the engine block

The E-series engine was originally designed as a transverse engine with integral gearbox, for this study a separate fabricated sump was used with a longitudinal configuration using a Sherpa gearbox. This enabled the Lucas dynamometer to be used in conjunction with the interfaced control electronics.

3.4.3.2 Production Implementation of Knock Sensor System

Following the successful trials of the E-series engine with the sensor location investigated by holographic interferometry, further studies were undertaken. A new passenger vehicle series was planned using the new engine management control system. The engine to be used was based around the O-series engine and therefore similar studies were undertaken initially using a standard O-series production engine. An example is shown in Plate 10. The modified cylinder block was later made available, known as the R-series and S-series, a result from this is shown in Plate 11, seen resonating at 6970 kHz. The lower pair of fringes demonstrate the location of the sensor currently used on Maestro and Montego production vehicles.

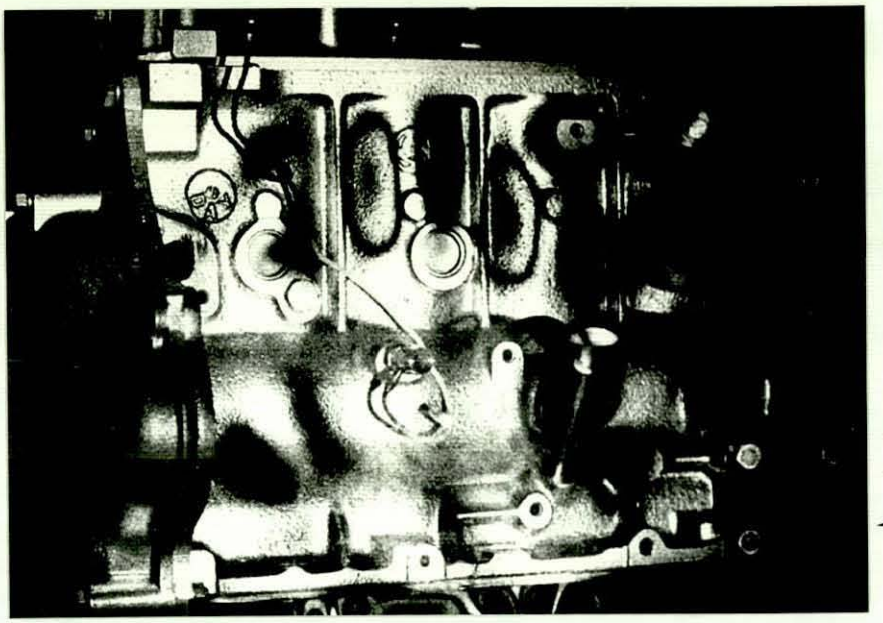

Plate 10.
O-Series engine vibrating at 7445Hz with 10lbf input
in-line with the dip stick

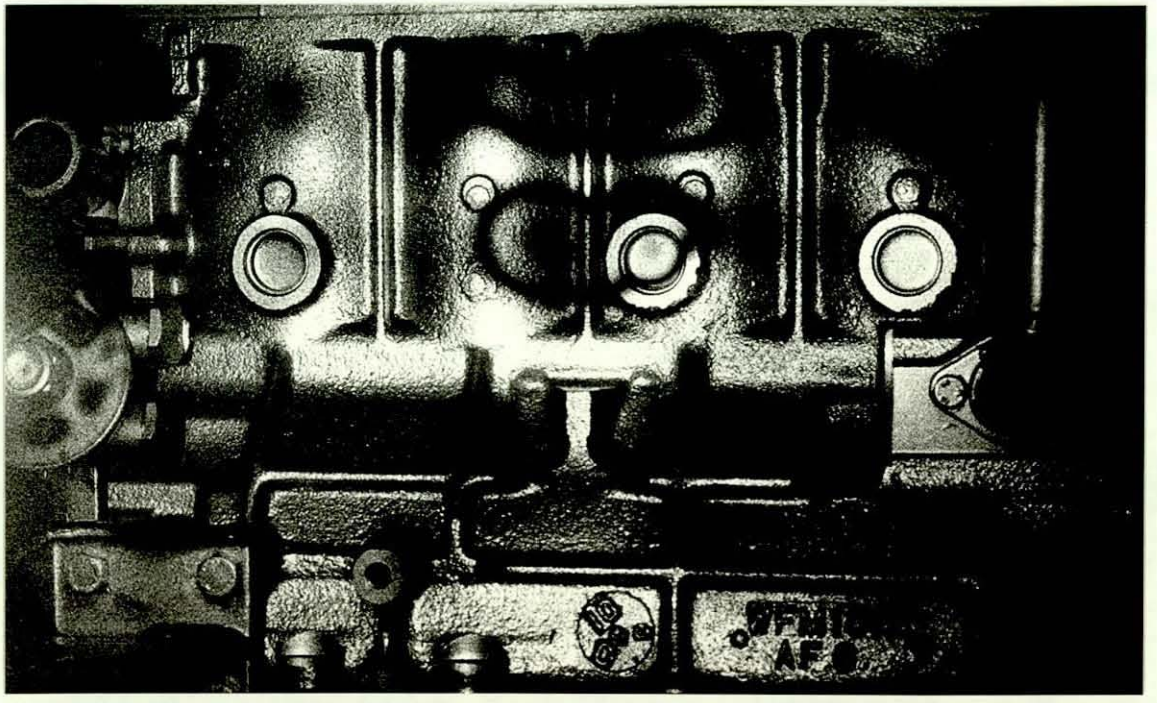

Plate 11.
R-Series engine vibrating at 6970Hz with 10lbf input
in the middle of the engine block

3.5 Conclusions

This chapter has examined the theoretical background of the various techniques concerning Holographic Interferometry. These have been verified with simple experiments and consideration of the optical arrangements for different displacements sensitivities. Engineering studies were undertaken to determine general suitability of the technique and successful novel engine component designs resulted.

- Experiments undertaken have enabled three engineering design studies to be successfully completed with Holographic Interferometry providing confidence in the technology.
- Refinement of the process enabled set-up of experimental equipment within four hours, although the component mounting required careful design and manufacture to avoid cross coupling into the optics.
- Difficulty was exhibited in obtaining in-plane data, results shown were for out-of-plane studies only.
- Arrangement of equipment and limited laser power required upto 30 minute exposure periods for holograms.
- Difficulty was encountered in establishing resonance conditions of components without auxiliary sensors.
- The technique was not considered suitable for daylight operation.
- Results required photographic or subsequent recording with a television camera to obtain suitable data for display.
- The process was prone to problems with photochemistry and holographic plate inhomogeneity and non-repeatability.
- The technique was not considered suitable for automation and operation by semi-skilled technicians.
- The quality of interferograms was seriously affected by movements $>\lambda/8$ during exposure periods. Control of industrial laboratories for periods greater than one second was difficult.

- Alternative interferometric processes were studied to ease the data acquisition process and dispense with the need for auxiliary sensors.
- Experimental verification of theoretical models is now possible with short lead times and suitable data density.

CHAPTER 4
DOUBLE PULSED HOLOGRAPHIC INTERFEROMETRY

4.0 Introduction

The laboratory constraints of Holographic Interferometry can be overcome in two ways; i) by using a common path interferometer (i.e., locate a reference beam return mirror close to the object such that any general environmental perturbations affect both arms of the interferometer), or ii) by using a pulsed laser to deliver the requisite exposure energy in a sufficiently short period of time to obviate the need for vibration isolation. The former technique whilst attractive, especially when only a continuous wave laser is available, generates experimental difficulties which though not insolvable require a high skill level of operation. The latter technique provides the basis for a self-contained instrument which was the objective of this research. The need to move away from the laboratory environment is twofold: firstly to perform measurements on the subjects working in-situ (a requirement any engineer will consider essential), secondly, to produce initial test data from which an overview can be acquired prior to detailed specific component testing. The need for this overview is essential when trying to undertake any experimental study where the component response to the rest of the system defines the design of the test rig to simulate the system response. The need for this isolation in a test rig is simply governed by the reduction of variables. Obviously in certain circumstances in-situ analysis is sufficient, however in the range of problems encountered to date, other than qualitative studies, all have been concerned with component redesign. The ability to work in isolation from the complete system will usually be the initial approach. Access to suitable pulsed laser equipment which could also be used for the laboratory testing would minimise initial capital outlay. The heart of this research is the generation of such equipment. This chapter will initially concentrate on the design of pulsed holographic arrangements and then explain the use of pulsed laser equipment in the tests undertaken.

A more detailed description of pulsed laser operation and design can be found in Appendix 1.

4.1 Holographic Constraints

The successful recording of a hologram using a continuous wave laser relies on all components remaining relatively motionless during the exposure period. The maximum displacement tolerated during a holographic recording is approximately $\lambda/10$. The available laser power, component stability and object velocity are the factors which determine the exposure time.

The alternative to the continuous wave laser is the pulsed laser which develops intense laser activity in short time intervals. The medium typically used within the laser is a synthetic single crystal of Aluminium Oxide (Al_2O_3) with 0.05% (by weight) of Chromium Oxide (Cr_2O_3) more usually known as Ruby. This type of laser is optically pumped (excited) by close coupled Xenon flashlamps. The broad band flashlamp discharge excites the chromium ions within the crystal and upon relaxation the ion emits a photon which can be cascaded into a pulse of laser energy. A more complete description of pulsed lasers, their operation and modifications undertaken to improve performance are detailed in Appendix 1. Typical pulse periods of a ruby laser are 1-3msec though a technique of energy storage, Q switching utilised within the cavity can reduce this to 10-20nsec (where 1 nsec = 1 x 10^{-9}sec). From the holography viewpoint this means displacement levels of $\lambda/10$ need only be held for a period of 20 nsec. Practically for an out-of-plane arrangement:

$$\text{Tolerable velocity} = \frac{\lambda/10}{20 \times 10^{-9}} \quad ms^{-1}$$

where λ for Ruby lasers is 6943 A or 0.694×10^{-6} m, hence ;

Maximum velocity of component = 34.7 ms^{-1}
during the exposure.

4.2 Fringe Pattern Analysis, The Zero Fringe Ambiguity

The first problem in the interpretation of double pulse fringe patterns is the determination of the zero order fringe (fringes of no displacement). The fringe pattern produced in a double exposure hologram has a co-sinusoidal fringe function which means a uniform displacement sensitivity and intensity distribution and so do not exhibit a bright zero order fringe. This is unlike the time-averaged interferograms which do have bright fringes and the fringes have a zero order Bessel function intensity distribution. The use of "quasi time-averaged pulsed holography" reported by Gordon [12] is a simple technique to identify the zero order regions. Using this technique, the fixed Q of the ruby laser produces two long duration pulses. In this way pulsed holograms can be obtained with a quasi-Bessel function describing the fringe pattern sensitivity. This technique is used in initial mode identification, and a subsequent Q switched double pulse hologram records the object motion for detailed analysis. The interrogation of the fringes to produce a displacement map is simply a case of modifying the sensitivity vector by the number of half wavelength fringes. When using cosine fringes no modification of the fringe field takes place because the zero order Bessel sensitivity function no longer applies.

4.3 Design of Experimental Arrangements

Two types of analyses were undertaken; firstly, where the component or device exhibited a single frequency vibration problem, and secondly where the excitation was present and combined with a low frequency, high amplitude general displacement. The former produced few experimental problems other than the triggering of the laser and the inevitable on-site complications. The latter presented an interesting dichotomy; double pulsed holography is exemplified as a technique for in-situ analysis of real world objects, however the data to be extracted is combined with rigid body data which serves only to mask and confuse the required

experimental data. Abramson [13] developed the technique of sandwich holography; two holographic plates, sandwiched together are rotated between the two exposures to record two separate holograms on each of the plates. By rotating one holographic plate relative to the other, the two temporally separated single pulse holograms can be combined. Whilst elegant in concept, it becomes hideously complicated with large structures which require considerable "a priori" knowledge of the output required, an unreasonable demand when attempting "fire fighting" type solutions in industrial environments. The technique developed here was to use common path interferometry to remove the rigid body motion by attaching a mirror onto a non-contributing portion of the component from which the reference beam could be reflected toward the hologram. In this way the rigid body motion would simultaneously displace both wavefronts and not contribute to the resultant interferogram. Mottier [14] originally proposed the idea whilst Waters [15] utilised a speckle reference beam derived from the object. For rotating objects Stetson [16] utilised a rotating prism within a hollow rotor electric motor to effectively de-rotate a rotating turbine fan and record double pulse vibration patterns. The initial experimental arrangement chosen for vibration studies is shown in Figure 4.1.

In this figure, a simplified laser is presented. The need for pre-amplifier extraction of the reference beam was proposed by Ansley and Siebert [17] in 1969 and Siebert [18] in 1971. They considered that the amplifier in the ruby laser introduced a frequency change hence reducing coherence. Cookson et al [19] demonstrated that with the original JK design of ruby laser this was not valid. One advantage of extracting the reference beam prior to the amplifier is the removal of sufficient energy whilst still enabling spatial filtering to be used. One problem with pulse durations of 15 nsec and energy levels of >5 mJ is the ionisation of air when the energy is focussed down with a bi-convex lens arrangement. Using a 25μ diamond pinhole provided by British Diamond Wire Drawers, spatial filtering of the reference beam could be achieved without need for a vacuum chamber.

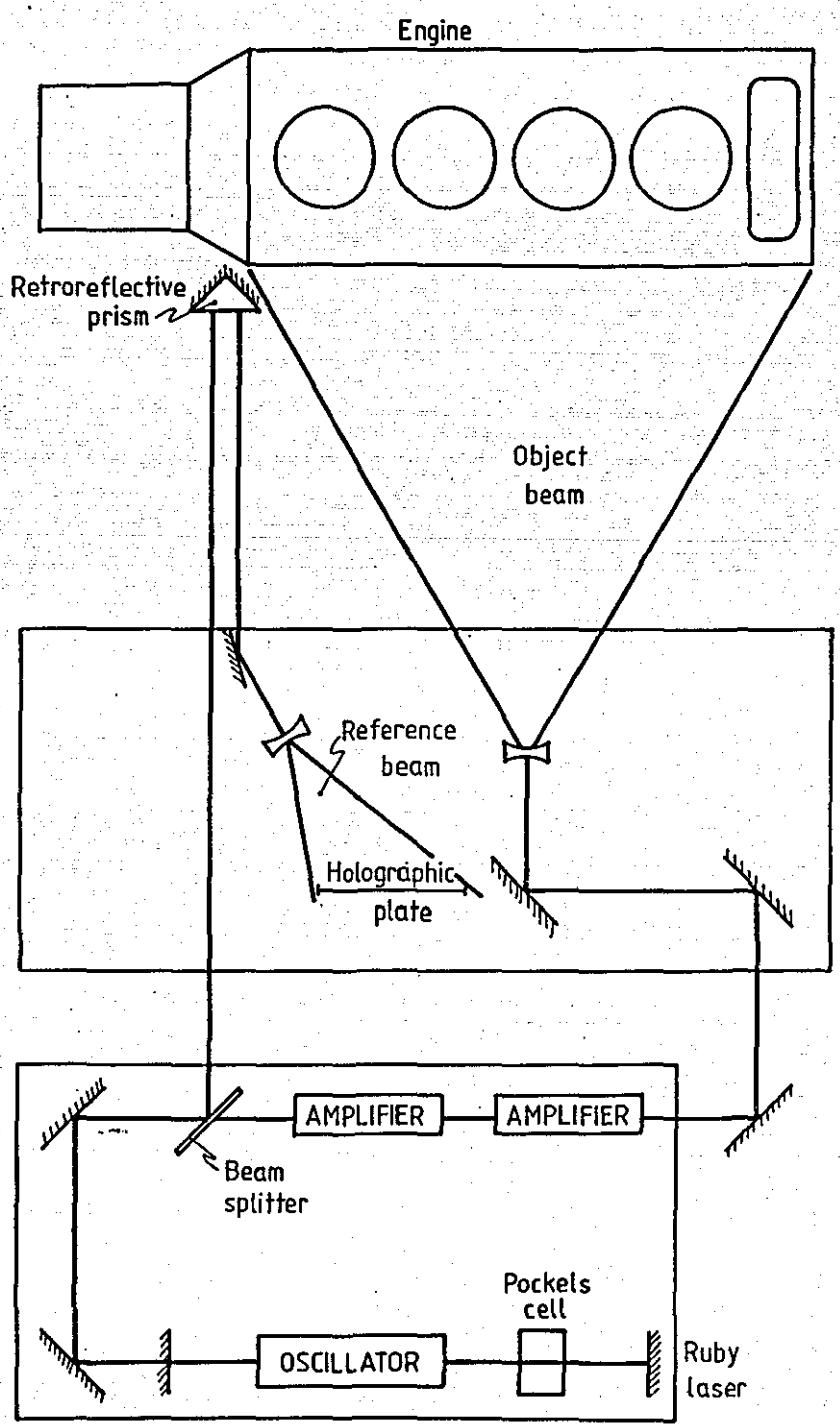

Figure 4.1
Experimental Arrangement for Vibration Studies using Double Pulse Holography

A novel way of producing the reference beam without modification to the laser axis is shown in Figure 4.2. The handicap of this approach was the reduction in oscillator output (4-5%) with the concomitant noise potential involving four additional optical surfaces. Other than for the initial double pulsed ESPI experiments using this laser, the arrangement was discarded. Preference was given to a single wedge beam splitter placed after the amplifiers.

At this point it was decided to combine the equipment and produce a portable holographic system. With the considerable volume occupied by the laser (even with an improved internal component density), the obvious location was either above or below the main optical arrangements. With maintenance in mind mounting the laser on the top proved to be a successful location. By rigidly coupling the laser on top of a purpose built 4 x 2' optical table, a compact arrangement was devised capable of moving up to and around the component as shown in Figure 4.3.

By using Tec-Optics dielectric mirrors (20 mm diameter) specified with an incidence angle of 45°, 100% reflection of the 694nm radiation could be achieved with no damage to the coatings. The energy density onto these mirrors did not exceed 1.5 Jcm^{-2}. By transferring the laser output onto the optical table with a 2 x 45° mirror periscope arrangement, polarization was preserved in the vertical axis. The optical stands and component holders were specifically designed for this arrangement and provided: good packing density, great flexibility, high rigidity and internal damping. The magnetic bases provided secure location with a degree of adjustment.

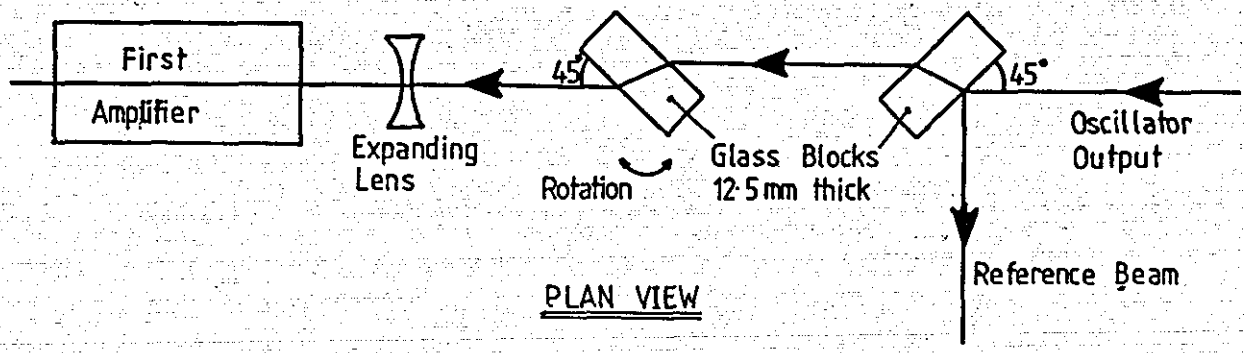

Figure 4.2
Optical Arrangement (Plan View) to Derive Reference Beam Prior to Amplification

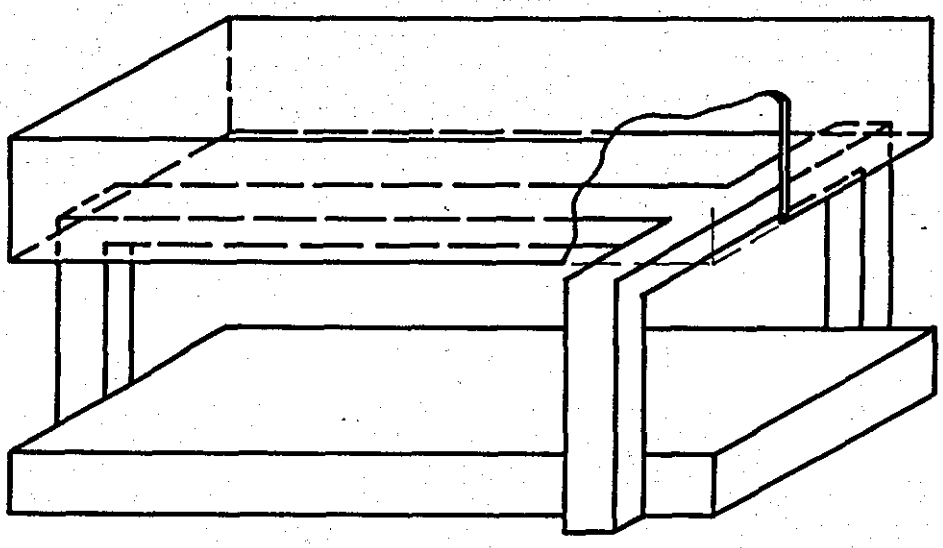

Figure 4.3
Mounting Arrangement of the Ruby Laser on the Table Simpler Vibration Studies

In circumstances where rigid body motion is not considered a problem, an alternative arrangement was devised which kept all optics upon the table. Thus the equipment could be positioned adjacent to the component and the test undertaken with little disturbance or setting up required. To compensate for the pathlength difference between the object and reference beams, a folded adjustable reference beam arrangement shown in Figure 4.4 proved suitable.

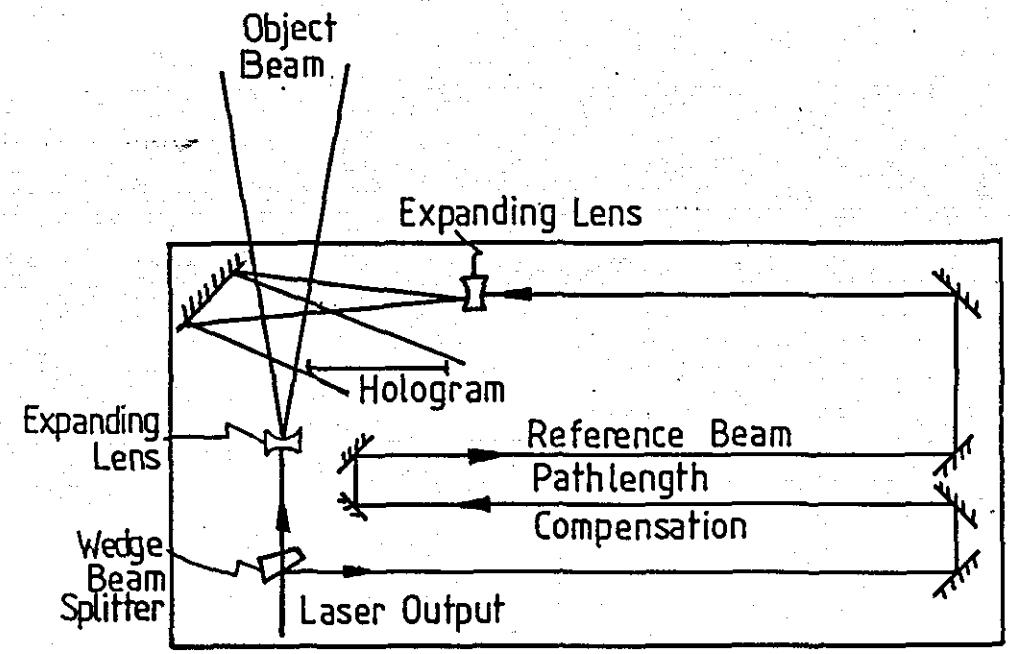

Figure 4.4
Plan View of the Table Arrangement for Simpler Vibration Studies

As discussed earlier, Section 2.3.1, the holographic emulsion requires at least double the recommended energy level with such short exposure periods. Various techniques were tried to improve the sensitivity of the plates; including pre-exposure to a flashlamp and ammonia soaking, but neither technique proved to be stable or repeatable. Babcock and James [20] discuss gaseous hydrogen hypersensitisation in-vacuo, Jenkins and Farnell [21] the use of various chemical approaches to infra-red emulsions, Albright [22] provides a comprehensive review on the subject though all authors concentrate on astronomical photographic material. The conclusion of these experiments was that the sensitisation techniques are too variable for industrial application. Depending upon the emulsion batch, between 6-10 $\mu J\ cm^{-2}$ was the energy level delivered onto the emulsion. Processing was as detailed:

Development:	2 minutes, Neofin Blue, 20°C.
Wash:	2 minutes.
Fix:	2 minutes, Ilford Hypam.
Wash:	2 minutes.
Bleach:	2 minutes, Ferric Nitrate, twice clearing time.
Object:Reference beam ratios - 1:6 to 1:10.	

Bi-concave lenses were used throughout for beam expansion, to avoid the problem of focussing the beam and increasing the energy density. This approach prevented material damage to the optics, ionisation of the air and stray reflections back into the amplifier causing damage to the oscillator. Unfortunately this did not enable spatial filtering of the beams to be undertaken and consequently surfaces had to be kept clean to prevent damage to the optics and reduce noise. Single lenses were unable to provide sufficient optical power for beam expansion and were combined in doublet and triplet arrangements. Scatter plates and holographic scatter plates, after Gates [23] and Webster et al [24] were tried but still required pre-expansion for the holographic units otherwise material damage would occur. Scatter plates produce a uniform beam but with random polarization. A solution involving minimal optics is shown in

Figure 4.5, where the surface reflectivity of ball bearings was used to expand the beam rapidly and retain polarization. The focal length was half the radius of curvature. The surface finish was adequate and since only one optical surface is employed minimal energy losses occur. The surface reflectivity of a hardened steel ball is < 100% of 694 nm and therefore occasional rotation of the ball was necessary to minimise blueing of the surface. Polishing to remove the surface discolouration was tried but proved unsuccessful. Unit cost was less than £5 and can therefore be considered a consumable. A range of different sized balls was used to provide a range of beam expansions.

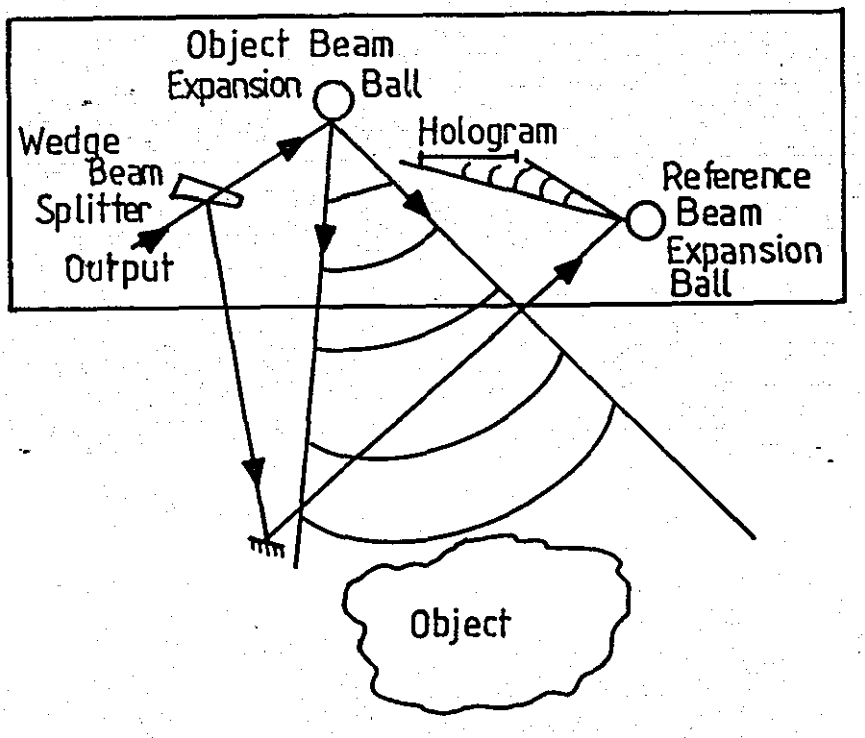

Figure 4.5
Plan View of Simplified Arrangement for
Vibration Studies with a Local Reference Beam

4.3.1 Laser Triggering

A hologram made of an object using a double pulsed laser will give a frozen fringe pattern representing the displacement undergone by the object in the time interval between the two pulses. The separation between the pulses must therefore be chosen to coincide with the peaks of object displacement, which with most vibration problems is found to be half the oscillation period ($\tau/2$). If the component displacement is greater than, say, 30-40 fringes, the delay between the fringes can be reduced. This will have the effect of sampling less of the displacement, but with prior knowledge of the nature of the waveform, the total displacement can be extrapolated.

Depending upon the vibration problem under investigation, a typical triggering scheme is shown in Figure 4.6.

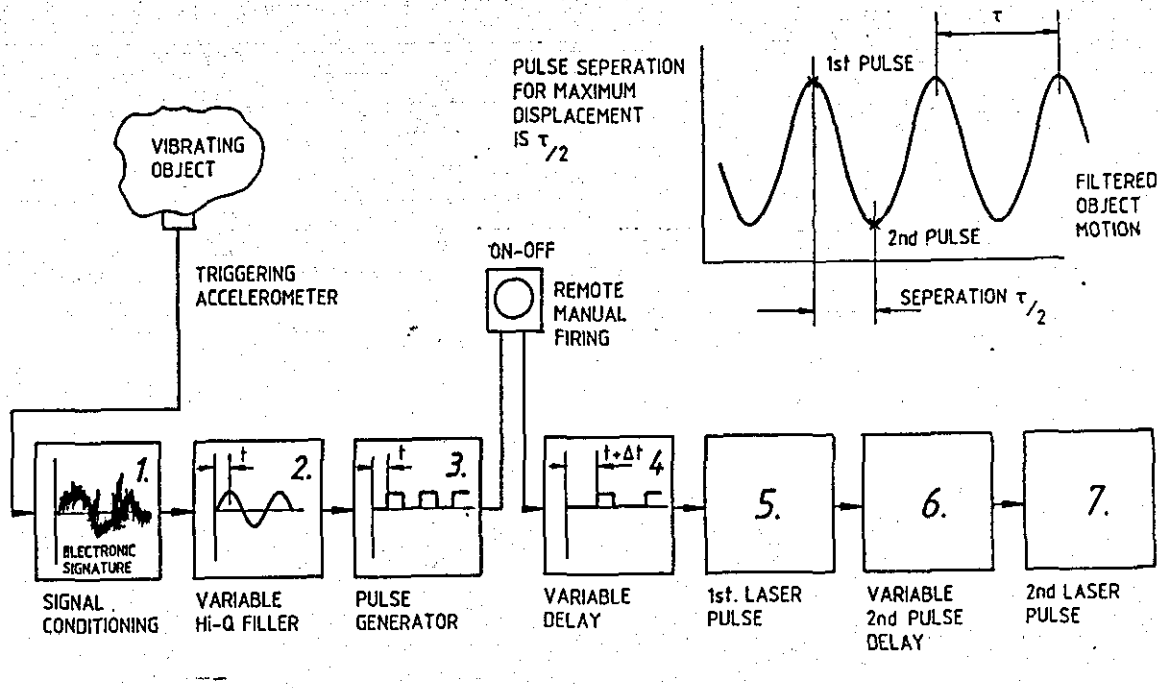

Figure 4.6
Laser Triggering, Control and Firing System

This system is designed to examine periodic displacements but if transients are to be studied, alternative sensors or direct feed from the source must be considered. The narrow band pass filter samples the required timing signal from the accelerometer which is then modified to provide the requisite pulse form to trigger the laser. To accommodate the rise time of the laser a delay amplifier is used to compensate and enable the firing of the first pulse to coincide with the first peak of displacement. A second delay amplifier is set with the necessary pulse separation to enable the second pulse to be fired and record the resulting double exposure interferogram.

For pulse separations of between 5 μs - 1 ms, two pulses can be extracted from a single fluorescence of the ruby rod by double pulsing of the Q switch. The shortest interval between pulses is determined by the drive electronics to the pockel cell, the longest by the length of the flashlamp pulse. A double pulsed hologram requires equal energy in each pulse and to achieve this the delay between flashlamp trigger, the first switch pulse, the supplied energy to the flashlamps, and the voltage to each of the Q switch pulses, must all be controlled. These parameters allow for selection of the pulses within the fluorescence envelope of the ruby rod.

For pulse separations of 1 ms - 5 s it is necessary to fire the flashlamps twice. This is achieved commercially by use of a second capacitor bank which is charged simultaneously with the first, each bank being used for each pulse. Caution must be exercised when working in the region 1 ms-5 μs when reduced energy is required for the second pulse and the flashlamps can remain in an ionised condition. It is within this working region that the initial analysis of most large structures occurs. The Department of Mechanical Engineering has two such double capacitor bank ruby lasers and use of these has allowed both laboratory and on-site investigations to take place. For pulse separation greater than five seconds, the recharging time within the capacitor banks is sufficiently short enough to enable a second pulse to be produced.

4.4 Experimental Study Using Double Pulsed Holographic Interferometry

The result shown in Plate 12 is the response of the front spoiler and grille of an Austin Maestro self excited with an engine speed of 2000 rpm. Plate 13 shows the results of an Austin Metro engine excited at 1200Hz using an electro-dynamic vibrator just visible at the top of the photograph. Both plate results were obtained using the arrangement in Figure 4.4.

Plate 12.
Austin Maestro Vibrating with Engine Speed of 2000 rpm

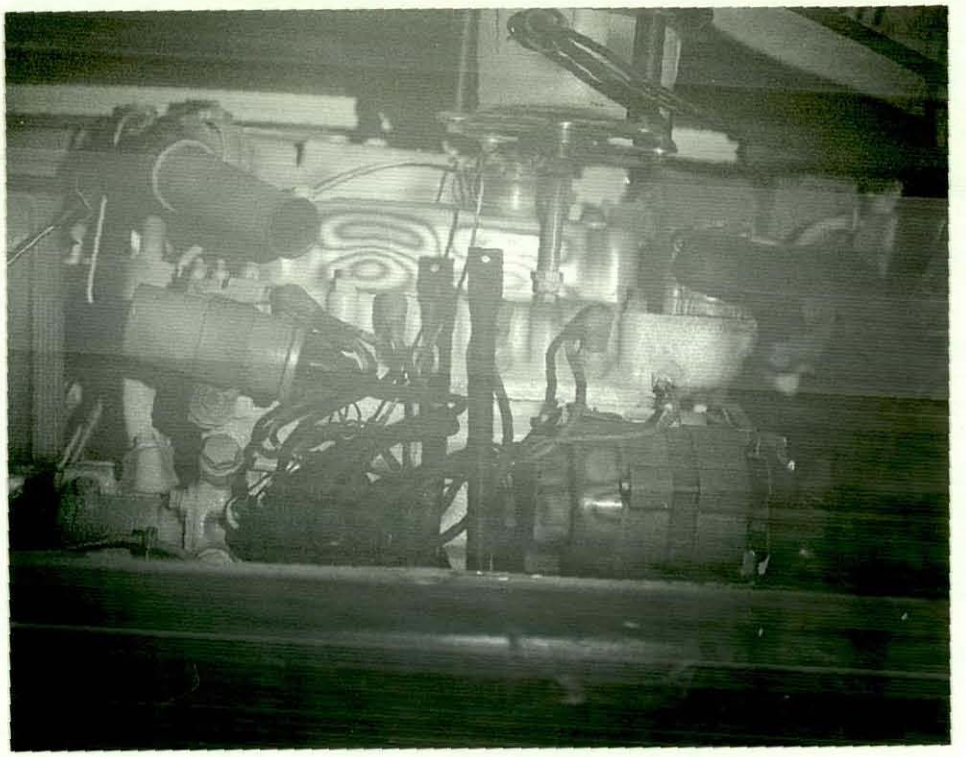

Plate 13.
Austin Metro Engine Vibrated at 1200Hz

The arrangements previously discussed were derived from experiments undertaken on automobiles with equipment being used to examine, in a qualitative fashion, the sources of noise in the engine compartment of passenger saloons. The testing of the arrangements in an arduous industrial environment was accomplished at Moffat Gas Compressor Station. The component under test, shown in Plate 14, was a four metre diameter centrifugal pump driven from a free power turbine. The turbine was supplied by hot gas generated by an industrial version of a Rolls Royce RB2-11 gas turbine engine. The purpose of the compressor, as one of a chain of compressors, was to pump high pressure gas along a 42 mile section of the gas grid. The section ran from the North Sea Gas receiving station across the border into England. The gas turbine was fuelled by

the natural gas it was pumping and therefore represented a self-contained pumping facility within the gas grid. With seasonal changes to the domestic consumption of gas, the pumping conditions of the station varied. During part of the seasonal variance, at a particular pumping demand, a resonant condition could be excited within the compressor unit.

Previous studies with conventional modal analysis using accelerometer matrices had identified the compressor and associated pipework to be resonating at 168 Hz, the source of the high level of vibration energy was unknown. The compressor back-plate was investigated using holographic interferometry arranged to examine the out of plane displacement. The input feed pipe and the outlet take-off pipe where also examined using the optical arrangement shown in Figure 4.7.

The trigger arrangement used for the firing of the laser was as shown in Figure 4.6. An accelerometer placed on the component surface was used to synchronise the initial pulse firing to a specific timing point on the object surface motion. After suitable bandpass filtering, a trigger signal was obtained as shown in Figure 4.8.

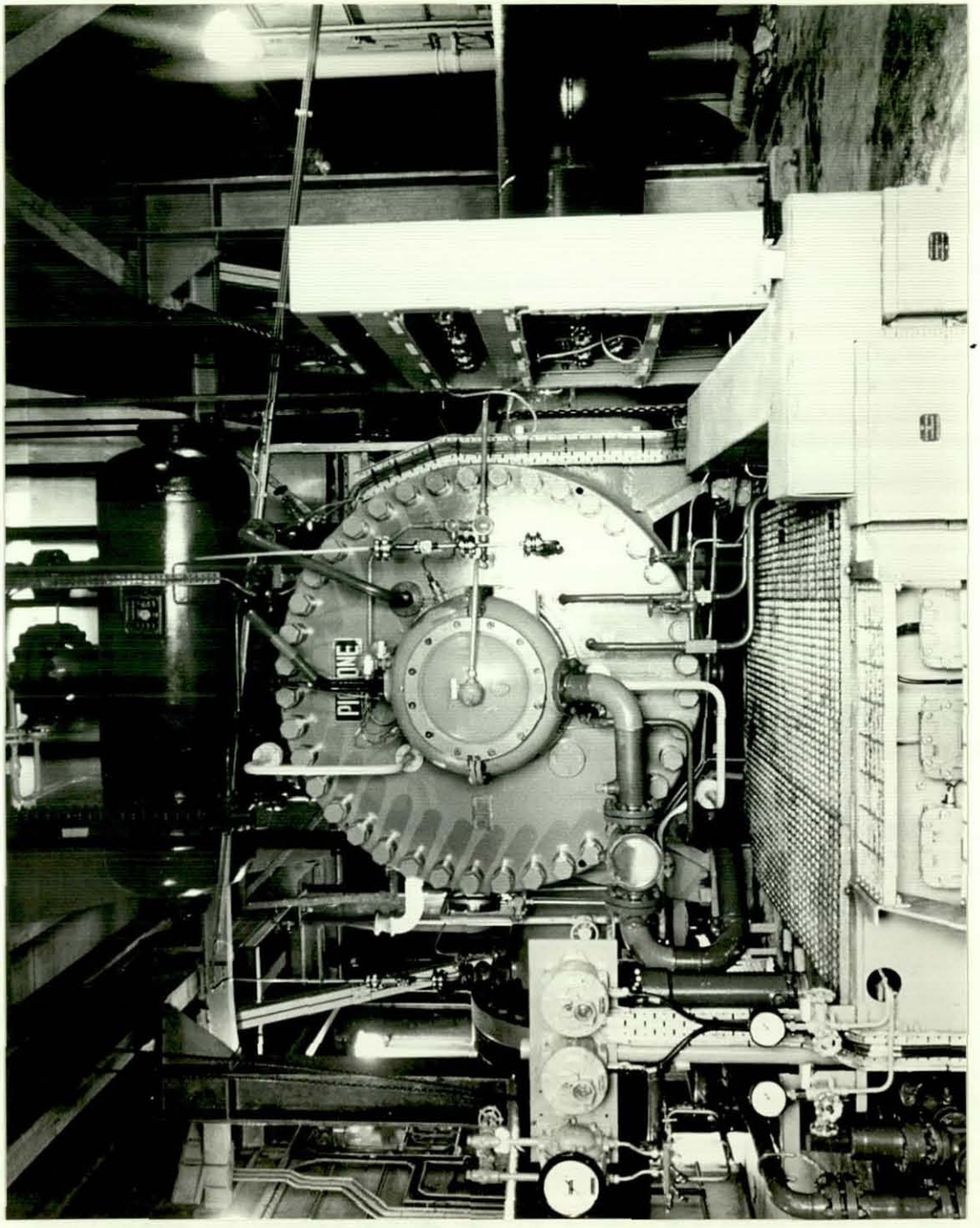

Plate 14.

Interior of the Compressor Station Showing
the 4m Diameter Backplate of the Compressor

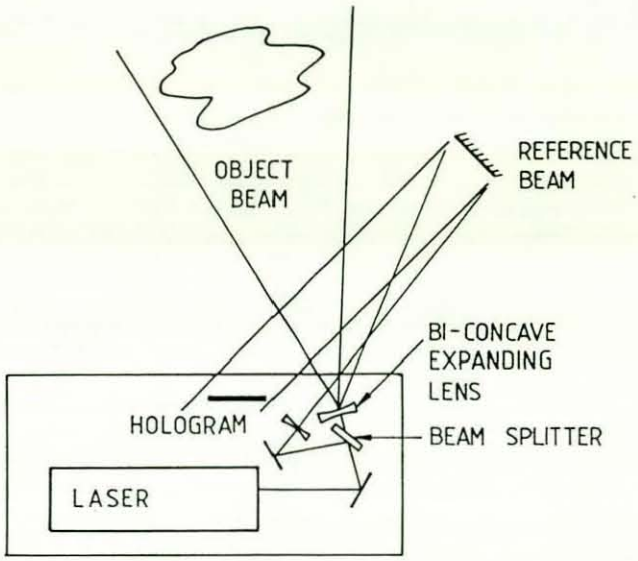

Figure 4.7
General Optical Arrangement Used at the Moffat Compressor Station

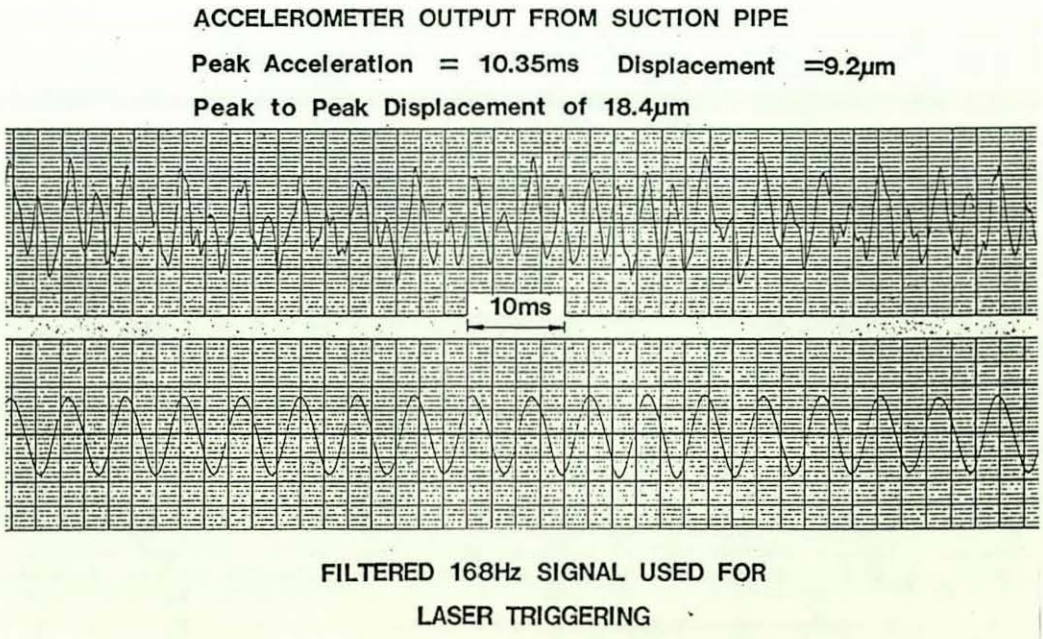

Figure 4.8
Filtered Accelerometer Signature Used for Initial
Pulse Timing of the Laser

4.4.1 Discussion of Results

Plate 15. The movement of the backplate of the compressor indicates a simple 'drum skin' panting mode although the source of this excitement is not readily observed.

Plate 16. The sequence shown appears to indicate the presence of a travelling wave set up between the two brackets which support the input feed pipe prior to coupling with the compressor. The results were obtained by changing the initial variable delay of the laser firing by upto ± 1.5 msec.

The maximum displacement observed is 48 fringes which corresponds to a displacement of;

$$(48/2) \times 0.694 = 16.7\ \mu m$$

This corresponds well with the measured displacement using accelerometers of 18.4 μm with an error of approximately 10%.

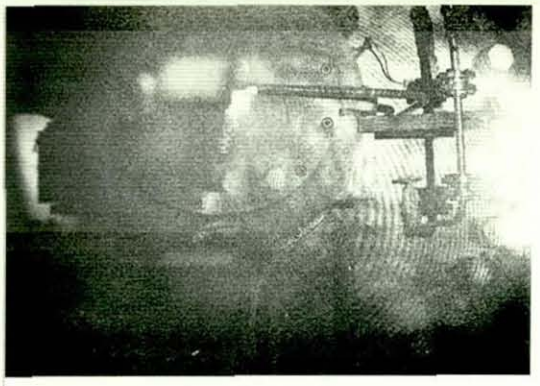

Fig. 2-1.

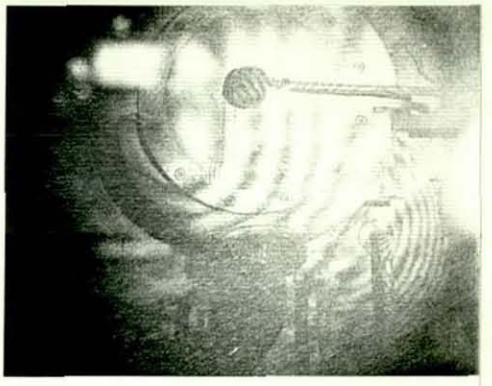

Fig. 2-2.

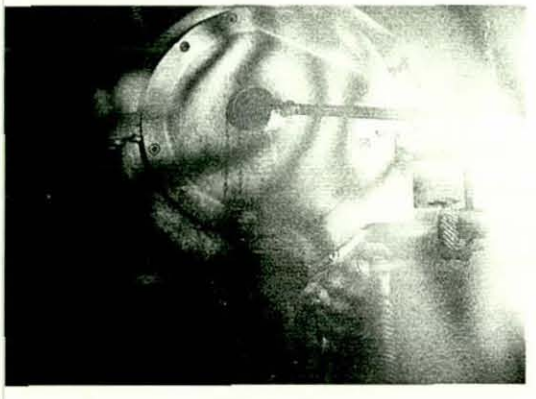

Fig.2-3.

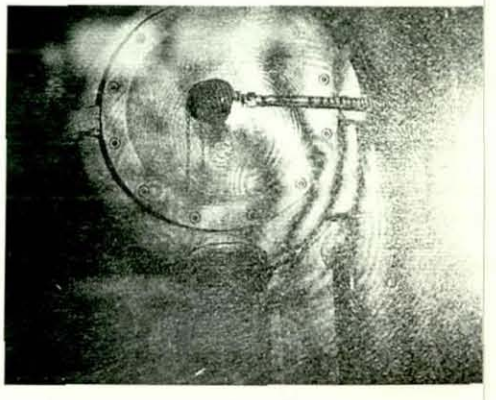

Fig. 2-4.

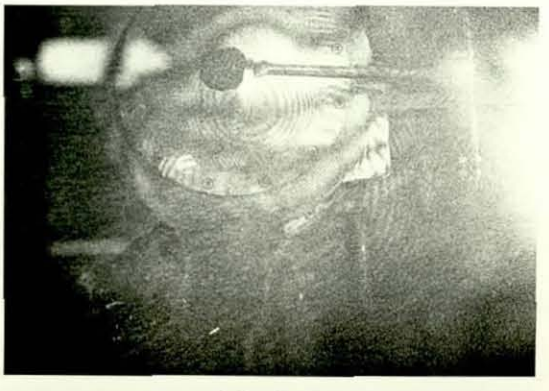

Fig. 2-5.

Plate 15.

Holographic Analysis of Backplate of Compressor

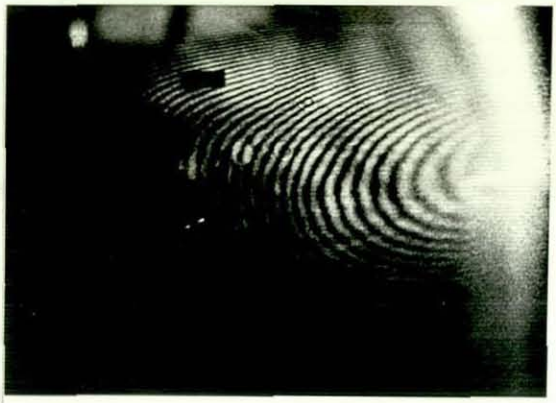

Fig. 1-1.

Fig. 1-2.

Fig. 1-3.

Fig. 1-4.

Fig. 1-5.

Fig. 1-6.

Plate 16.

Holographic Analysis of Input Feed Pipe with Varying Phase Delay to Laser Triggering

4.4.2 Error Analysis

With reference to Figure 4.9 and [6];

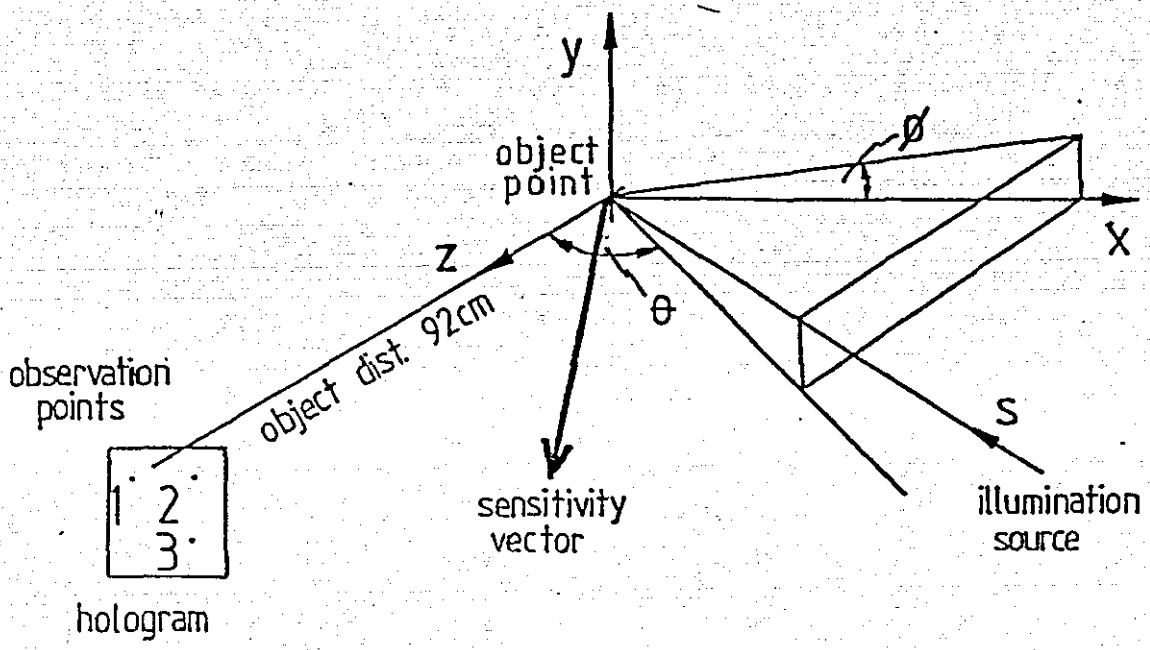

Figure 4.9
Generalised Viewing Arrangement of Pulsed Holograms
and Measurement Errors when Observations are made from 3 Points
(From Vest [6])

The errors associated with the three displacement vectors for the 4 x 5" Agfa 10E75 holographic plate are;

$$L_x = \pm 5\lambda, \quad L_y = \pm 7\lambda, \quad L_z = \pm \lambda/4$$

where $\lambda = 0.694\mu m$, therefore;

$$L_x \approx \pm 3.5\mu m \; L_y \approx \pm 4.9\mu m \; L_z \approx \pm 0.2\mu m.$$

4.5 Conclusions

This chapter has considered the use of pulsed holographic interferometry in an industrial environment. Successful studies using this technique led to better understanding of engineering problems and difficulties associated with the interpretation of data generated by this technique.

- The inherent low optical conversion efficiency of the ruby laser incurred problems which rendered it difficult to operate in anything other than a laboratory environment (See Appendix 2).
- Low sales volumes discourage the laser manufacturers from investing design effort to improve the operational aspects of the equipment.
- Replay of the holograms for quantitative analysis can be difficult with large image volumes. Argon ion pumped dye lasers can be used to correct for the replay distortions introduced with the change in replay wavelength.
- The short exposure periods inevitably led to high energy densities and consequently no focussed optical filtering techniques could be used to reduce optical noise introduced by contaminated optical surfaces.
- Holographic emulsions suffer from reciprocity law failure (as most photosensitive emulsions do), which further led to a reduction in photometric sensitivity by a factor of two.
- The working environment usually required darkness to minimise fogging of the holographic emulsion.
- Alternative recording media, eg. thermoplastic film, suffered from reduced photometric sensitivity at 694 nm as well as limited recording bandwidth, this in turn constrained the volume of the image recorded.
- The equipment could be used with careful optical design to record holograms in the most arduous and demanding industrial environments.
- In-situ examination of dynamic structural responses has proven to be a very powerful analytical technique which has been demonstrated as offering solutions to problems previously beyond the capability of conventional modal analytical techniques.

- Triggering of the laser from secondary transducers which synchronised the component motion with the firing of the laser enabled temporal, as well as spatial, examination of the structural response.
- Continual optimisation of the laser parameters did not facilitate change of the pulse separation period. Thermal lensing within the gain medium necessitated careful operation to maintain beam quality and repeatable intensities in each pulse.
- The size of the laser head, power supplies and associated control electronics mitigated against easy installation, thus making the system transportable compared with the portable requirements of some applications.
- The pulse separation period (10μs - >1ms) proved to be limiting with low frequency oscillations, <500 Hz. Peak to peak displacements of >20μm could be accommodated by minimising the sampled window of motion, thus interferograms could be made of transient events.
- Double pulsed holographic interferometry is a technology which will not find widespread appeal, despite the data quality and quantity, due to the problems associated with the laser equipment and the specialist knowledge needed in the design of the interferometer.

CHAPTER 5
ELECTRONIC SPECKLE PATTERN INTERFEROMETRY USING CONTINUOUS WAVE LASERS

5.0 Introduction

The successful use of Holographic Interferometry in providing complete engine dynamics studies as discussed in previous chapters, demonstrated the potential of this type of analytical equipment. It also highlighted problems which could not easily be overcome to allow the equipment to be developed into simple to use instrumentation. From the outset, this research attempted to identify the potential of wholefield interferometric methods for experimental analytical studies of engineering components. The use of television cameras within modified interferometers - pioneered by Butters et al at Loughborough - was identified as the approach most likely to produce instrumentation for industrial exploitation. The aim was to produce a self-contained instrument with in-situ working capability (as opposed to requiring pneumatically isolated optical tables) using pulsed lasers and providing automatic unambiguous fringe analysis. These objectives are dealt with in subsequent chapters. Previous attempts to commercialise equipment based upon Electronic Speckle Pattern Interferometry (ESPI) had failed due to; insufficient development, the relatively high cost of digital image processing electronics, under-engineered optical equipment, and limited applicability.

5.1 Background to Speckle and Electronic Speckle Pattern Correlation Interferometry

During the 1960's after the development of the laser and holographic interferometry, work began on studies of a secondary phenomenon of coherent illumination, that of Laser Speckle. Pioneered at the National Physical Laboratory at Teddington much activity centred on either the reduction of speckle, considered by most to be a nuisance and a problem to holographers, or using it in conjunction with low resolution recording media to perform interferometry. The basic speckle pattern image formation and background to speckle pattern correlation interferometry is given in Appendix 2.

A speckle pattern is observed when an optically rough surface is illuminated with coherent radiation. The reflection from the surface will be made up, as a wavefront, by a large number of reflections from the scattering points of the rough surface. Therefore at any viewpoint the surface will appear to comprise of a granular pattern made up from the coherent interference of all the individual scattering points on the surface. When the sources for this interference are not coaxial their interaction, across a scene, will produce a pattern which will vary in brightness across the scene (and within the individual speckle). It is not the objective of this work to attempt to modify the present theoretical models concerning speckle and its imaging. This is left to others, for example, Jones and Wykes [25], Montgomery [26] and Mendoza [27]. The objective of this work is to harness these models, where necessary, to enable the engineering of suitable instrumentation to proceed.

The speckle pattern can be combined with a uniform carrier wavefront to produce a phase referenced speckle pattern. The brightness distribution is affected depending upon the relative brightness of the speckle and the carrier (or reference) wavefronts. The combination of these two wavefronts will increase the overall size of the individual speckles by approximately two.

When observing speckle by eye, it will combine the light from a large number of scattering centres within the resolved area of view. This can be considered as multiple beam interferometry but because no reference position is available it contains little information of value. Groh [28] used this random pattern as a projection mask for fatigue analysis. A photographic negative of this pattern was positioned over the subject and as movement occurred the change in the object surface would shift the surface speckle and enable light to be transmitted, this could then be monitored via suitable sensors.

Hopkins & Tidbury [29] used a time averaging technique with a 35 mm camera recording the modes of vibration of vehicle body panels. The panels were coherently illuminated and whilst resonating were recorded with exposure periods much greater than the vibration periods. Areas of no movement recorded speckle patterns, areas of movements recorded speckle smears with the smear axis showing the surface velocity paths.

Archbold et al [30] reported in 1969 the first application of phase referenced speckle patterns. A small aperture within the imaging optics of the instrument produced a speckle pattern from an object coherently illuminated. A smooth reference beam, obtained from the same laser was added to the image and the resulting phase referenced speckle pattern observed by eye. When the optical path lengths and polarization vectors were matched, the intensity of speckles would be changed when the object surface was moved. The device has interferometric sensitivity and was proposed for vibration studies. In this case, when observing vibrating surfaces, the speckles would blur out (using the integration ability of the eye) in areas of movement and remain along the nodal lines. The instrument was initially known as a Laser Image Speckle Interferometer subsequently shortened to Speckle Interferometer. See Figure 5.1.

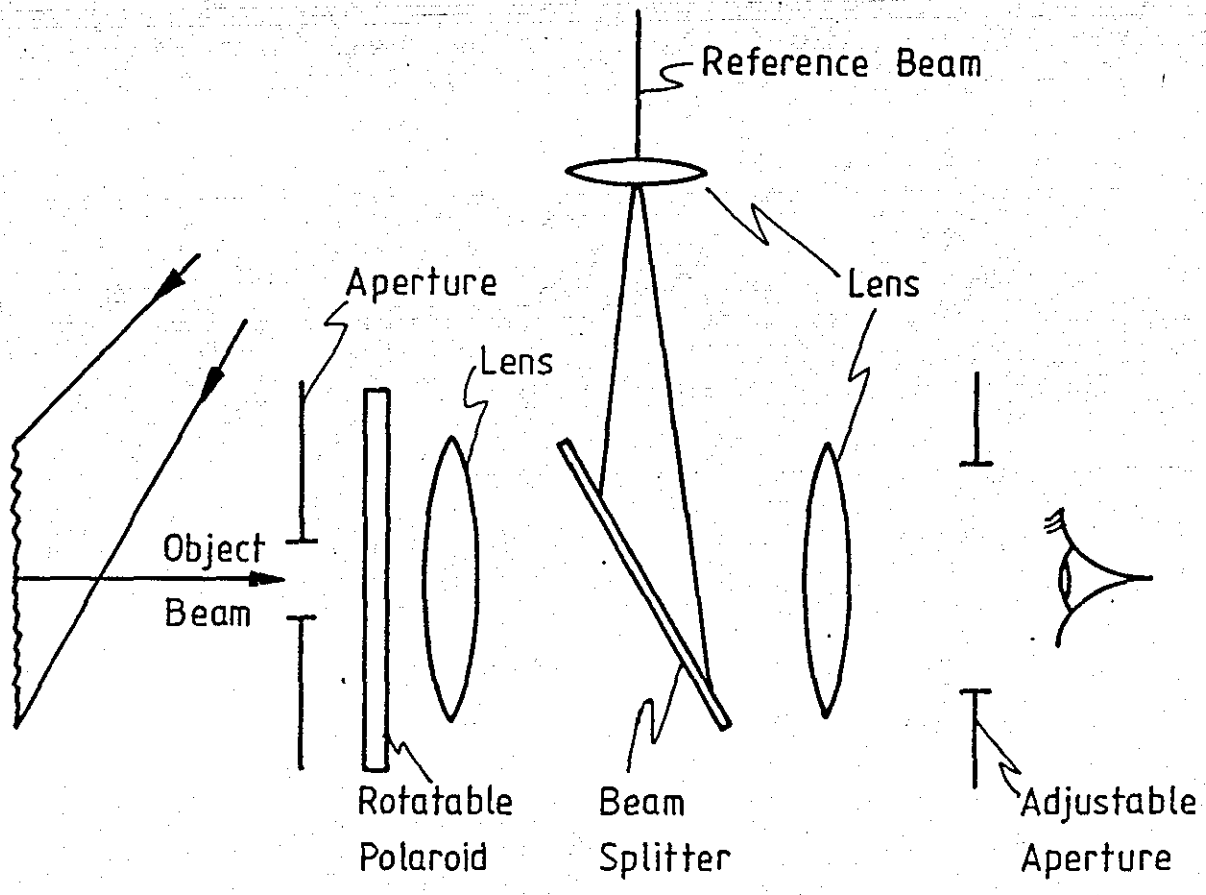

Figure 5.1
Out of plane Time Averaged Speckle Pattern Interferometer

Leendertz [31] developed a photographic process involving speckle interferometry for surface displacement analysis. Photographs of the phase referenced speckle patterns were made before and after surface deformation. A contact reversal of one of the images was then made and accurately aligned in contact with the other exposure (or performed in real time) providing a subtraction fringe pattern. A more convenient double exposure technique was simultaneously developed by Archibold et al at N.P.L. and Butters and Leendertz at Loughborough, though this used speckle addition with reduced fringe contrast. Burch [32] used optical Fourier filtering techniques to improve the fringe quality producing subtraction fringe patterns of higher visibility and definition.

The extension to include the video camera in conjunction with a speckle interferometer provided Butters & Leendertz [33] with a novel solution to problems posed by photographic recording. The combination of high photometric sensitivity and electronic processing provided a modified interferometer, which whilst unable to match the fringe quality of the Fourier filtered fringe patterns of Burch, generated fringe patterns in real time. A further innovation of Leendertz [34] was the combination of two illumination beams which provided correlation subtraction of in-plane speckle patterns.

To the author's knowledge ten companies in the US and Western Europe have attempted, or are presently selling, ESPI or ESPI type instruments; these include, Conspectum (Norway), Ealing Electro Optics (UK), EOS (German), Eumig (Swiss), Loughborough Consultants (UK), Newport Corporation (USA), Spectradata (German), United Technologies Research Centre (USA), Vibravision (Swedish) and Vinten (UK).

Of these, three companies account for most of the sales (60 at time of writing) Conspectum, Ealing and Newport. Eumig and Vinten are no longer available, EOS, Spectradata and UTRC are relative newcomers, Vibrovision has not advertised or promoted widely and is based on the work of Ek and Molin.

The Spectradata system is different from the rest with the incorporation of an in-plane system, Ealing have an in-plane option available. Ealing, EOS and Spectradata now have fringe pattern analysis software. Loughborough Consultants produce specialist equipment specific to problem solving based around the research at Loughborough University. Loughborough Consultants transferred technology from the University to Ealing, Newport and Vinten, they also assisted in the licensing of Conspectum for ESPI technology.

Other research groups have built in-house ESPI equipment which, because it is not marketed, does not require licensing from BTG. Industrial research groups who have attempted to build and utilise ESPI systems include; Jurid Werke (Germany) who have attempted to incorporate pulsed lasers and derotators to study brake problems on brake dynamometers, Rover Group to examine vehicle vibration, Westland Helicopters and Royal Aircraft Establishment, Farnborough, to examine delamination of composite structures and military establishments, eg MOD and US Naval Weapons to examine structural dynamics.

The technique of common path interferometry can be applied to most of the instruments to desensitize the equipment to local environmental perturbations. Løkberg et al [76] obtained high sensitivity results (1 nm) from human ear drums 'in vivo', a stroboscopic operation of an argon laser with an exposure period of 1 ms was used. The mark space ratio of the exposure period of a continuous wave laser requires higher average powers to be used. A review by Løkberg [77] expands on the application of stroboscopic illumination and demonstrates the ability of strobed results to provide high fringe densities (100 fringes across a television monitor).

The freedom from environmental constraints demonstrated by Cookson et al [51] using pulsed laser ESPI provides more efficient use of available energy but the practical constraints of the laser limited its industrial application. It is this background which directed the pulsed ESPI research.

5.2 General Description of Electronic Speckle Pattern Interferometry

The general arrangement for both the optical and electronic equipment is given in Figure 5.2.

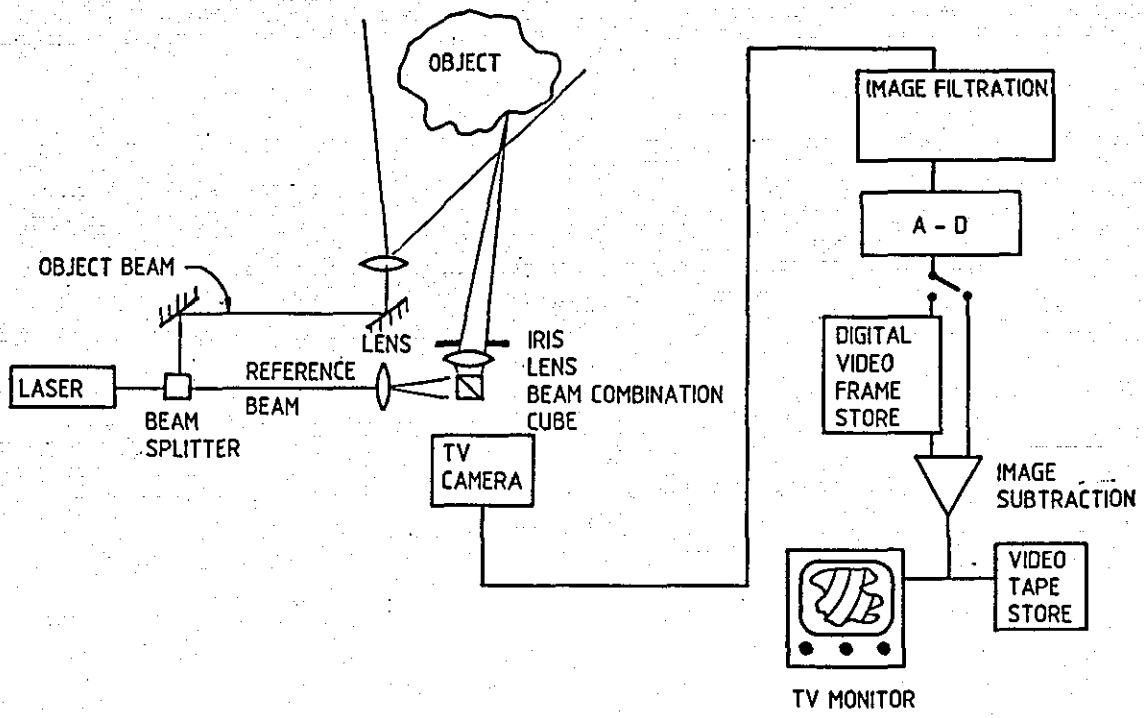

Figure 5.2

Schematic for the Optical and Electrical Configuration for An Out-of-Plane Sensitive Electronic Speckle Pattern Interferometer

The basic optical arrangement can be considered as a focussed image holographic system. The reference wavefront is mixed with the imaged wavefront using a beam splitter prior to the imaging sensor of the television camera. The object is illuminated usually with an expanding object beam whose axis is close to that of the axis of the imaging lens (see Section 4.2.2.1). These conditions sensitise the system for displacement along the axis of the imaging lens; i.e., out of plane (a similar holographic arrangement results in the observer seeing the object within the reference beam). The size of the speckles is governed by the size of the imaging lens aperture, thus enabling the matching of the speckles with the resolution of the television imaging sensor. The intensity of the resulting speckle interferogram then contains three main terms, from (1):

$$I = I_1 + I_2 + 2\sqrt{I_1 I_2} \cos \phi \quad \text{(see Section A2.3)}$$

The interference term $2\sqrt{I_1 I_2} \cos \phi$ is the information carrier in the video system and the other two terms can be considered as DC terms. The spatial frequencies of the interference term, when imaged by the television camera, range between 1-5MHz. Therefore filtration of the lower frequencies makes better use of the dynamic range of the video framestore. The enhanced signal can now be digitised (to a minimum of 8 bits to avoid degradation) before being stored in the digital framestore.

Every subsequent picture from the television camera undergoes similar processing, but bypasses the digital framestore and goes through an image correlator. Pixel by pixel correlation can be achieved by either addition or subtraction. The easiest way to achieve subtraction is to invert the live image and add the two images. Thus the addition of the inverted live image and stored image results in subtraction. Straight addition of the two images, whilst being identical with holographic double exposure or live fringe studies, does not make best use of the video system. The ability to subtract the two images enables static optical terms to be subtracted, furthermore any intensity variations across the image area

will be normalised. The result of the image subtraction is viewed on a television monitor after undergoing suitable re-configuration into an analogue video signal.

If the object generating the speckle pattern moves away from or toward the television camera the brightness of any individual speckle will vary cyclically from bright to dark to bright with every phase increment of π radians or $\lambda/2$ along this axis. Every speckle which undergoes this variation will have an independent initial intensity value because of the random nature of the speckle pattern.

The maximum number of fringes that can easily be identified across the image surface is approximately 40 and, whilst the system is capable of more, the fringe contrast begins to make visual perception difficult. Consequently the maximum displacement, using a helium neon laser (of wavelength approximately equal to 0.6μm) that can be considered at any one time is approximately 12μm. Displacements greater than this can be considered by simply readdressing the framestore at this maxima before continuing with the loading of the component. Obviously a record of this fringe pattern must be made prior to the new condition being made in the framestore. This 'staircase' loading technique can continue providing that a full record of all the stages is kept thus enabling an overall displaced shape to be eventually produced. Automatic fringe processing facilitates this (see Section 5.7). Since this is a correlation subtraction process, Denby, Leendertz [35] realised the potential for re-configuring the optics to provide a method of examining pure in-plane displacement.

5.2.1 Removal of Vibration Pattern Phase Ambiguity with Optical Phase Modulation

To overcome the problems of poor fringe visibility and loss of phase information, (as shown experimentally in Appendix 3), phase modulation within the reference beam can be introduced. This was reported by Lokberg and Hogmoen [36]. The simplest way of achieving this is to replace one of the passive reflective elements within the interferometer with one capable of being vibrated under both amplitude and frequency control. The object vibrates with amplitude $z_1(x,y)$ at point x,y and has an associated phase of $\phi_0(x,y)$. The vibrating mirror is oscillated with the same frequency f as the object but with an amplitude z_r and phase ϕ_r.

If the angle between the object illumination and observation is 5-10° then the image will be;

$$I(x',y') \alpha J_0^2 \left[\frac{4\pi}{\lambda}\left[z_0^2(x,y) + z_r^2 - 2Z_0(x,y)\, Z_r \cos(\phi_0(x,y) - \phi_r)\right]^{1/2}\right] \quad (42)$$

Therefore the maximum value will be reached when the phase and amplitude of the vibrating mirror match those of the object point (x,y). The value of this when trying to analyse complex fringe patterns is that areas of movement that are in phase will be easily identified. Consequently the phase relationship of these sites with adjacent areas of vibration can be determined by the phase change introduced with the reference beam. This technique is not only of value in vibration analysis but also in determining dynamic moduli of materials as reported by Rowland [37]. Stroboscopic modulation can be seen in Plate 17 where the relative phase between the two adjacent antinodes is 180°. Davies, Montgomery and Tyrer [38] used phase modulation, stroboscopic illumination and speckle noise reduction to analyse vehicle power trains and engines.

The usual method of exciting this mirror is to adhere it onto a piezoelectric crystal which is bonded onto the mirror support. Therefore this vibrating mirror is now a dynamic structure with its own associated resonant characteristics. Therefore the electronics controlling the amplitude and phase of vibrating mirror should take into account the system response. Tilt errors can also be introduced if care is not taken with the choice of the mirror within the interferometer. To remove the tilt and dynamic problems of the mirror an electro-optic transmission element can be used, the penalties here are higher driving voltages and cost. Experiments have been conducted with both systems, the former is favoured as suitable for the UART interface with the μVAX II computer system. For in-plane analysis one of the 45° mirrors can be vibrated.

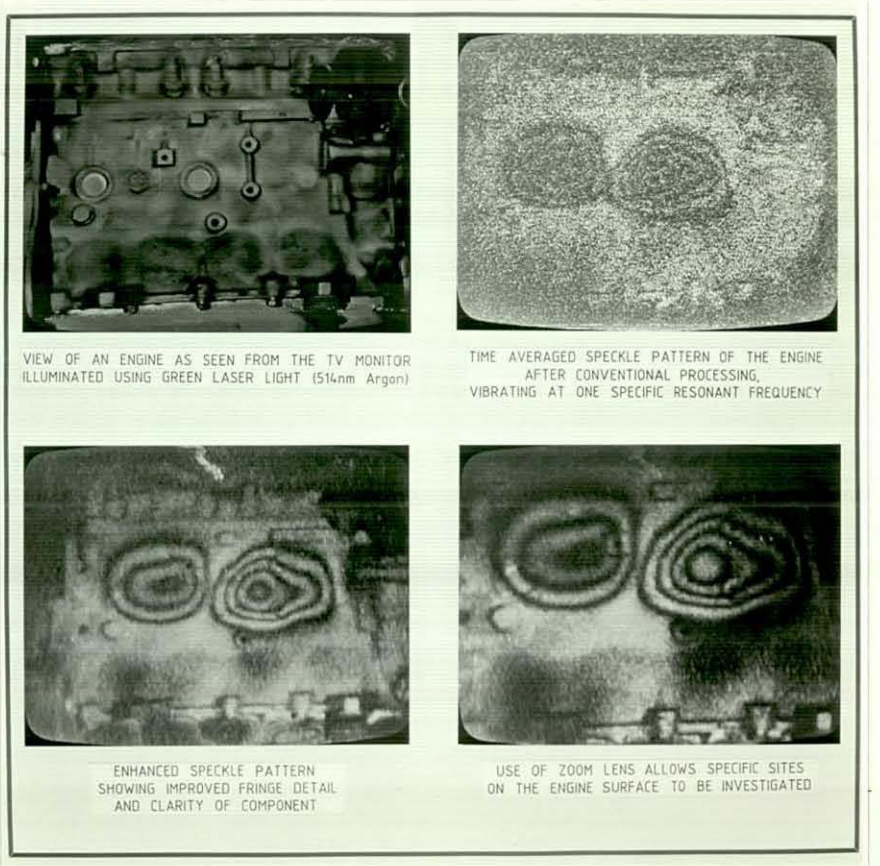

Plate 17.

Results from Stroboscopic ESPI Analysis of E-Series Engine with Speckle Decorrelation

5.2.2 Vibration Analysis Using Stroboscopic Techniques

As with Holographic Interferometry if the component is resonating with a higher frequency than the operating time of the television camera then a time averaged fringe pattern function will dominate. If the component response is imaged at specific timing points then a different interferometric sensitivity function can be used to describe the object motion. With large displacements (2μm and above) the Bessel function has reduced the fringe contrast to such an extent that observation is made too difficult, see Figure 3.3. The introduction of stroboscopic illumination originally reported by Pederson, Lokberg and Forre [39] changed the fringe function to a simple cosine^2 function. Therefore the fringe visibility is uniform over the whole object area.

As with stroboscopic holographic interferometry, the light pulses are usually synchronised with the peaks of displacement. Therefore the light modulation is at twice the frequency of the object vibration. The pulse duration is at most, 1/10th of the object vibration period. If the object motion produces too many fringes for good fringe contrast it is possible to work on sections of the sinusoidal response curve other than the peaks.

The resulting image will be described by,

$$I(x,y) \alpha \cos^2 [(4\pi/\lambda) z_0 (x,y)] \qquad (43)$$

With stroboscopic illumination and speckle noise reduction techniques it has been possible to image speckle fringes of 5 pixels width. The result shown in plate 18 was magnified using the zoom facility of the image processor to reveal a total fringe width of 5 pixels, around the four nodal extremeties. This suggests the system is capable of imaging over 100 fringes across a 512 pixel video picture. Assuming the basic Nyquist sampling requirements, it is suggested that the system could be able to image fringes 3 pixels wide within the aliasing constraints.

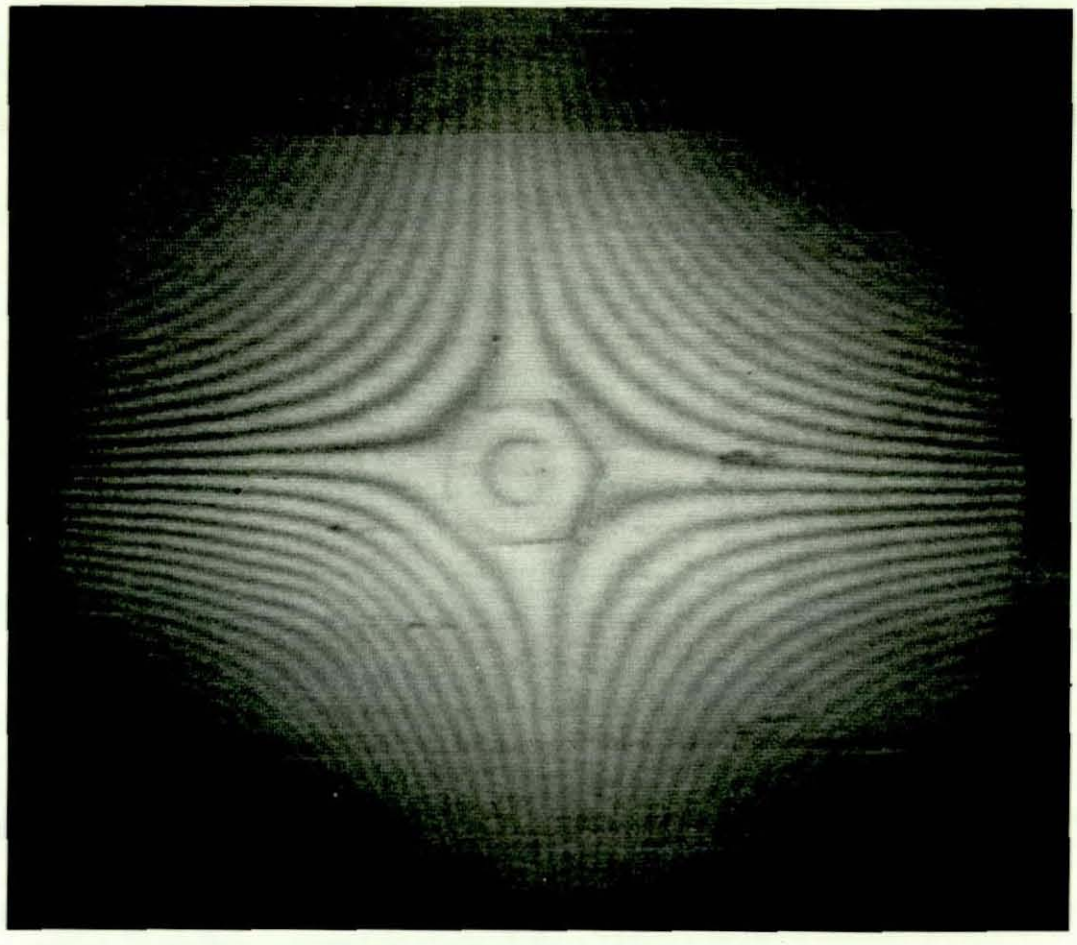

Plate 18.
Photograph of Digitally Averaged Vibration Pattern of a Centrally Mounted Metal Disc Resonating at 1.2kHz

A consequence of the stroboscopic illumination mark space ratio is the overall reduction in component illumination and to offset this light level reduction, more laser power is required. Clearly the interruption of a continuous beam is not optically efficient or cost effective. An alternative approach tried utilised the instantaneous extraction of the entire stored energy within the laser cavity to momentarily illuminate the surface. Such an approach was attempted using a cavity dumper supplied by

Coherent UK Ltd. The cavity dumper was used in conjunction with an Innova 90-5 argon ion laser and produced pulse energies of around 0.55μJ per pulse. The device worked by replacing the output mirror (typically 90% reflective) of the laser with one of 100% reflectance which could tilt via a piezoelectric transducer and allow the entire output of the laser tube to be removed as a pulse of energy. This approach depletes the excited population within the laser cavity requiring re-energisation before the next pulse can be extracted. Unfortunately the device relied on removal of the output mirror from the laser and the alignment of this external cavity system onto a pre-machined base linking laser and cavity dumper. The demands for continual alignment of the system during and prior to operation rendered the experiment impractical.

King at Loughborough has successfully demonstrated stroboscopic modulation of a 20 mWatt diode laser by modulating the power supply. The coherence length of the laser during continuous operation was greater than 1 metre but dropped to less than 5 mm during pulsed operation. The construction of the diode laser did not lend itself to interrupted operation, the thermal characteristics of the device being dramatically reduced, limited its useful operation for interferometric purposes. Frequency doubled YAG lasers have been successfully used to generate stroboscopic illumination even though the pulse duration was typically 10-20 nsec. This work is more fully covered in the next chapter.

5.3 Design of New ESPI Processing Electronics

The combination of a television camera with a Speckle Pattern Interferometer was achieved by Butters and Leendertz [33]. This arose from the need to simplify holographic arrangements to enable measurements to be made in real time. This combination enabled the data to be obtained optically and processed electronically. This combination produced an instrument technology with exactly the same

sensitivity as holographic interferometry but without the inherent photographic needs. This instrument has been named the Electronic Speckle Pattern Interferometer, with the acronym ESPI. In this work ESPI will refer to both the interferometer and to interferometry.

The optical arrangement for ESPI is identical with that of Speckle Pattern Interferometers and for non-destructive testing it can be used for the same applications as Holographic Interferometry. The major feature of ESPI is that it enables real time operation with the resultant fringe patterns being displayed on a television monitor. The usual requirements for photographic processing and plate relocation are dispensed with as is the need for a second image transducer to record the fringe pattern.

The advantage of a television camera in being the primary image transducer is that it enables the fringe position to be accurately digitised without the errors introduced by the second imaging system as necessary in holography. Subsequent errors in the image processing of the fringes can be related to the precision of the television camera (CCD arrays having the best geometric precision).

With ESPI the picture is an intensity map produced by a phase referenced speckle pattern. Subsequent video processing of the picture can be used to enhance the interference term and remove the remaining non-contributory object and reference beams. The correlation process can be performed by either addition or subtraction and to achieve the correlation one image must be retained within the system. Originally video tape recorders were used as the image store but these are now superseded by digital framestores.

Initially, large digital framestores manufactured by Pantak using discrete 16 Kbyte memory devices were used. The framestore consisted of 96 memory integrated circuits which made up the 512 x 512 x 6 bit digital video framestore. Subsequently this was superseded by a stand alone single board framestore manufactured by FOR-A, again of 512 x 512 x 6

bit construction, but utilising only 24 x 64 Kbyte memories. The analogue electronics used previously on the larger Pantak system was reduced such that three piggyback daughter boards could be added to the FOR-A system making a stand alone ESPI subtraction system. This was then commercialised by J.D. Jacksons who now supply Ealing Electro Optics with complete systems. Further development replaced some of the analogue technology with digital techniques. This approach still proved to be time consuming in setting up and the final picture amplification resulted in poor use of the dynamic range. It was necessary to further improve the signal conditioning and reduce the calibration and set-up requirements of these additional circuits. Experiments into maximising the speckle frequency signal content using optimised bandwidth filtration were conducted utilising the Kontron high resolution digital image processing system. The results of this work were then implemented into a single digital pre-processor daughter board which plugged directly into the host mother board of the FOR-A. This technology was commercially exploited with licence arrangements and supply of circuit boards to Newport Corporation.

Further research concerning the extraction of optimised ESPI fringe contrast has concentrated on the filtration techniques which work on single lines of the television picture. New designs have enabled subtraction and floating low frequency filtration to work on each television line. Thus low frequency detail, including any daylight or non coherent image content, is locally filtered out. This approach renders the system insensitive to intensity changes across the image area. A further advantage is the ability to provide total daylight immunity without requiring global averaging filtration which introduces the inevitable loss of speckle signal. The Daylight Immunity Device (DID) has an optimised bandwidth filter of 1.1 - 5 MHz which is maximised around 1.5 MHz. The DID is a self-contained preprocessor system which can be used in conjunction with any of the ESPI electronic systems.

For a more complete analysis of the DID, please see Appendix 4.

Finally, the move to computer processing of the fringe pattern required, the combination of ESPI pre-processing electronics with computer addressable framestores. After performance trials of all IBM compatible framestores, the Imaging Technology IS100 was chosen, this sits on the host bus of IBM-AT and IBM compatible microcomputers. The pre-processing electronics consists of a "half slot" board which plugs into the host bus adjacent to the framestore. The IS100 can be configured as either a one 512 x 512 x 8 bit or two 512 x 512 x 6 bit framestore and utilises twelve 256 Kbyte memory devices. By way of comparison, storage of a single 512 x 512 x 6 bit image would require 6 such memory I.C.'s as compared with the original 96 for the Pantak. Consequently these new designs have given; better fringe contrast, a considerable cost saving, improved facilities and increased equipment reliability.

5.4 Electronic Speckle Pattern Decorrelation

During 1984 discussions took place with Newport Corporation concerning the potential exploitation of ESPI. It became apparent that marketing of such optical instrumentation would be prejudiced because of the relatively low fringe quality compared with Holographic Interferometry and unless the fringe contrast of ESPI could be brought to near holographic quality it was suggested no American market would exist. An idea put forward by Pinnow of Newport Corporation compared the problem with that of fibre optic communication which led him to suggest that ideas used for coherent noise reduction in fibres may be applicable to ESPI. Simultaneously, Montgomery at Loughborough had independently proposed analogue electronic fringe improvement [26]. It was therefore timely to combine efforts with Montgomery to attempt fringe enhancements. The approach of the author was to concentrate on digital pre- and post-processing of ESPI images, while Montgomery concentrated on the necessary optical hardware and develop analogue systems. Initially, a Microconsultants Interlect 100 image processor was

loaned to the author for various N.D.T investigations. This led to the loan of a Trappix 55/256 which produced the results shown in Plate 18.

If an interferometer is used for vibration analysis in an environment where fringe drift is encountered, then simple picture integration over some time period (usually expressed by the number of image frames) can be advantageous in minimising the contribution of the ambient fringe position to any fixed fringe pattern. Alternatively, when using the FOR-A store a facility provided is to continuously update the framestore and thereby subtract the previous image from the current one. Any long time varying drift will be continuously subtracted away from the steady state vibration fringe pattern. Integration here of the output will yield a vibration fringe pattern with some immunity to environmental drift. However, the fringe visibility will be fixed by the underlying speckle content of the image beam.

Speckle noise in ESPI is very similar to the granularity problem in holography where the use of coherent light introduces granulation in both the recording process and reconstruction. Martinssen and Spiller [66] discuss the problem and conclude that speckle reduction is not possible at the recording stage by continuous speckle decorrelation because the granulation is the information carrier. An alternative is to ensemble average a number of different speckle images each containing the same fringe pattern. In ESPI the speckle pattern cannot be moved significantly during a single frame otherwise incoherent imaging would result. Nakadate et al [67] average an ESPI shearing pattern over 60 frames to increase the signal to noise ratio of their video images by reducing the time variant electronic noise. The principle of ensemble averaging of random noise is not new and is commonplace in radar and telecommunications. Speckle decorrelation can be obtained by altering one or more of the following parameters; viewing direction, illumination direction, laser wavelength, introducing a phase change to the illuminating wavefront or the scattered light from the object. Slettemoen [68] suggests changing the viewing direction using a rotating

double slit aperture, movement of the aperture by its own width would completely decorrelate the pattern. Lokberg & Slettemoen [40] suggest an easier method of object beam tilt. Creath and Slettemoen [69] subtract the stored pattern of a vibrating object from the live pattern of the vibrating object and introduce a π phase change between reference and object beams.

The speckle averaging makes use of the integration features available within computer based framestores and a rotating diffuser screen. Diffuser screens have included a double back-to-back type using commercially available diffuser glass, though the optimum was found to be a disc of acid etched diffuser glass attached to a geared down 12 volt d.c. electric motor. Montgomery [26] has shown the necessary translation speed of the diffuser to be within the range of 10-40μms^{-1}.

The benefit of digital manipulation of individual speckle images should increase the utility of this technique and require far fewer images than were required for the simple integration examples shown.

5.5 New Optical Design of Interferometer

A previous attempt at commercialisation of ESPI technology had taken place with a licence arrangement with Vintens Ltd.. The optical arrangement is shown in Figure 5.3.

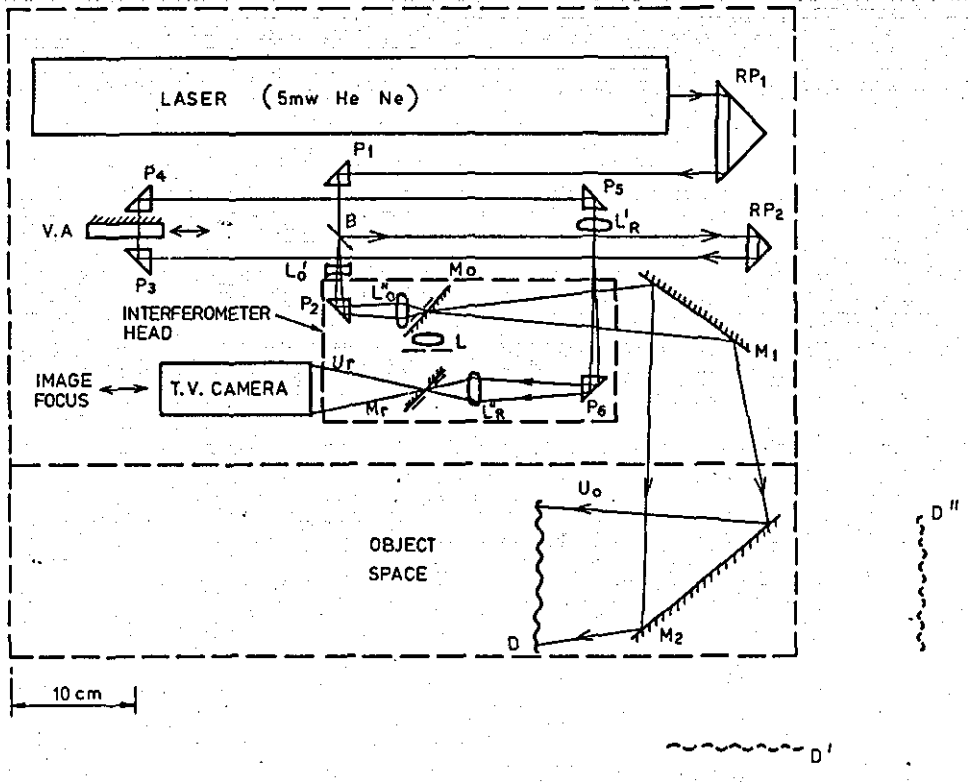

Figure 5.3
Optical Arrangement of the Vinten ESPI

As can be seen, the arrangement is costly because of the number of optical elements used, the complex layout caused consequent alignment problems and suffered poor performance due to optical losses and optical noise. The weight of the unit required two men to lift the interferometer. No opportunity for reference beam path length compensation was provided and operation was achieved on multiples of the laser coherence length. Fixed focus, single element imaging lenses were used which required the television camera to be translated for final focussing of the object.

The concept of the "hole in the mirror" illumination and observation (M_1 and M_2) is one technique intended to maintain conjugacy of the object and reference beams. Unfortunately, it is difficult in practice to use and also presents considerable manufacturing problems. It was therefore not surprising to learn of Vinten's poor sales performance.

Fundamental to any in-service operation of an interferometer is simplicity of design and consequent use. Experience gained in attempting to implement ESPI within the automobile industry, enabled a list of primary and secondary design specification to be produced.

5.5.1 Instrument Specification

Primary Objectives

- Ease of operation by non-specialist operators,technicians.
- Low maintenance. (Enclosed optics to minimise cleaning requirements-service call 1/annum).
- Minimal operator realignment. (Limited to adjustments of; object area, focus, path length compensation and beam ratios).
- Variable image area. (Use of interchangeable zoom imaging lenses).

Secondary Objectives

- Cost. (Less than £30K, identified by market research).
- Size and weight. (Easily man manageable).
- 240V operation. (Requiring no special services).
- Capable of accepting alternative laser sources. (Argon Ion),
- Expandable to include: stroboscopic illumination, phase modulation, speckle decorrelation and contouring.

5.5.2 Initial Concept

Instruments designed by Bergquist and constructed by Roulstone, had concentrated on turret lens construction to provide some degree of variable imaging capability. Extending this principle led to the incorporation of a variable zoom lens as used by small format, single lens reflex camera manufacturers. Advantages of this approach yielded high quality, low cost optics designed for operation with a stand off from the film plane of ≈45mm. Use of Zuiko (Olympus) lenses confirmed the suitability, leaving sufficient access behind the lens for the reference beam combination optics. The arrangement still provided well corrected imaging onto the television camera. The use of 1° wedge beam combiners had been common place as the alternative to the "hole-in-the-mirror" arrangement. However, this introduced astigmatism into the focussed image. A pellicle beam combiner was tried, (a thin plastic membrane), but was found to be highly susceptible to airborne acoustic energy which resulted in dynamic excitation of the beam combiner. Finally a 25mm cube beam splitter, initially 50:50 (transmitting:reflecting), finally, 95:5 ration was used to provide high quality object and reference beam combination. An arrangement for minimum number of optics is given in Figure 5.4.

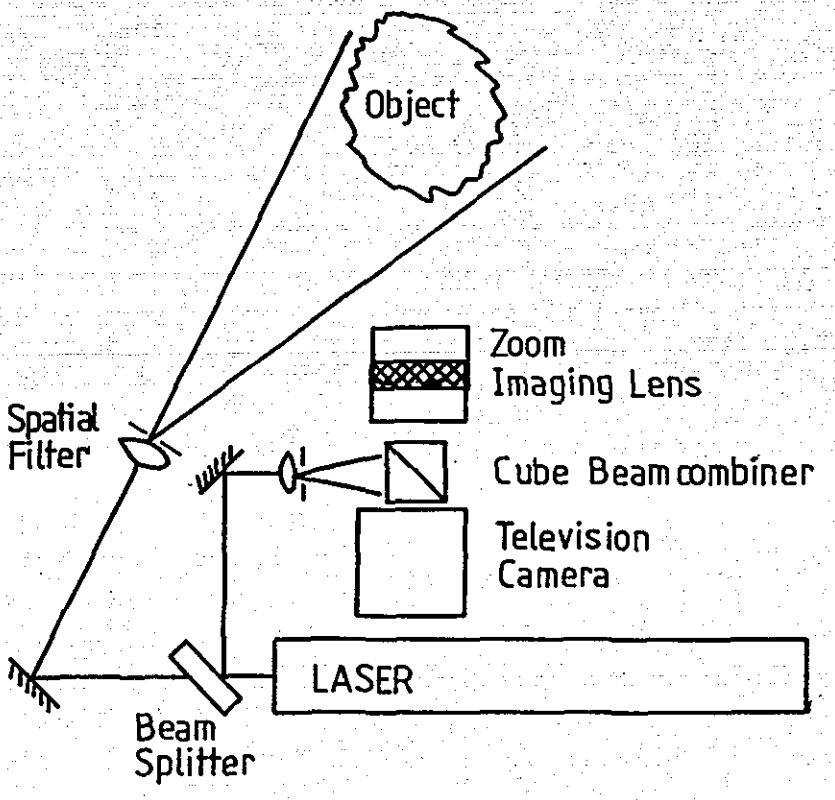

Figure 5.4
Arrangement for ESPI with Minimal Optics

The spatial filters are not obligatory, though the improvement to fringe quality, due to uniform local intensity, is considerable for time-averaged vibration studies. Similar to the Vinten design, object location is dependant upon multiples of the coherence length of the laser used. Montgomery [26] has experimentally analysed fringe contrast from these designs and shown for the first five coherence planes that the fringe contrast was uniform.

In practical terms, the ability to initially optimise object illumination and then match the reference path length has many advantages, notably: ease of set up, reduction in set up time and removal of coherence measurement errors. The ability to dial up necessary compensation and adjust by visual confirmation from the television monitor is of value to the operator.

Changing the axis of the laser to match the television camera with a steering mirror, whilst introducing a further optical surface provides: compact design, ease of initial alignment, room for auxiliary optics and the input mirror for a second laser. The final design shown in Figure 5.5 was presented to all commercially interested parties.

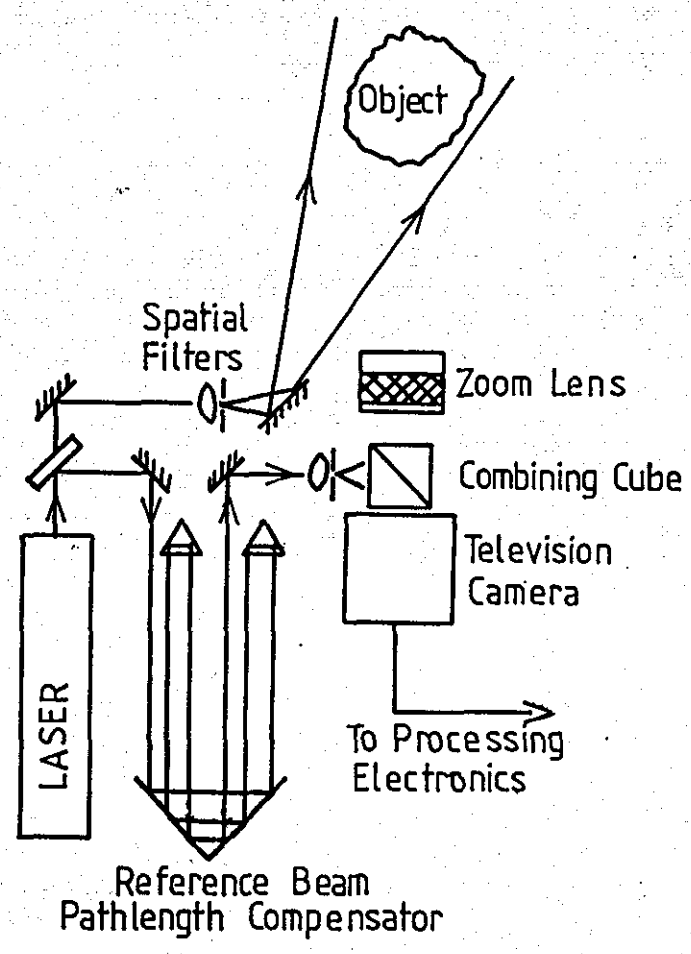

Figure 5.5
Modified ESPI Arrangement for Out-of-Plane Studies

The design of the reference beam path length compensator used a 150mm travel linear translation bearing with a maximum horizontal runout of greater than 1μ over the travel. NPK of Japan provided a single rail of suitable specification such that after five or seven passes of the compensator the laser beam would still focus through the reference beam spatial filter pinhole. The moving carriage of the compensator carried the smaller prisms in an attempt to minimise changes of load along the length of the high precision ground rail. Individual tilt and rotation of the prisms allowed for initial alignment, a fixed target array was used for alignment purposes.

To facilitate object illumination, a final object beam steering mirror was introduced to allow manipulation in both horizontal and vertical axes. Here problems were encountered with conventional commercially available mirror mounts. The requirement was for a compact mirror which could be adjusted from above, and once adjusted, locked off in position. This led to the design of a novel mirror mount which as a kinematic principle has now been applied to various optical mounts.

5.5.3 Novel Mirror Mounts

Examination of commercially available mirror mounts, Figures 5.6 and 5.7, show them both reliant on the precision of the operating screw threads for angular precision, and thread straightness of lack of axial crosstalk. Examination of the former showed itself to have high susceptibility to axial crosstalk (in x and y axis) when used to tilt a laser beam independently in the x and y axes. The runout was primarily a function of thread straightness and the precision by which the ball end to the thread had been applied. Furthermore, neither design lent itself to vertical actuation. The need for optical alignment without introducing dust required a transparent cover which itself could protect the internal components but could be penetrated and sealed by the adjustment screws.

Initial ideas concentrated on taper ended screw threads and moving wedges. Both became expensive to manufacture and still relied upon the thread precision and straightness. The final design was published by Bramley, Roulstone and Tyrer as Patent Number 8529687. The novelty being derived from the ball on ball motion to transfer vertical operation to horizontal movement by means of the contacting tangent between the two ball diameters. Thus with both balls fixed in opposed tubes the motion could be transmitted through the angle between the two tubes. A further advantage is gained when balls of different diameters are used. In this instance the transmitted motion is factored as a function of the square root of the difference of squares of the ball diameters, ie. either a magnification or reduction to the operating screw thread pitch. The design as shown in Figure 5.8 overcomes the axial crosstalk of the screw thread and enables vertical actuation. This mechanism of displacement was also adopted in the construction of spatial filters. The reduction in operational volume of the device means that stacking of components in compact trains and positioning devices in corners of boxes is possible. To date, one licensee, Ealing Electro Optics PLC., has undertaken manufacture of these mirror mounts.

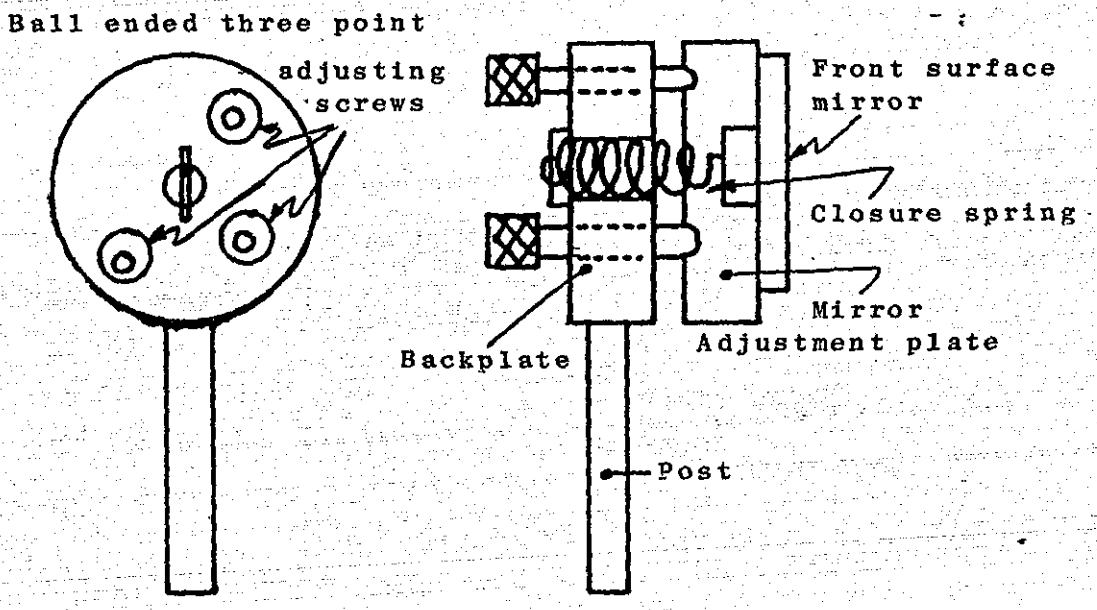

Figure 5.6
Typical Design of Screw Operated Tilting Mirror Mount

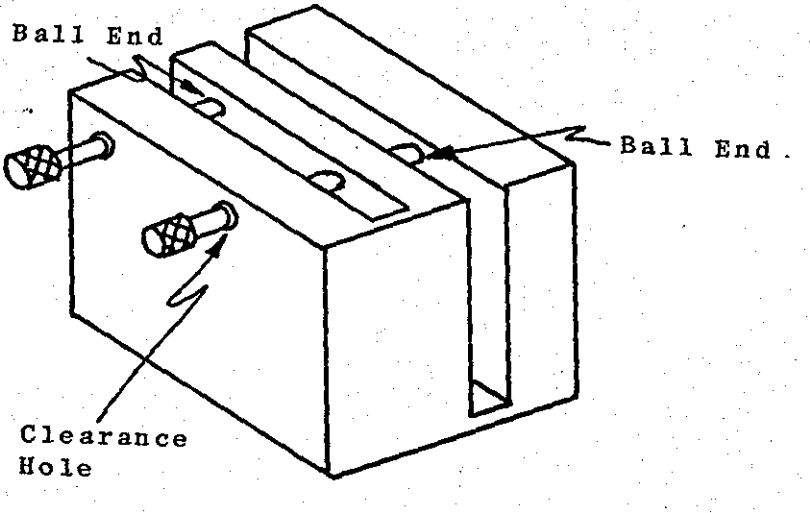

Figure 5.7
Typical Design of a Flexural Plate Mirror Mount

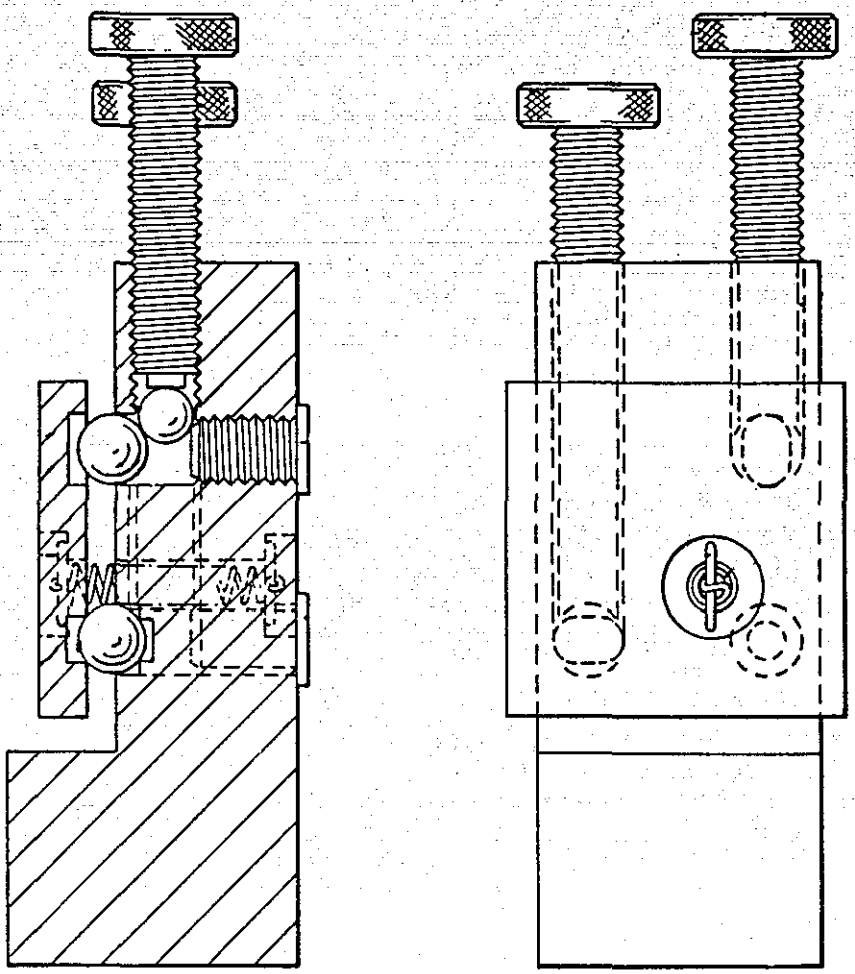

Figure 5.8
High Precision Kinematic Mirror Mount
Employing Novel Vertical Actuation

5.5.4 Final Design of Continuous Wave Optical Head

Based on the experience gained from the previous designs, a specification for a new optical head was produced. It was the intention of this specification to combine all the attributes of recent inventions as well as providing an integrated test bed to evaluate performance of two different method of reference beam phase modulation. The need was driven by the fringe pattern analysis work (see next section), which required a system capable of being interfaced to the host mini computer. The specification considered operational and facility features. The final specification is given below:

OPTICAL HEAD

OPERATIONAL FEATURES

- On board Helium Neon laser.
- Interchangeable zoom lens.
- Vertically adjusted spatial filters with removable pinhole carriages.
- Transparent dust shield.
- High strength of weight ration.
- High base internal damping.
- Thermal barriers and enclosures.
- All components rigidly mounted to base.

FACILITY FEATURES

- Stroboscopic illumination using either mechanical or electro-optic shutters.
- Phase modulation of reference beam using either piezo electric mirrors or electro-optics delays.
- External laser input, argon ion.
- Rotatable output mirror for decorrelation.

The final outline is given in Figure 5.9. The base utilised an aluminium honeycombed composite of 50mm thickness onto which was bonded a mild steel skin on both sides to minimise any differential expansion. The steel skin formed the fixture base which was marked out and finished prior to final bonding onto the aluminium. The laser was mounted using two collars which were positioned using posts of suitable height. The laser

was additionally enclosed with aluminium plate and a separate vented lid to minimise thermal input into the interferometer. The working height of the interferometer was determined by the reference beam compensation leg. The centre height of the prisms on their adjustment sled and fixed to the moving carriage of the NPK rail was considered to be the tallest of all the components.

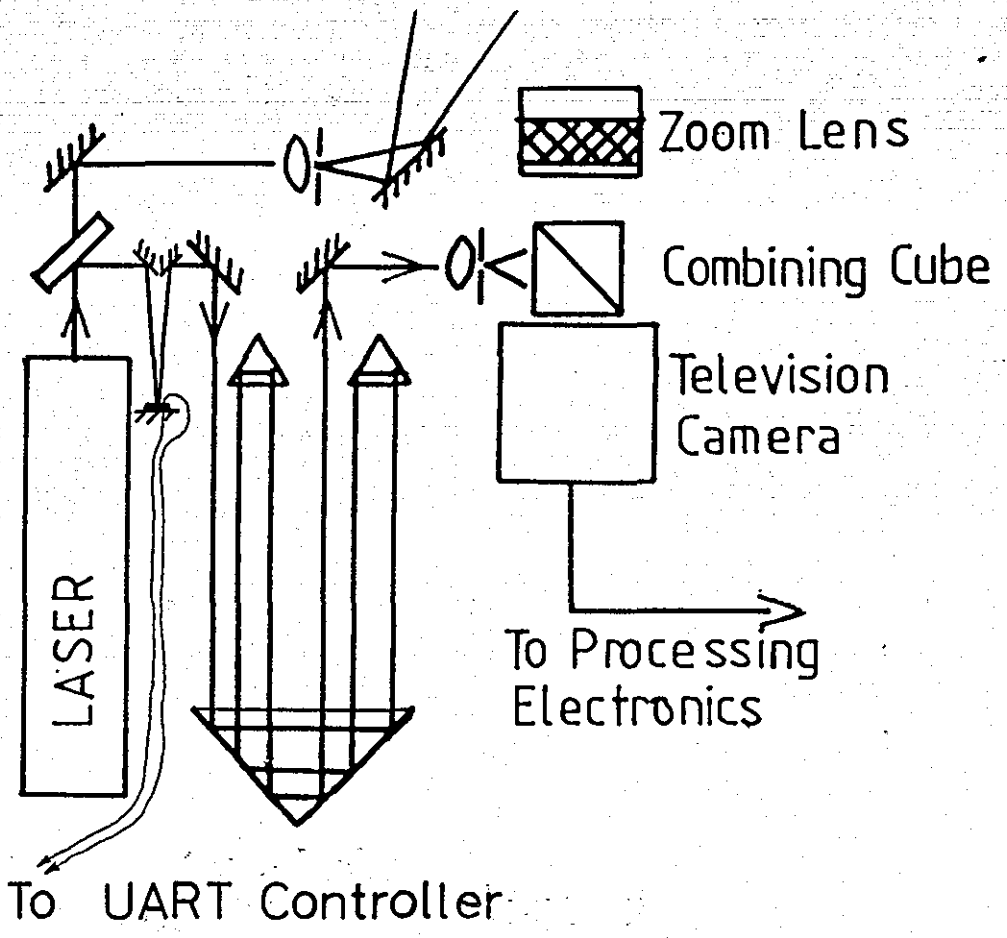

Figure 5.9
Continuous Wave ESPI System with Computer Interactive Optical Phase Stepping

The television camera initially chosen was a high resolution (1254 lines), extended red super chalnicon manufactured by J.D Jackson. This was fixed onto a focussing table, which could be moved axially via the focussing screw. A low profile, aluminium, single rail construction was chosen. A milled vee groove on either side of the rail provided the location. The television camera height controlled the overall height of the system.

All optics that required adjustment were manufactured with vertical operation (previously described), thus all adjusting screws were elongated to penetrate through the transparent dust shield. This permitted optical alignment without the ingress of dust. The spatial filters (object and reference beam) whilst having x and y adjustment of the pinhole were not provisioned with vertical z adjustment of the focussing lens as the horizontal adjustment was sufficient. For quick alignment checks (necessary when an auxiliary laser is being introduced), the entire pinhole carriage can be removed beneath the base plate of the spatial filter.

Interfringe interpolation accuracy is determined by positional error of the phase shift within the reference beam. In an attempt to determine this experimentally, two methods were conceived;

1. A mirror mounted onto a piezo electric translator.
2. Variable electro-optical delay crystal using the pockel effect.

The consequence of such an approach is shown diagrammatically in Figure 5.10 and 5.11 with a lateral translation of the beam leading to a percieved component of tilt to the interferometer.

Schwider et al [70] have considered these in more detail, in particular the errors associated with the precision of the applied phase, extraneous fringes and optical noise. Here the work is concerned with a Twyman Green interferometer in an attempt to determine phase to within $\lambda/200$. The ability to repeat and average determinations enable precisons on fringes of high contrast to be successfully obtained. In this work the emphasis is toward the rapid acquisition of data from events which may not be repeatable.

Cheng and Wyant [71] examine the sensitivity of a phase shifting interferometer to non-linearities in the piezo electric tranducer and calibration errors. Using a 4 phase shift method of $\pi/2$ increments (each labelled A, B, C, D respectively) an initial phase determination can be made using A-C, and a second determination using B-D, an average is then taken of the two. Non-uniformities in the PZT are also considered and they examine the need for better calibration and compensated algorithms. The approach taken was to utilise piezo-ceramic crystals for the phase shifting transducer which exhibit the combined advantages of low driving voltages (a 10 volt range being adequate) and improved manufactured linearity. In the manufacture of these elements significant bulk shrinkage (70-80%) of the component volume during firing leads to inhomogenities within the crystal.

One technique to minimise the effects of non-linearities associated with this manufacturing process is to segment each crystal into thirds. A composite crystal is then made by combining three matched segments, which provides more uniform transalation characteristics. Such a crystal was purchased and used in this work.

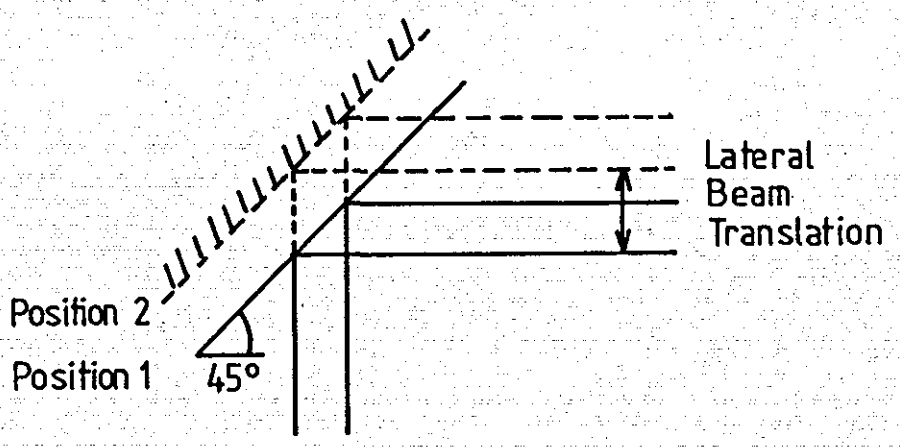

Figure 5.10
Lateral Beam Translation with a 45° Moving Mirror

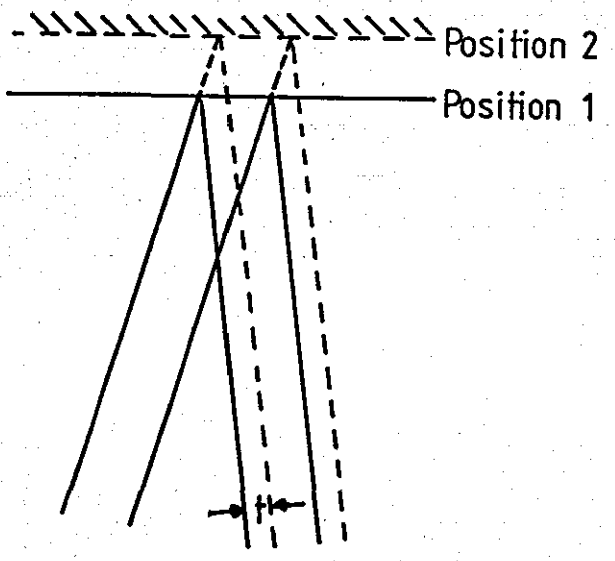

Figure 5.11
Reduced Lateral Beam Translation Using Acute Angle Reflection

The quality of the piezo device governs the overall accuracy, high precision devices are composite structures made up from three wedges of material. The performance of the elements is matched prior to assembly, thus a uniform linear translation of the mirror takes place. Recent piezo capacitive devices have been acquired which produce the requisite levels of movement with a change of 1.6 volts. These avail themselves to direct connection to the digital to analogue interface of the computer. Previously, 600-800 volts vas necessary which required a voltage amplifier to be interfaced to the computer. The arrangement described in 5.11 was chosen as introducing no measurable errors.

The electro optic cell selected was a modified Electro Optics Designs pockel cell. The crystal is elongated and the beam is passed back through the device with a corner cube as shown in Figure 5.12.

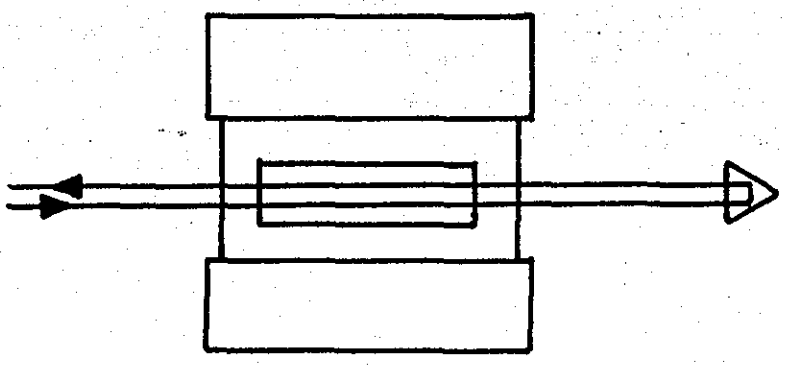

Figure 5.12
Double Pass Phase Modulation using an EOD Pockel Cell

The primary reason for undertaking this arrangement was the elimination of moving parts, thus overcoming dynamic resonant problems and tilt components as discussed previously. The unit proved itself experimentally, however the following factors mitigate against its use in commercial systems:

1. Cost, £4.5K.
2. Driving voltage, 1500V.
3. Power supply size and weight.
4. Electro optic head volume compared with a piezo capacitive mirror.

Consequently the pockel cell was removed and the mirror used for all subsequent work.

5.6 Three Dimensional Vibration Analysis Using Time-Averaged ESPI

The optical arrangements necessary for out-of-plane and in- plane sensitivities are discussed in Appendix 2. Little work has been reported which utilises the advantage of ESPI for such combined, yet independent analysis. Whilst requiring three illumination arrangements, the potential exists for sequential analysis by one television camera or simultaneous viewing with three television cameras. The desire to investigate the three dimensional aspects was promoted with the need generated by Metal Box PLC. A collaborative request was made for assistance in the design of ultrasonic can manufacturing equipment. Here the need was to design a resonant structure at 20kHz which would operate with high energy efficiency and good separation of any other adjacent resonant and coupled modes. The envisaged process relied on resonant operation to effect a considerable friction reduction during the necking operation of metal cans.

Experiments were performed which demonstrated the ability of ESPI to yield information about the mode shape of an ultrasonically excited die block. However, the usual out of plane study, whilst providing confidence of the technology performance at that frequency (20kHz), did not yield all the necessary information.

In-plane ESPI had previously only been applied to measurement of surface displacement and strain. Praeter [52] has observed in plane strain in rotating objects, but no reports have been found using a twin object beam interferometer to measure vibration. Lokberg [41] has studied in-plane vibration modes using an out-of-plane interferometer and viewing the object at an angle, so that the sensitivity vector gave a combination of in-plane and out-of-plane components. The main advantage of this system is that only one optical arrangement is needed. Disadvantages are that the object appears distorted because it is viewed obliquely, and calculating the three dimensional amplitudes gives the same computational problems as for holographic interferometry. These problems can be overcome by using one out-of-plane and two in-plane ESPI systems to measure three mutually perpendicular components of amplitude. When viewing a surface at the normal it is possible to acquire directly the in-plane and out-of-plane components, thus for any object geometry it is easy to obtain the resultant amplitude and direction at a point by adding the three components vectorially. The ideal arrangement is to have an optical rig which enables all three views to be taken either simultaneously or sequentially without moving the object. Hence quantitative measurements can be made by counting fringe orders from the nodal fringe to give amplitude in the direction of the sensitivity vector at that point. Vector addition of the components then gives the overall surface amplitude. It should be noted that the sensitivity vector varies across the object, especially when diverging beams are used. However, if the divergence angle and viewing angle are small, the variations can usually be neglected except for very accurate measurements.

The object chosen to demonstrate this technique was a thick, hollow cylinder, approximately 170mm outside diameter and 40mm thick, made of an aluminium alloy. Its lower order resonant modes fall into three classes: radial, torsional and rotational, whose principal vibration components are radial, axial and tangential respectively. When the cylinder is viewed axially end-on, axial vibrations correspond to out-of-plane motion, whilst radial and tangential components are both in-plane.

The cylinder was excited by a magnetostrictive transducer mounted radially on the outside diameter, and driven by a signal generator with variable frequency and power output. Firstly it was viewed axially using an out-of-plane ESPI system with an argon ion laser. The excitation frequency was increased gradually whilst observing the time-average fringe patterns in real time on a video monitor. This enabled all the resonant frequencies to be identified rapidly, and the fringe patterns for each mode to be recorded on video tape for subsequent analysis. The optical arrangement was then changed to give a system with horizontal in-plane sensitivity and the analysis repeated and finally the vertical in plane component was examined. Figure 5.13 shows the three fringe patterns observed at 24.00kHz. In all, more than ten resonant modes were observed in the frequency range 13 to 27kHz.

A finite element analysis of the cylinder was also undertaken to predict the natural frequencies and corresponding mode shapes. From the results of the analysis, contour plots of out-of-plane, and horizontal and vertical in-plane, components of amplitude were produced. These could be compared with the ESPI fringe patterns to help identify the resonant modes, and to see how the mode shapes observed in practice vary from the theoretical predictions. Figure 5.13 shows Finite Element predictions of a resonant mode at 24.24kHz, which corresponded closely to the experimental fringe patterns. The predicted mode is a second order rotational mode, having symmetry about horizontal and vertical axes, with the inside and outside of the cylinder rotating in opposite directions in between. The observed in-plane fringe patterns individually give little

indication of the type of vibration mode, so it is necessary to combine them. This has been done by superimposition and plotting the component vectors wherever two fringes intersect. The amplitude of the vector is scaled from the fringe function, and the phase (shown as direction at an arbitrary point in time) changes through 180 whenever a nodal fringe is crossed. Adding the two vectors at each intersection point gives the total in plane vibration pattern as shown in Figure 5.13. This shows the two axes of symmetry and the rotation about nodal points, providing additional verification that the mode is as predicted. It would be possible to add the out-of-plane components and produce an isometric plot of the mode shape, but in a case like this the mode can be more easily visualised and categorised by considering the combined in-plane components separately. It can be seen that the out-of-plane nodal lines coincide with the maximum in-plane amplitudes, and where there is little in-plane motion along the vertical and horizontal axes the object is vibrating out-of-plane.

The results presented demonstrate that by using three ESPI viewing arrangements it is possible to observe all three dimensional vibration modes. Because the three sets of results represent mutually independent components, interpretation of the mode shape is very much simpler than with holographic interferometry or similar techniques. Predominantly in-plane modes require only a simple vector addition of two fringe patterns. This process can be extended to add all three results for complete visualisation of complex three dimensional mode shapes. Such an approach, using either single or combined patterns, is particularly attractive to vibration engineers. Furthermore, the procedure of data reduction and fringe pattern interpretation is ideally suited to automation by computer as discussed in the next section.

This work has also demonstrated the compatibility of ESPI and Finite Element techniques as complementary to vibration analysis. Finite Element methods are clearly very powerful predictive tools, and often extremely useful at the design stage. It is at the stages of prototype evaluation, development and quality control that experimental verification is essential. Mode shapes can be easily analysed and compared with predictions, and as demonstrated this can indicate distortion due to operating conditions, fabrication stresses, material defects, etc. Resonant frequencies can be accurately measured by observing the peak response and the amplitude response for a given excitation can be measured quantitatively. The Finite Element model used in this analysis did not take account of mechanical damping. ESPI has also identified combination modes which were not originally predicted. However, once the boundary conditions for a given mode have been verified, the Finite Element technique can provide useful information on internal strains which cannot always be obtained experimentally. A more complete analysis of this work is presented in reference [42] by Shellabear and Tyrer.

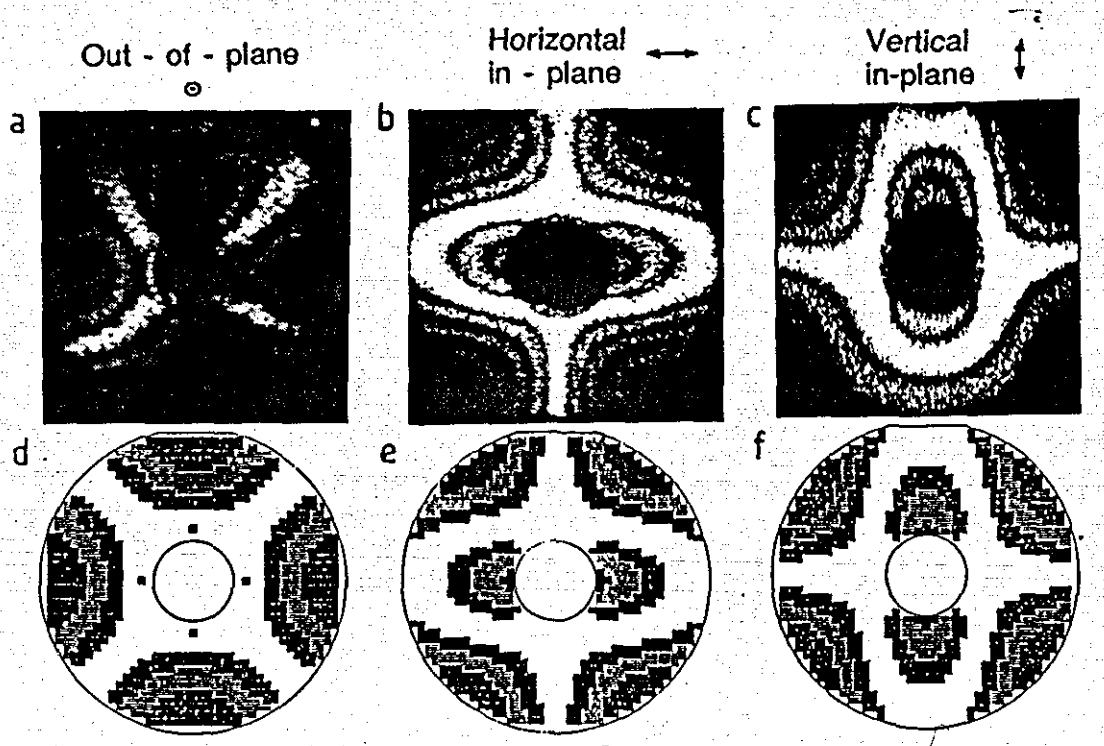

(a,b,c) ESPI fringe patterns
(d,e,f) computer FEM predictions
(g) in-plane amplitude vectors from (b) and (c)

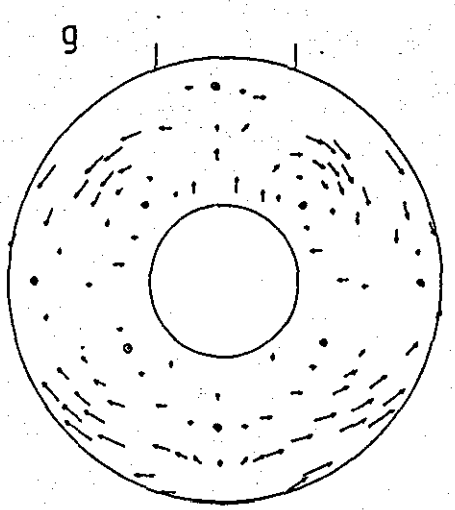

Figure 5.13
Vibration Analysis of Thick Aluminium Cylinder
at 24 kHz Using Both ESPI and Finite Element Methods

5.7 Computer Based Fringe Pattern Analysis

The automated extraction of data from ESPI fringe patterns has been highlighted in Figure 1 because it was felt that an end user would not have the desire to interpret such data. The successful transfer of ESPI technology to the instrument manufacturers had required activity to be undertaken in this area. It was necessary to build an optical system capable of producing enhanced information suitable for the computer based image processor. It was also necessary to evaluate the various methods of fringe pattern detection. Having chosen the most appropriate means to develop software to manipulate fringe patterns into a suitable matrix of unambiguous data, the display of the data could be tailored to suit end user requirements.

Several specific problems arise in ESPI fringe analysis, due mainly to the presence of a high level of spatial frequency noise. The difficulty lies in the reduction of this noise, which constitutes the information carrier. The interferometric phase referenced speckle pattern is contained within a spatial frequency band of 1.0 MHz - 4.5 MHz within the noise. The image is modulated with a random intensity of the information carrier (speckle). The resultant fringe pattern contains fringes which have a definable function but do not contain displacement phase (sense) resulting in data ambiguity. Local changes in surface illumination and non-homogeneous reference beams can render variable contrast across a fringe field. These issues render simple techniques of image processing ineffective when used in isolation. The image after subtraction contains both optical and electronic noise which gives rise to intrinsically poor signal to noise ratios. Electronic noise is inherent within the television camera electronic processing and digital storage. The optical noise is composed of the residual statistical speckle produced by the coherent object beam and the optical surfaces within the interferometer. A distinct overlap in frequency exists between noise and signal at some spatial frequencies.

Thus the fringes are discontinuous making them difficult to locate in two dimensional space using conventional thresholding and tracking techniques.

The method of optical noise reduction discussed earlier is relevant only to time averaged fringe patterns. However, the intention was to develop a system able to undertake analysis on any ESPI fringe pattern, which meant the rejection of speckle averaging as a noise reduction technique. The fringe patterns could therefore have either a Bessel or cosinusoidal function requiring user preferred input sensitivities to be introduced.

ESPI correlation fringes have an intensity distribution caused by the displacement of the object surface along the sensitivity vector. Since the amplitude and phase are not explicitly detected, the direction (sense) of the displacement along this vector can not be easily deduced. This ambiguity requires additional information to provision the sense of displacement. Early analyses of interferometric results were of a qualitative nature where the characteristics of fringe patterns were sought, such as; concentration of fringes around one location, changes in the structure of a pre-determined structure or fringe field. The approach is not to rely upon such a-priori knowledge and enable a unique solution to be produced. Initial attempts at computer assisted fringe pattern detection required the location of fringes, deducing the fringe order number and extracting point wise information by fringe counting and interpolation.

A survey of potential techniques used in other types of optical fringe pattern analysis highlighted five methods:

i) Simple fringe tracking.
ii) Spatial synchronous detection.
iii) Phase heterodyning.
iv) Digital transforms.
v) Phase stepping.

5.7.1 Evaluation of Various Methods of Fringe Detection

5.7.1.1 Fringe Tracking

This is essentially an intensity tracking process involving binarisation, thinning and edge or peak detection. Little knowledge of the fringe pattern characteristics is required, but most earlier methods involved operator guidance to some extent. The general methodology is; filter, identify and track peaks or troughs, number the fringes, calculate the measurement parameter.

The two main problems to be overcome are noisy fringe data and images with large variations in local contrast. Most fringe tracking routines can not cope with high noise or varying contrast without extensive operator guidance. Some systems rely upon the user guiding a cursor or light pen, Hurden [43], to determine fringe position. Such systems are prone to positional error and rely heavily upon skill and individual judgement. They can also be very tedious to use and dealing with large amounts of data in this way is not feasible.

High spatial frequency noise can be reduced by low-pass filtering by local averaging (mask) techniques. High spatial frequency noise is a more difficult problem and is less amenable to mask filtering, although satisfactory results can be achieved at the expense of fringe visibility in some cases.

Assigning of fringe order numbers can be performed by the operator if the zero order fringe position is known or if prior information is available.

5.7.1.2 Spatial Synchronous Detection

Spatial synchronous detection provides a facility for the introduction of 'tilt' to the interferogram. This is usually accomplished by angular displacement of a mirror in the interferometer, which in turn causes the fringe pattern to rotate/translate in the field of view.

By careful manipulation of the optical geometry, it is possible to obtain a new set of fringes symmetrically distributed about the horizontal or vertical axis of the field of view. The measurement parameter is then encoded in the departure of the fringes from the expected symmetrical distribution. It is then a simple task to assign fringe order numbers according to the pattern symmetry (eg. left to right for vertical fringes). These procedures yield phase directly and obviate the need for assigning fringe numbers, although identification of the zero order is still necessary. Green [44] has demonstrated the technique suitable for ESPI fringe processing.

5.7.1.3 Phase Heterodyning

When measuring surface displacement or form it is not possible to distinguish between concave and convex features given only a single interferogram and no other information. This ambiguity may be removed by determining the displacement at a given point in terms of phase difference produced by an optical path change.

Heterodyne interferometers are specifically designed to extract phase information and have been used very successfully in holographic interferometry for several years by Dandliker [45]. They are capable of very high resolution and usually form part of an automatic data processing system. They are rather more complex and expensive to construct than a conventional holographic interferometer, and require high bandwidth detectors making them unsuitable for direct video interfacing to an image processor.

A Twyman-Green heterodyne interferometer forms the basic frame work of a typical instrument. The two interfering beams are shifted a very small amount in optical frequency, ($\Delta\omega_1$ and $\Delta\omega_2$) using electro-optic Bragg cells. For each beam, then,

$$E_1 = E_{01} \cos [(\omega + \Delta\omega_1)\, t + \psi_1] \qquad (44)$$

$$E_2 = E_{02} \cos [(\omega + \Delta\omega_2)\, t + \psi_2] \qquad (45)$$

where E is the optical field amplitude, ω is the angular frequency and ψ the phase. A photodiode detector is used to sample the interferogram at a point in the hologram plane (x,y). An a.c. photocurrent will be produced as the two frequencies modulate, such that $i = (E_1 + E_2)$ which will be time averaged over the finite detector bandwidth δv. This bandwidth is chosen such that; $\delta v > (\Delta\omega_1 - \Delta\omega_2)$ but $\delta v << \omega$.

The photocurrent is given by;

$$i \alpha\ E_{01}E_{02} < \cos[(\Delta\omega_1 - \Delta\omega_2)t + \psi_1 - \psi_2] > \qquad (46)$$

and hence the phase $(\psi_1 - \psi_2)$ of the a.c. photocurrent generated at (x,y) equals the phase of the interferogram at this position. The photodetector output can then in principle be calibrated to yield displacement information directly when coupled to an electronic phase meter. The detector can be moved across the interferogram or an array of detectors can be sampled, depending on speed and spatial resolution requirements.

Phase values are unaffected by stationary noise or local variations in fringe contrast, data ambiguity is removed and the remaining fringe analysis process greatly simplified. Accuracy of fringe determination can be as high as 1/1000 of a cycle (π/500). Drawbacks include; cost, detector bandwidth and spatial resolution. Furthermore, it is not possible to use a conventional TV camera and video interface as the value of δv would be too low. Typical values of $(\Delta\omega_1 - \Delta\omega_2)$ are in the order of 5-100 KHz, whereas a television camera operates at a field rate of 50 Hz.

5.7.1.4 Digital Transforms

If the fringe pattern under investigation has a certain spatial symmetry, eg. as in the case of speckle photography where sets of straight, parallel fringes of a $\cos^2$ intensity profile are formed, it is possible to extract fringe spacings on a spatial frequency basis.

It is sometimes necessary to apply 'tilt' to the fringe pattern in order to provide the necessary symmetry for spatial frequency analysis so that phase may be determined. Assuming such an intensity distribution g(x,y) in the fringe pattern, it can be shown that;

$$g(x,y) = a(x,y) + c(x,y)\exp(2\pi j f_o x) + c^*(x,y)\exp(-2\pi j f_o x) \quad (47)$$

where a(x,y) is a function representing the background (d.c.) intensity, f_o is the fringe spatial frequency and c(x,y) is a function incorporating the amplitude and phase of the fringe pattern as:

$$c(x,y) = (b(x,y)/2)\exp(j\ \psi\ (x,y) \quad (48)$$

This component represents the information carrier, ie. the term containing the phase description. It is assumed that the fringe function is one dimensional; that the fringes are vertical and parallel, then a digital Fourier transform (DFT) applied in the x direction only will produce a result of the form;

$$G(f,y) = A(f,y) + C(f+f_o,y) \quad (49)$$

where f is the spatial frequency in the x direction. The second term in the right-hand side of the equation (49) involving $C(f+f_o,y)$ can be extracted from the transformed image by masking of the coefficients in the power spectrum (using a suitable filter mask centred on f_o). If this is then d.c. shifted to the origin and the inverse transform applied, an image involving only c(x,y) will result, ie. that of equation (48).
This image may be reduced to a phase description $\psi(x,y)$ pixel for pixel by

applying;

$$\psi(x,y) = \tan^{-1} [\mathrm{Im} (c(x,y)) / \mathrm{Re}(c(x,y))] \qquad (50)$$

where Re and Im are the real and imaginary parts of the complex function c(x,y). This approach has the advantage that it requires only one interferogram to produce phase information. Its main advantages include noise sensitivity, the requirement for tilt (which is not always feasible), and the computationally intensive application of digital transforms. This last feature is becoming less of a problem with high speed digital hardware now available which provides digital Fourier transform capability on a custom built chip. Huntley [46] has successfully examined both Fourier and Walsh transforms applied to ESPI.

5.7.1.5 Phase Stepping

The Quasi-Heterodyne or phase stepping method is well established in the fields of holographic and speckle interferometry. The technique involves similar principles to phase heterodyning, but allows the use of a TV camera and video frame store as a recording medium. This makes the instrumentation much simpler and allows direct interfacing to a computer image processing system. Several discrete increments in the phase of one of the interferometer beams shifts the position of the fringes, producing a set of values of intensity at each point I(x,y). These are effectively sampled versions of the heterodyne a.c. signal change.

In its usual implementation, the phase is stepped using a piezo translator or electro-optic cell by $2\pi/k$ in (k-1) equal steps where k is an integer. It is normal practice to restrict the value of k to 3, 4 or even 5 as a compromise between accuracy of determination of the phase $\phi(x,y)$ and protracted computational effort. The choice of k=3 is most usual, although other variations have included unequal phase steps and continuous rather than discrete shifts in phase. Nakadate [47], Creath [48] and Robinson [49] have all demonstrated techniques based upon the measurement of the

difference of phase. The approach taken here was to measure the phase of the difference*, requiring the phase stepping of fringe patterns which requires, for two steps, only three interference fringe maps, compared with six images for their approach. Whilst requiring fewer images, it also has the added advantage of improved use of the framestore resolution originally reported by Kerr and Tyrer [50].

Mathematically, it can be illustrated that for the two step method (k=3), with a shift of $\Delta\phi = 2\pi/3$, the Fourier series coefficients $\alpha_1(x,y)$ and $\beta_1(x,y)$ are given by;

$$\alpha_1(x,y) = \Sigma_{N=1,k}\ I_N\ (x,y)\ \cos(2\pi N/k) \qquad (51)$$

$$\beta_1(x,y) = \Sigma_{N=1,k}\ I_N\ (x,y)\ \sin(2\pi N/k) \qquad (52)$$

where N is the image number and $I_N(x,y)$ is the intensity (gray level) of a pixel located at (x,y) in image N. A solution for the phase is then;

$$\phi(x,y) = \tan^{-1}\ (\beta_1(x,y) / \alpha_1(x,y)) \qquad (53)$$

A solution for phase in terms of pixel gray level is;

$$\phi(x,y) = \tan^{-1}\ \{\sqrt{3}[(I_1-I_2) / (2I_3-I_1-I_2)]\} \qquad (54)$$

Three images are required to evaluate the phase map $\phi(x,y)$ of a test surface image pixel for pixel. If images are digitised at a spatial resolution of 256 x 256 pixels it is then necessary to process 196,608 pieces of information with arithmetic and trigonometric calculations. This process must be repeated (in the case of displacement measurement) after deformation of the test surface and a difference obtained between the two resultant phase maps. This differing process yields the surface displacement in terms of phase and is usually obtained by subtracting the values of the phase maps.

*As originally proposed in SERC grant application GR/D/24647 September 1984

Even with the use of arctangent look-up tables the total processing time involving 2^{17} operations of equation (54), can be in the order of minutes, particularly in the case of the 4 step (k=5) approach. Environmental sensitivity of the technique increases with k to such an extent that large errors in I_N (x,y) due to drift can occur in all but the most carefully controlled conditions.

Phase stepping was identified as the most appropriate fringe processing technique to undertaken ESPI fringe pattern analysis.

5.7.2 The Development of a Phase Stepping Approach for ESPI

Procurement of a suitable image processing system was initially delayed when problems became apparent with the Trappix system. Poor sampling at the analogue input stage and various software faults eventually meant that this system had to be rejected and the procurement process repeated. Before taking delivery of the new system from Kontron Bildanalyse, work continued on a smaller system base around a DEC pdp 11.23 microcomputer. The INTELLECT 100 system was here for the initial software development and testing, the work being continued on the Kontron system after trials, software modification and system tuning.

This work concentrated on the digital phase stepping approach described in Section 5.7.1.5. This method best suited the ESPI application and offered potential solutions to the problems described in 5.7. In order to investigate possible ways of applying this method to ESPI fringe processing, a toolkit of computer algorithms was produced to simulate easily interpretable sets of raw data and the corresponding processed results. Variation of certain parameters of the data enabled the effects of noise, fringe modulation depth (visibility) and phase step errors to be examined.

Included in this work was the building of the ESPI rig (Figure 5.9) which eventually only utilised a mirror mounted on a piezo-electric crystal (PZT) in the reference beam path to achieve the phase stepping. An asynchronous input/output device (UART) was designed and built to allow control of the PZT mirror by the computer software. The mirror was pre-calibrated in a Michelson interferometer by fringe counting and interpolation to establish the PZT voltage versus phase response.

Initial tests of the phase stepping algorithm consisted of processing a series of computer generated sine wave patterns in order to produce a phase map at 256x256 pixel resolution. Because of the one dimensional, cyclic nature of the data, results could be easily predicted and interpreted. It was during this stage that the idea of processing speckle fringes rather than raw interferograms was developed and shown to be feasible. This novel "phase of differences"* approach was to become the cornerstone of the fringe analysis process. One advantage of this approach was the ability to observe the quality of the fringe patterns prior to processing.

The next stage involved the investigation of the effects of low modulation and reduced SNR on the phase maps, choosing various pixel wavelength values to test the consequences of under-sampling. The final stage was to repeat the above processes for actual ESPI fringe data obtained from the breadboard rig and to measure and compare gray level modulation for small phase displacements at various points in the processing chain.

Modulation of signals from the TV camera were compared with those levels obtained after passing through the ESPI rectifier, the modulation being measured on a line for line basis such that the average intensity (gray level) value for a line of n pixels was given by;

$$1/n \sum_{i=1}^{n} \left| I_i - (I + \delta I)_i \right| \qquad (55)$$

where I_i is the gray level of the i^{th} pixel and $(I+\delta I)$ is the gray level of the i^{th} pixel after a small phase step.

*See footnote P.142

The work carried out highlighted the need for major improvements in the ESPI processing electronics in order to enable the phase stepping approach to function to full advantage. More specifically, four main problems were evident:

1. Digitised output from the store or TV camera had a greatly reduced gray scale range, sometimes as low as 33% of the available levels.
2. Modulation depth produced by phase stepping was much lower when measured direct from the TV camera images than after rectification in the ESPI store, showing the need for extra video pre-processing.
3. Existing equipment did not produce TV signal information to CCIR standards with black levels below 0 volts and no proper clamps. White video levels varied from below 0.7 to over 1.0 volts depending on the store and camera combination. Black and white level clipping of the TV signal by the image processor input stage was thus degrading the data.
4. Video signals digitised by the image processor contained frequency bandwidths in excess of 8 MHz. Experiments have shown that essential speckle data are contained at video frequencies of 1 - 5 MHz. The image processor input Analogue to Digital Converter (ADC) should have a sample rate and response linearity in excess of 20 MHz to prevent aliasing. The use of anti-aliasing filters by some manufacturers may reduce the full bandwidth of the ADC to undesirably low levels. The use of a phase-locked loop is advantageous to insure that video synchronisation prevents pixel mis-match or lost data.

Effort was then diverted into improving the ESPI electronics and building and testing a video pre-processor unit, described earlier. The main advantages of the phase stepping approach have been demonstrated in that;

- An inherently less noisy image results.
- Areas of low modulation may be identified and removed.
- Displacement direction is unambiguous.
- Resolution of around 1/25th of a fringe is possible.

Nakadate and Saito [47] used a four step phase of difference approach and identified the sensitivity of the phase stepping technique to the inherent speckle noise. The spatial frequency distribution of a speckle pattern and the fringe pattern density can lead to an overlap between noise and signal. This makes the fringe extreme (minima or maxima) hard to locate in two dimensional space. Nakadate proposed a correction filter which could be of assistance especially at the phase boundaries where the technique is most sensitive. The results of the simulation work by Kerr and Tyrer [72] led to the design of the new generation of pre-processing electronics, see Appendix 4. The improved modulation depth (seen in Fig A4.5 for example) enabled less severe digital filtering to be used. The judicious use of convolution filters can increase the signal to noise ratio whilst minimising the reduction to fringe quality. Nakadate and Saito, for example, require eight iterations of an 11 x 11 median filter, the results shown in Plate 19 required three passes of a 5 x 5 filter. A more detailed analysis of the noise terms, including the use of a Fourier transform filter method, can be found in Kerr, Mendoza and Tyrer [73]. This work further helped in the refinement of the pre-processing electronics by West.

The phase stepped results detailed have been analysed without requiring additional processing, such as the lack of data arising from shadows, holes, etc. The component under test was windowed with a user defined mask, the computer programme started at the upper left corner of the window and integrated the grey levels along a video line to establish displacement. The determination of numerical data from interferometric fringe patterns has been the responsibility of Kerr (for example, as contained in [50]), at Loughborough.

The fringe processing routines used in this study have validated the initial objective of extracting numerical data from ESPI fringe patterns in an unambiguous fashion without operator intervention, and have been extensively studied by Kerr.

Results presented from this work are seen in Plates 19-23. Plate 19 demonstrates the three initial images used to produce the computed image. The component was a cantilever metal beam which was displaced by means of a differential micrometer. Plate 20 shows the isometric plot of this displacement. To demonstrate the ability of the system to handle unkown data, the beam was initially displaced toward the camera (Plate 21.1) and the system reset before the beam was displaced away from the camera (Plate 21.2). No additional information was given to the computer prior to the printing of the line profiles. The dotted outline on the profiles is the expected theoretical position. Plate 22 shows a torsion plate used to determine the fuller operation of the system. Plate 23 shows the data, results and isometric plot highlighting the twisted aspect of the plate under a 50gm load.

The phase stepping of ESPI fringe patterns enables both static and vibration results to be processed. The technique relies on fringe patterns of a consistent optical function which is problematic if time-averaged fringe patterns are used. It is capable of working on the data generated by pulsed or strobed laser systems and is thus appropriate to the needs of double pulsed ESPI.

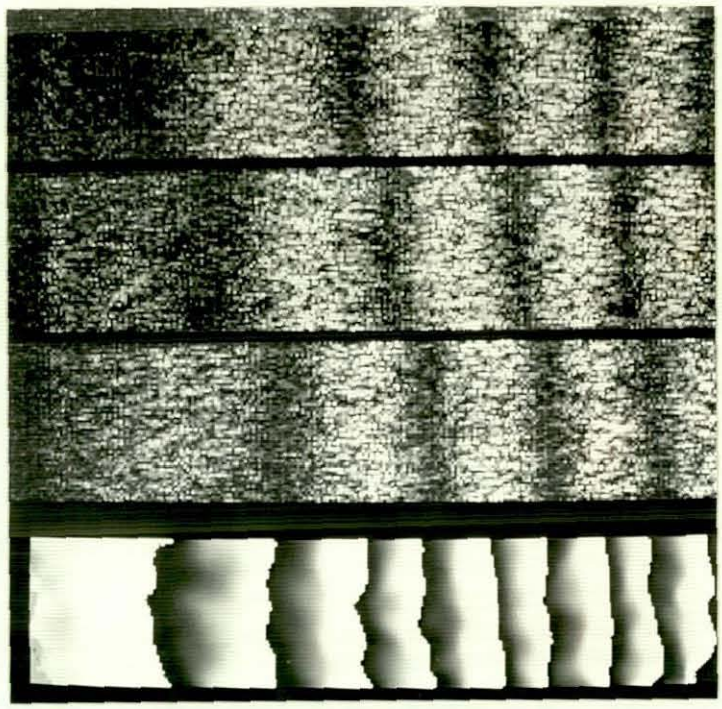

Plate 19. Three Phase Stepped Fringe Patterns and the Computed Result

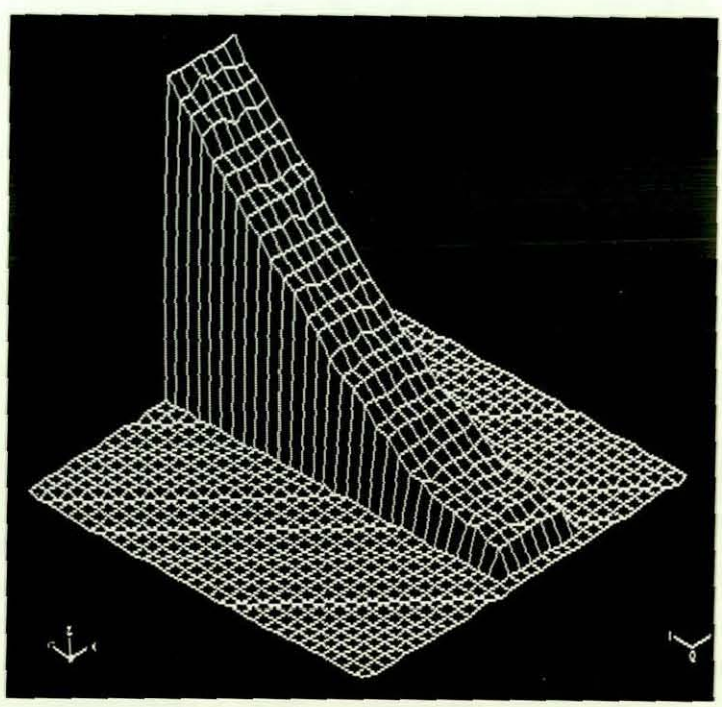

Plate 20. Isometric Wire Mesh Plot of the Results from Plate 19.

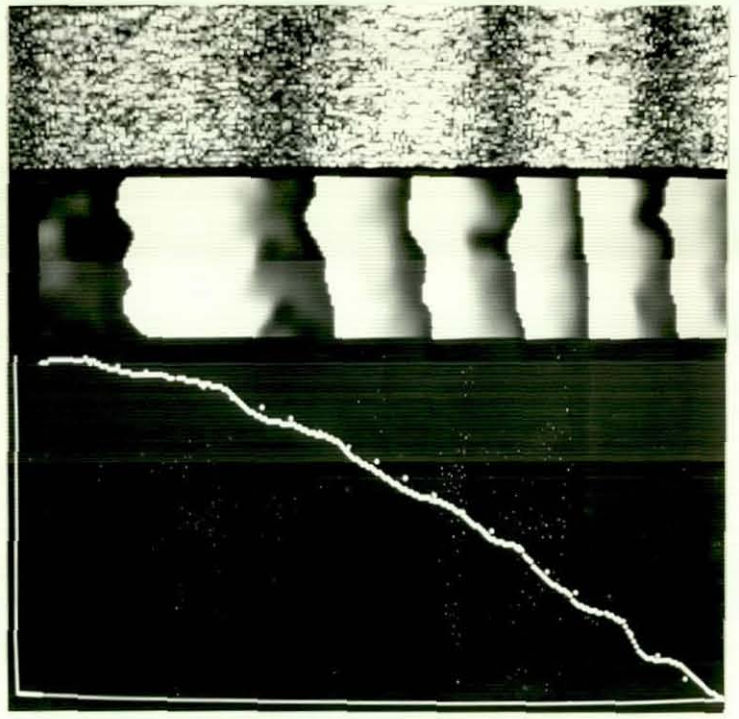

Plate 21.1 Displacement Toward the Camera

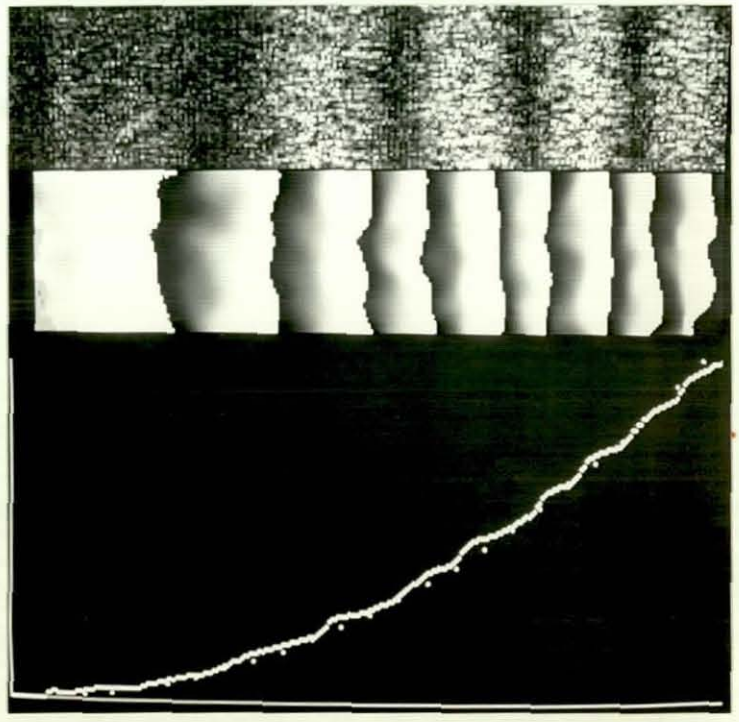

Plate 21.2 Displacement Away from the Camera

Plate 21. Cantilever beam analysis showing unambiguous analysis of displacement. Line profiles of numerical data are given under the phase images.

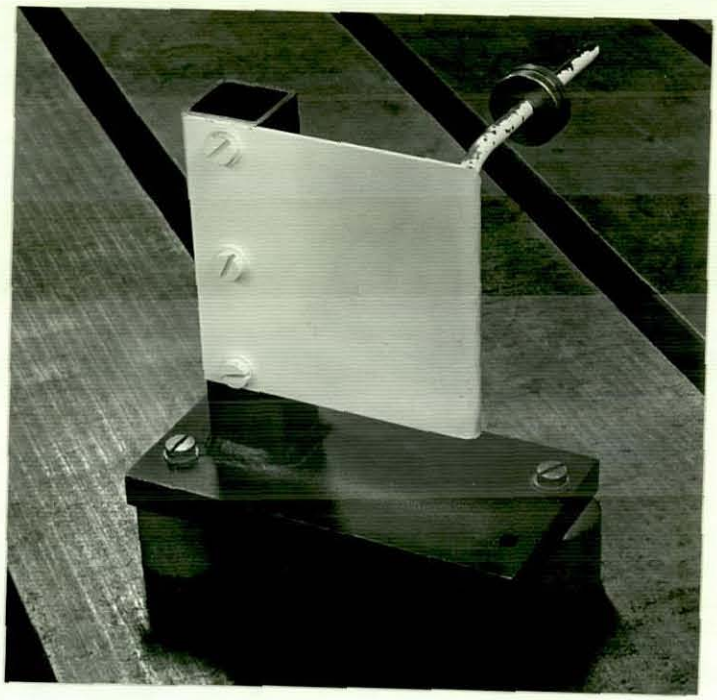

Plate 22. Torsion Plate Used

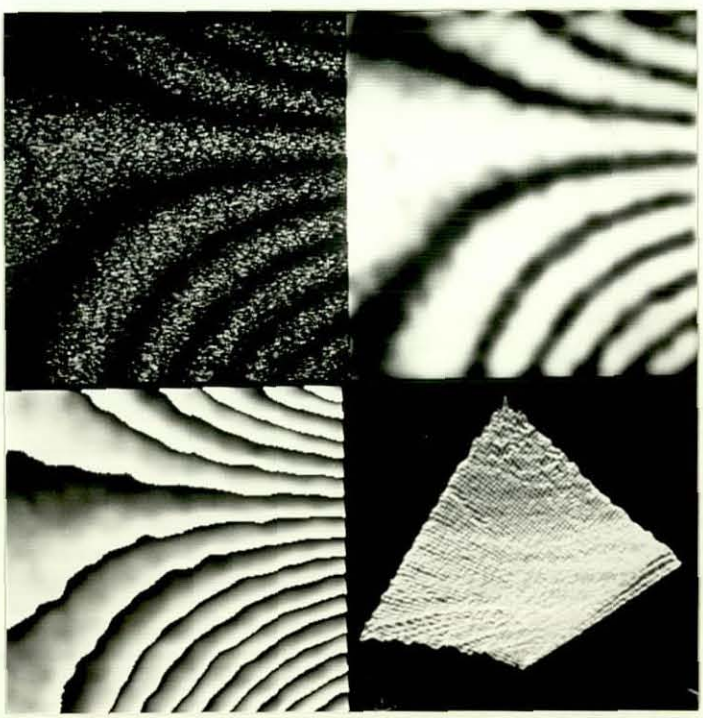

Plate 23. Automatic Fringe Analysis of Torsion Plate,
Showing Raw Data, Filtered Plot, Computed Image and Isometric Plot

5.8 Conclusions

This chapter has shown that correlation interferometry provides displacement fringe pattern data which is in a form more suitable to engineers than is holographic interferometry. The optics and electronics received considerable research and design effort in order to configure them to a form suitable for manufacturers and in order to present high contrast fringe patterns. Automatic data interpretation using computer based image processing was evolved to handle the different forms of interferometric fringe patterns. The conclusions are summarised below.

- Strobing removed the intensity variation which makes the technique more amenable for data analysis provided that phase ambiguity is removed and the zero order detected.
- Strobing and phase shifting removed the data ambiguity. The mark space ratio of the illumination period was important to the fringe function.
- Prefiltering of the signal made better use of the framestore and rendered improved fringe contrast with fringes of the cosine^2 form.
- Daylight immunity was necessary and could be produced by bandpass filtering of the speckle frequency in the region of 1.5-5 MHz. The combination of daylight immunity and image processing upon a half slot, plug-in board, enabled high quality fringes to be produced using an IBM compatible computer. This used a commercially available digital framestore with no modification to store or computer.
- The presentation of ESPI vibration fringe patterns could be improved to near holographic quality fringes, using integration of multiple images by the speckle decorrelation technique. Results have been obtained with fringewidths of only five pixels.
- The understanding of some of the end user requirements and the problems of manufacture enabled a prototype instrument specification to be produced.
- The production of a prototype optical instrument aided in attracting potential licensees.

- The need for high quality, compact optical arrangements led to the production of the novel kinematic mirror mounts. The technique of vertical manipulation was successfully transferred to other optical devices.
- The confidence generated by successful commercial manufacture of ESPI led to the growth of industrial utilisation of such instrumentation which then provided further direction for the technology. This concentrated on the need for three dimensional analysis, computerised fringe pattern analysis and pulsed laser ESPI.
- The ability of ESPI to map three dimensional surface displacements or amplitude vectors of suitable density and quality has been reported. Here the combined in plane analyses are unique in their ability to show, in real time, the distribution of sub micron displacement mode patterns.
- The introduction of computerised fringe processing was accomplished in a complementary fashion to the interferometric equipment.
- The approach taken necessitated an understanding of the equipment and techniques available but also took the end user and double pulse ESPI requirements into account. The requirement at every stage was to derive data in a useful and unambiguous form.
- An analysis of potential fringe processing approaches revealed phase stepping to be suitable. It handled the data quality, was sufficiently robust in handling the experimental fringe pattern intensity and contrast variations, was capable of operating without additional prompting and could automatically output meaningful information.
- Sub-fringe interpolation has been achieved to a level of better than 4% accuracy.
- With these stages in place, the evolution of suitable complementary double pulsed equipment was considered to be the final requirement.

CHAPTER 6
DOUBLE PULSED SPECKLE PATTERN INTERFEROMETRY

6.0 Introduction

The development of suitable double pulsed ESPI equipment was one of the final goals of this project. The preceding chapters have highlighted: the useful engineering data that can be obtained by interferometry, the ability for double pulsed holography to be used at an industrial location, and that ESPI could be made into suitable instrumentation which could be used to produce meaningful quantitative data.

The combination of double pulsed ruby lasers with ESPI had been demonstrated by Cookson, Butters and Pollard [51] in 1978 using analogue electronics. Some equipment had been supplied to Praeter at City University in London, who undertakes in-plane strain analysis on rotating components [52].

The performance of the Cookson equipment had been limited by the ruby laser used at that time. This was modified considerably in the early part of this project to provide a more controllable and stable laser (see Section A1.5). The initial work concentrated on out-of-plane studies, which were considered to place the tightest constraints of beam pointing and laser stability. The first part of the work attempted to combine digital framestores of limited band width (6 bit) to pulsed ESPI.

6.1 Image Recording Mechanism

The pulse separation is usually half the period of oscillation (τ) under study. Typically this will vary between 50 μs to 5 ms (10 KHz - 100 Hz) which is shorter than the television frame period 20 ms. However, the persistence of the imaging tube of the television camera can be used to store and add the two speckle interferograms, before transmission to the processing electronics. The triggering of the laser coincident with the displacement required will activate the camera as shown in Figure 6.1.

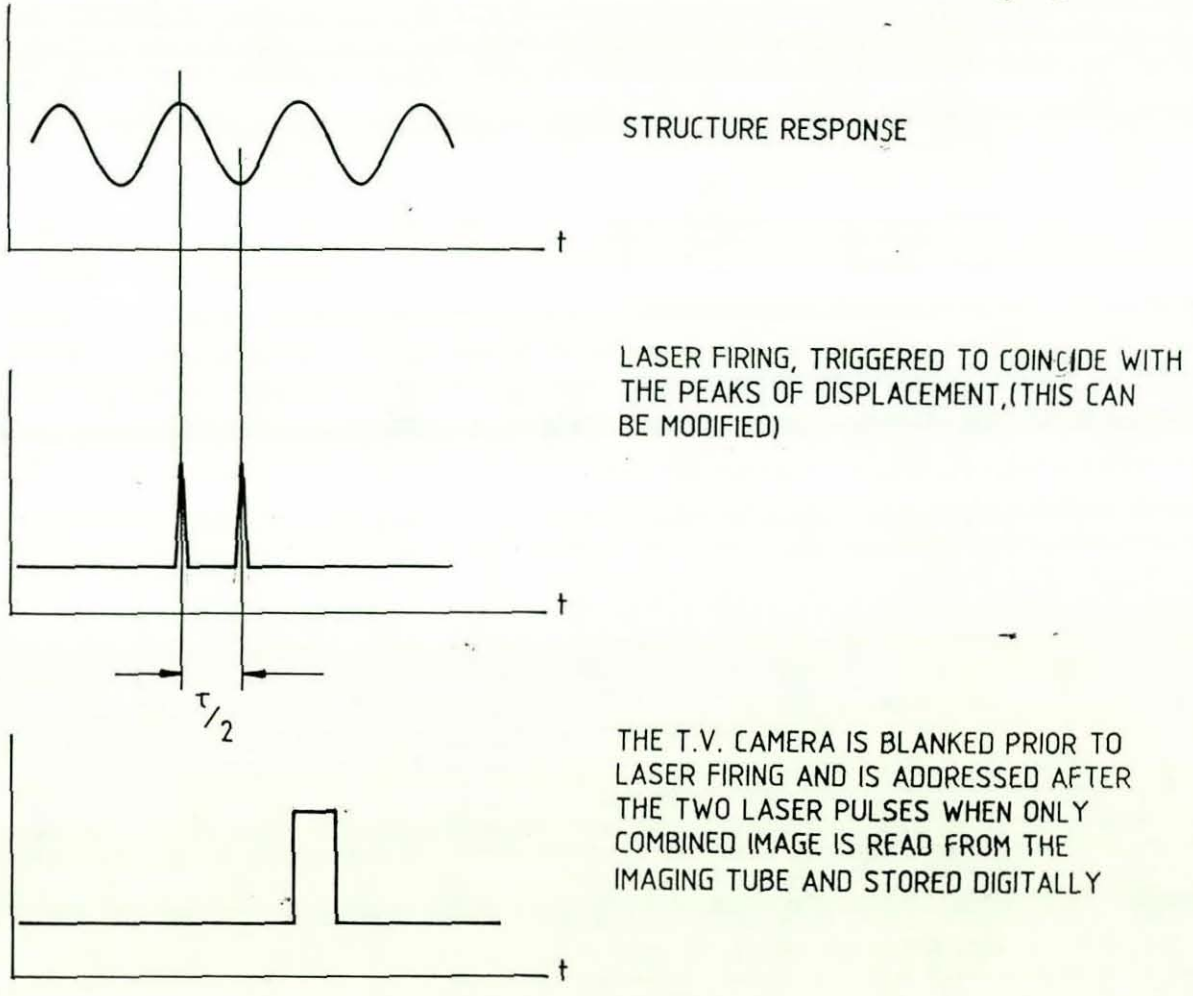

Figure 6.1
Double Pulsed ESPI Operation

The camera field coils are switched off, the first laser pulse is synchronised with the object motion as described in Figure 4.6. Any laser pulse build up times (typically 1 ms) can be accommodated by the first variable delay such that the laser fires on the peak of displacement of the next oscillation. The pulse separation is determined by the period of the object oscillation but for maximum displacement this is $\tau/2$ and is controlled by the second variable delay. Immediately after the second pulse the camera field coils are switched on and the combined interferogram read off the faceplate of the imaging tube. Thus correlation fringes with lines of equal phase change will be produced, these will be addition fringes from the surface displacement of a form given in Section A2.3.2.

The image is then filtered, digitised and stored within a digital framestore. With this type of operation there is no need for the subtraction system, although it can be used to subtract the background optical noise if stored into a second framestore which is then subtracted from the interferogram to enhance the overall fringe quality.

Alternatively, after the first pulse the frame is read into one framestore, 20 to 1000ms later the second pulse is fired and the next frame is stored in a second framestore. Subtraction of these frames gives higher contrast subtraction correlation fringes than those obtained by addition, see equations A2(17) and A2(20). The minimum time delay in this case is set by the time taken to scan one frame in a chalnicon type tube.

As with stroboscopic ESPI, if the displacement is in excess of 30 fringes then undersampling of the displacement can be used to reduce the fringe numbers. Thus extrapolation to the maxima can be achieved knowing the function of the excitation and the amount of under-sampling, determined by the reduced pulse separation. For pulse separations of between 10 μs - 1 ms, two pulses can be extracted from a single fluorescent pulse of the ruby rod by double pulsing the Q switch. The shortest interval between pulses is determined by the drive electronics to the Pockel cell

and the build up of sufficient energy within the ruby rod. The longest interval between pulses is determined by the fluorescent period of the ruby which is typically 1.5 ms depending upon the flashlamp type used.

6.2 Double Pulsed ESPI with Ruby Lasers

With double pulsed holography the recording medium, usually silver halide, is very forgiving in terms of the relative intensity of the two pulses. Hence a successful hologram can be produced even when the pulse intensities are not equal. With ESPI however, the television camera is usually operating at the maximum tube gain and any addition variation will overload the framestores and produce no result. This places a constraint upon the quality of the ruby laser pulses. Due to the inherent inefficiency of the ruby laser, heating occurs within the ruby rods during each operation of the laser. This heating affects the laser pulse and therefore stabilisation of the laser prior to each firing is required. Consequently, instead of the laser repetition rate being better than 10 per minute, it is reduced to 1 per minute, this is unacceptable for on-site analysis.

The arrangement used is derived from Figure 4.2, hence in Figure 6.2 the reference beam is again removed from the oscillator beam prior to amplification. Path length compensation was achieved using dielectric coated mirrors and an optical rail. To reduce the noise content in the reference beam, spatial filtering with a diamond pinhole was used. The energy density was sufficient to damage the adhesive used in microscope objective lenses, therefore simple short focal length lenses were used. The first result of the system is shown in Plate 24, here a vibrating metal disc is used as the target.

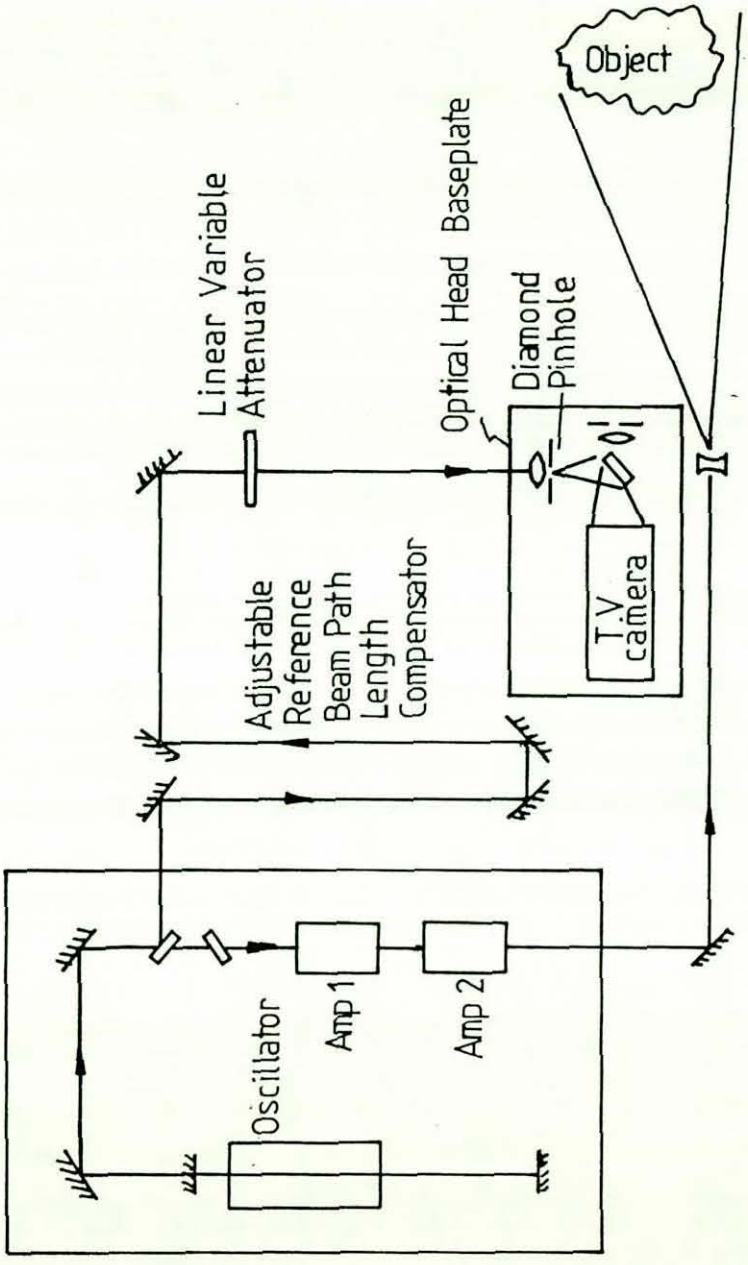

Figure 6.2
Optical Arrangement for Double Pulsed ESPI
using a Ruby Laser

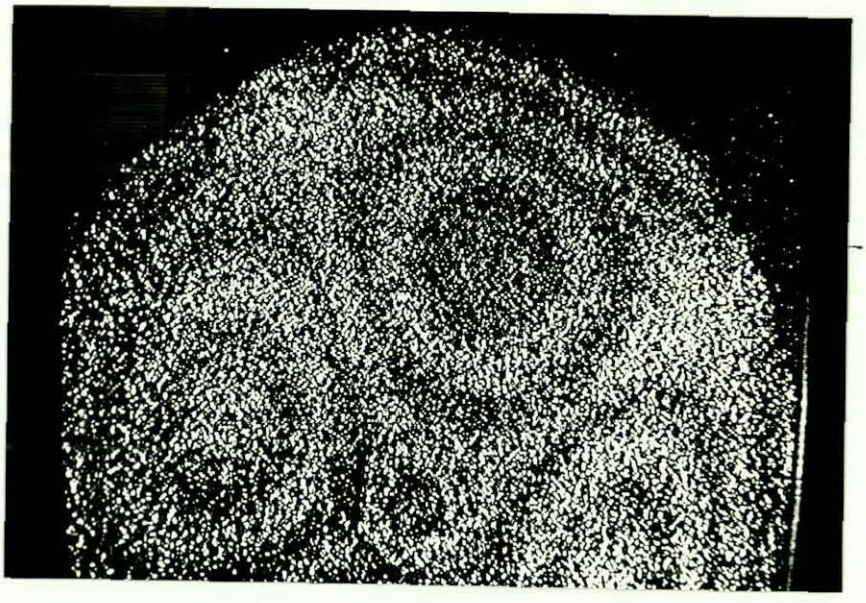

Plate 24.
First Pulsed ESPI Result of Vibrating Metal Disc

Modifications to the camera control unit included a facility which enabled the scan coils to be activated immediately after the second laser pulse, the image could then be selected from the next ten frames from the camera. It was found that the fourth frame from the camera contained the best fringe contrast. The arrangement used a simple imaging lens such that the reference beam expansion lens could be conjugate with the imaging lens. This meant that the two images appearing on the faceplate of the camera appeared to be derived from the same source. Focussing was accomplished by moving the camera on its slotted baseplate, the camera could then be locked in position.

A J.D. Jackson camera was used with a Toshiba chalnicon tube, a chalnicon was chosen for its high sensitivity at 694 nm, the ruby laser wavelength. Figure 6.3 shows the performance of chalnicon and vidicon tubes against illumination wavelength. To avoid Newton's rings on the faceplate of the imaging tube a 1° wedge was cemented onto it.

Studies were undertaken to determine methods for increased thermal energy extraction involving redesign of the cooling circuit of the oscillator and amplifiers, increased cooling capacity and alternative cooling media. Discussions with JK Lasers concerning the fluting of the rods to increase the energy extraction from the ruby suggested this would prejudice the flashlamp coupling and the resultant laser mode structure.

Whilst this demonstrated the potential of pulsed ESPI as an investigative tool, the associated laser problems suggested the need for an alternative laser type. Alexandrite (an Allied Corporation manufactured crystal) is still as yet in the research phase and is not commercially available. YLF has been very difficult to manufacture and very limited numbers of lasers have been built, confidence is very low for an improvement of supply. The only other solid state pulsed laser available is the Neodymium Yttrium Aluminum Garnet based laser (Nd.YAG).

FEATURES:

(1) Ultra High Sensitivity
(2) Low Dark Current
(3) Wide Spectral Range
(4) Image Burn Resistant
(5) No Blooming
(6) High Resolution

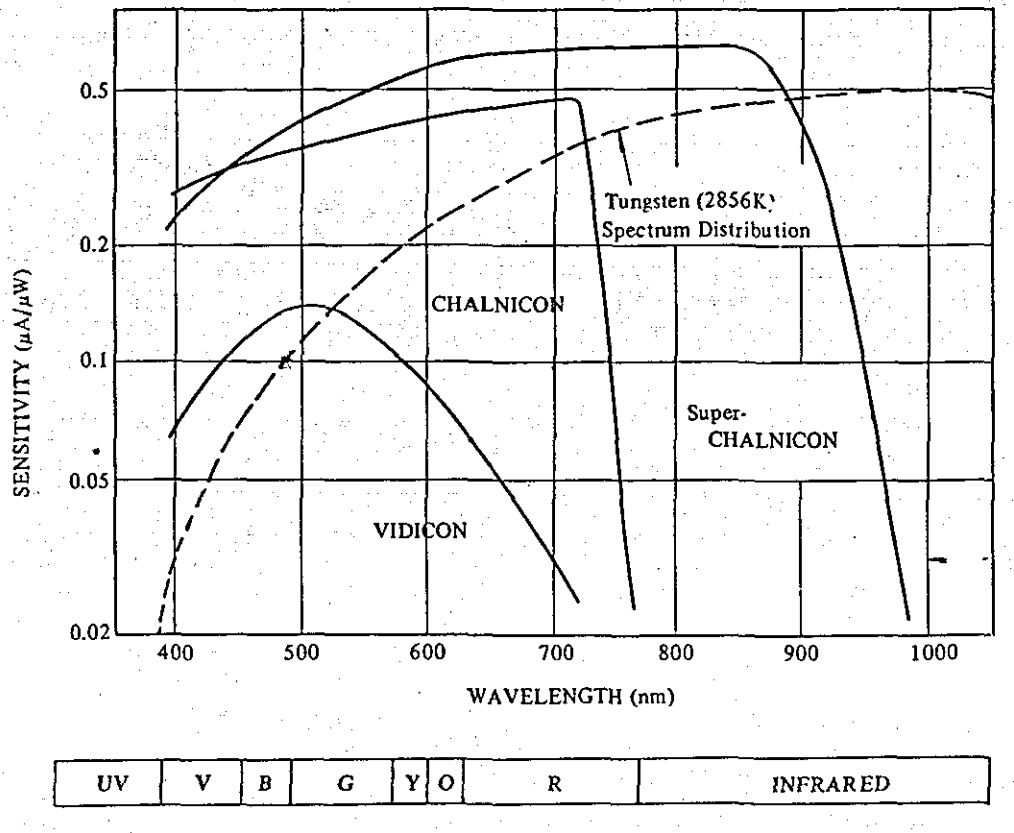

Figure 6.3
Plot of Optical Sensitivity Against Wavelength for Super-Chalnicon - Cd Te_{1-x} Se_x Target Camera Tubes

6.3 Double Pulsed ESPI with Nd.YAG Lasers

The need for on site or in-situ inspection has been identified and the potential for invasive real time measurement is considerable. The use of ruby lasers in combination with ESPI proved a useful demonstration but could not be considered a total solution. This realisation drove forward a search for alternative pulsed lasers which would be suitable. It was therefore necessary that a specification for such a system be drawn up. The key points identified were that the system should;

- be portable and self contained,
- have a high repetition rate linked to TV frame rates,
- be able to work in an underwater environment,
- operate at a wavelength to match available imaging transducers, and
- be commercially manufactured and supported.

Initially the YAG laser was discounted due to: a wavelength of 1.06 μm, mode quality, mode repeatability, double pulse limitations and repetition rates. Discussions with Spectron Lasers and JK Lasers clarified some of these points but highlighted other restrictions, the final laser specification was as follows:

Pulse repetition rate	- 25 Hz
Mode structure	- TEM_{00}
Coherence	- > 0.5 m
Output wavelength	- 530 nm
Energy per pulse	- > 20 mJ
External triggering and synchronisation.	
Double pulse operation.	

The YAG laser has usually been commercially available principally for material processing where it is used at 1.06 μm. The Neodymium (Nd) doping of the Yttrium Aluminium oxide crystal ($Y_3Al_5O_{12}$) with

concentrations of between 0.5 and 2.0% produce the highest output powers of any four level material. The crystal will emit in three groups centred around 0.914, 1.06 and 1.35 μm respectively, the 1.06 μm group being the easiest to excite. Nd doping of glass will also produce 1.06 μm output, it is easier to make large glass rods and Nd glass is preferred for lasers whose main purpose is to deliver large bursts of energy. The major disadvantage of glass is its lower relative thermal conductivity compared with YAG which imposes limitation on continuous and high repetition application. Furthermore the line width of the output is very wide, therefore only a very short coherence length is available.

The Nd.YAG laser is inherently much more optically efficient, typically (2 to 3%) compared with the ruby laser (0.5%), which means that it can operate using much smaller power supplies and at higher frequencies (up to continuous operation). The laser output is not affected by the operating frequency once thermal equilibrium has been achieved. Thus with lower input energy requirements and better thermal conductivity, the YAG can be successfully operated at 50 Hz, with no thermal or energy associated degradation of the laser output.

Mode control can be achieved in the same way as with ruby lasers (see Section A1.8) with Fabry-Perot etalons and pinholes for mode selection.

The pulse duration with Q switched operation is 12-20 nsec as compared to 20-30 nsec for ruby. With fixed Q operation the pulse duration is approximately 0.2 msec compared to 1 msec with ruby. Therefore the maximum pulse separation is reduced by one-fifth of the ruby equivalent.

The Nd.YAG crystal takes much longer to grow than ruby, therefore it is considerably more expensive and difficult to get rods longer than 200 mm. The high gain characteristics of YAG also means it is limited in the amount of energy which can be stored in the rod when Q switching. This is because the fluorescent decay rate increases due to amplifications. Thus the rod is limited to half a Joule of stored energy compared to

several Joules for ruby and therefore 150 mJ is the maximum available for a Q switched oscillator. To operate in TEM_{00} mode reduces this output by a factor of 10, a further reduction (50%) will be introduced with the line narrowing etalons and therefore amplification is necessary.

Camera selection to match the fundamental 1.06 μm wavelength limits the choice to extended red sensitive vidicons, see Figure 6.4. Comparing sensitivity of the super chalnicon at 0.69 μm and the extended vidicon at 1.06 μ shows a reduction from 0.60 A/W to 0.015 A/W (a reduction of 40). Therefore it was necessary to consider secondary harmonic generation of the laser frequency and by using a potassium dihydrogen phosphate (KDP) crystal, conversion efficiencies of between 20 -- 50% have been possible. Thus 0.53 μm radiation (green) and 1.06 μm are the combined output wavelengths from the laser. The design of the laser chassis enables the fundamental wavelengths to be filtered out allowing all conventional television camera tubes to be used. The original extended red sensitive chalnicon was used for both systems, the gain of 40 for the camera sensitivity (0.5 A/W) was at the cost of 50% laser output reduction and the KDP crystal.

Water has a transmission window at 530 nm which will enable such equipment to operate underwater. The debris in the water generates Mie scattering and reflected backscatter from suspended particles. It is possible by gating the camera to record the two returned wavefronts and amplification can be achieved (if required) by an image intensifier. An experiment was undertaken to test a gated and intensified television camera manufactured by Osprey within an ESPI system. The results were satisfactory, however, the cost at greater than £20K prohibited purchase and preliminary tests were only carried out on a camera loaned by CEGB Marchwood laboratories.

The desired laser operating frequency is determined by the television system, 50Hz for UK and Europe, 60Hz for the U.S.A. Unfortunately, the initial lasers could not operate above 25Hz. Therefore those lasers were

synchronised to record every second field. This reduced fringe contrast because of the 2:1 interlace used with video equipment and produced a television picture whose resolution was only 256 x 512. When operated in a non-interlaced mode with 50Hz operating lasers, the resolution was increased.

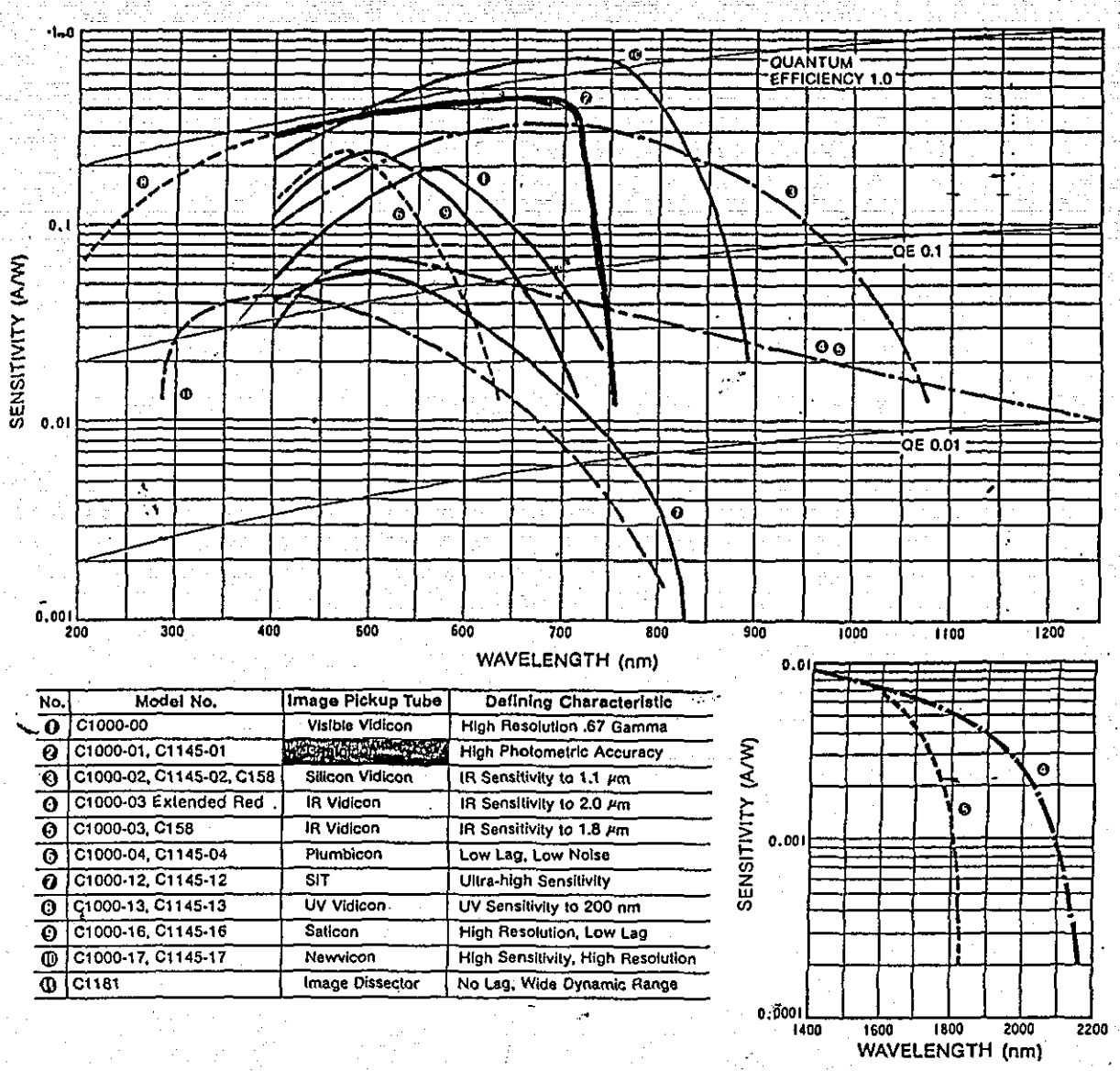

No.	Model No.	Image Pickup Tube	Defining Characteristic
❶	C1000-00	Visible Vidicon	High Resolution .67 Gamma
❷	C1000-01, C1145-01	[illegible]	High Photometric Accuracy
❸	C1000-02, C1145-02, C158	Silicon Vidicon	IR Sensitivity to 1.1 μm
❹	C1000-03 Extended Red	IR Vidicon	IR Sensitivity to 2.0 μm
❺	C1000-03, C158	IR Vidicon	IR Sensitivity to 1.8 μm
❻	C1000-04, C1145-04	Plumbicon	Low Lag, Low Noise
❼	C1000-12, C1145-12	SIT	Ultra-high Sensitivity
❽	C1000-13, C1145-13	UV Vidicon	UV Sensitivity to 200 nm
❾	C1000-16, C1145-16	Saticon	High Resolution, Low Lag
❿	C1000-17, C1145-17	Newvicon	High Sensitivity, High Resolution
⓫	C1181	Image Dissector	No Lag, Wide Dynamic Range

Figure 6.4
Plot of Optical Sensitivity Against Wavelength
for Various Imaging Television Camera Tubes

6.3.1 Nd.YAG ESPI System Design

As described previously, it is necessary to trigger the laser from the component under test, and with reference to Figure 4.6, the overall system can be described. Since the laser and camera are synchronised together their triggering signal is taken from the sensor. Three pulses are necessary: one to trigger the laser, the second for the camera control, the third to activate the framestores, as shown in Figure 6.5.

If the component is not being studied under self-excitation it is necessary to provide the requisite input to the structure. Figure 6.6 shows various methods of excitation with either electro-dynamic or piezoelectric transducers. A further output can be taken to the phase stepping optics within the interferometer to enable automated analysis of the data (see Section 5.7.2). If the component is rotating, the image of the component can be rendered stationary using an image-derotator. This approach is different to that of Praeter [52], who relies on subsequent position correlation of a rotating object to provide in-plane studies. With a derotator the normal three vectors of displacement can still be studied. Using Praeter's method, only in-plane measurements are taken. The output from the surface mounted accelerometer is used in the same way as previously, see Figure 6.5.

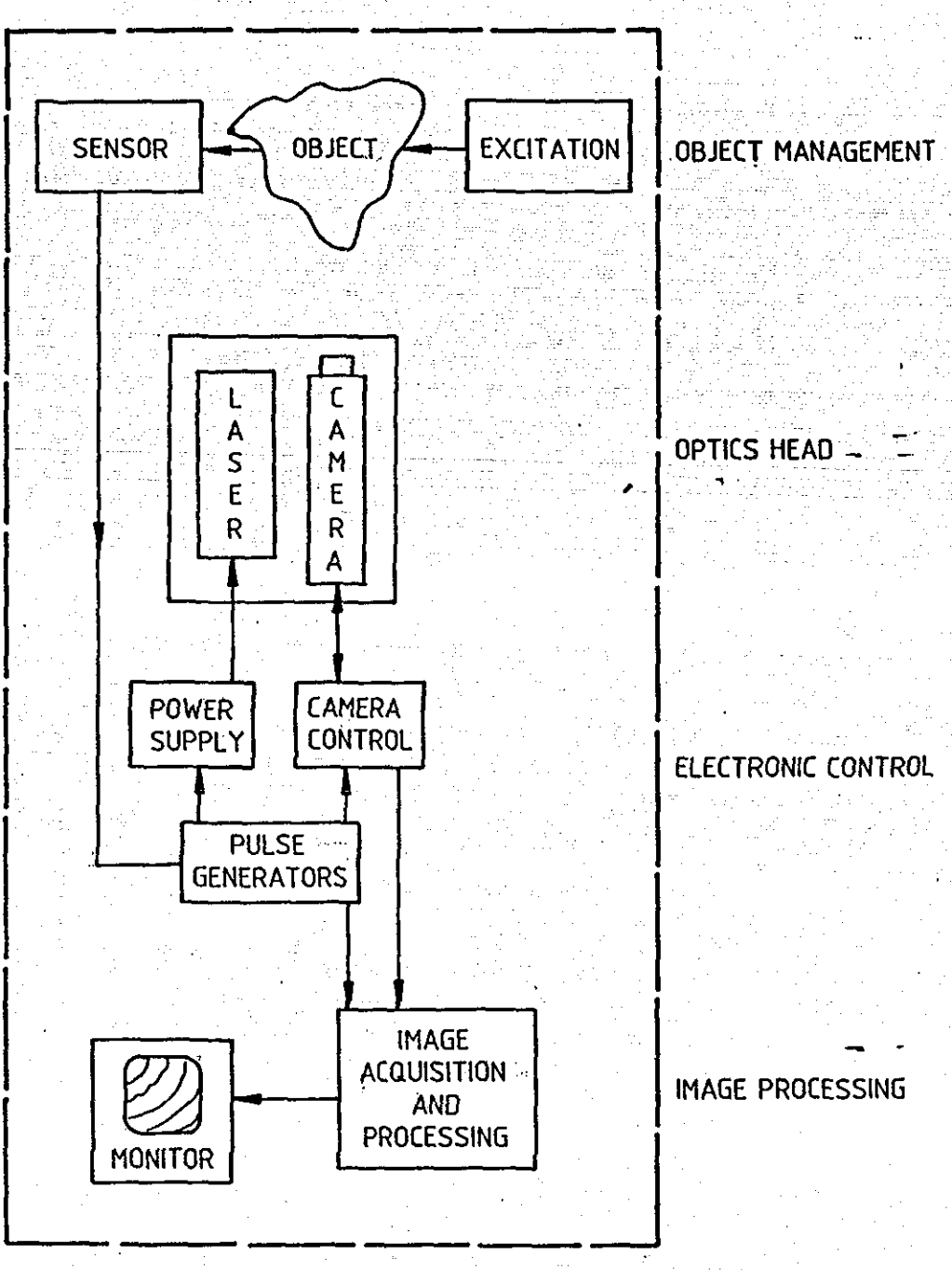

Figure 6.5
Block Diagram of Pulsed ESPI System

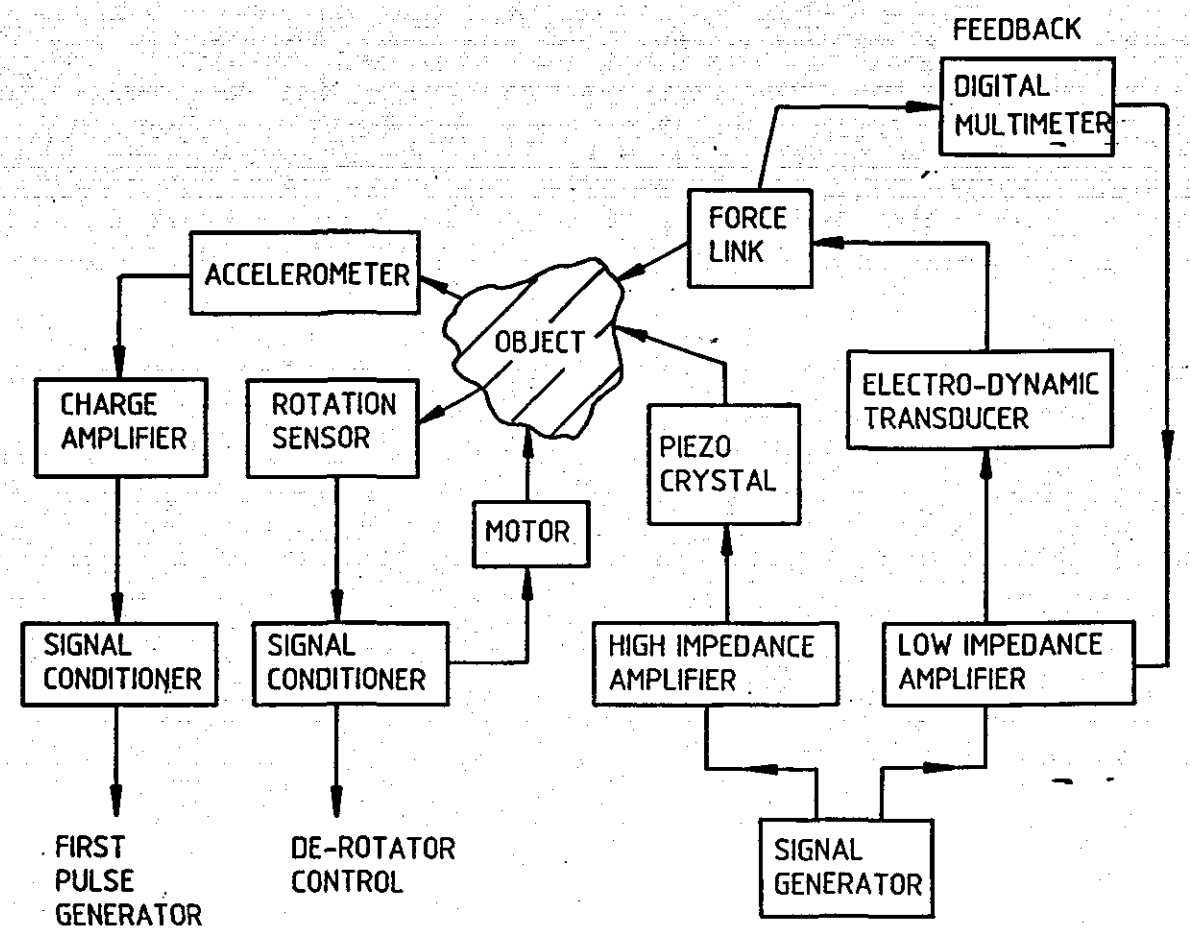

Figure 6.6
Object Management for Pulsed ESPI System

6.3.2 Optical Head Arrangement

Figure 6.7 shows the general arrangement of the laser, optics and camera. The results obtained from such equipment are shown in Plate 25 which also includes the experimental prototype used to obtain these results.

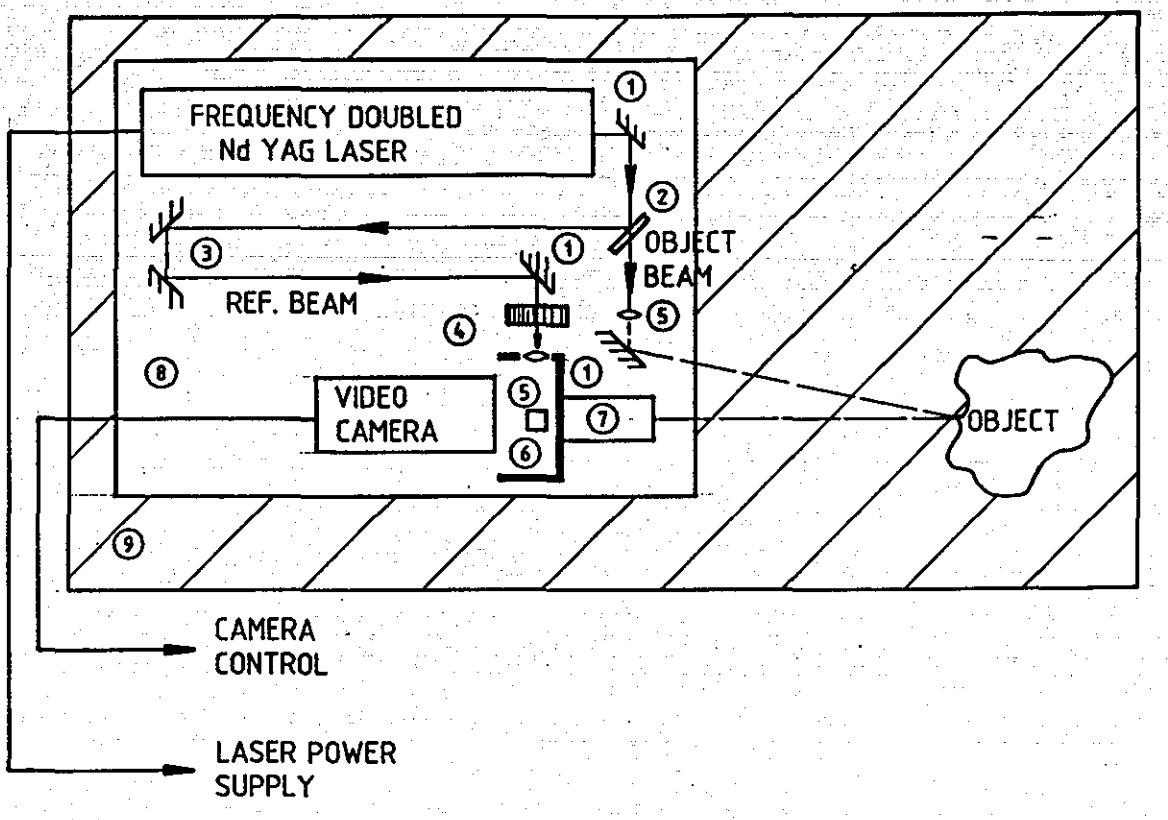

① MIRRORS COATED TO REFLECT AT 530 nm
② BEAM SPLITTING WEDGE
③ PATH LENGTH COMPENSATION LEG
④ VARIABLE NEUTRAL DENSITY FILTER
⑤ EXPANDING LENS AND SPATIAL FILTER
⑥ BEAM COMBINING CUBE
⑦ 28 - 135 mm ZOOM LENS
⑧ OPTICS BASE
⑨ OPTICS TABLE FOR MOUNTING OPTICS HEAD AND OBJECT

Figure 6.7
Experimental Optics Head Used for Double Pulsed ESPI

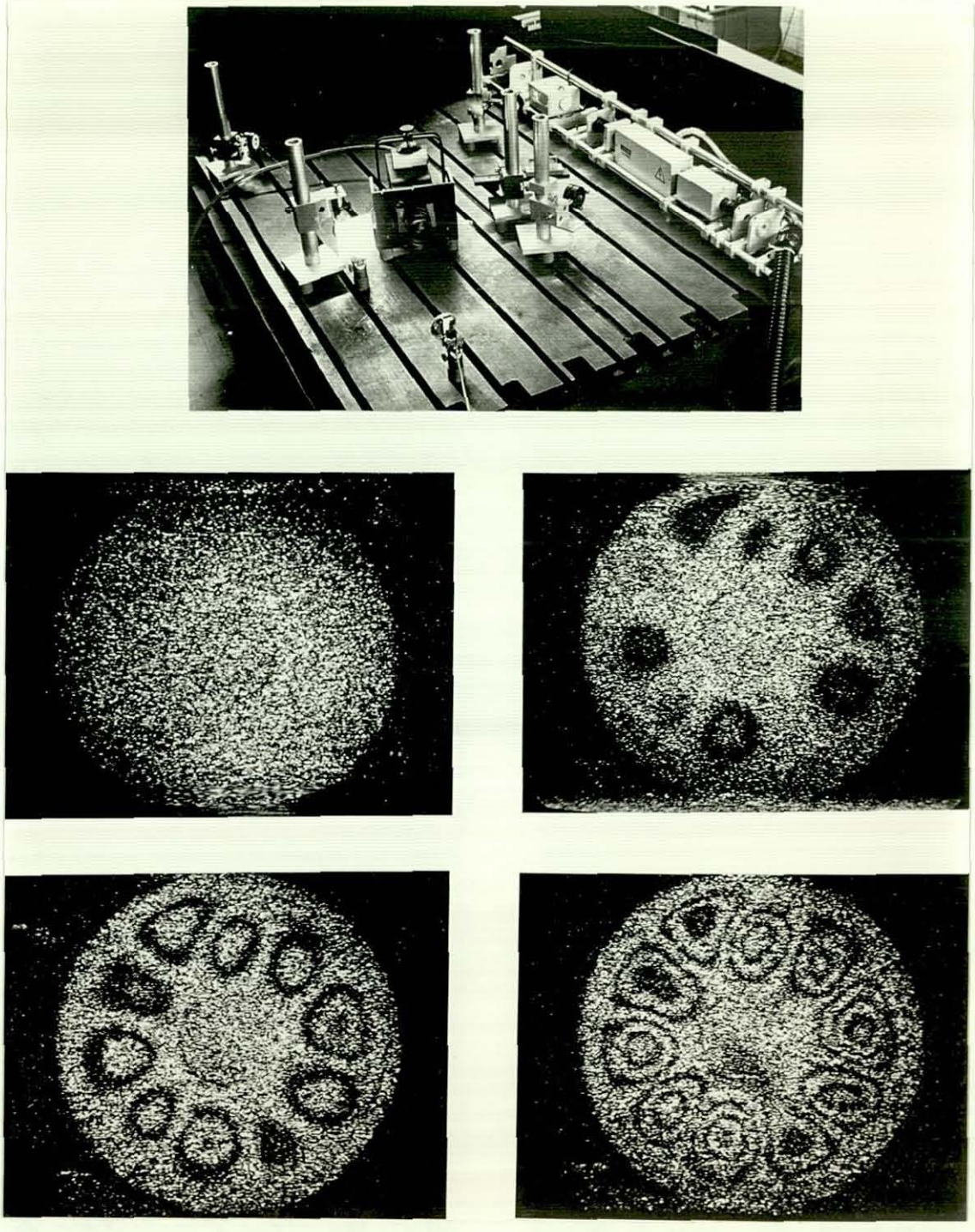

Plate 25.

Series of Results Demonstrating Animation of Object Movement Using Prototype Spectron Laser

6.3.3 Electronic Control and Image Processing

From Figure 6.8, the output from surface sensor is processed to produce the requisite trigger for the first pulse generator. This initiates the laser and provides the triggering of the second pulse generator which can delay the sensor pulse until the laser has operated when it energises the camera field coils, etc. Once the video image is available the third pulse will initiate the framestores.

The subtraction mode can be used either to remove the background optical noise or, if the pulse separation is longer than 40 msec, two framestores can be used in conjunction with conventional processing, see Figure 6.9. Initially this was achieved using two modified FOR-A framestores and more recently with a multi-page IS100 framestore in a Victor 286 microcomputer. This second system is shown in Plate 26. The system combines all necessary optics, laser and CCD television camera in one self-contained module. The object illumination can also be phase stepped to provide the necessary images for the automatic fringe analysis system.

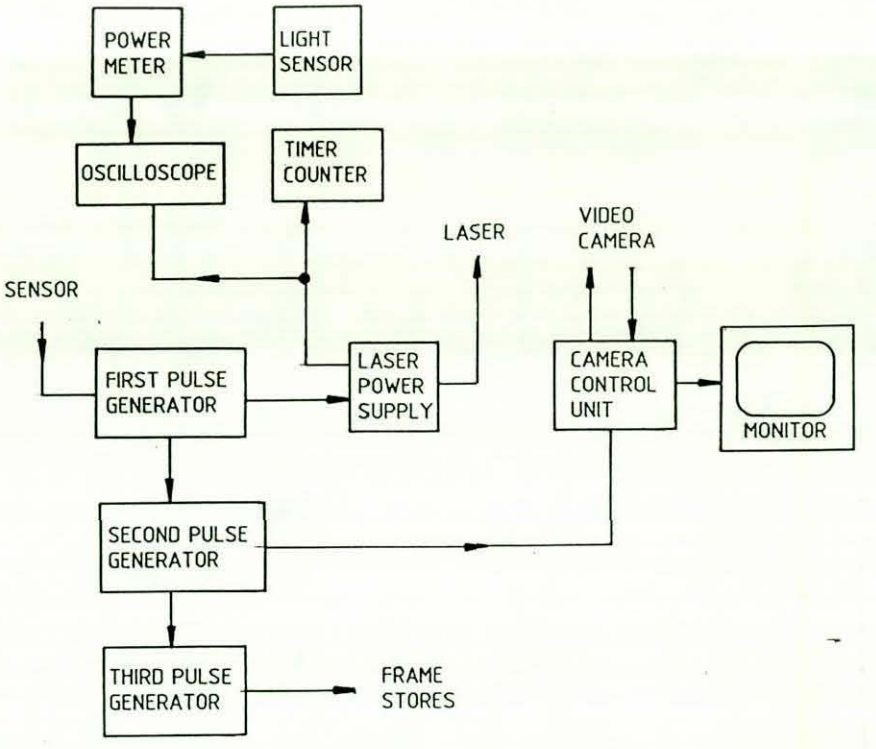

Figure 6.8
Electronic Control

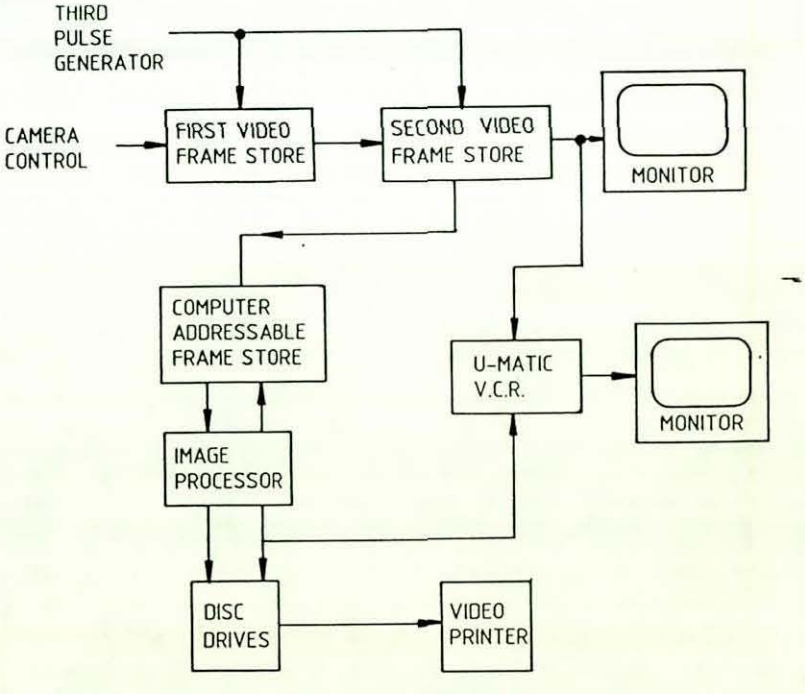

Figure 6.9
Image Processing Arrangement for Double Pulsed ESPI

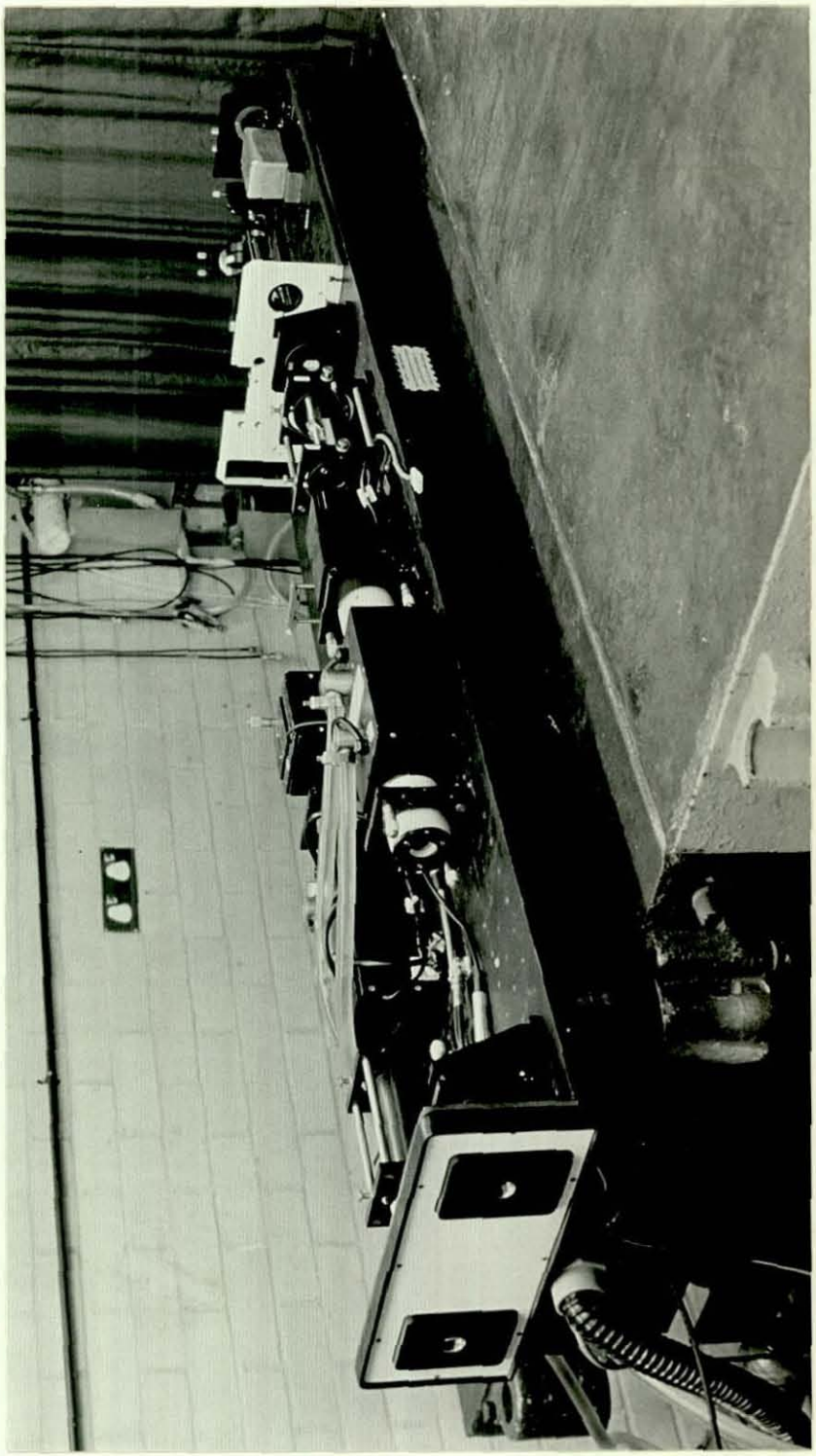

Plate 26.
Lumonics Double Pulsed Frequency Doubled
Nd.YAG Laser Based ESPI System

6.4 Computer Based Fringe Pattern Analysis of Nd.YAG Interferograms

Three fringe patterns produced by the Lumonics Nd.YAG laser were successfully phase stepped by 120° to provide the requisite data set for the fringe pattern analysis equipment. A result from the vibrating, clamped metal plate is shown in Plate 27. The laser was synchronised with the oscillator whilst the reference beam was phase stepped twice in $\pi/3$ increments, at the television frame rate. Three successive frames from the television camera were used for the image processor.

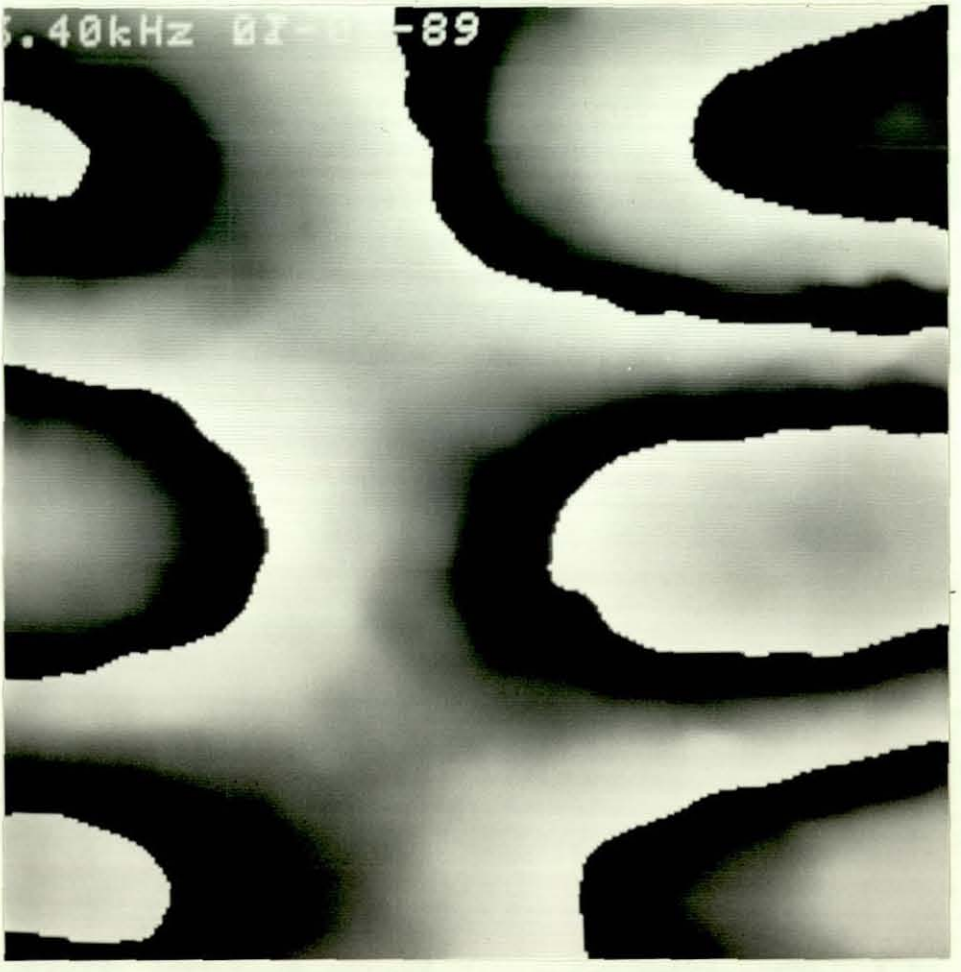

Plate 27.
Phase Stepped Double Pulsed Nd.YAG Results
of a 150mm Square Metal Plate Vibrating at 3.4kHz

6.5 Twin Laser Pulsed ESPI

The constraint governing the maximum and minimum period between the two laser pulses is the fluorescence period of the excited species within the laser crystal. Ruby has a longer maximum pulse separation at ≈1msec, whilst YAG is ≈250 μsec. Twin flashlamp excitation of the crystal has been successfully used as has twin excitation of a single flashlamp. Adjustment of the interval between pulses will, in all cases, produce a change in relative pulse energies. This is due to the variation of Q switch delays and pockel cell driver voltages. Nd.YAG can operate with higher optical conversion efficiency than ruby, enabling higher repetition rates, although operation beyond 25Hz was too demanding for the currently available Lumonics double pulse pockel cell driver systems. The high frequency operational instabilities of the pockel cell result in variable pulse to pulse energy and degraded laser beam pointing. The problem of beam pointing manifests itself as arbitrary fringes seen across the whole object fringe pattern or as fringe pattern drift.

Conventional accelerometer based vibration analysis relies upon time varying velocity changes, thus providing information which is temporally continuous, but spatially discontinuous. Double pulsed ESPI, on the other hand, provides data which is spatially continuous but temporally contiguous. A requirement therefore exists for a device which combines both continuous temporal and spatial information. One method of achieving greater temporal sampling interferometrically is illustrated in Figure 6.10.

Pulse 1 is synchronized with one peak of displacement, pulse 2 is also synchronized but an increasing delay between pulses is introduced. This could be produced by modifying the arrangement shown in Figure A.3. Unfortunately, using conventional double pulsed lasers each successive pair of pulses would require re-adjustment of several laser parameters which would not be practically possible with 50Hz operation.

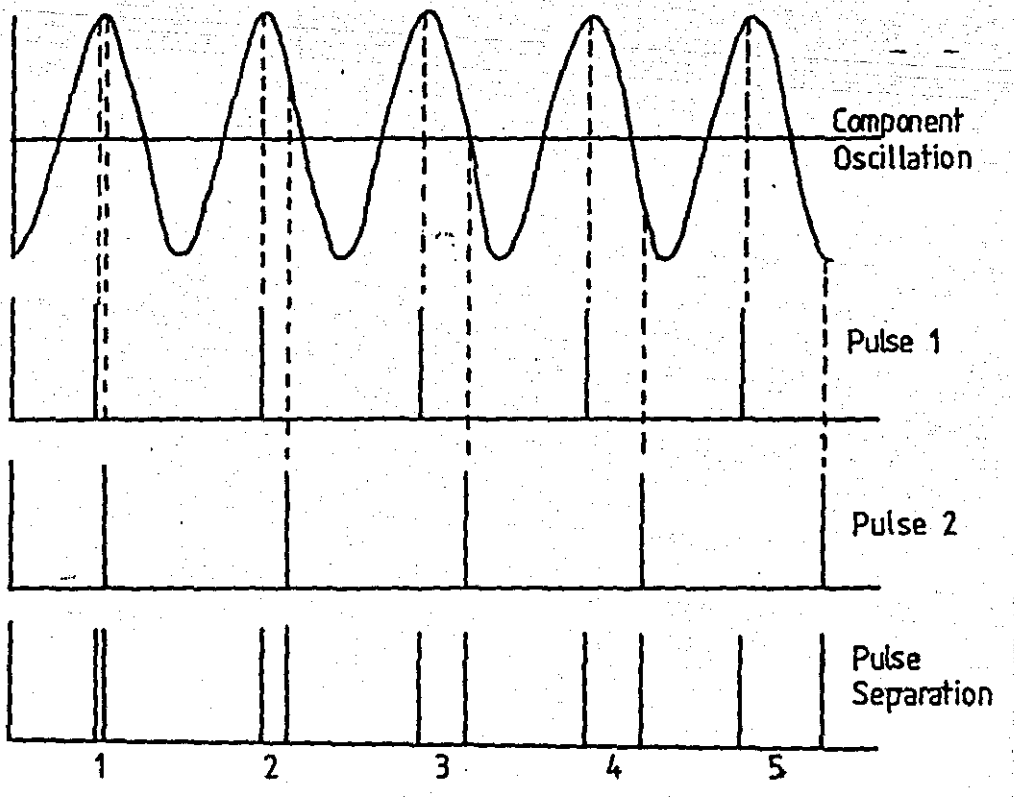

Figure 6.10
Triggering Arrangement for Temporally Modulated
Twin Laser Pulsed Interferometry.

However, this would not be the case if two separate lasers were used. In order to do this within an interferometer, it would require that the two pulsed lasers were combined such that the output beams appear to emanate from a single source. Thus each laser is individually operating as a single pulsed laser with each being individually synchronized from time varying triggers. Consequently, each laser can be fully optimised for best individual performance and exhibit minimal pulse to pulse variability, no matter what the relative pulse separation is.

The concept of twin laser interferometry is believed to be original, the necessity being driven by a need to continuously vary the pulse separation without need to alter the individual laser performance. A patent, No. 8613635, covering this work, was applied for in June 1986 which summarised the invention as "appropriate by use of separate sources of variable phase relationship to generate the respective pulses at times which are not interdependent as is the case where a common source is used".

Initially, trials were undertaken which used two separate laser oscillators which fed into a common laser amplifier, see Figure 6.11. The reasons for this were twofold:-

(i) To ensure a common source for the optical output of the laser.

(ii) To ensure a consistent wavelength should any frequency shift exist between the two oscillators.

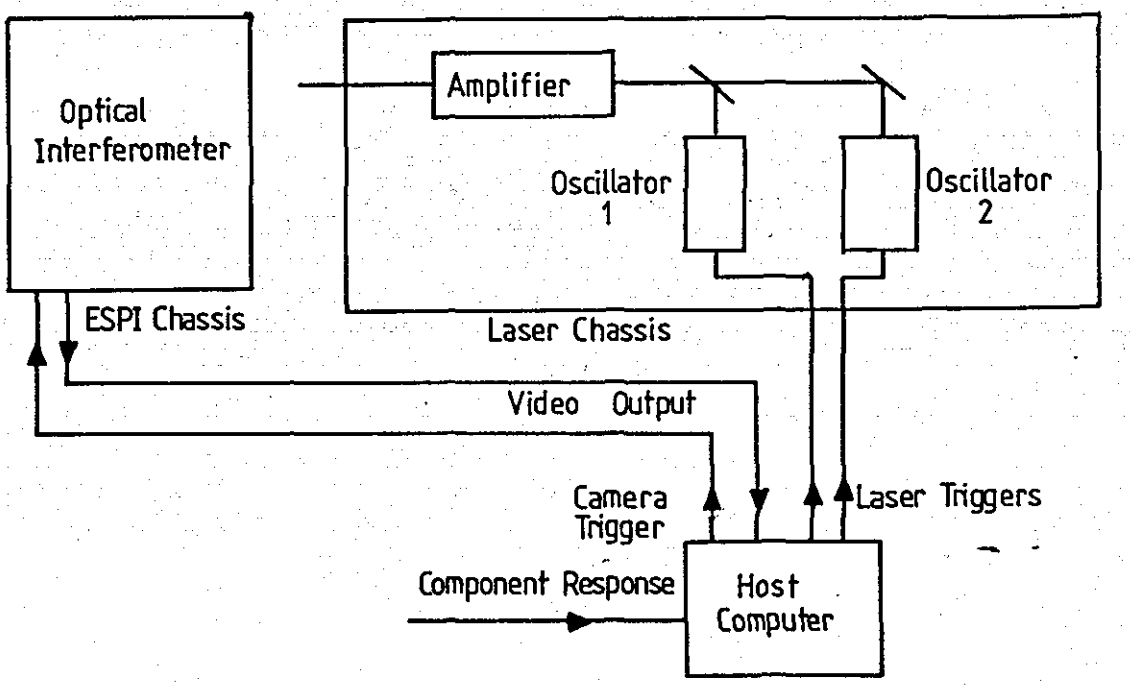

Figure 6.11
Schematic Arrangement of Twin Laser Oscillator ESPI System

Unfortunately, the laser dynamics which constrain the oscillators similarly constrain the amplifier. Thus having energised the amplifier crystal, the first laser pulse from oscillator 1 extracts all the gain available and the system reverts back to a single pulse oscillator-amplifier arrangement with a second weaker pulse as a result of the depleted amplifier absorbing some of the second oscillator energy.

Therefore, it was necessary to design and construct a double oscillator, double amplifier laser - effectively two complete lasers sharing the same optical chassis, see Figure 6.12. Whilst Park et al [53] have suggested the use of injection seeding for frequency stability of a single oscillator, it is suggested here that a novel approach may be taken by using a single seeder to excite two oscillators, thereby ensuring similarity. This was done to remove the possibility of unwanted double pulse contouring (a consequence of frequency difference). A further advantage of seeding is that when a narrow band source is used, the system will retain that narrow bandwidth. Thus long coherence length of the lasers is achieved without the need for intracavity etalons and the energy loss (approx 45-50%) associated with Fabry Perot etalons is no longer suffered. To retain long term thermal stability and the conjugacy of the two lasers, three bar invar rail arrangements are used to mount all laser components.

With the release from the constraints imposed by the fluorescence of a single Nd.YAG crystal, a minimum pulse separation of less than 10 nsec is achievable. The pulse separation needs to be greater than the pulse duration, so intervals of greater than 10 nsec are used.

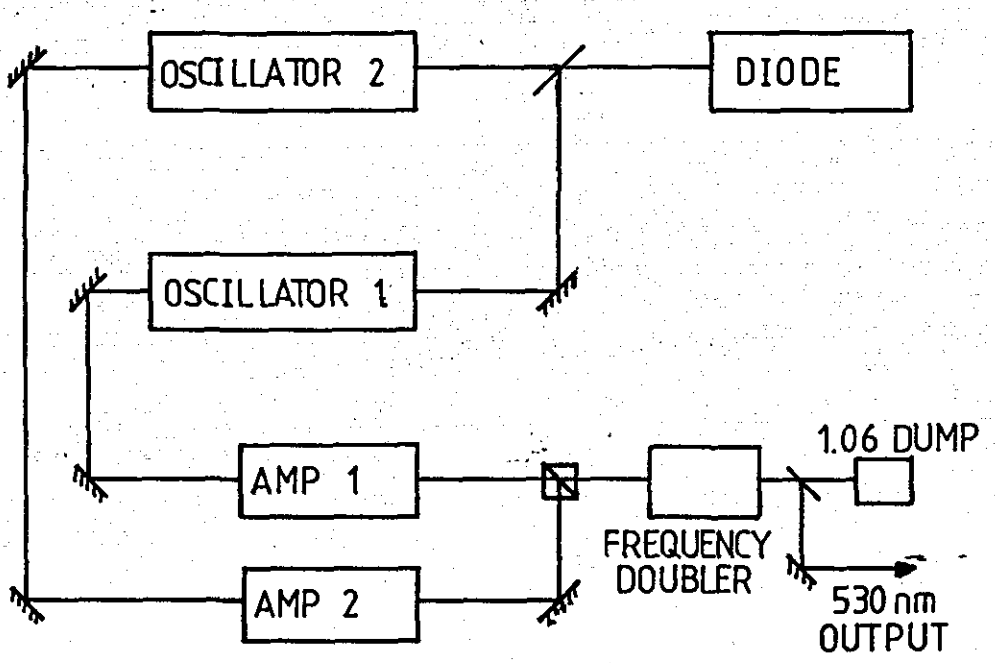

Figure 6.12
Arrangement of Twin Seeded Oscillator/Amplifier
Nd.YAG Lasers with Frequency Doubling

6.5.1 An Overview of Injection Seeding of Solid State Lasers

In the solid state ruby lasers used for the holographic experiments and the initial Nd.YAG ESPI laser, the amplifier is injected with a line narrowed Q switched pulse from the oscillator. The principal can be extended with injection of the oscillator from a very narrow linewidth beam whilst the Q switch is open. Rahn [54], put forward principles of stabilising the injection of a Nd.YAG laser, which formed the basis of the seeding approach taken in this work. Injection seeding requires the seed laser emission to be orders of magnitude more intense than the noise emissions present within the oscillator cavity. This relies on the seed frequency being within the bandwidth of the laser cavity. Consequently, the pulse developing out of the seed signal will saturate the gain medium and extract the desired energy prior to any coincidental activity from any noise emission. Thus competitive amplification of noise emission is inhibited.

The free spectral range of the oscillator enables many different longitudinal modes to exist with a frequency spacing given by:

$$\Delta\nu = \frac{c}{2L}$$

where ν = Frequency spacing,
c = Velocity of Light,
L = Optical Path Length of the laser resonator.

The resonator length is 0.6m

$$\Delta\nu = \frac{3\times10^{8}}{2\times0.6} = 250 \text{ MHz}$$

The Nd.YAG gain curve is approximately 120 GHz taken at the Full Width Half Maximum (FWHM) point, and can therefore, support many competitive modes. As discussed in Appendix 1, various methods for suppression of the transverse modes and selection of a longitudinal mode exist. Usually spatial filtering with an aperture for transverse modes,

and narrow bandwidth optical filtering for longitudinal modes are preferred. A semi-conductor laser utilises a different electro-optical mechanism for photon generation than that discussed in Appendix A1.8. This mechanism relies upon emissions based on the band gap energy which is uniquely determined for a pure semi-conductor at a given temperature and pressure. With precise control of the diode operating currents and with temperature stabilisation, a very narrow line width can be continuously achieved with average powers > 1 milliwatt. This is at least 5 orders of magnitude greater than the spontaneous noise level within the solid state (Nd.YAG) material. Usually, with unseeded operation, the Optical Build-up Time during Q switched operation is typically 45 nsec, requiring the competitive generation of emission within that interval. With seeded operation no reliance is made upon the spontaneous time lag and injection can take place 30 nsec after initiation, reducing the Optical Build-up Time and ensuring total gain removal prior to the noise build-up some 15 nsec later. The energy level associated with the injected single mode will be in the order of 10^3 times more intense than any other longitudinal mode.

6.5.2 Matching the Seed Laser to the Nd.YAG Oscillator

The seeding diode laser and Nd.YAG oscillator have two separate chasses and are consequently independent in frequency control and stability. Frequency matching of the narrow bandwidth diode laser to the broad spectrum of line frequencies of the YAG chassis is achieved with active control of the YAG cavity length. The rear reflector of the chassis is mechanically translated with a piezo electric crystal, which is controlled via a feedback loop. Temperature stabilisation of the cooling water provides some additional control, which although much slower to react will tune the overall operating frequency of the cavity. The primary purpose of the cooling water is to maintain long term frequency stability.

The minimum Q switch build-up time of a correctly matched seed and oscillator pair corresponds with the maximum injection seeded energy output. Therefore, the rear piezo electric frequency tuning mirror can be manipulated with reference to the Q switch build-up time. The eventual control loop employed in Figure 6.13, is taken from the Spectron Laser Control Handbook [55].

To minimise the Q switch build-up time, the control electronics develop an error signal using the derivative of the build-up time with respect to the host cavity length (dTb/dL). When the error signal is minimum, the Q switch build-up time is at its minimum value for that host cavity mode. The error signal can be integrated over a time period to produce the control voltage for the piezo tuning element. The derivative (dTb/dL) is developed by dithering the cavity length and measuring the change in build-up time. This dither is produced by translating, in an alternating fashion, the piezo about an average position. The exact frequency of the pulsed laser is determined by the cavity length, thus it is desirable to minimise the dither to maintain a stable output frequency.

The frequency of the seed laser can be tuned with temperature and its output can be tuned to the centre of the host lasers gain curve. This produces the most effective and stable seeding and has the highest seeded output power from the Nd.YAG.

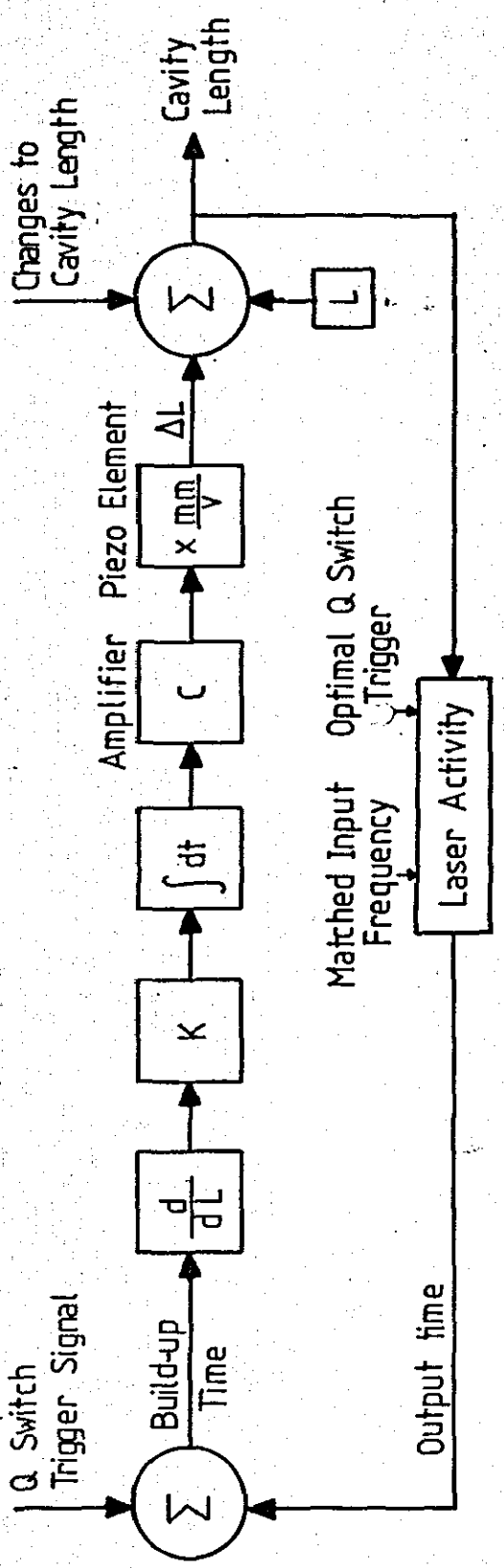

Figure 6.13
Control of Piezo Electric Frequency Tuning Mirror

6.5.3 Coupling the Seed Laser to the Nd.YAG Laser

The Nd.YAG laser still utilises an intracavity aperture to ensure diffraction limited performance which requires the seed laser to input a collimated beam of small diameter. Prior to coupling to the Nd.YAG laser the diode must be protected from any radiation propagating back from the host laser beam because of the leaking rear reflector. The energy levels available could destroy the seed laser and to decouple the two lasers a Faraday Isolator is used. This also ensures the seed laser preserves frequency stability with no optical feedback. The diode laser does not have a preferential polarisation axis, consequently a half wave plate is inserted between the diode and the Faraday Isolator. The extinction ratio required by the Faraday Isolator to protect the seed laser is of the order of 50db. To ensure this high extinction ratio, the isolator demands temperature stabilisation to maintain performance. The overall arrangement is shown in Figure 6.14.

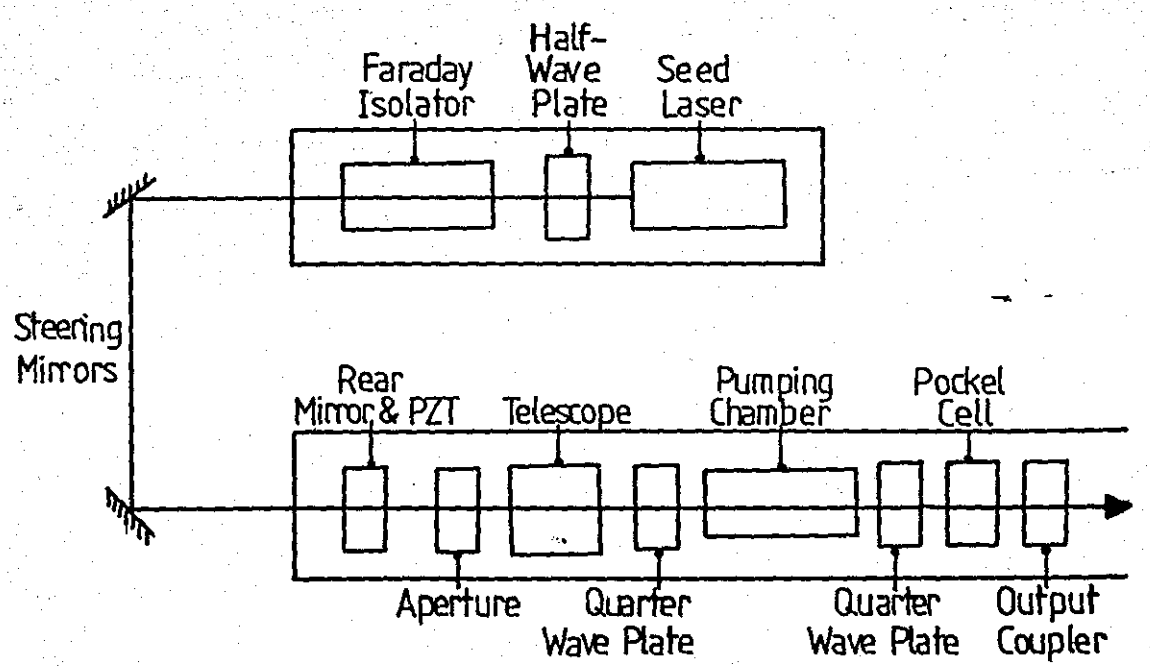

Figure 6.14
Component Arrangement of A Diode Seeded Nd.YAG Laser

6.5.4 Combination of Twin Output Beams

Efficient recombination of the two amplified laser pulses is achieved with a polarising beam combiner cube. The combiner chosen required a low optical insertion loss and high efficiency combination. No amplitude beamsplitter could survive the incident energy densities nor provide efficient coupling. A polarisation beam splitting cube is used successfully to handle high input energies and divide in the ratio:

$$\frac{I\ trans}{I\ refl} = \cot^2 \psi$$

where ψ is the angle the incident electric vector makes with the vertical.

Used in reverse, when one beam is presented in the vertical and the other in the horizontal, the combination will be achieved with neglible insertion loss. The output will still retain the orthogonal relationship between the electric vectors of the beams. Hence the two output pulses, whilst coaxial, would be rotated relative to one another by 90° and therefore not mutually coherent. The solution to this problem was achieved using the frequency doubling crystal. The input acceptance angle to the KD*P is to within 45° of its aligned axis. The frequency doubled output would be aligned with the principle crystal axis, whilst the fundamental residual energy would transmit through with no re-orientation. A half wave plate is then used to re-orientate the electric vector of the doubled output back from 45° to the vertical. A dichroic mirror is used to split off the doubled output from the fundamental. The residual 1.06μm energy is then absorbed in a tubular beam dump.

The optical combination was achieved by adjusting the output combining arrangement aligning laser 2 into the beam path of laser 1. Final adjustment is achieved using an interferometer initially set up for laser 1. With the framestore in subtraction mode, laser 1 is turned off and laser 2 turned on. Fringes are seen across the image as a result of the misalignment, which can be minimised using the x, y mirror adjustment of the beam combination optics. A setting is thereby determined with both lasers now truly coaxial.

6.5.5 Results Obtained from Twin Pulsed ESPI

It was highly satisfying, when after installing and commissioning the laser, results were obtained immediately from the interferometer. To examine the interferometric quality of each laser, the oscillators were operated individually. A difference in fringe contrast was observed in fringes over the test object, (the clamped metal plate) with laser 2 unable to exactly match the quality of laser 1. Occasional momentary loss of the fringe pattern was observed, this being attributed to the oscillator cavity piezo mirrors coming to the end of its compensating travel followed by automatic resetting and during this period coherence is lost. Initially each laser was triggered internally and the plate oscillated independently producing fringe patterns which varied in density depending upon the beat frequencies of the oscillation against the 50Hz internal trigger. Triggering the laser from the oscillator successfully phase locked the fringe pattern and produced stable results. The interferometric depth of field available from the laser is greater than 1m. A 10 ns pulse produces a light beam 3.0m long. Thus for adequate coherent light to combine at the television camera and produce high contrast fringes path length compensation is necessary for maximum depth of field. Early out of plane results are shown in Plate 28, where to demonstrate the flexibility of the system, results are presented of the author's hand pushing against the optical table. The final result, Plate 29, is of the author holding a vibrating plate oscillating at 13040 Hz, demonstrating the ability of twin pulsed ESPI to examine objects totally independent of the interferometer.

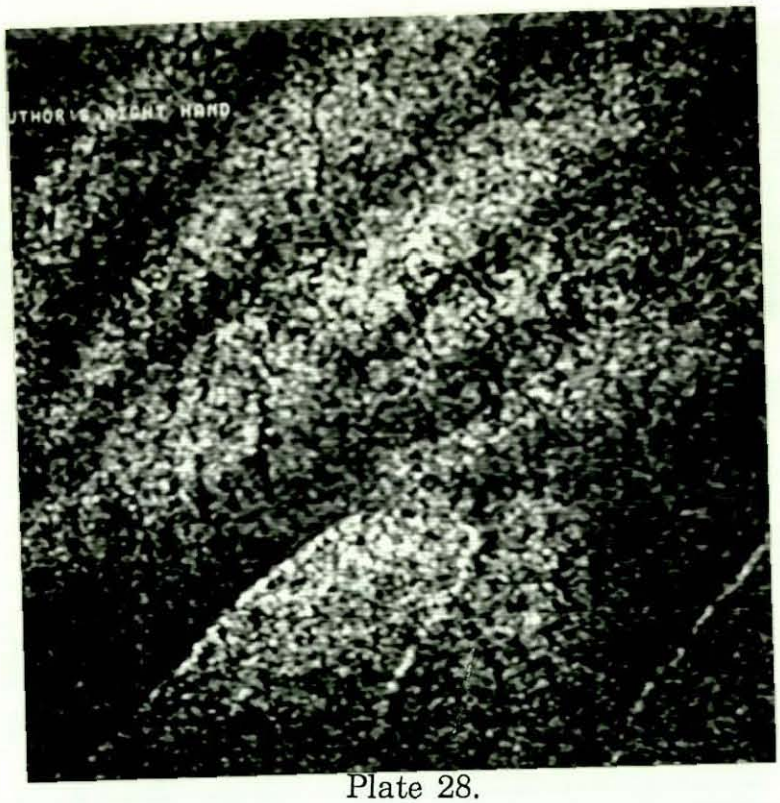

Plate 28.

Twin Pulse ESPI Fringe Patterns of a Hand Pushing Against the Fixed Optical Table

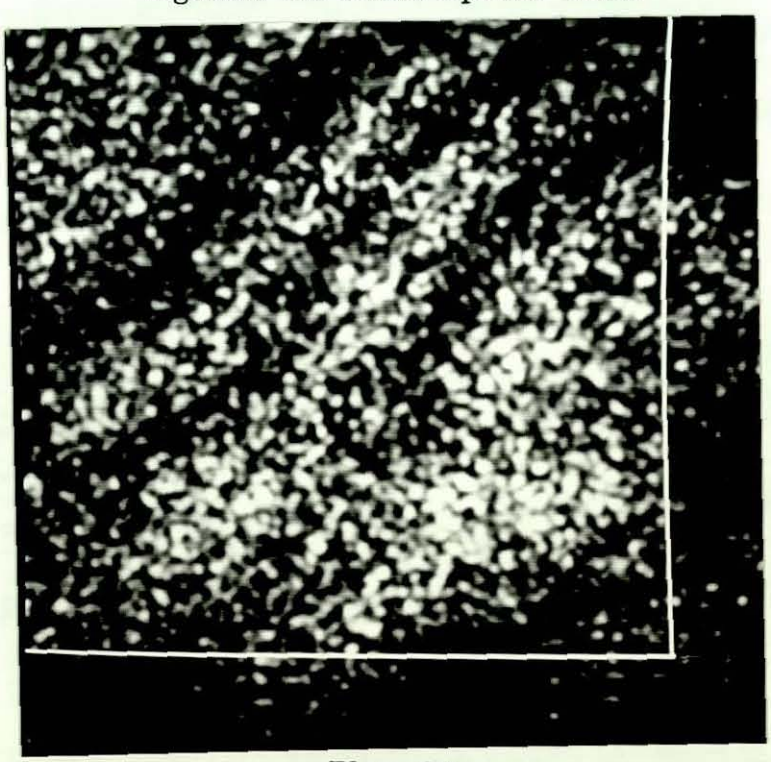

Plate 29.

Twin Pulsed ESPI Results of a Handheld Clamped Metal Plate Oscillating at 13,040Hz

6.5.6 Post Processing of Twin ESPI Fringe Patterns

As shown in Appendix A2.3.2, addition fringe patterns have a $\cos^2$ function on top of the combined object and reference background terms. The raw data gathered for a twin pulse interferogram is shown in Plate 30. If the reference beam optical noise is initially stored and subtracted using a framestore, the result is seen in Plate 31. Creath and Slettemoen [74] reported similar results for the CW case. With no amplification of brightness and contrast, fringe patterns are difficult to observe although adjusting the contrast of the television monitor can assist this.

To verify the concept of interference between the two different laser pulses, each laser (in single pulse operation) was operated in a stroboscopic manner to obtain the conventional subtraction result as seen in Plate 32. This result is obtained from using laser 2, (identical results were obtained from laser 1), with the plate vibrating at 1350 Hz. Verification of twin pulse mode was achieved by synchronising the positive peak of the surface displacement with laser 1 and the negative peak with laser 2. Plate 33 shows the result of subtracting the images each obtained from a separate laser. The fringe visibility is comparable with that of Plate 32. A major breakthrough in twin pulsed addition fringe visibility was obtained when a second framestore was utilised. A combined interferogram of the surface at rest was stored in a second framestore and the live twin pulse image subtracted from it, effectively undertaking a further correlation subtraction of the fringe pattern from the rest condition. This may be of benefit in identifying and separating bulk body motion from surface displacement. The result can be seen in Plate 34.

An advantage of this approach is the ability to post process data recorded on videotape, Plate 34 was produced from data originally captured using a U Matic videotape recorder and played back via the video processors. Thus source data recorded using the pulsed equipment during an in-situ analysis provides the opportunity for repetitive sequential analysis which may be of benefit during complex modal study.

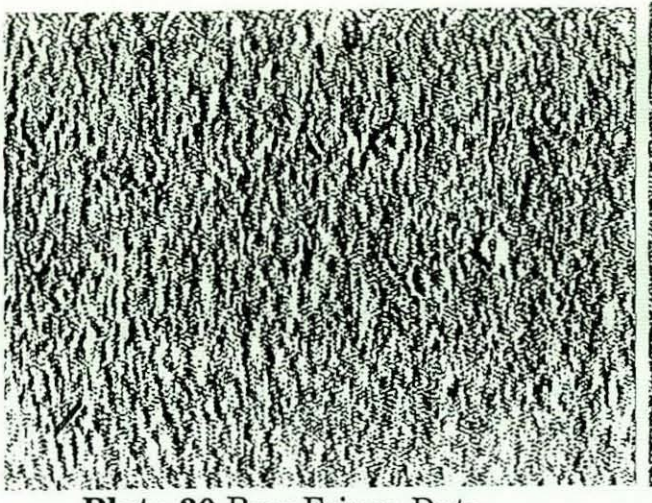

Plate 30 Raw Fringe Data from Twin Pulse Addition

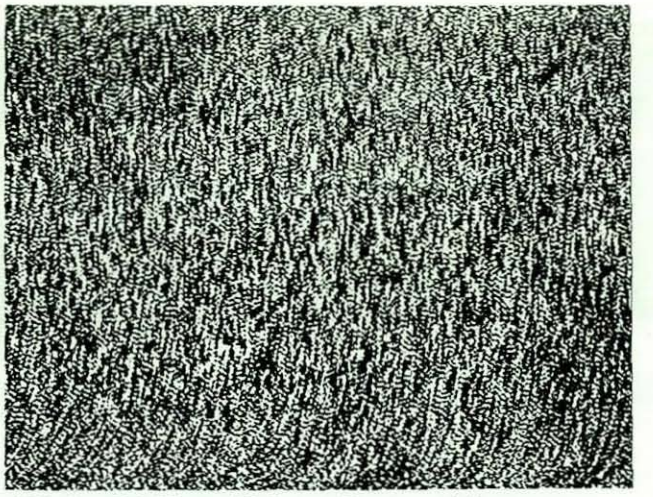

Plate 31 Raw Fringe Data with Reference Beam Noise Subtracted

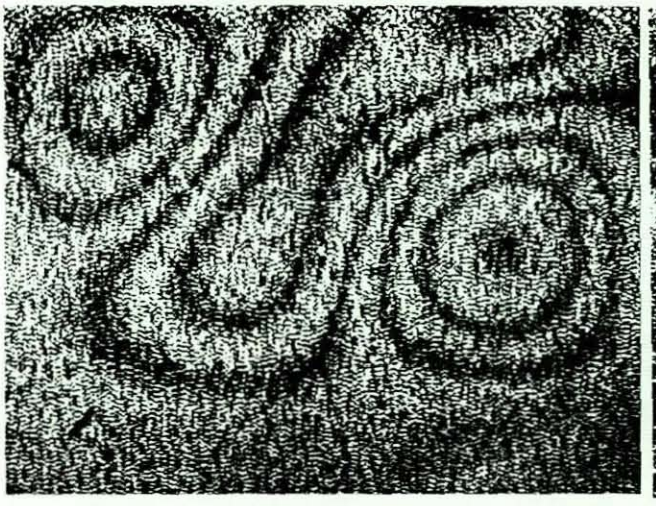

Plate 32 Stroboscopic Subtraction Fringes Produced using Laser 2

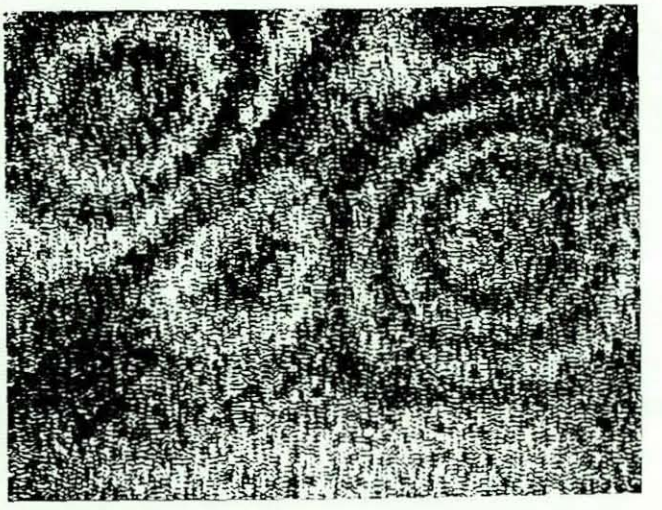

Plate 33 Stroboscopic Subtraction Fringes using a Pulse from Laser 1 and a Pulse from Laser 2

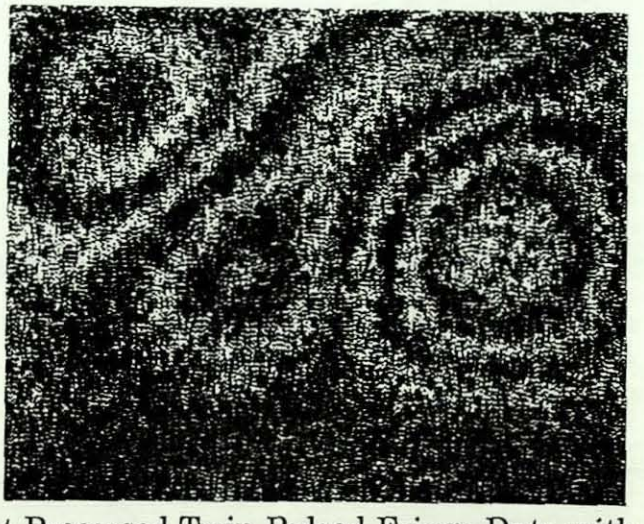

Plate 34 Post Processed Twin Pulsed Fringe Data with Background Subtracted using Second Framestore

6.6 Conclusions

This chapter has concluded the programme of work as laid down in Chapter 1. The final objective has been the production of an ESPI system that could operate free from the constraints of the laboratory. The equipment produced was suitable for combination with the computer based fringe analysis equipment described earlier.

- Previous work involving pulsed ESPI relied upon a ruby laser as the source. Experiments proved this laser type to be difficult to work with and capable of only limited double pulse repetition rates (1 pulse every 5 seconds).
- After a review of commercially available pulsed laser types it was decided to modify a Nd.YAG laser to double pulse operation. The laser chosen was able to operate at 25Hz and a frequency doubling crystal was used to produce 530nm (green) coherent radiation.
- The use of frequency doubling and CCD television cameras provided equipment of adequate photometric sensitivity, enabling an object size of $1m^2$ to be illuminated with 35mJ of output energy.
- CCD cameras were successfully used to store two pulse images prior to input to the digital framestore.
- New image filtering electronics were designed to accommodate the pulse to pulse variation in laser beam intensity.
- Full digital control of the image acquisition system and laser triggering was achieved using a micro-computer.
- Double pulse ESPI fringe patterns were successfully produced using the computer based fringe analysis software. The results provided both amplitude and phase information over an entire vibrating object.
- Frequency line narrowing using intra cavity etalons led to unexpected laser beam pointing instabilities. A coherence length of >1m was available using line narrowing.

- Fringe contrast was reduced using every alternate television picture field, (a consequence of using 25Hz operation), effectively reducing the image resolution to 256 horizontal by 512 vertical lines. 50Hz operation was beyond the Lumonics Nd.YAG laser, the poor power factor of the charging system required a 60 amp supply to maintain 25Hz.
- To overcome the limited pulse separation period available from Nd.YAG a twin pulse solution was proposed. Seeding of the two laser oscillator/amplifier combinations by a common narrow bandwidth diode laser ensured output with a long coherence length. Using diode seeding provided higher output energy than the previous filtered Nd.YAG laser design.
- A twin laser was successfully produced with improved output intensity and beam pointing stabilities over the previous double pulsed design.
- Twin pulsed ESPI was successfully demonstrated, verifying the concept first proposed in 1986.
- Fringe contrast enhancement was possible for double pulse or twin pulse results when the camera lens was blocked and the framestore was loaded with the residual system noise (mostly from within the reference beam). Subsequent operation of the system yielded higher fringe contrast when the noise component was continuously subtracted.

CHAPTER 7
CONCLUSIONS

The primary objective of this work was to produce an instrument which could undertake wholefield inspection and displacement measurement utilising a non-contacting technology. The instrument had to permit operation by engineers not necessarily familiar with the underlying technology and produce results in a meaningful form. Whilst optical technology was considered suitable, two objectives remained. These were;

i) To identify an effective quantitative measuring technique.
ii) That a chosen route could eventually result in a practical instrument.

Of the possible techniques widely cited in the literature, Holographic Interferometry was identified as partly meeting these objectives. The use of double pulsed lasers extended the technique to undertake work in an industrial environment. Recognition of the experimental difficulties in using Holographic Interferometry in practical engineering studies suggested Electronic Speckle Pattern Interferometry (ESPI) to be a more suitable technique. Re-design and reconfiguration of the Speckle Pattern interferometer, combined with research into the processing electronics produced equipment of suitable form able to be exploited by external manufacturers. Further research led to successful computer based fringe analysis capable of automatically reducing the fringe pattern to meaningful data. The final effort was the combination of ESPI with novel pulsed lasers to produce the prototype for the required instrument technology. Conclusions drawn from this research are discussed in the following pages.

Holographic Interferometry was one technique originally considered as offering a number of desirable features. Experimental work undertaken provided data which confirmed the potential of the technique for solving problems but also highlighted some difficulties. The available recording media were examined to determine whether an automated recording process could be produced. The problems encountered suggested this was difficult to achieve in a general instrument. The recording materials investigated highlighted the need for high illumination levels due to the inherent low photometric sensitivity of the recording media. To record holograms of large objects, greater than $1m^2$, exposure times of the order of seconds required laser output powers of >1 Watt. Whilst this could be achieved experimentally, the technique suffered from environmental disturbances, a $\lambda/8$ variation in relative pathlength during exposure would seriously reduce the brightness of the hologram. A technique tried to combat this was common path interferometry, which reduced the experimental susceptability to external changes but was not always experimentally practical.

Considerable effort was required to extract quantitative data from the holograms. In order to perform a complete three dimensional displacement analysis a number of holographic views must be recorded, each requiring the same demanding environmental stability. To determine the cartesian displacement vectors, (x, y and z) from the hologram, requires intensive computational reduction from a number of fringe patterns recorded using secondary imaging transducers, either photographic or video. Error analysis of the experimental arrangement highlighted a number of practical restrictions which lead to data uncertainties. Qualitative analysis using Holographic Interferometry had been very successful and resulted in useful analytical data which was used in three different engineering design programmes. Unfortunately, attempts to quantify the data to provide strain values relied upon double differentiation of the fringe field, a process that is highly sensitive to fringe position errors. These experiments provided the confidence that optical interferometry was able to produce data of suitable displacement sensitivity, with results that

were acceptable to other engineers. No arrangement could be determined which provided the basis for a measuring instrument. The lessons learnt in this instance steered the research toward double pulsed lasers and Electronic Speckle Pattern Interferometry.

Double Pulsed Holographic Interferometry. Experiments were undertaken to extend the capability of Holographic Interferometry using double pulsed ruby lasers. This work was necessary to determine the possible limits of the technique. Aside from the equipment limitations, the experiments demonstrated a reduction of photometric sensitivity by a factor of two in the silver halide recording material when used with pulsed lasers. This was due to the short exposure times from the Q switched ruby laser, defined by Reciprocity Law failure. The experiments did provide confidence that with suitable design effort, interferometric arrangements could be constructed that could work in the most arduous of industrial environments.

Triggering of the laser from a secondary transducer resulted in various electronic configurations which successfully provided temporal and spatial investigations of vibrating component surfaces. However, the problems of data extraction common to holographic techniques led to questions about data quality and interpretation. This in turn initiated a search for alternative interferometric techniques. During this work three requirements were identified as essential to further the original objectives, these were;

(i) The optical technique must provide three-dimensional data in a form not requiring further reduction prior to engineering evaluation.

(ii) Results must be able to be interfaced to some form of automatic data reduction system capable of extracting meaningful information.

(iii) The technique should be able to be configured to render it insensitive to environmental changes.

These conclusions led to the choice of ESPI as a more suitable candidate technology.

Electronic Speckle Pattern Interferometry. Correlation interferometers were able to satisfy the requirement of providing three dimensional data without further reduction but needed to be investigated in order to determine if it was able to fulfil the remaining objectives. ESPI had been known of for 10 years prior to the start of this research but had failed to become an industrially recognised technique. It was not user friendly and although attempts were made to commercialise the technology, these had failed due to cost, setting up complexities and restrictions on inspection size.

Previous work had introduced equipment constraints that were not fully compatible with the underlying principles of ESPI. Jones and Wkyes [25] in their examination of the limitations of ESPI stated (page 196), "it should be noted that only out-of-plane sensitive time averaged fringes can be observed", and also (page 197) that "the ESPI system must use a high F-number (small lens aperture) viewing system". These examples were common of the folklore surrounding ESPI and were proven to be incorrect. Experiments undertaken have refined in-plane time averaged ESPI such that high contrast fringe patterns have been obtained from systems operated using F1.4 lenses.

This work has produced designs of interferometers which have been subsequently manufactured by Ealing Electro-Optics and Newport Corporation. The re-designs of the processing electronics have also been licensed and incorporated within their equipment. The design of the existing analogue ESPI processing electronics produced fringes of good visual quality, but to achieve this were highly contrast stretched. Thus the actual $\cos^2$ fringe function had been replaced by one of a near square wave type. Sub-fringe interpolation could not be accurately performed. New digital processing electronics were produced which did not affect the resultant fringe pattern intensity distribution, were compact, simple in

construction and easy to maintain. The restoration of the correct fringe function provided suitable input data for the fringe pattern analysis. After a review of available fringe processing techniques, two step phase stepping was chosen. Other workers had decided to assign phase values to all image pixels before and after displacement, then compute the resultant values knowing the phase and intensity. This approach required a total of six images to perform a complete analysis. The approach taken here was to step the fringe pattern twice (by $-2\pi/3$ and $+2\pi/3$) and compute the displacement from three images. This required less computer memory and computational effort. A reason for this approach was to use existing fringe patterns displayed upon the television monitor. Thus data acquisition remote from the image processor could be contemplated.

The fringe analysis work was pursued in the initial stages using a large 1024 x 1024 μVax mini computer based image processor able to undertake solutions within reasonable timescales. The use of 1024 pixels was an attempt to increase the data density. The approach taken has shown this to be unnesseccary with the phase stepping approach proving successful in tackling the fringe pattern reduction of ESPI fringe patterns using 512x512 pixels. It was also the range of different interferometric arrangements and fringe pattern types, which required an automatic system to work on both pulsed and continuous wave equipment. The demands imposed by the image processors required improvement of the electronic pre-processing. The hardware 'piggybacked' onto the mother board of stand-alone framestore equipment. The availability of lower cost personal computers with suitable high definition plug-in framestore cards enabled further advanced pre-processing solutions to be implemented within the micro-computer. Data processing requirements and further analysis of the ESPI fringe pattern image content led to new floating level filtration and band pass image filtration. The combination of specific pre-processing hardware, micro computer and multipage framestores resulted in this equipment being able to undertake image acquisition and fringe pattern processing in less than 15 seconds. This processing time was a factor of four faster than the μVax II based equipment.

The construction of hybrid in-plane and out-of-plane sensitive interferometers provided the necessary test bed for the image processing equipment. The generation of processed three dimensional displacement data in cartesian coordinate form is considered highly significant to real world engineering design studies.

Attempts to incorporate a pulsed ruby laser in a speckle interferometer, whilst experimentally successful, were significant in identifying problems which were endemic of that laser type. Limitations of repetition rate and pulse to pulse intensity stability could not be sufficiently improved upon even after two re-designs of the equipment. An alternative laser type was identified which could provide suitable pulsed energy. The frequency doubled Nd.YAG pulsed lasers for ESPI resulted in real time, high repetition (50Hz) pulsed results, one advantage being the ability to provide animation of a surface resonant motion.

The gain in sensitivity of the imaging system at 530 nm for scanned image tubes (0.45 A/W) was two orders of magnitude better than at the fundamental 1060 nm laser wavelength (0.02 A/W). This was achieved with the expense of a 50% reduction in output energy due to the frequency doubling. Presently with CCD television camera areas of $>1m^2$ can be illuminated with a 35 mJ/pulse of laser energy. An early concern of whether the imaging mechanism of the CCD would work with the double pulse illumination system proved unfounded. CCD cameras coped adequately with the task and provided imaging precision of the data previously unobtainable with scanned vacuum tubes.

The consequences of energy variability and the demands of digital storage required that new floating level filtration electronics be designed, and this provided the additional benefit of increasing the capability to handle the uneven intensity distribution of the reference beam. Initial experiments were hampered by signal degradation arising from: successive analogue and digital conversions, the local timing circuits not being synchronised via a master source and attenuation throughout numerous pieces of

electronic equipment. The combination of all image filtration, image acquisition, fringe pattern enhancement and fringe pattern analysis within one microcomputer based system has resulted in reduced noise and improvements in fringe pattern quality. A further advantage of this approach was the reduction in equipment used, leading to a hardware cost savings.

The new twin pulse laser design was very successful, it achieved a trebling of the optical energy output with half the electrical energy requirement of the previous system. The line narrowing with the diode laser seeding provided the necessary improvement to beam pointing. In practical terms, the laser became as easy to use as a continuous wave laser. The individual maximum pulse energy output of 100 mJ/pulse of 530 nm energy compares with the single line output of a 30 watt argon ion laser.

Considering the operational requirements, the pulse timing flexibility was considerably improved. Any pulse separation from 10 nsec upto 20 msec (20 msec being the camera operating cycle time) is achievable, with a maximum energy of 100 mJ/pulse of consistent output. The output energy was no longer dependent upon laser timing, nor subject to the continual electronic adjustment previously needed for the Nd.YAG or ruby lasers. Double pulsed addition fringe pattern quality was enhanced by initially storing the system residual noise into a framestore and subtracting this from the live image.

The final results have achieved the original objectives, although the path taken did not follow the original plan, this was revised as the research progressed. It is inevitable that any research work will generate more questions than are immediately answerable. Some of these questions are posed in the following chapter whilst others are being addressed by additional researchers working within this field.

CHAPTER 8
FURTHER WORK

One objective of this research was to produce an instrument capable of optical whole field inspection displaying results in a meaningful form. The new twin pulsed laser technology has extended the use of the instrumentation outside of the laboratory and into real world environments. This work has generated new areas which should form the basis of new research to extend and consolidate that already achieved to date. The new ideas fall within four categories: Optical head design, laser design, electronics/image processing, and new application areas. Each of these areas are addressed in the following sections.

Optical Head Design

The value of simple out-of-plane studies is limited, the ability of ESPI to visualise the three separate cartesian co-ordinate displacement vectors (x, y and z) has been shown to have application in the study of vibration problems. The combination of two in-plane systems and one out-of-plane arrangement has been demonstrated on a laboratory basis. The combination of these arrangements within a single head could provide an instrument with greater flexibility. Viewing with a single lens and imaging onto three cameras would enable the three separate images to be acquired either sequentially or in parallel. Some metallic surfaces are able to preserve the polarisation of reflected laser light. It is possible to use this property to advantage by illuminating the surface with two or more beams whose electric vectors are at different angles relative to one another. Therefore concurrent imaging would take place via a single lens if a polarisation beam splitter is used to produce the requisite images. These images can be phase stepped independently and automatically analysed by separate framestores. The present computer framestores are only able to handle a single camera input. The concepts could also apply to rotating components with the addition of an image derotator. Though at present the combination of pulsed YAG ESPI with an image derotator has not yet been demonstrated.

Laser Design

The technique of diode seeding two laser cavities can be extended to three or more YAG laser oscillators. This would make single phase step, three pulse ESPI a potential tool for transient vibration analysis. The present Nd.YAG oscillators are large three rail arrangements, the space requirement for the laser components could be reduced if the new mirror mount concept was incorporated for all elements. Furthermore the line selection with seed lasers ensures adequate coherence without frequency narrowing etalons. The potential for compact seeded Nd.YAG lasers is considerable, one benefit here is the possibility of a hand portable tool. The recent use of slab injection of YAG rods for higher output energies could be equally applied to the single frequency Nd.YAG types and assist in the construction of compact lasers. Here, transverse pumping is used along the axis of the rod as opposed to the present method of longitudinal injection at the rear mirror.

Image Processing

The recent availability of computer framestore cards with on-board transputers has potential for high speed image fourier filtration and other computationally intensive processes without needing to access the main computer bus. This could replace the initial pre-processing stages which presently use look-up tables with more advanced logical operations prior to storage. The ability to implement the transputer operations in 'C' programming language is a great advantage, although awareness of parallel programming techniques is necessary.

Recent advances in neural networking applied with optical pre-processing could enable the noisy speckle fringes to be enhanced with any data holes being filled by the use of associated imaging techniques. These techniques could be applied to fringe pattern analysis replacing the current fringe processing techniques which utilise two dimensional vectoral analysis. One method of neural networking requires a spatial light modulator to be included in the imaging system prior to the television camera. A further use of spatial light modulators could be for real time optical image

filtering (Fourier, Mellin, etc.) and also fringe pattern enhancement. The construction of matched Vander Lugt filters for image spatial filtering could remove the high frequency, speckle information leaving lower frequency fringe detail if some intermediate real time optical memory could be devised (such as a BSO crystal).

Applications

The imaging speed of a Nd.YAG system is presently limited by the pulse duration (typically 10nsec). The introduction of an extended optical delay line into one arm of the interferometer would reduce the interference potential of the two beams. The television camera could be synchronised with the shortened interference period and gating of the camera could then ensure the non-contributory parts of the two beams did not illuminate the camera faceplate. The consequence here would be to image with sub nano second possibilities. Components at high speed or with high levels of displacement could be imaged. The ability of the twin laser to generate pulses of suitable intervals would enable ultra fast phenomena to be analysed by interferometry. Finally, it would be interesting to attempt to analyse components underwater with a design of submergible interferometer.

There is considerable potential for new research and types of interferometers able to solve engineering and scientific problems. The awareness of the technical community to the advantages of ESPI is now growing and helped by the availability of commercial instrumentation should drive the future research utilising ESPI.

REFERENCES

1. Gabor, J.D., "A new microscope principle", Nature, 1948, 161, 777.

2. Gabor, J.D., "Microscopy by reconstructed wavefronts", 1949, Proc. Roy. Soc. A 197, 454.

3. Gabor, J.D., "Microscopy by reconstructed wavefronts II", 1951, Proc. Phy. Soc. B64, 449.

4. Leith E.N. and Upatnieks, J., "Wavefront reconstruction with diffused illumination and three dimensional objects", J. Opt. Soc. Am., 1964, 54, 1295-1301.

5. Denisyuk, Y. N., "On the reproduction of the optical properties of an object by the wave field of its scattered radiation", 1963, Optics and Spectroscopy, 15, 279-84.

6. Vest, C.M., "Holographic Interferometry", Pub. John Wiley, 1979.

7. Erf, R.K, "Holographic Non-destructive testing". Pub. Academic Press, 1974.

8. Caulfield, H.J., "Handbook of Optical Holography", Pub. Academic Press, 1979.

9. Powell, R.L., Stetson, K.A., "Interferometric vibration analysis by wavefront reconstruction", J.Opt.Soc.Am., 1965, 55, 1593-1598.

10. Osterberg, H, "An interferometric method of studying the vibrations of an oscillating quartz plate", J.Opt.Soc.Am., 1932, 22, 19-35.

11. Ostrovsky, Y.I., Butusov,M,M., Ostrovskaya,G.V., "Interferometry by holography", Springer-Verlag, 1977.

12. Gordon, A.L., "Fixed Q Pulsed holographic interferometry", Opt. and Lasers in Eng., 1985, 6, 25-33.

13. Abramson, N., "The marking and evaluation of holograms", pub., Academic Press, 1981.

14. Mottier, F.M., "Holography of randomly moving objects", App. Phys. Lett. 1969, 15, 44-45.

15. Waters, J.P., "Object motion compensation by speckle reference beam interferometry", App.Opt., 1972, 11, 630-6.

16. Stetson, K.A., "The use of an image derotator in hologram interferometry and speckle photography of rotating objects", Exp. Mech., 1978, 18, 67-73.

17. Ansley, D.A. and Siebert, L.D., "Coherent pulse laser holography", 1969 Proc. SPIE vol 15, 127-130.

18. Siebert, L.D., "Holographic coherence length of a pulse laser", App. Opt., 1971, 10, 3, 632-637.

19. Cookson, J., Butters,J.N., Pollard,H.C., "Pulsed lasers in ESPI", Opt.& Laser Tech., 1978, 6, 119-124.

20. Babcock, T.A. and James, T.H., "Use of hydrogen hypersensitisation to diminish recombination and produce emulsion coatings of high quantum efficiency", Jnl. Photo Scie., 1976, 24, 19-23.

21. Jenkins, R.L. and Farnell, G.C., "Chemical hypersensitisation of infra red emulsions", Jnl. Photo. Scie., 1976, 24, 41-49.

22. Albright, G.S., "Methods of hypersensitisation in astronomical photography - a state of the art review", Jnl. Photo Scie., 1976, 24, 115-118

23. Gates, J.W., "Holography with scatter plates", Jnl. Phys. E., Scie. Instr., 1968, 1, 989-994.

24. Webster, J.M., Tozer, B.A., Davis, C.R., "Holography of large volumes using holographic scatter plates", Opt. and Laser Tech., 1979, 6, 157-159

25. Jones, R. and Wykes, C., "Holographic and speckle interferometry". Cambridge University Press, 1983.

26. Montgomery, P.C. PhD. Thesis, "Forward looking innovations in ESPI"., Loughborough University, 1987.

27. Mendoza Santoyo, F., PhD. Thesis, "On the underlying optical mechanisms of ESPI", Loughborough University 1988.

28. Groh, G., "Engineering uses of laser produced speckle patterns", in "Engineering Use of Holography", Robertson, E.R., and Harvey, J.M., Eds., Cambridge University Press, 1970.

29. Hopkins, J.J. and Tidbury, G.H., "A note on the interpretation of laser speckle patterns of vibrating panels to yield information concerning mode shapes", 1977, Optica Acta, 24, 7, 773-778.

30. Archbold,E., Burch, J.M., Ennos, A.E., Taylor, P.A., 1969., Nature, 222, 263-5.

31. Leendertz, J.A., "Interferometric displacement measurement on scattering surfaces using speckle effect, 1970, Jnl. Phys E., Sci Instrum, 3, 214.

32. Burch, J.M. and Tokarski, J.M.J., 1968, Optica Acta, 15, 101.

33. Butters, J.N., Leendertz, J.A., "Holographic & Video techniques applied to engineering measurement", Jnl. of Meas.& Cont., 1971, 4, 344-50.

34. Butters, J.N., Leendertz, J.A., "A double exposure technique for speckle pattern interferometry", J.Phys.E.Sci.Inst., 1971, 4, 277-279.

35. Denby, D., Leendertz, J.A., "Plane surface strain examination by speckle pattern interferometry using electronic processing", Jn. of Strain Analysis, 1974, 9, 1, 17-25.

36. Lokberg, O.J. and Hogmoen, K., 1976, Jnl. Phy. E., vol. 9, 847.

37. Rowland, A.C. in "Holographic Measurement, Speckle and Allied Phenomena", 1985, Proc. RPS and CEGB, London.

38. Davies, J.C., Montgomery, P.C. and Tyrer, J.R., "The application of ESPI to modal analysis", 1985, Proc. ISATA, Graz, Austria, 73-92.

39. Pederson, Lokberg, Forre, "Holographic vibration measurement using a TV speckle interferometer with silicon target vidicons", Opt.Comm., 1974, 12, 4, 425.

40. Lokberg, O.J., Slettermoen, G.A., "Improved fringe definition by speckle averaging in ESPI", ICO - 13, Conf.Japan, 1984.

41. Lokberg, O.J., "Mapping of in-plane vibration modes by ESPI", Opt.Eng. 24,356-359,1985.

42. Shellabear, M.C., Tyrer, J.R., "3 Dimensional analysis of volume vibration by ESPI", Proc. SPIE 1084, 1989, London, U.K., 252-261.

43. Hurden, A.P.M., "An instrument for vibration mode analysis using ESPI", NDT Int.,1982, 6, 143-148.

44. Green, R.J., Walker, J.G., Robinson, D.W., "Investigation of the Fourier transform method of fringe pattern analysis", Proc.FASIG, L.U.T., 1896, 45-47.

45. Dandliker, R., Ienichen, B., Mottier, F.M., "High resolution hologram interferometry by electronic phase measurement", Opt.Comm., 1973, 9, 412.

46. Huntley, J.M., "Fast transforms for speckle photography fringe analysis", Proc.FASIG, L.U.T., 1986, 147-162.

47. Nakadate, S., Saito, H., "Fringe scanning speckle pattern interferometry", Appl.Opt., 1985, 24, 14, 2172-2180.

48. Creath, K., ""Phase shifting speckle interferometry", Appl.Opt., 1985, 24, 18, 3053-3058.

49. Robinson, D.W., Williams, D.C., Opt.Comm., 1986, 57, 26-30.

50. Kerr, D., Tyrer, J.R., Proc.SPIE., 1987, San Diego, 379-389.

51. Cookson, J., Butters,J.N., Pollard,H.C., "Pulsed lasers in ESPI", Opt.& Laser Tech., 1978, 6, 119-124.

52. Praeter, R.W., "ESPI for rotating structures using a pulsed laser", SPIE. 398, 1983, Geneva, 225-228.

53. Park,Y.K.,Guiliani,G.,Byer,R.L., "Stable single axial mode operation of an unstable-resonator Nd.YAG oscillator by injection locking", Opt. Lett. 1980, 5, 96.

54. Rahn,L.A., "Feedback stabilisation of an injection seeded Nd.YAG laser", Appl.Opt., 1985, 24, 940.

55. Spectron Laser Systems, Injection Seeded System User Manual, Rugby, 1989.

56. Lengyel, B.A., "Lasers", second edition, pub. John Wiley and Sons, 1971, 87-88.

57. Goodman, J.W., Laser speckle and related phenomena., Dainty J.C., Ed. 1975, Springer Verlag, 39.

58. McKechnie, T.S., 1974, Optic 39, 258.

59. Dainty,JC., Optica Acta., 1971, 18, 327.

60. Ennos, A.E., in "Laser Speckle and Related Phenomena", edited by Dainty, J.C., 1975, Springer Verlag.

61. Tyrer, J.R., MSc Thesis, "Experimental investigation into the fringe contrast of time averaged ESPI", Cranfield Institute of Technology, 1981.

62. Burch, J.M in Optical Instruments and Techniques, 1970, Oriel Press, 213-229.

63. Goodman, J., "Introduction to Fourier optics", 1968, Pub. McGraw Hill, New York.

64. Born, M. and Wolf, E. "Principles of Optics", 4th ed., Pergamon Press, 1970., p. 395, eqn. 9

65. Herbert, D.P., 1983, Optics and Lasers in Engineering, 4, 229-239.

66. Martienssen, W., Spiller, S., "Holographic Reconstruction without Granulation", Phys.Lett., 1967, 24A, 2, 126-127.

67. Nakadate, S., Yatagai, T., Saito, H., "ESPI Using Digital Image Processing Techniques", Appl.Opt., 1980, 19, 11, 1879-1883.

68. Slettemoen, G.A., "ESPI Based on a Speckle Reference Beam", Appl.Opt., 1980, 19, 4, 616-623.

69. Creath, K., Slettemoen, G.A., "Vibration Observation Techniques for Digital Speckle Pattern Interferometry", Jn.Opt.Soc.Am., 1985, 2, 10, 1629-1636.

70. Schwider, J., Burrow, R., Elssner, E., Grzanna, J., Spolaczky, R., Merkel, K., "Digital Wave-front Measuring Interferometry: Some Systematic Error Sources", 1983, Appl.Opt., 22, 21, 3421-3432.

71. Cheng, Y.Y., Wyant, J., "Phase Shifter Calibration in Phase Shifting Interferometry", App.Opt., 1985, 24, 18, 3049-3052.

72. Kerr, D., Tyrer, J.R., "Use of High Resolution Real Time Image Processing Techniques in Generation and analysis of ESPI Fringe Patterns", Optics Lasers.Eng., 1988, 8, 109-121.

73. Kerr, D., Mendoza Santoyo, F., Tyrer, J.R., "Manipulation of the Fourier Components of Speckle Fringe Patterns as Part of an Interferometric Analaysis Process", Jn.Mod.Opt., 1989, 36, 2, 195-204.

74. Creath, K., Slettemoen, G.A., "Vibration-Observation Techniques for Digital Speckle Pattern Interferometry", Jn.Opt.Soc.Am.A, 2, 10, 1629-1636.

75. Koliopoulos, C.L., "Avoiding Phase-Measuring Interferometry's Pitfalls", Oct. 1988, Photonics Spectra, 169-176.

76. Løkberg O J, Høgmoen K, Holge O M, "Vibration Measurement on the Human Ear Drum in vivo" 1979, Applied Optics, 18, 6, 763-765.

77. Løkberg O J "The Ultimate Holographic Tool for Vibration Analysis?" 1984, Jnl Acoust Soc Am, 75, 6, 1783-1791.

APPENDIX 1
PULSED RUBY LASERS AND THEIR OPERATION

A1.0 Introduction

A single crystal of Al_2O_3 is more usually known as sapphire. The crystal lattice has a cubic symmetry, the chromium oxide puts a small distortion along one of the cubic diagonals. As a result of this distortion the true symmetry of the crystal is rhombohedral with the symmetry element having a three-fold axis of rotation. Thus the crystal is uniaxial with the optical axis coinciding with the three-fold axis. Ruby crystals are synthetically grown specifically for lasers. The rods are core drilled from the large crystals with the cylinder axis at 60° or 90° to the optical axis.

Ruby with 0.05 chromium is pale pink having 1.58×10^{19} Chromium (Cr^{3+}) ions per cubic centimetre. If the concentration is increased tenfold the ruby is the more familiar red colour however the chromium ions will start to interact at this concentration.

A1.1 Construction of a Ruby Laser

The dimensions of the ruby rods vary between 0.25 inch - 0.375 inch diameter and 4 - 8 inch length. The end faces are ground and polished, to be plane and parallel, though a recent trend is to introduce a 1° vertical offset to eliminate laser action within the rod itself. The ruby rod is irradiated with optical energy from one or more xenon flashlamps typically for 3 msec. The usual arrangements for coupling of the optical energy to the laser rod is shown in Figure A1. The helical arrangement, Figure A1.1, gives the best cross sectional laser beam profile and is used for the oscillator and amplifier of the Apollo ruby laser. Unfortunately it is an expensive flashlamp to manufacture and the thermal expansion results in a continued uncoiling and coiling of the flashlamp. This leads

to regular fatigue failure of the flashlamps which at £600 is not an inconsequential replacement cost. The coupling efficiency of the optical energy of the flashlamp into the rod is the lowest of the five configurations. The close coupling arrangement of Figures A1.2 and A1.4 are more efficient, per unit length of flashlamp, than the helical arrangement but provide a lower quality far field mode structure to the output beam. The elliptical arrangement, Figure A1.3 is a good compromise for coupling efficiency and improved far field mode structure. The JK lasers used rely on a double elliptical pumping configuration. Figure A1.5 shows an experimental arrangement used for long pulse separation double pulse lasers which has been evaluated within the laboratories in an attempt to overcome existing equipment constraints. Whilst successful, it was still hampered by the constraints of ruby laser excitation and was not pursued due to the overwhelming advantages of the Nd.YAG laser. Double or multiple flashlamp excitation reduces the non-uniformity of the coupling. This non-uniformity has two adverse effects on the quality of the output beam:

(i) thermal gradients and consequential stressing within the laser rod leading to optical path distortion,

(ii) preferential formation of asymmetric beam modes of little value in holography.

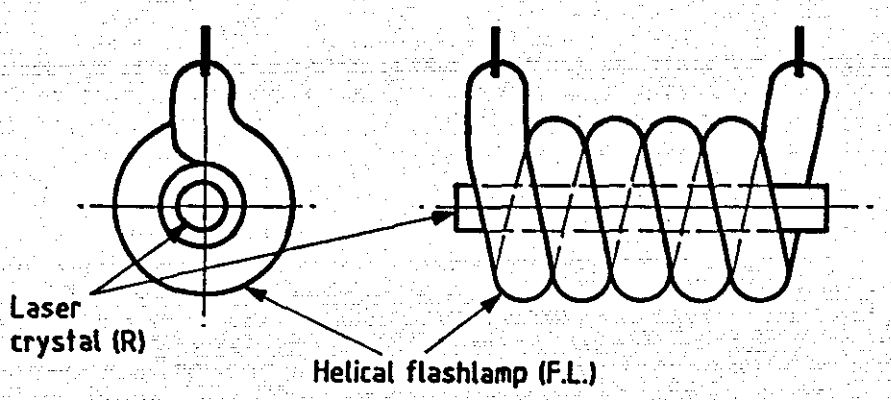

Fig. A1.1
Helical
flashlamp
arrangement

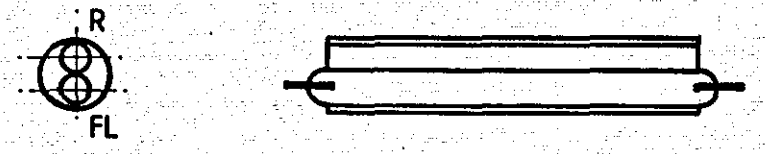

Fig. A1.2
Close
coupled
arrangement

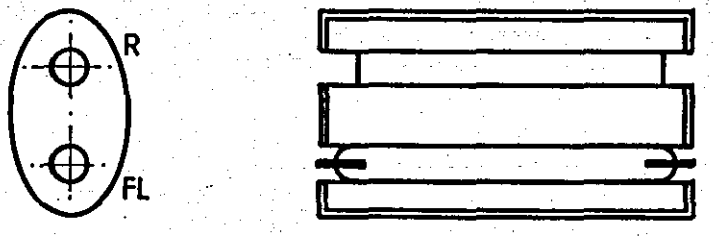

Fig. A1.3
Elliptical
cylinder
configuration

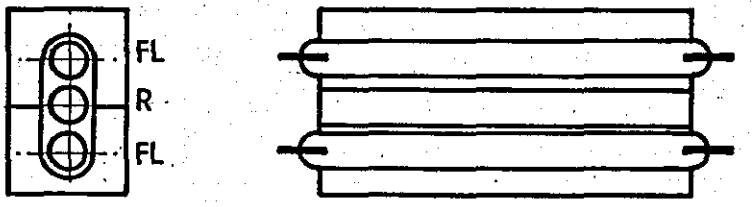

Fig. A1.4
Twin flashlamps
in close
coupling

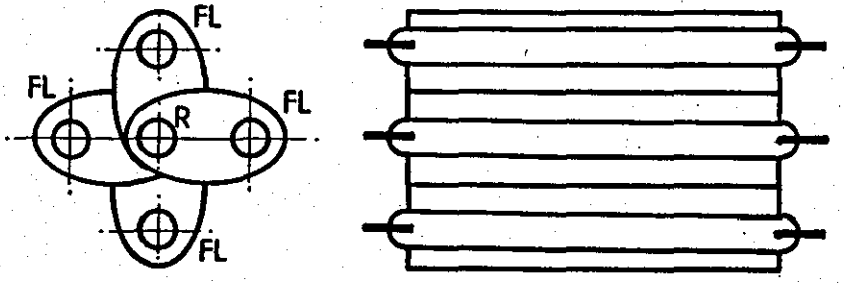

Fig. A1.5
Quadruple
flashlamp in
four way
elliptical
housing

Figure A1

Various Optical Pumping Arrangements for a Solid State Laser

A1.2 Optical Excitation of Ruby Lasers

The technique of optical pumping relies on a change of energy state of the laser rod material from a ground state up to an excited state by excitation of the active material by the flashlamps. The pumping light must be directed into the laser rod with a high degree of efficiency since inefficiencies result in heating and inhibit the necessary thresholds of excitation.

The energy rise needed to raise chromium from the ground state to the excited state is approximately 4.8×10^{-12} erg per atom. At least half the resident chromium atoms must be excited otherwise light amplification cannot take place. As stated earlier the chromium density is 1.58×10^{19} cm^{-3}, therefore the optical energy coupled into the rod must exceed (note 1 Joule = 1×10^{7} ergs);

$$1/2 \times 4.8 \times 10^{-12} \times 1.58 \times 10^{19} = 3.79 \times 10^{7} \text{ ergs cm}^{-3}$$

$$\text{Coupled energy needed} = 3.79 \text{ J cm}^{-3}$$

The oscillator on the JK ruby laser is 1/4 x 4" giving 16.38 cm^3 which requires the coupled energy to be 62.08 J.

Xenon flashlamps convert between 5% and 10% of the supplied electrical energy into UV and blue/green radiation (the spectral output is affected by the current density within the flashlamps). Current lamps are coated inside of the tube with UV fluorescent material to improve the blue/green output. The ruby rod does not absorb all of the flashlamp optical output, coupling is affected by the design of the pumping arrangements and coatings of the reflectors used.

Therefore assuming 40% coupling efficiency, the total energy requirement will be;

Coupled energy requirement x Coupling efficiency x Optical/electrical conversion efficiency

= 3.79 x 100/40 x 100/10 = 94.75 ≈95 J cm^{-3}

For the JK oscillator rod the energy requirement will be;

16.38 x 94.75 = 1552 J

This energy level is high, the fastest cycle time of the oscillator is 10 seconds and so the coolant system must be able to remove approximately 150 Watts of energy for the oscillator alone.

A1.3 Ruby Laser Beam Quality

It was necessary to modify the cooling equipment used by the JK laser and improve the coolant flow pattern. Initially the oscillator and two amplifiers were cooled in series. This was modified to a parallel manifold arrangement after poor beam repeatability was attributed to insufficient cooling.

The oscillator rod does not emit a uniphase wavefront across its diameter even though the rod is cylindrical with anti-reflection coated end faces. The oscillator was modified to enable a 2 mm diameter aperture to be translated across the oscillator cavity in both horizontal and vertical axes. (Previously a rotary head with different diameter apertures was used at a fixed central position). The aperture enables a uniphase TEM_{00} beam to be extracted from the oscillator with maximum output energy.

Associated with uneven beam cross-section is the generation of different modes of excitation. These modes must compete within the crystal for supply of energy from the excited atoms in order to propagate. Consequently the aperture is also used to select the single fundamental Gaussian mode within the output beam. Furthermore hot spots associated with the flashlamp coupling and focussing can be avoided.

A1.4 Pulse Forming Technique

The orientation of the optical axis of the ruby crystal with respect to the cylindrical axis can affect the output polarisation. A Glan-Thomson or Brewster stack can be used to enhance the polarisation of the oscillator intra-cavity beam to the vertical axis. An optical shutter is used within the cavity to block lasing activity and enable the excitation within the laser crystal to build up to store the energy above the threshold level. When peak excitation is reached or the control electronics require a pulse the energy is released. This technique is known as Q-switching and the shutter used is either a Pockel cell or Kerr cell.

The functional element within these two devices is a material which becomes birefringent under the influence of an external driving electric field. The usual method of operation is to cause a $\lambda/4$ retardation of any laser output which upon reflection from the rear reflector undergoes another $\lambda/4$ retardation becoming linearly polarised again only at 90° to its original axis. The polariser will absorb this radiation (typically with an extinction ratio of greater than 100:1) thereby stopping the radiation passing through the crystal and becoming amplified. Therefore whilst some energy will leak, most will be retained effectively integrating the energy from the flashlamps. At the desired time the voltage to the Q-switch is switched off and the polarising effect is removed, allowing oscillations to build up within the cavity. The amplification process takes place with the partial reflecting output mirror emitting the laser pulse.

The threshold of the laser crystal is controlled when the amplification per unit length (α) reaches:

$$\alpha = \frac{Y}{L}$$

where L is the length of the crystal and Y the loss of radiation during passage through the crystal.

α is proportional to the population inversion (the number of atoms excited from the ground state to the meta stable condition prior to emitting a photon and returning to the ground state), and during pumping the population increases. Laser oscillation cannot be achieved until the threshold is reached, once gained it quickly builds up until the population is exhausted. Therefore the loss rate controls the inversion.

The Pockel cell used had a driving voltage of 5 Kv however upon removing this voltage the decay rate of the birefringent material is 1-3 μsec, controlled by hysteresis and residual piezo electric effects within the crystal. To reduce this the Pockel cell is over-driven with a negative bias of 5-600 V. This overcomes these effects and can, depending upon the circuits used, be as short as 3-5 nsec although for holographic lasers it is advantageous for the mode structure if the opening of the shutter is around 400 nsec.

A1.4.1 Double Pulse Operation

After an initial pulse the exciting flash is still present and it is possible for energy to be stored again such that once the threshold is passed lasing action can be repeated. The typical recovery time for a ruby is 10 μsec, after which a second pulse can then be initiated. With reference to Figure A1.2, for holography the two pulses must be of similar energies and providing the pulse separation (between the two pulses) is within the flashlamp excitation and no longer than 1 msec a balance can be achieved.

The method of operation is as follows:

(i) Optimise the initial delay between the firing synchronisation pulse and the maximum threshold energy. At this stage the second pulse is disabled.

(ii) The pulse separation is controlled by a differential potentiometer as the Pockel cell controller.

(iii) After firing, the relative intensity between the two pulses is monitored on a digital storage scope. Pulse variation is achieved by adjustment to the amplitude adjustments for pulses 1 or 2 (this modifies the Pockel cell voltage) on the Pockel cell controller or adjustment of the initial delay to bias the second pulse preferentially against the first. This later technique is used only for longer pulse separations 750-1000 μsec.

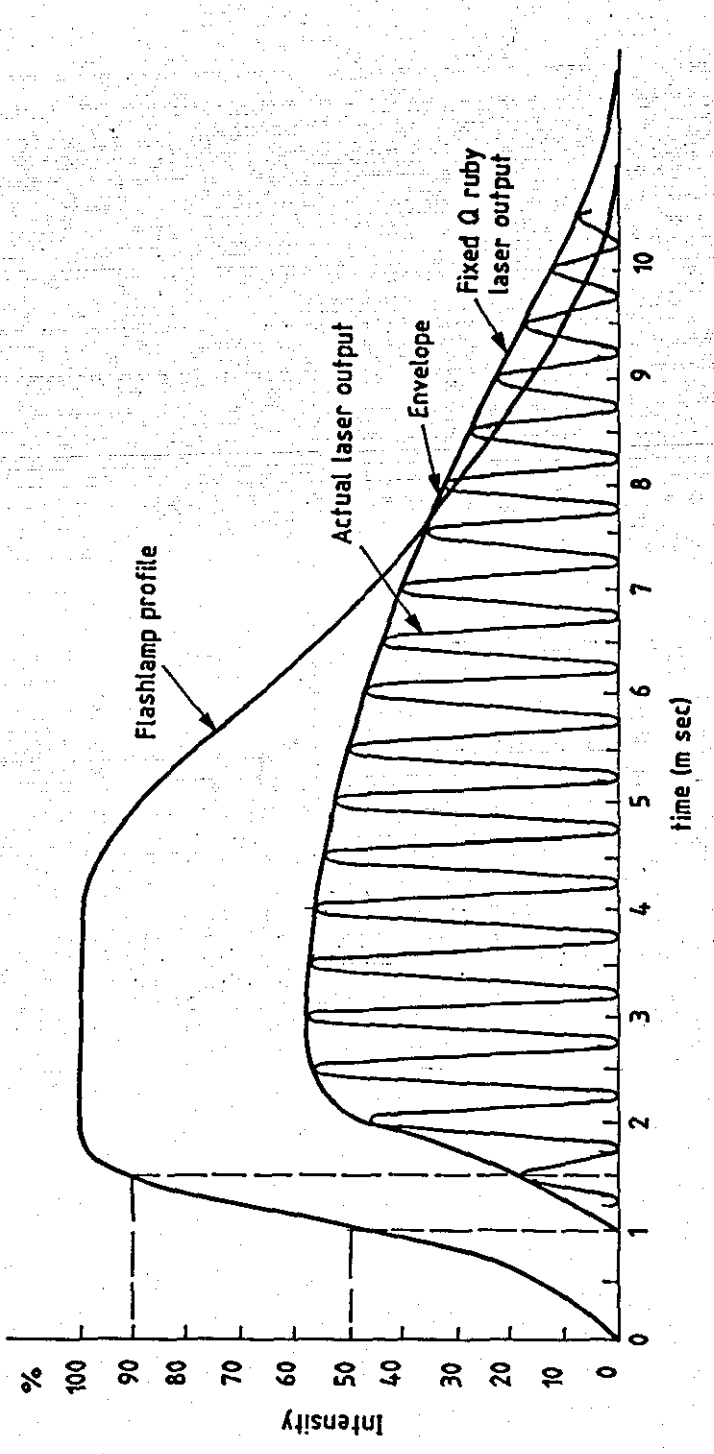

Figure A1.2
Plot of the Flashlamp and Fixed Q Outputs Against Time

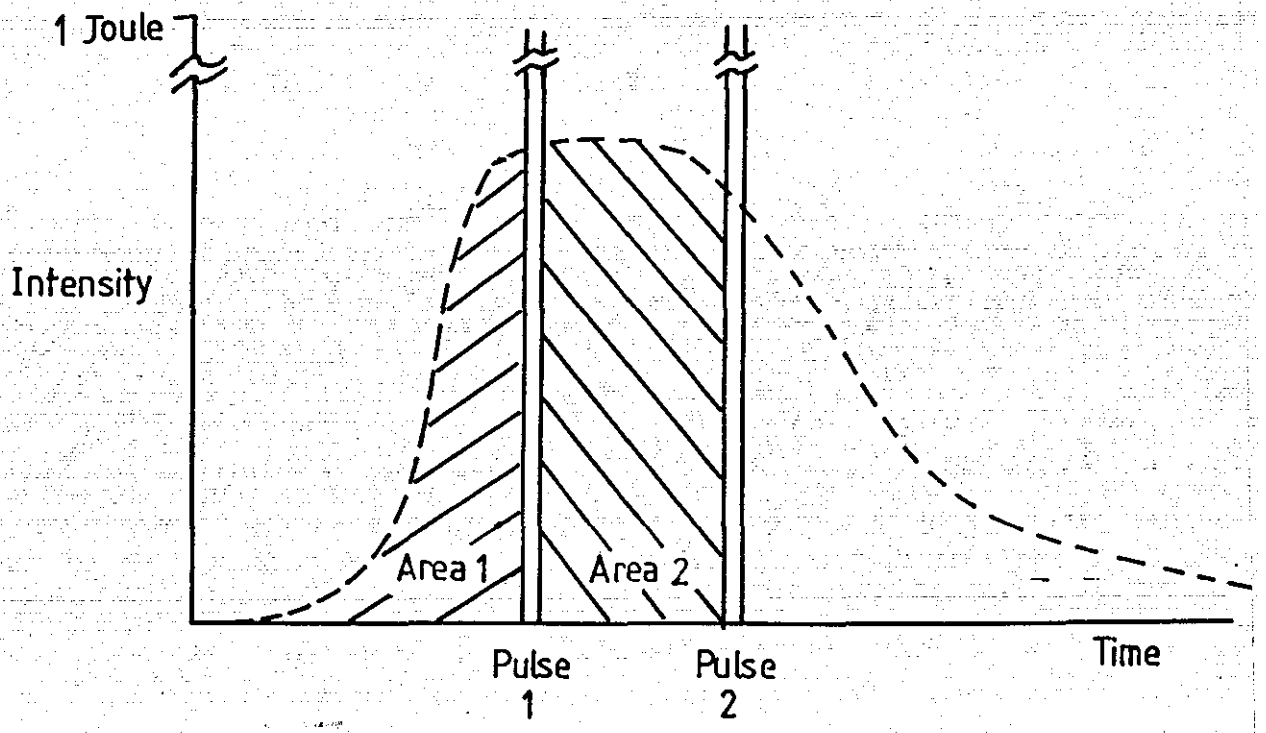

Figure A1.3
Plot of Energy Intensity Against Time,
Showing the Balancing of the Two Output Pulses

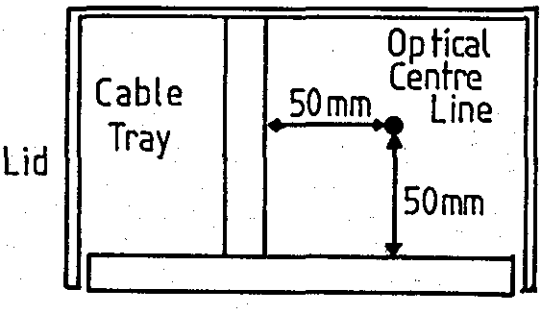

Figure A1.4
Cross-section of Laser Chassis

A1.5 Laser Chassis Modifications

At the start of the project the existing double pulse JK ruby laser had a single optical rail of 3 m length. The chassis section and inverted offset "T" section is shown in Figure A1.4.

The structural and thermal rigidity were inadequate which meant continual adjustment to the laser to maintain performance. Moving the laser made realignment necessary and changes to the laboratory temperature overnight necessitated a soak time of between 1 and 2 hours in the morning. The chassis was rebuilt as shown in the schematic, Figure A1.5, greatly improved structural stiffness. The tolerance to thermal drift was also improved though not significantly and three point mounting with adjustable feet was introduced to provide height and levelling ability. A three bar invar resonator for the oscillator was considered but cost and time were prohibitive. The compromise design proved adequate requiring only occasional adjustment during a day's operation.

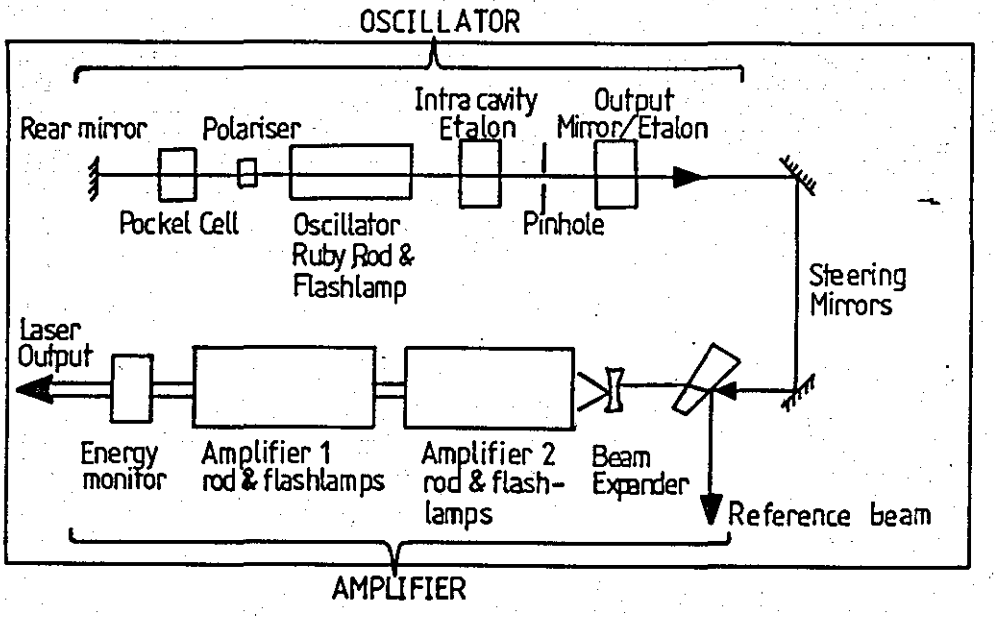

Figure A1.5

Schematic of Modified JK Laser Chassis Used for Holography and ESPI

A1.6 Fixed Q Operation of a Ruby Laser

Pulsed solid state lasers can be operated in several ways depending upon construction and laser crystal used. This simplest type of resonator is shown in Figure A1.6.

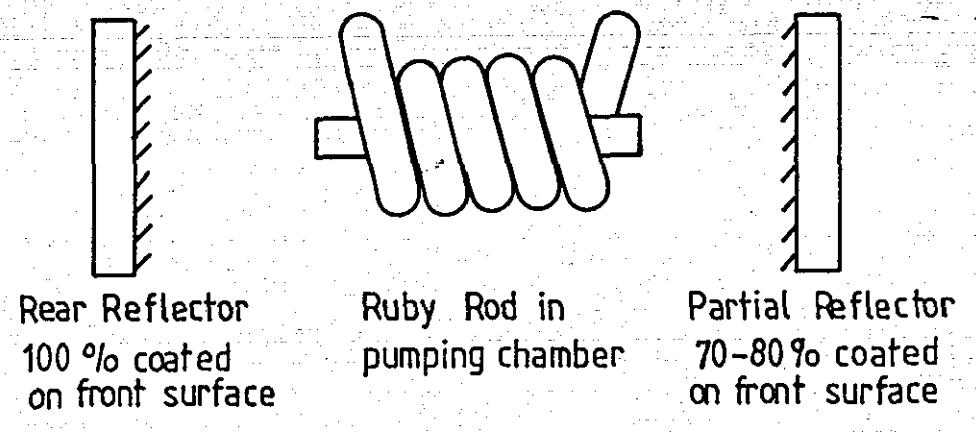

Figure A1.6
Simple Ruby Laser Resonator

The flash lamp increases the stored energy in the rod until there is sufficient radiation travelling between the reflectors for amplification to take place. The laser oscillation rapidly reduces the stored energy and is thus a self-quenching process. After an initial pulse of approximately one microsecond duration the energy level must be restored before reaching threshold again. Thus in the fixed Q mode the stored energy level is clamped at this level, and the laser output will pulsate for the duration of the excitation and the laser output profile will follow the flashlamp profile. See Figure A1.7.

The term Q is used here is defined as:

$$Q = \frac{\text{Energy stored}}{\text{Energy dissipated per cycle}}$$

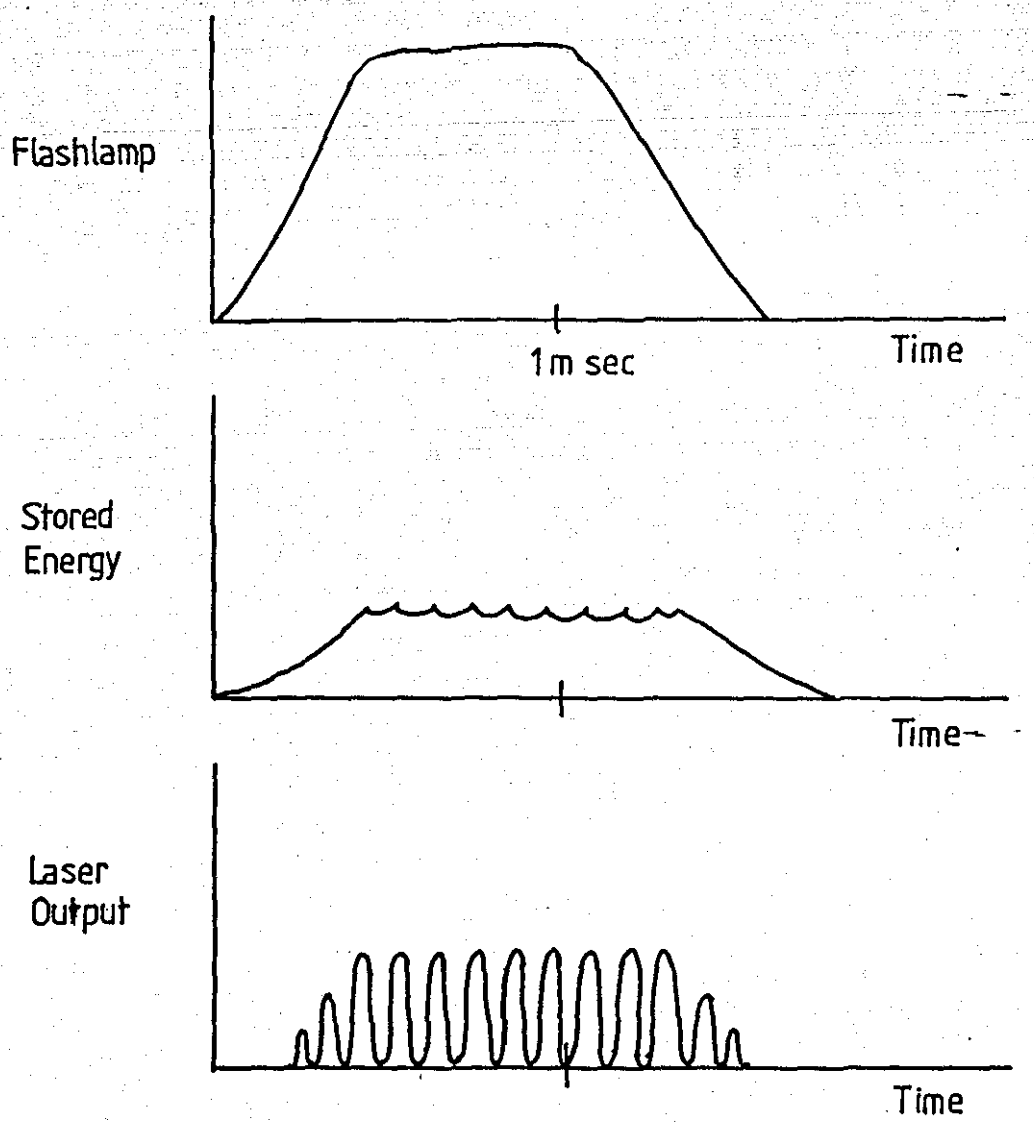

Figure A1.7
Fixed Q Pulsed Laser Operation

A1.7 Q Switched Operation of a Ruby Laser

In the Q switched mode, a high speed shutter is inserted into the optical resonator. The shutter is initially closed, thereby preventing laser activity, whilst the flashlamp excites the ruby. Energy is stored within the rod and builds up as shown in Figure A1.8. Before the energy begins to decay (as determined by the fluorescence of the ruby) the shutter is opened. The Q of the optical cavity is switched from a low to a high value. Consequently the energy is rapidly released in a single giant pulse which lasts for between 5 and 50 nanoseconds. This depletes most of the energy stored in the rod prior to the shutter being activated.

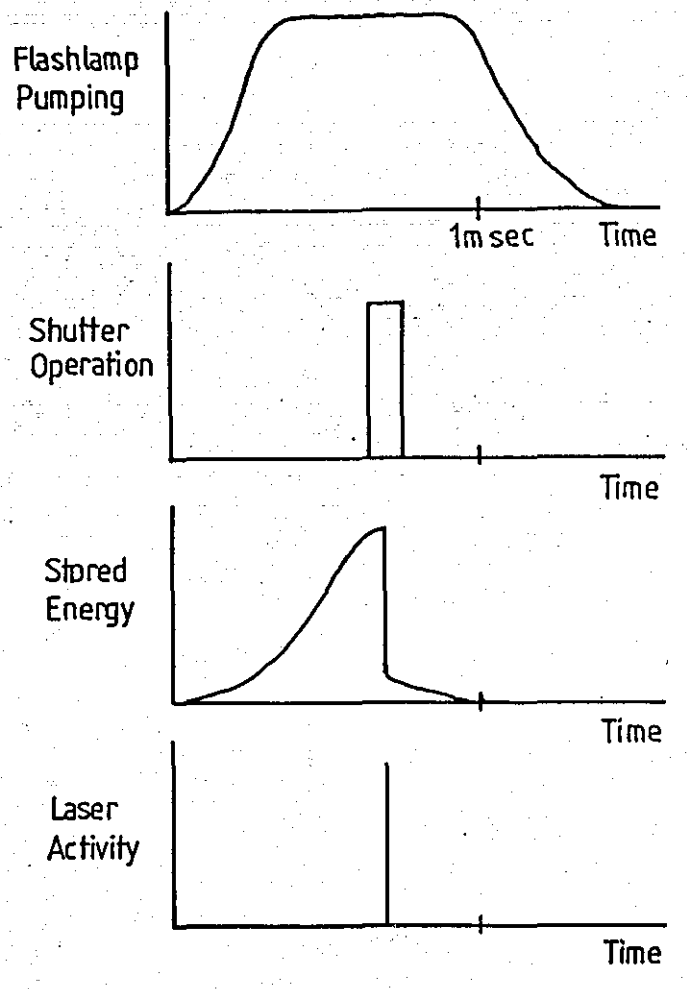

Figure A1.8
Plot Showing the Operations of Q Switched Laser Relative to Time

A1.8 Laser Mode Control

A simple laser cavity as shown in Figure A1.6 can generate coherent light in a number of different transverse and longitudinal modes simultaneously during operation. It will operate at several discrete wavelengths which are a function of the optical cavity wavelength. These are spaced at wavelength intervals of $\lambda^2/2L$, where λ is the mean laser wavelength and L the optical length of the cavity. The longitudinal modes affect the line width of the laser output as shown in Figure A1.9.

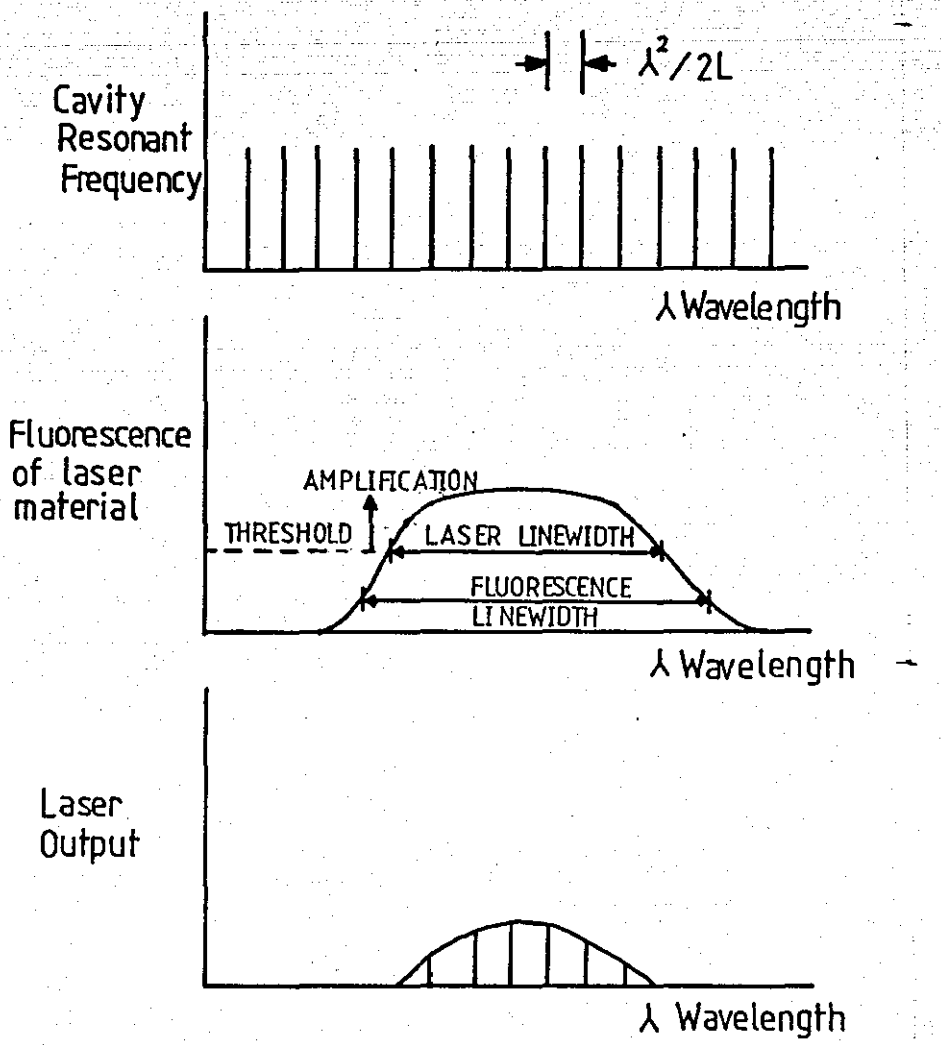

Figure A1.9
Output of a Simple Laser Without Mode Selection

The transverse modes influence the intensity profile across the beam and the eventual phase characteristics of the output beam. A multi-transverse beam is ill defined in phase and intensity, Figure A1.10, shows the fundamental transverse electromagnetic (TEM) modes of a laser beam.

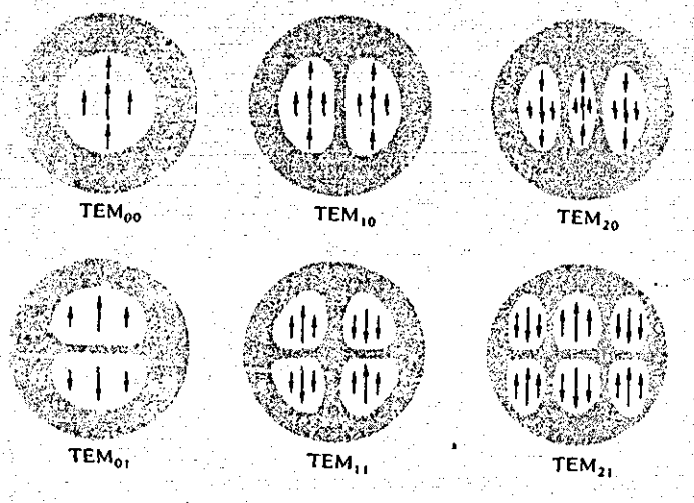

Figure A1.10
Energy Distribution Produced by Transverse
Electromagnetic ($TEM_{m,n}$) Modes and the Assigned Nomenclature

To reduce the number of oscillating longitudinal modes of the cavity a wavelength selector is introduced. The most commonly used are Fabry-Perot resonators or Etalons, which are either intra-cavity devices or resonant output reflectors replacing the output mirror. In principal they are transmission line filters which because of the proximity of cavity modes must be thermally controlled to preserve operation. Figure A1.11 (a modification of the diagrams presented by Lengyel [56]) shows diagrammatically the operation of a Fabry Perot etalon. Both surfaces of the etalon are semi-reflecting (60%R) and provide a resonant structure whose wavelength can be altered by introducing tilt.

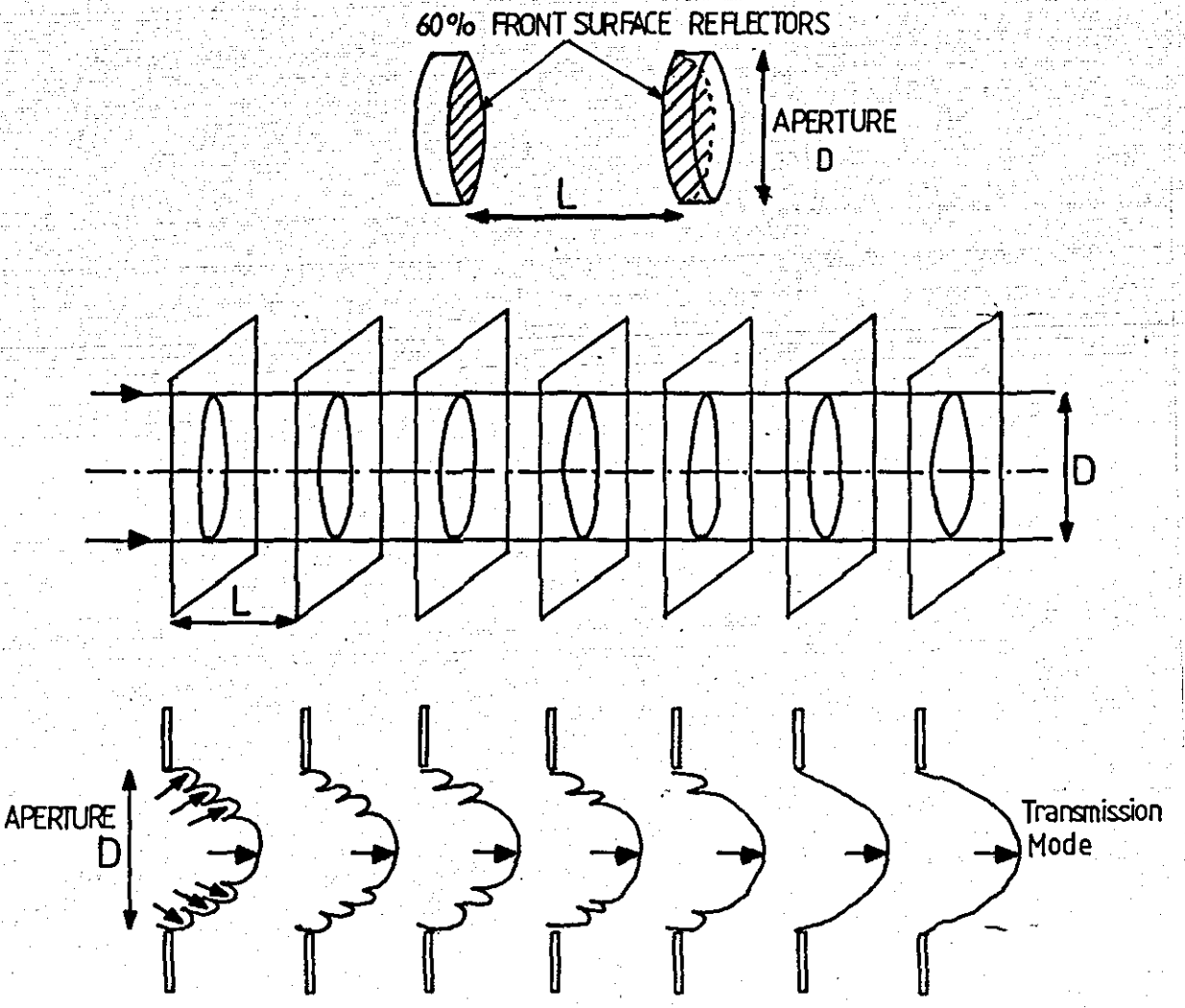

Figure A1.11
Single Transmission Mode Selection of a Fabry Perot Etalon

Initially the etalon is aligned normal to the transmitted beam. Tilt is introduced by a micrometer onto one of the axes of support thereby changing the relative pathlength between the two reflectors. Consequently only one of the laser wavelengths can mutually resonate within the laser and etalon cavities. In practice the quality or finesse of the etalon necessitates two being used, one as an intra-cavity device the second as the output mirror giving a reduction in transmitted energy typically by 50%. Control of the temporal coherence is effected by the inclusion of frequency selecting etalons.

Spatial beam control of a ruby laser is achieved by inserting a 2 mm aperture into the resonator. The single mode has a Gaussian beam intensity profile and consequently a uniphase wavefront. Again this produces a reduction in the output energy, unfortunately, no advantage is to be gained by increasing the laser rod diameter above 6 mm (1/4 inch) to increase the coupled energy. The output beam divergence of a TEM_{00} laser is diffraction limited, TEM_{00} performance is achieved in practice and the divergence of the output beam is increased because of the inclusion of beam expansion optics. These lenses are used to expand the oscillator output prior to the amplifier to improve the saturation of the amplifier rod and increase the amplification factor to ≈40. No collimating optics are used after the telescope, at the laser exit the beam output diameter is approximately 10 mm.

APPENDIX 2
SPECKLE IMAGE FORMATION AND CORRELATION INTERFEROMETRY

A2.0 Speckle Pattern Formation Theory

Goodman [57] considers the autocorrelation function and power spectral density of the second order statistical properties of speckle. The derivation for a uniform and square plate area L x L metres yields $R_1(\Delta x,\Delta y)$ the autocorrelation function to be;

$$R_1(\Delta x,\Delta y) = \langle I\rangle^2 \left[1 + \mathrm{sinc}^2 \frac{L\Delta x}{z} \mathrm{sinc}^2 \frac{L\Delta y}{z}\right] \qquad (A2.1)$$

The average size of a speckle being Δx and taken when $\mathrm{sinc}^2 (L\Delta x/\Delta z)$ first falls to zero. This distance is denoted as σx and z is the distance from the incident surface to the observation plane and σx and is given then as,

$$\sigma x = \frac{\lambda z}{L} \qquad (A2.2)$$

McKechnie [58] provided an experimental investigation of the intensity statistics of a speckle pattern, following on from the work of Dainty [59], and estimated the probability density functions of the intensity of the speckle pattern with 23,000 measurements. These results verified the negative exponential probability density function of:

$$p(I) = 1/I_0 e^{-I/I_0} \qquad (A2.3)$$

where p(I) is the speckle brightness probability, I_0 is the average brightness, I the actual brightness.

Ennos [60] proposes the idea of two types of speckle; objective and subjective, to which he suggests different speckle size.

A2.1.1 Objective Speckle

A flat screen held at a distance (L) from the illuminated surface will have a speckle pattern projected onto it. The average size of the speckle depends upon the angle subtended by the screen (α). For a circular illuminated patch of diameter (D), the speckle diameter (σ_0) formed at the screen at distance (L) when illuminated with light of wavelength λ, will be given by:

$$\sigma_0 \approx \frac{1.2\,\lambda\,L}{D} \qquad \text{(A2.4)}$$

If a screen with a hole in it is now interposed between the viewer and the surface and if the hole is small (say 1 mm), the speckle size observed is large. Any increase in the size of the aperture will reduce this size. See Figure A2.1.

A2.1.2 Subjective Speckle

This speckle type is formed by imaging a coherently illuminated rough surface with a lens. It is a high frequency modulation of the intensity that would be obtained if illuminated with incoherent light.

The average diameter (σ_s) of this speckle type is given by:

$$\sigma_s \approx 1.2(1 + M)\,\lambda F \qquad \text{(A2.5)}$$

where M is the magnification power of the lens, F is the aperture ratio of the lens (i.e. F number), $M = V/U$, where U is the object distance and V the image distance. The subjective speckle is the equivalent of the objective speckle that would be generated if the lens pupil became the scattering surface. See Figure A2.2.

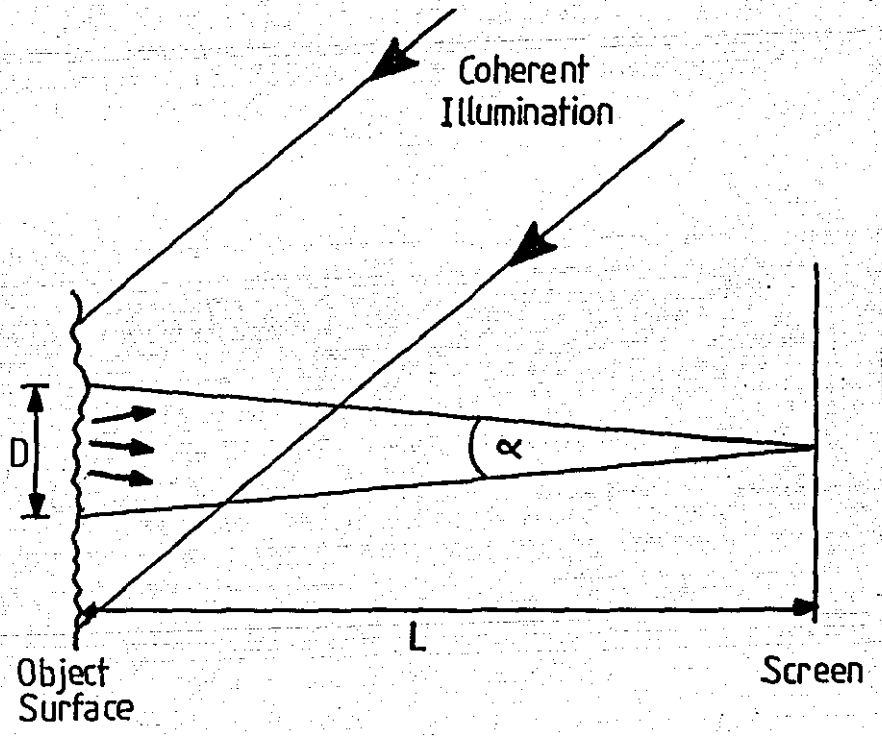

Figure A2.1
Objective Speckle

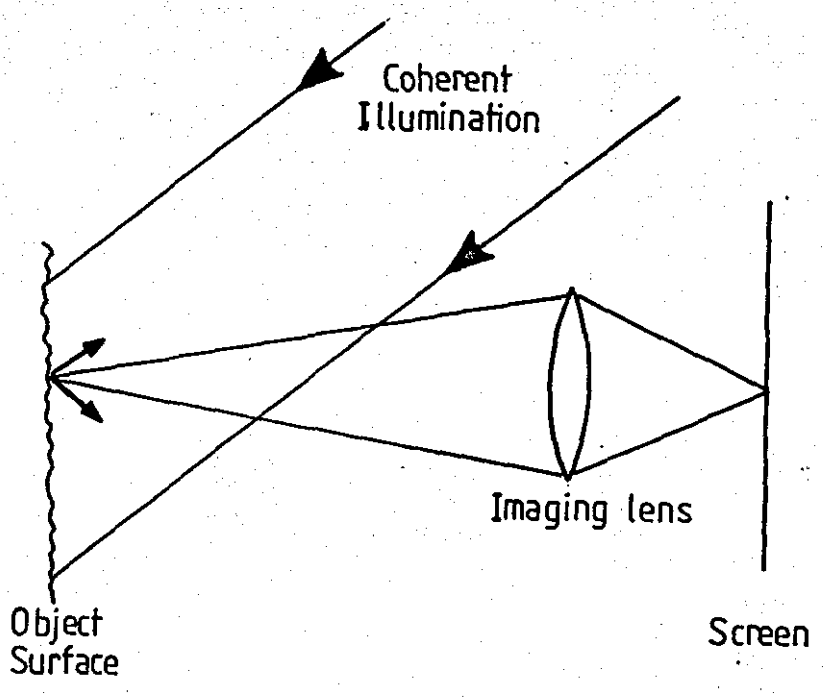

Figure A2.2
Subjective Speckle

The brightness distribution of a speckle depends upon whether or not it is fully developed. A fully developed pattern is obtained only when all the waves contributing to a particular speckle are coherent and implies that the surface must not depolarise the light. Should a depolarising surface be used, the speckle derived can be considered as the incoherent superimposition of two independent speckle patterns, mutually polarised at right angles to each other.

In the case of a fully developed pattern, the most probable brightness value is zero, thus there will be more dark speckles than of any other brightness. For a partially developed pattern, the most probable brightness value is half the average brightness. Experimental work carried out on the surface finish of an object for laser speckle substantiates this theory. Shot blasted surfaces which do not depolarise the light give fewer bright speckles than a silver painted surface which does give some depolarisation to the returning object beam.

Tyrer [61] identified matt silver spray as a convenient material for both speckle and holography providing little depolarisation, good surface reflectivity and reduced flare when compared with bright metallic surface finishes. Matt white paint is another popular surface finish but this will depolarise the returning object wavefront, thus providing undeveloped speckle patterns. This leads to a higher noise term in the object beam because of the reduced interference term relative to the apparent object to reference beam ratios. Experiments were undertaken in which polarising filters were attached to the imaging lens of the ESPI systems matched to the reference beam polarisation. This produced improved fringe contrast when compared to the unpolarised object beam from matt white painted surfaces. The use of shot peening, bead and sand blasting whilst yielding good reflectivity with reduced flare, introduced changes to the surface material characteristics of the component under test which rendered these techniques unsuitable. Burch [62] considers the brightness distribution of fully developed speckle patterns when combined with a uniform wavefront and derives the expression:

$$P(I) = (2/I_0) \exp[-(1 - 2I/I_0)] \, I_o \, (2\ 2I/I_0) \qquad \text{(A2.6)}$$

This is illustrated in Figure A2.3

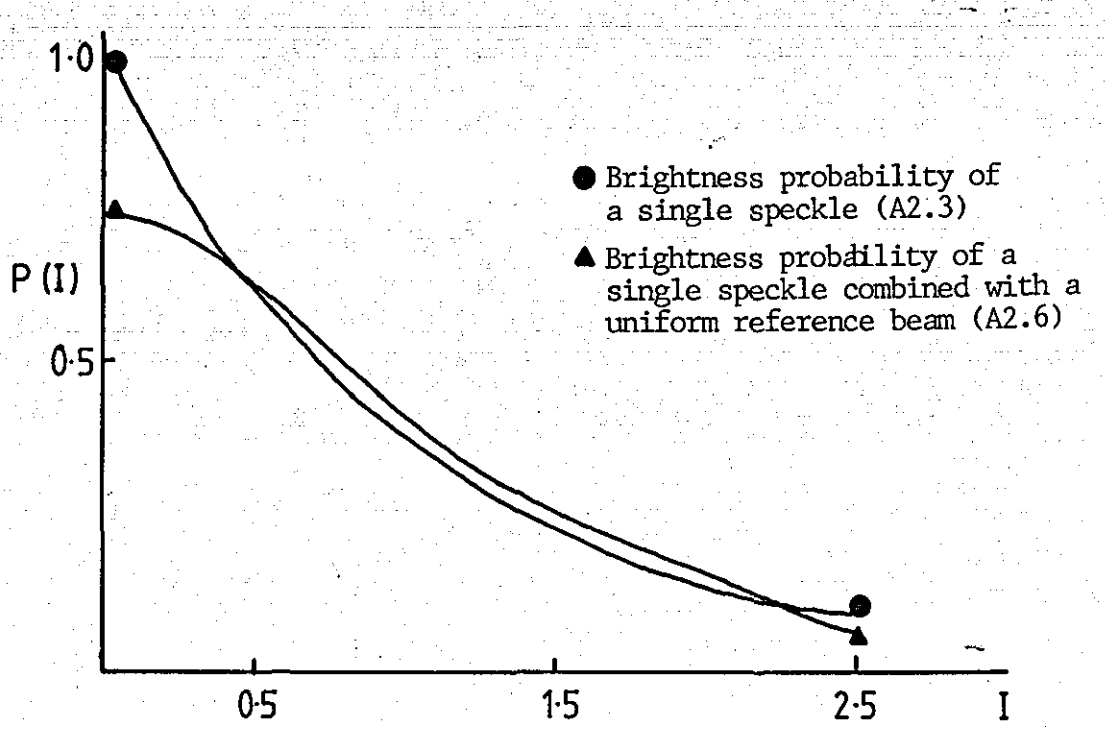

Figure A2.3
Plot of the Probability Density Functions of the
Brightness Distribution of Equations (A2.3) and (A2.6)

Jones and Wykes [25] derive their formulation for speckle size from Goodman [63], they define the subjective or image plane speckle size as twice the resolution limit of a lens system as defined by diffraction theory; i.e.

$$\sigma_s \approx \frac{2.4\,\lambda V}{a} \qquad \text{(A2.7)}$$

where V is the distance from the lens to image plane, a the diameter of the lens aperture.

They also propose the minimum speckle size would be given by:-

$$\sigma_{min} \approx \frac{\lambda V}{a} \qquad \text{(A2.8)}$$

Born and Wolf [64], suggest for coherent systems, the initial resolution limit may have a larger numerical factor 1.54 instead of 1.2 as suggested by Ennos in (A2.4). They go on to state that the factor is somewhat arbitrary depending upon the form of the object, aperture and sensitivity of the imaging transducer. Mendoza [27] points out that the television camera imaging surface is non-square and the asymmetry of the photodetectors (whether CCD at ≈17 x 9 μm or scanned image tube 23 x 15 μm) means that the resolving power is different in the horizontal and vertical directions. Furthermore he states that with the tendency for ESPI systems to be operated at aperture levels larger than defined by any of the suggested theories, then "....it can be safely said that due to the presence of high spatial frequencies dominating the complex pattern of interference and thus the inability of the system to resolve it, the total intensity present on each pixel is averaged to give a mean intensity per pixel".

This statement is substantiated by the author who has successfully operated speckle equipment with aperture ratios of F1.4 and a 50 mm focal length (V) with the object 0.5m from the lens (U), and λ = 0.633 µm. Applying these parameters to the various models presented gives the following:

Equation (A2.5) yields σ_s = 1.17 µm with a = 35.7 mm and M = 0.1.
Equation (A2.7) yields σ_s = 2.12 µm.
Equation (A2.8) yields σ_s = 0.89 µm.
Born and Wolf modified (A2.5) yields σ_s = 1.50 µm.

Obviously there is significant variation between the models, which in practical terms do not appear to limit the imaging capacity of the system.

A2.2 Optical Arrangements for In-Plane Displacement Sensitive Correlation Interferometers

By appreciating that the illumination of the surface need not be restricted to a single beam, Leendertz utilised one of the unique attributes of correlation interferometers, that of sensitivity to a single in-plane vector. See Figure A2.4.

The surface is illuminated with two beams derived from the same laser source. One beam can be considered as the object beam, the other as the reference beam, in this arrangement the surface illumination is composed of the resultant interference fringes. The fringe spacing of these fringes is controlled by the angle between them and the axis of the fringes is along the bisector between the two beams. The surface of the object is illuminated with these interference fringes and the derived speckle pattern is directly influenced by the illumination intensity pattern. The speckle pattern is recorded and the state of the surface is modified resulting in displacement, thus the corresponding speckle traverse across the illuminating fringe pattern. The intensity of any one speckle will vary cyclically across the traversed fringes. If any displacement occurs to the surface in the other in-plane vector or along the bisector of the included angle (usually the viewing axis), no change will occur to the illumination intensity and produce no change in the speckle intensity. Consequently the sensitivity is totally independent to motion in these other two displacement axes. Hence there is no need to undertake a generalised analysis in order to extract any single displacement vector (see Figure A2.4).

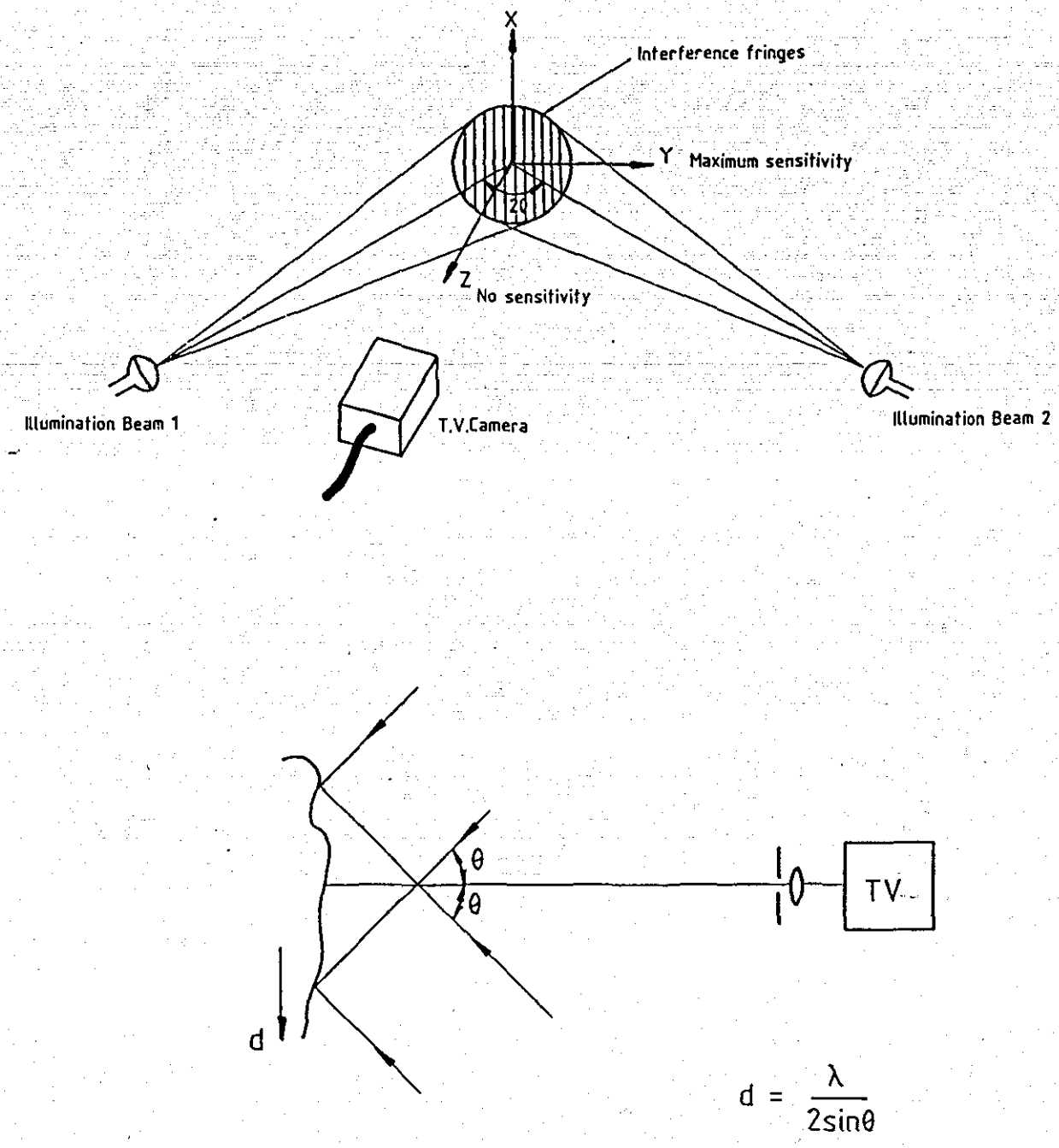

Figure A2.4
Sensitivity Description for an In-Plane Correlation Interferometer

A2.2.1 Optical Arrangements for Out-of-Plane Displacement Sensitive Interferometers

Figure A2.5 shows an arrangement that is sensitive to displacement along the camera axis. The figure is a schematic, but the sensitivity will be controlled by the angle between the camera axis and the illuminating source. The source coincident with the camera axis produces a pure out of plane sensitive system.

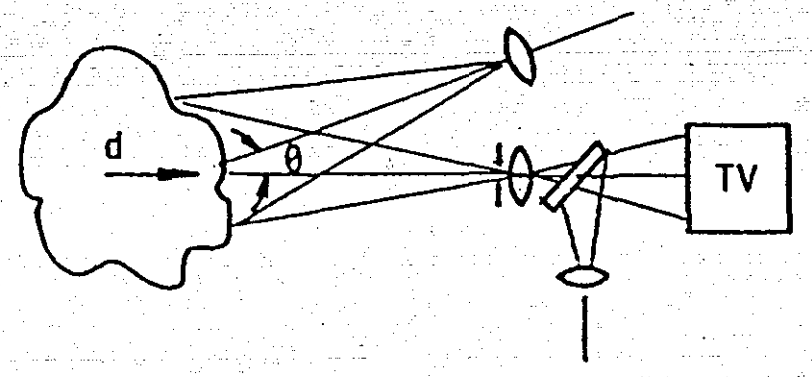

$$d = \frac{\lambda}{(1+\cos\theta)}$$

λ = wavelength of laser
d = displacement and along axis indicated

Figure A2.5
Sensitivity of an Out of Plane Interferometer

If the geometry of the system departs from this, with either or both of the viewing and illumination directions angled to this axis this general vector equation holds:

$$\phi = (n_0 - n_s).d\,2\frac{\pi}{\lambda}$$ where n_0 = illumination direction
n_s = viewing direction
d = displacement

Even if the illumination vector is rotated to a maximum of 15° and the viewing vector is as shown, the system retains maximum sensitivity. This allows for practical experimental layouts with maximum light efficiency.

A derivative of the out-of-plane system developed by Herbert [65], Figure A2.6, enables the object illumination and imaging to be achieved with the same lens. With this arrangement a microscopic objective could be used to examine areas 1 mm^2.

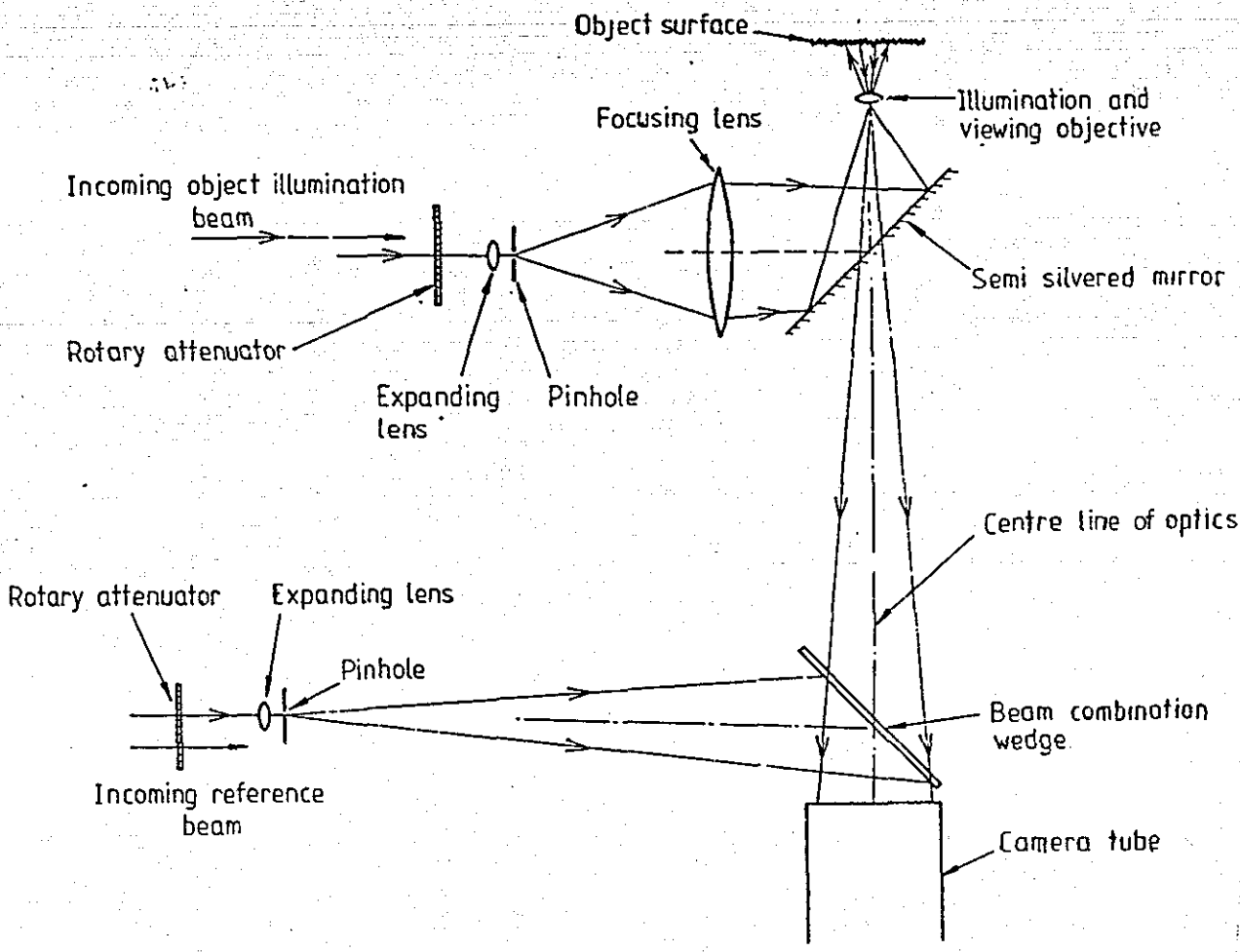

Figure A2.6
Speckle Microscopy Optical Arrangement to Investigate Small Areas of Surfaces

A2.3 Principles of Speckle Pattern Correlation Fringe Formation

In intensity interferometers, one measures two intensities I_1 and I_2 (the subscripts refer to either different times or points in space) and forms the average product. As was shown earlier in a complex Gaussian system (1) gives;

$$I_1 + I_2 + 2\sqrt{I_1 I_2} \cos \phi \qquad (1)$$

When considering the speckle case the object wave phase information ϕ_0 is composed of the object speckle pattern phase ϕ_{0S} and a random background speckle pattern phase ϕ_B. The latter usually remains constant providing the surface does not decorrelate the speckle pattern. Therefore the object wavefront can be described as earlier (8) as:

$$U_0(x,y) = a_0(x,y) \exp [j\phi_0(x,y)] \qquad (8)$$

and the total Irradiance (I) seen by the recording device is;

$$I = UU^*$$

where U is the complex amplitude and U^* is its conjugate.

In this case we have two wavefronts combined, one reflected from the object, the second the reference beam. The reference beam may be a uniphase spherical or collimated beam, though speckle reference beam from scattering surfaces have been successfully used. Assuming both beams to be linearly polarised, or have polarised content then

$$\begin{aligned} I &= |U_0 + U_R|^2 \\ &= (U_0 + U_R)(U_0^* + U_R^*) \end{aligned} \qquad (A2.9)$$

the subscripts 0 and R refer to object and reference wave amplitudes.

Assuming that U_R will have the same form as U_0;

$$I = |a_0(x,y) \exp [j\phi_0(x,y)] + a_R(x,y) \exp [j\phi_R(x,y)]|^2 \quad \text{(A2.10)}$$

Dropping the positional indicators;

$$I = [a_0 \exp j\phi_0 + a_R \exp j\phi_R][a_0 \exp(-j\phi_0) + a_R \exp(-j\phi_R)] \quad \text{(A2.11)}$$

$$I = a_0^2 + a_R^2 + a_0a_R [\exp j(\phi_0 - \phi_R) + \exp j(\phi_R - \phi_0)] \quad \text{(A2.12)}$$

$$= a_0^2 + a_R^2 + a_0a_R [\exp j(\phi_0 - \phi_R) + \exp(-j)(\phi_0 - \phi_R)] \quad \text{(A2.13)}$$

$$I = a_0^2 + a_R^2 + 2a_0a_R \cos (\phi_0 - \phi_R) \quad \text{(A2.14)}$$

$$I = I_0 + I_R + 2\sqrt{I_0}I_R \cos (\phi_0 - \phi_R) \quad \text{(A2.15)}$$

A2.3.1 Subtraction Correlation

Assume I_1 to represent the wavefront of the surface at the initial or rest condition and I_2 to be the wavefront after displacement. The detector (the television camera) will record the individual intensity signals and the initial image I_1 will be retained within the framestore. Subsequent to storage of I_1, the electronics automatically switch to the subtraction mode, where the current television picture is subtracted pixel by pixel from the stored image. Thus the output signal will be proportional to the difference between the two input signals. Let V_1 represent the consequential voltage produced by the video system to the input I_1 and V_2 the response to I_2 then V_S represents the subtracted output voltage;

$$V_S = V_1 - V_2 \; \alpha \; I_1 - I_2$$

let $\phi_0 - \phi_R = \phi_1$ rem: $\phi_0 = \phi_{0S} + \phi_B$

$$V_S = [I_R + I_O + 2\sqrt{I_R}I_O \cos(\phi_1)] - [I_R + I_0 + 2\, I_RI_0 \cos (\phi_1 + \Delta\phi)] \quad \text{(A2.16)}$$

$$= 2\sqrt{I_R}I_0[\cos \phi_1 - \cos(\phi_1 + \Delta\phi)]$$

$$= 2\sqrt{I_R}I_0(-2) \sin \frac{(\phi + \phi_1 + \Delta\phi)}{2} \sin \frac{(\phi + \phi_1 - \Delta\phi)}{2}$$

$$= 2\sqrt{I_R}I_0(-2) \sin \frac{(2\phi_1 + \Delta\phi)}{2} \sin \frac{(-\Delta\phi)}{2}$$

$$= 4\sqrt{I_R}I_0 \sin \frac{(\phi_1 + \Delta\phi)}{2} \sin \frac{(\Delta\phi)}{2} \qquad \text{(A2.17)}$$

This yields both positive and negative voltages, however the video system responds only to positive signals, therefore to maximise the output signal the subtracted result is assigned absolute values. Previously it had been assumed rectification of the signal would be satisfactory however this has the effect of doubling the spatial frequency of the signal. The present system developed by West at Loughborough utilises this advantage of digital electronics to assign absolute values and thereby retain the original spatial frequencies. Hence any pixel output voltage or brightness (B) is proportional to;

$$B \alpha I_R I_0 \sin^2 \frac{(\phi_1 + \Delta\phi)}{2} \sin^2 \frac{(\Delta\phi)}{2} \qquad \text{(A2.18)}$$

thus B will be maximised for ϕ values of π, 3π, 5π, etc. and will be minimised for ϕ values of 0, 2π, 4π, etc. Thus the zero order fringe pattern will be dark and the consequent fringes will be modulated with a $\sin^2$ function. For maximum correlation then,

$\Delta\phi = (2m + 1)\pi$, where m is an integer number;

i.e. displacement (d) for an out of plane system is given by;

$$d = \frac{(n - 1/2)\lambda}{2} \qquad \text{for n bright fringes,}$$

and for minimum correlation, $\Delta\phi = 2m\pi$ ie. when

$$d = \frac{n\lambda}{2} \qquad \text{for n dark fringes}$$

A2.3.2 Addition Correlation

For stroboscopic and double pulsed systems I_1 will be combined with I_2. This will unfortunately mean that any background noise terms will not be subtracted. The output voltage V_s will be given by;

$$V_s = V_1 + V_2 \alpha I_1 + I_2$$

$$= 2I_1 + 2I_2 + 4\sqrt{I_1 I_2}[\cos(\phi_1) + \cos(\phi_1 + \Delta\phi)] \qquad \text{(A2.19)}$$

$$= 2I_1 + 2I_2 + 4\sqrt{I_1 I_2}[2\cos(\tfrac{\phi_1+\phi_1+\Delta\phi}{2})\cos(\tfrac{\phi_1-(\phi_1+\Delta\phi)}{2})]$$

$$= 2I_1 + 2I_2 + 4\sqrt{I_1 I_2}[2\cos(\tfrac{2\phi_1+\Delta\phi}{2})\cos(\tfrac{-\Delta\phi}{2})]$$

$$= 2I_1 + 2I_2 + 4\sqrt{I_1 I_2}[\cos(\phi_1 + \tfrac{\Delta\phi}{2})\cos(\tfrac{-\Delta\phi}{2})] \qquad \text{(A2.20)}$$

Using the same processing electronics to process the signal,

$$B \alpha I_1 I_2 \cos^2(\phi_1 + \tfrac{\Delta\phi}{2})\cos^2(\tfrac{\Delta\phi}{2}) \qquad \text{(A2.21)}$$

B_{max} will be given with ϕ values of 0, 2π, 4π, etc.

B_{min} will be given with ϕ values of π, 3π, 5π, etc.

i.e. the zero order fringe will be bright as with holographic interferometry c.f. (38). Though the background signal level will be higher than with subtraction leading to a reduced fringe contrast.

Assume an average speckle diameter of 1.4μm, (this value being the average of the four values on page 228), and pixel size of 17 x 9μm, then each CCD pixel element could contain ≈100 individual speckles with a system operating at f1.4.

However, equation A2.16 is valid only when A2.15 is considered for a single pixel. Thus a modification to A2.16 is required;

$$V_g = \sum_{i=0}^{100} [I_R + I_O + 2\sqrt{I_R I_O}\cos(\phi_1)] - [I_R + I_O + 2\sqrt{I_R} + I_O \cos(\phi_1 + \Delta\phi)]$$

$$= \sum_{i=0}^{100} 4\sqrt{I_R I_O} \sin\frac{(\phi_1 + \Delta\phi)}{2} \sin\frac{(\Delta\phi)}{2} \qquad \text{(A2.29)}$$

Goodman [57] suggests the r.m.s signal to noise ratio of the intensity can be considered to vary with the $[M]^{1/4}$ where M is the number of speckle correlation cells within a measurement aperture which in the case above would yield an SNR change of approximately 10, this is shown experimentally in Figure A4.2. Burch [62], examines the gamma variate from Rayleigh and derives a family of curves which demonstrates this function. It is suggested that for the double pulse mode, equation A2.21 could be modified and be of the form;

$$F(\Delta\phi\ j) = \Sigma_i\, a_i \cos\left(\phi_i + \frac{\Delta\phi}{2} + \frac{a_j}{2}\right) \cos\frac{(\Delta\phi)}{2} \qquad \text{(A2.30)}$$

where a_j takes the values O and ± 2π/3 used for the phase stepping, and i is the speckle number. In the limit all the cross products would tend to zero and the $\cos^2$ terms average toward 0.5. If the speckle number is 100, then a 10% deviation will be expected and this could be different for each of the phase steps leading to uncertainty in the final deduced phase angle. Thus the fringe accuracy can not approach that of conventional interferometry, Koliopoulos [75], suggests at best λ/3000 achievable, practical optical test figures of λ/100 to λ/300 and in workshop environments λ/20 to λ/50.

A2.3.3 Time-Averaged Correlation

As with holographic interferometry if the surface oscillates sinusoidally, the position of any point on that surface can be determined in time by (22):

$$Z(x,y,t) = z(x,y) \sin \omega t \qquad (22)$$

The response of the silver halide emulsion when integrating the object wave with an exposure greater than the period (τ) of the vibrating surface is then taken from (26):

$$I(x,y) = a^2(x,y) J_o^2 \left[\frac{4\pi z}{\lambda}(x,y)\right] \qquad (26)$$

Using speckle correlation the general form of this equation is modified when combined with (A2.15),

$$I = I_0 + I_R + 2\sqrt{I_0 I_R} \cos(\phi_0 - \phi_R) \qquad (A2.15)$$

where the phase term is now modified by the J_0^2 term from the vibrating surface,

$$\text{thus} \quad I = I_R + I_0 + 2\sqrt{I_R I_0} \cos(\phi_0 - \phi_R) J_0^2 \left[\frac{4\pi z}{\lambda}\right] \qquad (A2.22)$$

or the phase of the returning object wavefront will be modulated in time as:

$$\Delta\phi(t) = \Delta\phi \cos \omega t \qquad (A2.23)$$

thus (A2.15) modifies to:

$$I(t) = I_0 + I_R \, 2\sqrt{I_R I_0} \cos(\phi_0 - \phi_R + \Delta\phi \cos \omega t) \qquad (A2.24)$$

$$I = \frac{1}{\tau} \int_0^{\tau} I(t)dt \qquad \text{(A2.25)}$$

Combining (A2.24) and (A2.25);

$$I = I_0 + I_R \frac{2\sqrt{I_R I_0}}{\tau} \int_0^{\tau} \cos(\phi_0 - \phi_R + \Delta\phi \cos \omega t)dt \qquad \text{(A2.26)}$$

This can again be evaluated using the Bessel function,

$$\frac{j\pi^n}{2\pi} \int_0^{2\pi} e^{jx\cos\alpha} e^{jn\alpha} \, d\alpha = J_n(x)$$

$$J_0(x) = \frac{1}{2\pi} \int_0^{2\pi} \exp j(x \cos\alpha) \, d\alpha \qquad \text{(A2.27)}$$

thus (A2.26) reduces to,

$$I = I_0 + I_R + 2\sqrt{I_0 I_R} \, J_0^2 \left(\frac{4\pi z}{\lambda}\right) \cos(\phi_0 - \phi_R) \qquad \text{(A2.28)}$$

The values of $J_0^2(x)$ are plotted in Figure A2.7, with minima at 2.40, 5.52, etc. and maxima at 0, 3.83, etc.

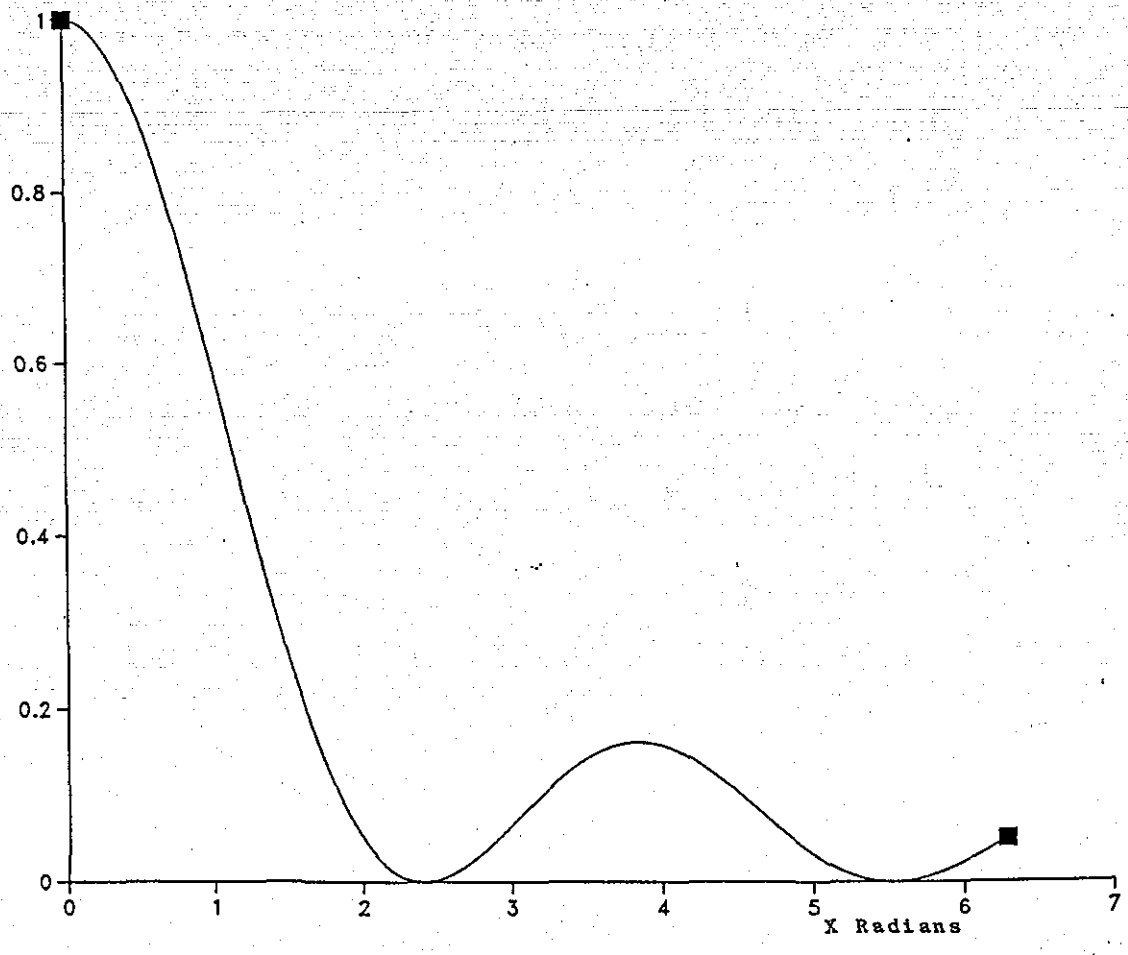

Figure A2.7
Plot of $J_0^2(x)$ against x

APPENDIX 3

EXPERIMENTAL VIBRATION STUDY USING TIME-AVERAGED ESPI ON A CLAMPED SQUARE METAL PLATE

As discussed in Holographic Interferometry, Chapter 2, comparison can be made with theoretical models. In this instance the first six modes of the plate are examined and a study made of the results.

A3.0 Theoretical Analysis

The following result is drawn from [41], which proposes that the natural frequencies for a fully clamped square plate are given by;

$$\text{Natural Frequency} = \frac{\beta}{2\pi}\sqrt{\frac{Et^2}{\rho L^4(1-\nu)^2}} \quad \text{Hz}$$

where; E = Youngs Modulus (Nm^{-2}),
t = thickness (m),
ρ = density ($kg\ m^{-3}$),
L = length of side (m),
ν = Poissons Ratio.

β is a value dependant upon the mode number of the solution.
For this experiment, the first six modes were considered, the corresponding values of B are given below:

Mode	Value of β
1	10.40
2	21.21
3	31.29
4	38.04
5	38.22
6	47.73

The material used was an 18/8 stainless steel with a Poisson ratio of 0.30.

A3.1 Experimental Details

$E = 201 \times 10^9\ Nm^{-2}$, $t = 0.001$ m,

$\rho = 7900\ kgm^{-3}$, $L = 0.1524$ m,

$\nu = 0.3$.

$$fn = \frac{\beta}{2\pi}\sqrt{\frac{201 \times 10^9 \times 0.001^2}{7900 \times 0.1524^4(1-0.3^2)}} \quad Hz$$

Using this value, a table of the first six modes can be constructed as shown in Table C.

Mode	β	Natural Frequency Hz	Experimental Result Hz
1	10.40	377	400
2	21.21	769	730,790
3	31.29	1134	1130
4	38.04	1378	1325
5	38.22	1385	1350
6	47.73	1729	1700

Table C. Comparison of Experimental and Theoretical Resonant Frequencies of 150x150 mm Clamped Metal Plate

Figure A3.1 illustrates the mode shapes. The material used was rolled sheet stock stainless steel and therefore has a preferential rolling axis which is an important factor in the asymmetry of results produced of Mode 2. Rather than provide a complete modal analysis, the purpose of the experiment was to demonstrate the quality of fringe patterns using ESPI compared with Holographic Interferometric experiments. Furthermore, with suitable refinement of technique and model, a direct comparison between model and experiment is possible. One advantage of ESPI is the ability to visualise coupled modes which theoretical models have difficulty with. This is due to the requirements of specific material variables, definition of actual boundary conditions and very high computational overheads. This work has been further investigated by Shellabear and Tyrer [42] in subsequent three dimensional vibration analysis studies of thick cylinders.

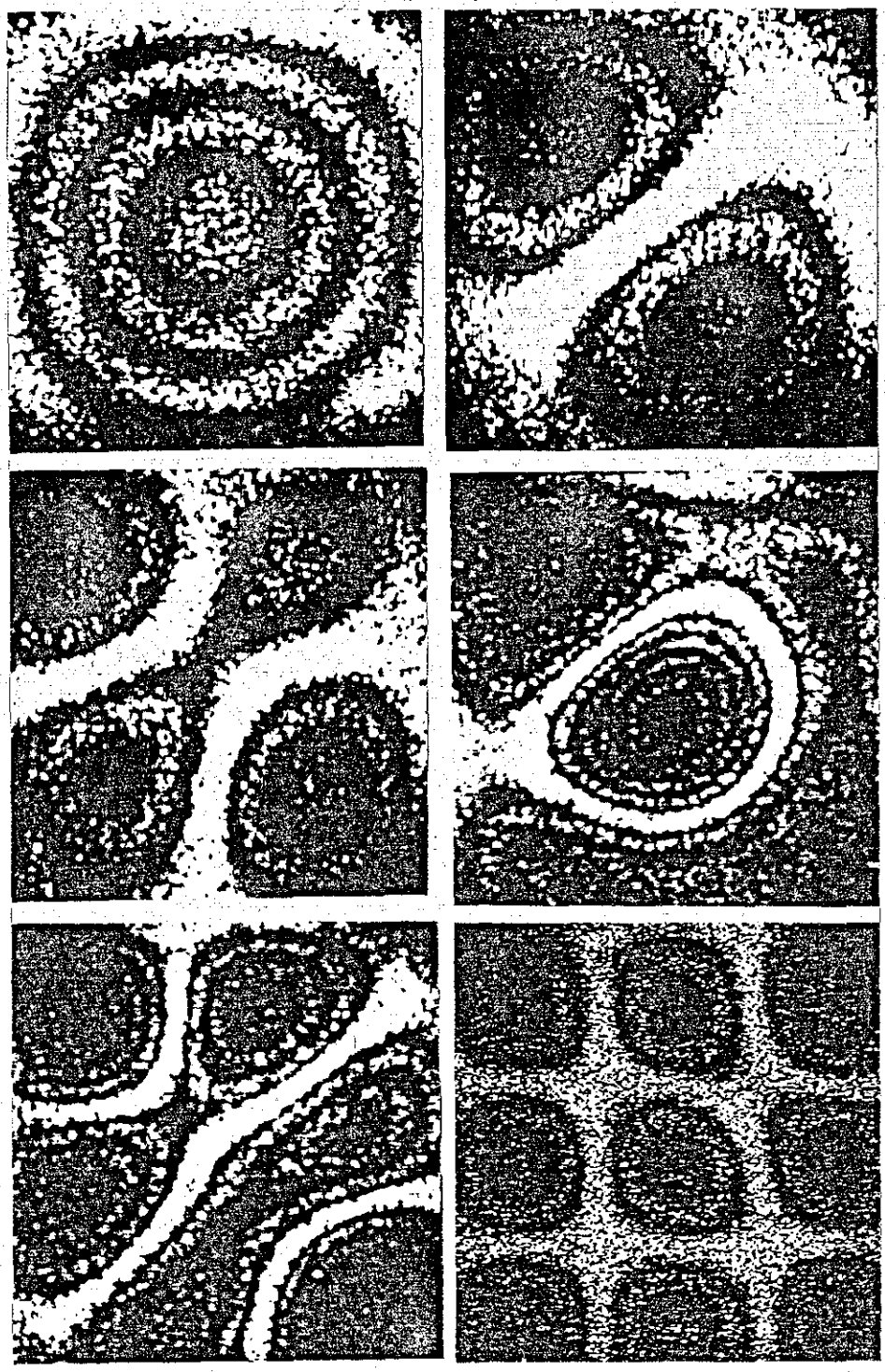

Figure A3.1
Clamped Metal Plate Mode Shapes

APPENDIX 4

NEW ESPI PROCESSING ELECTRONICS

A4.0 Description of Daylight Immunity Device

There are two sections to the Daylight Immunity Device (DID), the first half is concerned with synchronisation and blanking, the second half with signal conditioning. The video image is fed directly to the synchronisation part and is black level clamped. This clamp is sufficient to cope with the large differences in input signal level. The sync pulses are detected by a comparator which can produce the necessary front and rear porch of the blanking pulses. The levels are adjustable and allows the timing to be set for both RS170 and CC1R video signals - a description of UK standard video is given in Figure A4.1. The output of the comparator provides a pulse of which detection of the leading edge supplies the blanking for the duration of the sync pulse and back porch. The trailing edge provides the duration of the front porch and sync pulse. By overlapping the two blanking pulses no instability arises in the blanking signal. These signals are combined in a nand gate, a further nand gate inverts the sync pulse to provide composite sync at TTL levels.

The video component of the signal is fed via a buffer to the filter circuit where it is amplified and inverted. The gain can be adjusted to compensate for the actual image requirements and an offset allows independent adjustment of the video signal with respect to the blanking and this prevents negative video signals. The signal is then inverted to ensure correct polarity and sets the output threshold to within 700 mV (the video signal component of the 0-1 volt composite output).

The synchronisation pulse is then added to provide the working signal for input to the framestore. The elements of this self contained unit formed the basis of the modular concept which is attached to the computer based framestore systems. Modification to the final stage of the system requires the internal sync oscillator of the framestore board to lock the pre-processor to the

framestore ensuring improved stability of the fringes.

Figure A4.2 shows the video level of a fringe pattern using no pre- or post-processing. The fringe pattern is formed by the subtraction of a pure speckled video image and a modulation depth of approx 10% is apparent. Figure A4.3 shows the same component (a cantilever bend plate) using the filtered and amplified arrangements on the FOR-A system with an output modulation depth of, at best, 35%. Figure A4.4 shows a video print of the fringe pattern with unity contrast and brightness (the comparable result with no video processing was of insufficient quality to print). Figure A4.5 shows the results of the DID applied to a FOR-A system, full modulation of the output is achieved. The results obtained were for a 7 fringe displacement and the video line shown is line 353. The corresponding result, Figure A4.6, shows this visually. Whilst acknowledging that the underlying speckle fringe pattern modulation is low (approx 10%), the use of the DID prior to the framestore ensures optimised use of the grey levels available within the memory.

A4.1 Results

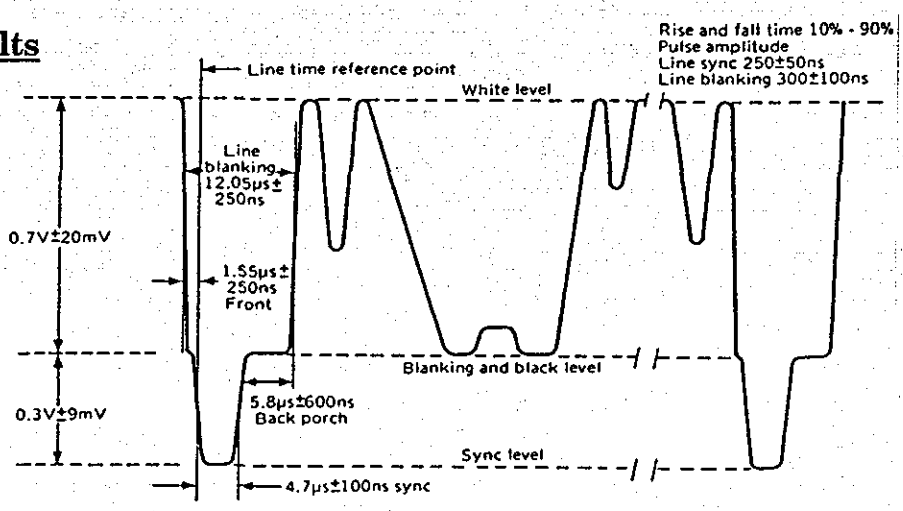

Figure A4.1

A typical line waveform of a TV signal. At the end of each line is a synchronising pulse. The amplitude of the analogue video waveform corresponds to the picture brightness at any particular moment. All levels and waveform timings must be precise in a modern TV system. Timings are for UK 625-line systems.

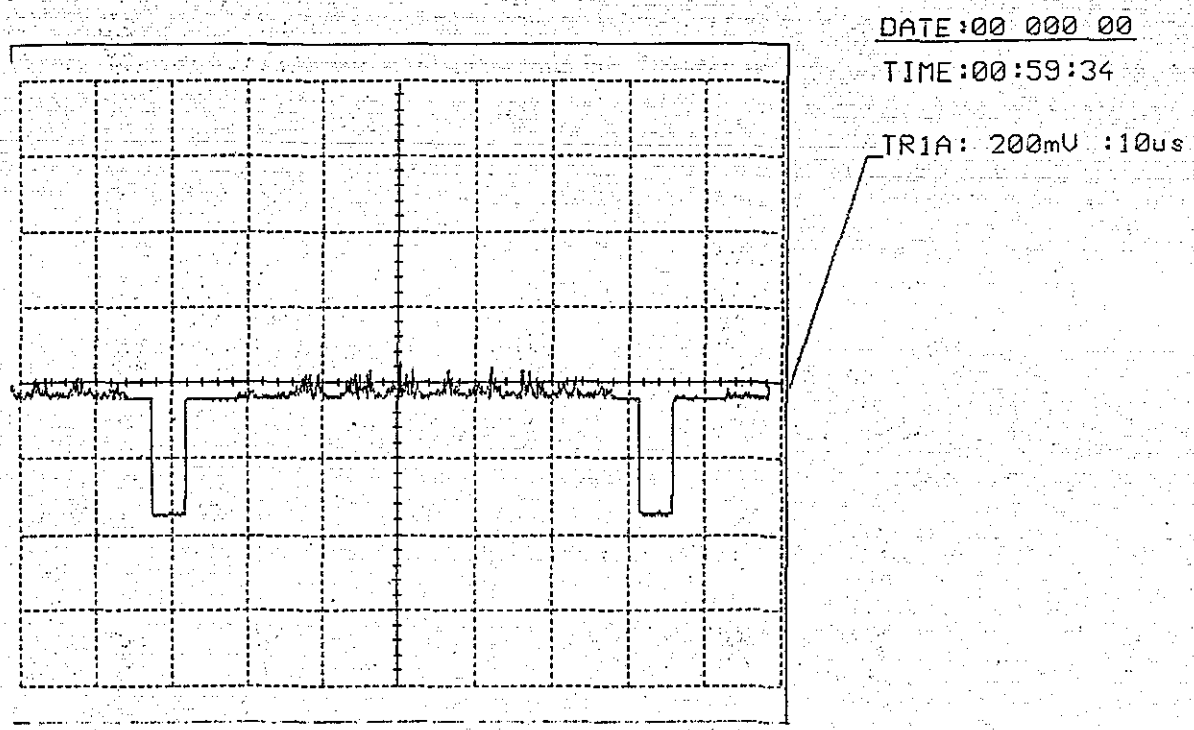

Figure A4.2

Video Level of a Seven Fringe Displacement Pattern Formed by the Subtraction of two Phase Referenced Speckle Patterns and no Additional Video Processing

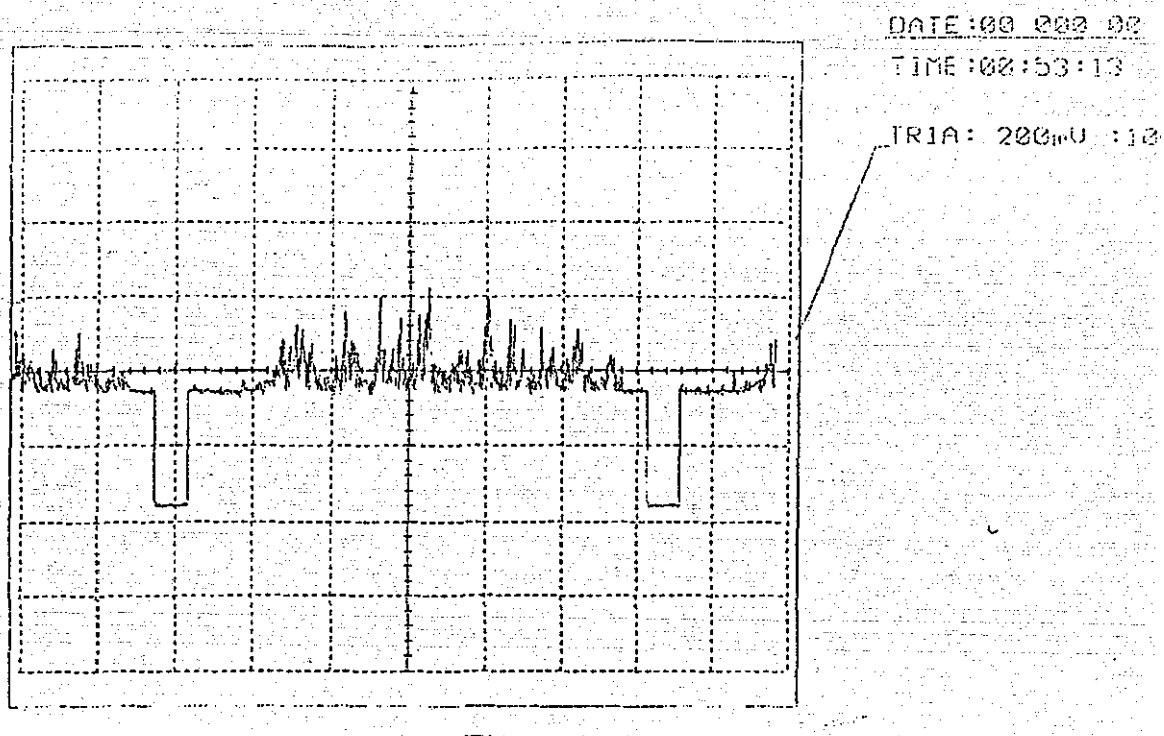

Figure A4.3
Video Level of a seven Fringe Displacement Pattern
Formed by the Subtraction System in the
Filtered FOR-A System

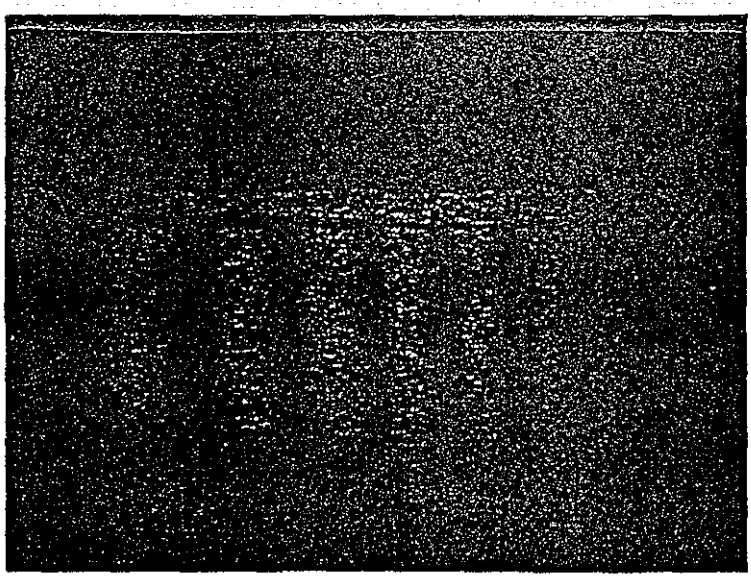

Figure A4.4
Photograph of the Video Image of above (A4.3),
Unity Brightness and Contrast have been used

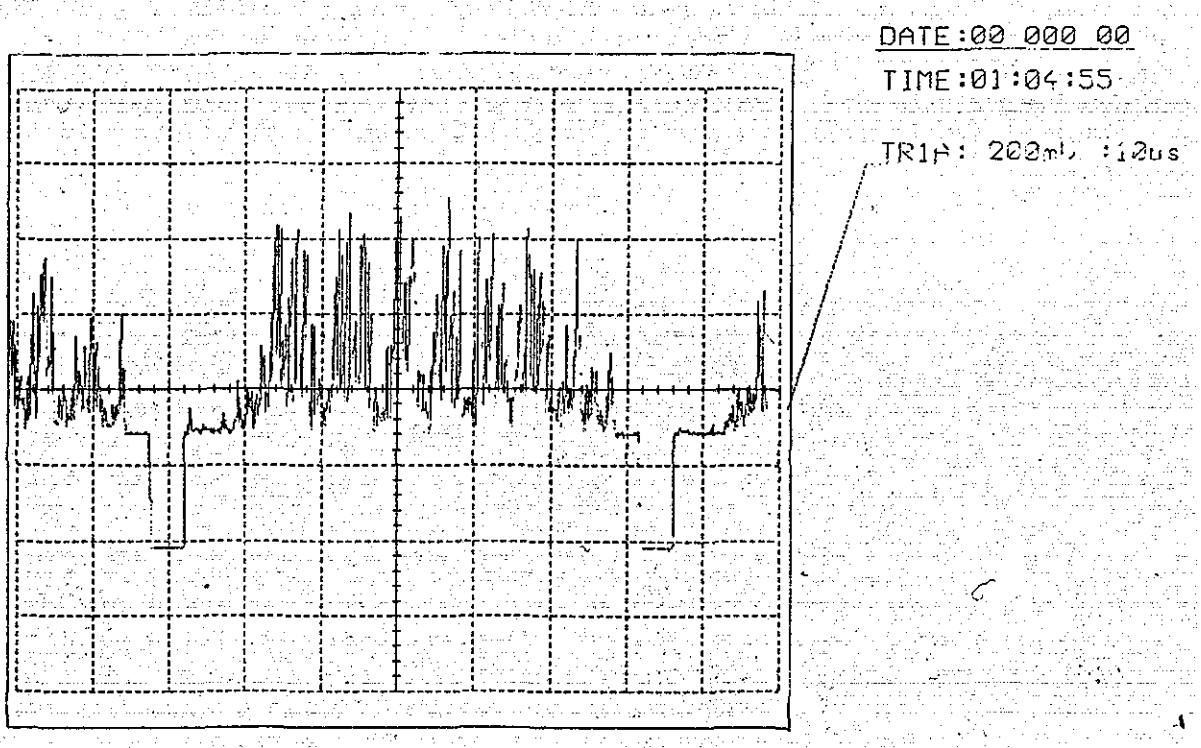

Figure A4.5
Video Level of a Seven Fringe Displacement Pattern
Formed after Pre-Processing using the DID Electronics
and the Subtraction System in the Filtered FOR-A System

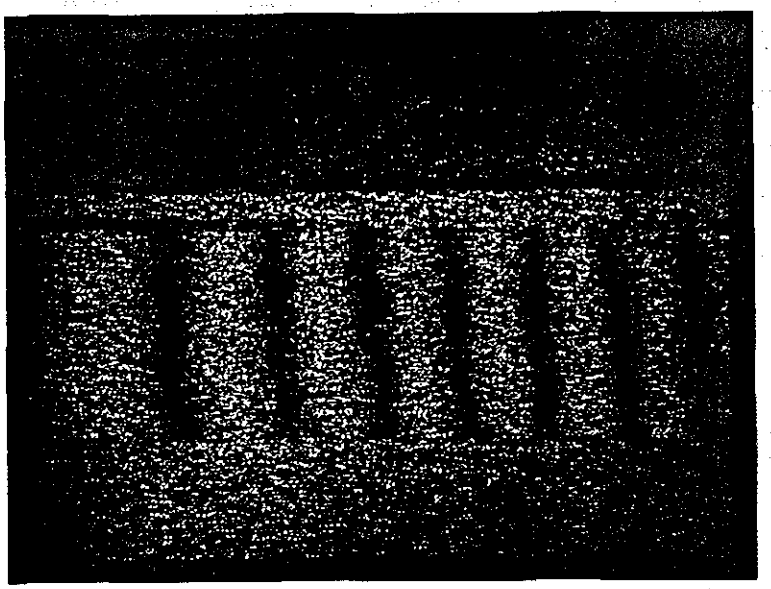

Figure A4.6
Photograph of the Video Image of above (A4.5),
Full Modulation, Unity Brightness and Contrast have been used